SYNTHESIS OF GYROSCOPE LIKE COMPLEXES VIA ALKENE METATHESIS: THE EFFECT OF LIGAND SUBSTITUTIONS ON ROTATIONAL BARRIERS

A Dissertation

by

GEORGETTE MARIE LANG

Submitted to the Office of Graduate and Professional Studies of
Texas A&M University
in partial fulfillment of the requirements for the degree of

DOCTOR OF PHILOSOPHY

Chair of Committee,	John A. Gladysz
Committee Members,	Donald J. Darensbourg
	Hongcai Zhou
	Jorge Seminario
Head of Department,	Simon North

August 2016

Major Subject: Chemistry

ABSTRACT

Major objectives of this dissertation involve the synthesis of gyroscope like complexes based upon dibridgehead diphosphine and diarsine cages, complexes with neutral dipolar rotors, and reactivity and rotational behavior of such complexes.

Ring closing metathesis and hydrogenation reactions of *trans*-$Fe(CO)_3(P((CH_2)_mCH{=}CH_2)_3)_2$ (m = 4-8) yield *trans*-$\overline{Fe(CO)_3(P((CH_2)_n)_3P)}$ (n = 2m+2). Reactions with NO^+ BF_4^- and $[H(OEt_2)_2]^+$ BAr_f^- (BAr_f = B(3,5-$C_6H_3(CF_3)_2)_4$) give the cations *trans*-$[\overline{Fe(CO)_2(NO)(P((CH_2)_n)_3P)}]^+$ BF_4^- and *mer,trans*-$[\overline{Fe(CO)_3(H)(P((CH_2)_n)_3P)}]^+$ BAr_f^- (n = 10, 12, 14). The rotational dynamics of these complexes are probed by variable temperature NMR spectroscopy. As opposed to those with larger values of n, the rotators of *trans*-$[\overline{Fe(CO)_2(NO)(P((CH_2)_n)_3P)}]^+$ BF_4^- (n = 10, 12) and *mer,trans*-$[\overline{Fe(CO)_3(H)(P((CH_2)_n)_3P)}]^+$ BAr_f^- (n = 10), show slow rotation on the NMR timescale at room temperature. VT-NMR data yield $\Delta H^{\ddagger}/\Delta S^{\ddagger}$ values (kcal/mol and eu) of 8.3/–28.4 and 9.5/–6.5 for $Fe(CO)_2(NO)^+$ rotation (n = 10, 12), and 6.1/–23.5 for $Fe(CO)_3(H)^+$ rotation (n = 12).

Reaction of arsines $As((CH_2)_mCH{=}CH_2)_3$ (m = 4-6) with (BDA)$Fe(CO)_3$ (BDA = benzylideneacetone) yield *trans*-$Fe(CO)_3(As((CH_2)_mCH{=}CH_2)_3)_2$. Metathesis and hydrogenation reactions afford *trans*-$\overline{Fe(CO)_3(As((CH_2)_n)_3As)}$ (n = 10, 12, 14). Previously discussed analogous reactions give *trans*-$[\overline{Fe(CO)_2(NO)(As((CH_2)_n)_3As)}]^+$ BF_4^- and *mer,trans*-$[\overline{Fe(CO)_3(H)(As((CH_2)_n)_3As)}]^+$ BAr_f^-. VT-NMR data give $\Delta H^{\ddagger}/\Delta S^{\ddagger}$

values of 7.7/–22.1 and 5.4/–22.7 for $Fe(CO)_2(NO)^+$ and $Fe(CO)_3(H)^+$ rotation (n = 12) which are distinctly lower than those in diphosphine analogs.

Reactions of *trans*-$Fe(CO)_3(P((CH_2)_mCH=CH_2)_3)_2$ (m = 4-8) with NO^+ BF_4^- afford *trans*-$[Fe(CO)_2(NO)(P((CH_2)_mCH=CH_2)_3)_2]^+$ BF_4^-. Further substitution is effected with Bu_4N^+ X^- (X = Cl, Br, I, CN) to give *trans*-$Fe(CO)(NO)(X)(P((CH_2)_mCH=CH_2)_3)_2$.

Three synthetic routes to gyroscope-like complexes *trans*-$\overbrace{Fe(CO)(NO)(X)(P((CH_2)_n)_3P)}$ (n/X = 4-8/Cl, Br, I, CN) are described. (1) Reaction of *trans*-$[\overbrace{Fe(CO)_2(NO)(P((CH_2)_{14})_3P)}]^+$ BF_4^- with Bu_4N^+ X^- gives *trans*-$\overbrace{Fe(CO)(NO)(X)(P((CH_2)_{14})_3P)}$. (2) Treatment of the acyclic complexes *trans*-$Fe(CO)(NO)(X)(P((CH_2)_mCH=CH_2)_3)_2$ with Grubbs' catalyst affords *trans*-$\overbrace{Fe(CO)(NO)(X)(P((CH_2)_mCH=CH(CH_2)_m)_3P)}$. (3) Similar reactions with *trans*-$[Fe(CO)_2(NO)(P((CH_2)_mCH=CH_2)_3)_2]^+$ BF_4^- can give *trans*-$[\overbrace{Fe(CO)_2(NO)(P((CH_2)_n)_3P)}]^+$ BF_4^-. Consistent with NMR data, crystal structures of *trans*-$\overbrace{Fe(CO)(NO)(X)(P((CH_2)_{14})_3P)}$ (X = Cl, Br, CN) indicate that the void space within the diphosphine cages appears sufficient for Fe(CO)(NO)(X) rotation.

DEDICATION

This dissertation is dedicated to my mother Tania and boyfriend Jason. Your love and support have been invaluable to me throughout this entire process and I wouldn't have been able to do it without you.

ACKNOWLEDGEMENTS

First and foremost, I would like to thank my research advisor, Dr. John Gladysz. For years, he has put forth much effort towards my research and recently much time and effort on this dissertation. I have learned a lot from him. I would also like to thank my committee members, Dr. Don Darensbourg, Dr. Hongcai Zhou, and Dr. Jorge Seminario. I would also like to thank Dr. Janet Blümel.

The Gladysz group has evolved a lot over the years and many people have come in and out of Reed McDonald. I want to thank everyone for your friendships and chemical discussions, but there are a few that I would like to acknowledge specifically. First and foremost I would like to thank Paul Zeits who taught me so much in my first years. He put up with me as a fledgling graduate student and helped me to gain confidence as a researcher. Melissa Clough, Kyle Lewis, and Alexander Estrada have been the best lab mates I could have ever asked for. Thanks for making lab, not only educational, but also fun. There have been several post docs that have mentored me in different ways. Dr. Yoshihiro Kobayashi, Dr. Juan Guerrero-Leal and Dr. Coralie Thomas thanks for being such wonderful people and such a wonderful source of knowledge. A special thanks to Dr. Tobias Fiedler. You were a great co-glovebox czar with me and you helped me get through making figures for this dissertation. Without you I would probably still be making a table of contents graphic for my second paper. Bryan Stewart you have helped me navigate the world of Adobe Illustrator and have helped to

keep me sane throughout the entire dissertation writing process. For his help with many of the NMR experiments described in this work, thank you to Greg Wylie.

To my mom, I have no words to describe what your support has meant over the last 31 years of my life. I could not have done this without you. You have never lost faith in me and you pushed me to always do my best even if I wasn't the best. You taught me that there was always a lesson to learn in everything that I did. That drive to learn has brought me to where I am today. Thank you for being the best person I know.

Dad and Rainey, thank you both for loving and supporting me. I hope that in the future we will be able to spend much more time together now that I am done with my dissertation.

Barbara and Gerald, thanks for welcoming me into your family and encouraging me as if I was one of your own.

Mrs. Jamie and Mr. Gary Cislaghi, you have supported me on my educational journey at every turn. Thank you for paying for me to apply to several different colleges and to take the GRE, and for genuinely being interested in what I was doing. It has all meant more than you know and I will forever be grateful.

Heather Stevens, you are the sister I never had. Thank you so much for rooting me on from afar. Thanks for always having my back.

I am so grateful for the friends I have met while in graduate school. Thank you Danielle Crouthers/Fair for the laughs, the love, the coffee, the wine, the chemistry discussions, and the mutual love for dramatic television. Ashley Cardenal, you are so

smart and driven. Thank you for always letting me vent and being a person who I felt actually understood.

Last, but certainly not least, I would to acknowledge Jason Denny. Being in a relationship with a fellow chemist graduate student has not always been easy, but I wouldn't change a thing. You have provided me with so much love and support over the last several years. Thank you for your immense help with this dissertation, for listening to me complain constantly, and for always reminding me to KEEP GOING. I can't wait for life together as a pair of chemists.

TABLE OF CONTENTS

Page

LIST OF FIGURES

Page

Page

Page

Page

Page

LIST OF TABLES

LIST OF SCHEMES

Page

1. INTRODUCTION

1.1 Gyroscopes: inspiration and historical perspective

At the outset, let us stand up for playing. Often mistaken for a kid's domain, playing opens up new fields of experience even for the "grown-ups". Possibly, it is one of the prerequisites of the creative process, in the sense that dealing playfully with known ideas provides new ways of thinking. Scientists are no exception. On the contrary, in the area of supramolecular chemistry, with all the model-like realizations of macroscopic objects at a molecular level, the drive to play seems to be followed strongly.– Christoph A. Schalley[1]

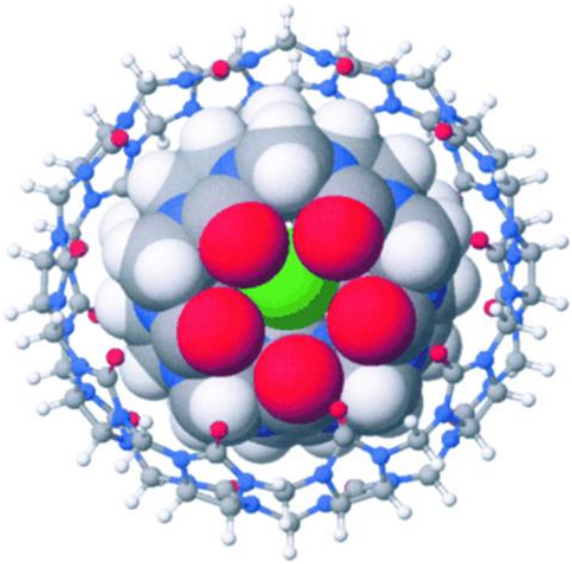

Figure 1-1. A gyroscane: a cucurbituril inside a larger cucurbituril (encapsulating a chloride ion). *Reproduced from Schalley, C. A. *Angew. Chem. Int. Ed*. 2002, 41, 1513-1515 with permission of John Wiley & Sons, Inc.

Christoph A. Schalley references the publication by Day, Blanch, and coworkers of a "gyroscane" shown in Figure 1-1.[2] In his opinion, the synthesis of the gyroscane

demonstrates that thinking playfully about chemistry and molecular level reconstruction of toys and macroscopic machines "leads to thrilling chemical problems, and that finding solutions often leads to a significant increase in our chemical knowledge."[1] This is a great preface to our work in the area of molecular gyroscopes.

In 1817, Johann von Bohnenberger, a mathematics and astronomy professor in Germany, described the first device closely resembling modern mechanical gyroscopes.[3] Almost 40 years later, French scientist Jean Foucault sought to develop an instrument to demonstrate the rotation and precession of the earth about its axis. A replica of his device is depicted in Figure 1-2 (left).[4] Since the 1800s, gyroscopes have come to greatly impact our everyday lives and today's technology. They are used as anti-roll stabilizers in high speed trains, space station orientation and navigational systems, virtual reality headsets, and self-leveling pool tables on cruise ships.[5] The combination of gyroscopes and accelerometers in consumer electronics allows for more accuracy and precision in the devices' direction and motion sensing. [6]

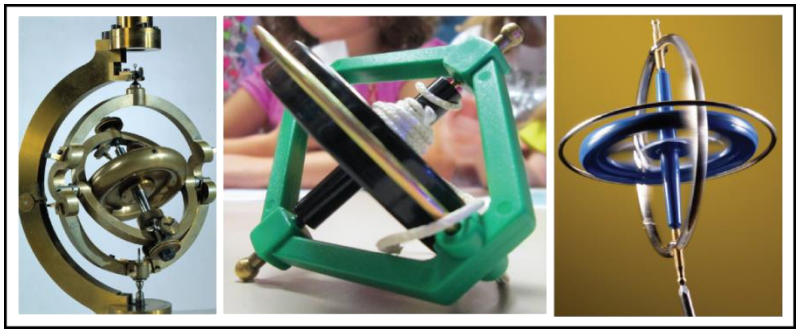

Figure 1-2. Foucault gyroscope (left) and present-day toy and model versions (middle, right).

1.2 Molecular rotors

Molecular gyroscopes and compasses are considered a categorical subset of molecular rotors. A molecular rotor is divided into two structural components: (1) the rotator; the portion of the system that rotates against the rest and (2) the stator; the portion with the larger moment of inertia. The stator is the stationary part of the system with respect to which the rotator turns.[7] In a molecular compass, the motion of the rotator would mimic the behavior of a macroscopic compass needle. This requires the rotator to have some kind of polar or polarizable group that would respond to an external electric field.[8b,9]

1.3 Molecular gyroscopes in the chemical literature

In addition to the Gladysz group, other groups have developed systems of gyroscope like complexes. These include the groups of Rose,[10] Gray,[11] Lambert,[12] Garcia-Garibay,[8] and Setaka.[13] The first reference of complexes as "gyroscopes" in the chemical literature emerges with Rose and coworkers in 1985 with the synthesis of what they refer to as "gyroscope like porphyrins."[10] A representation of these molecules is shown in Figure 1-3 (**I**). The basic structure resembles a two spoke gyroscope. The porphyrin core could serve as the rotator, while the peripheral 'handles' could serve as the stator. However, rotation of the porphyrin moiety is impossible due to steric bulk of the stator.[10]

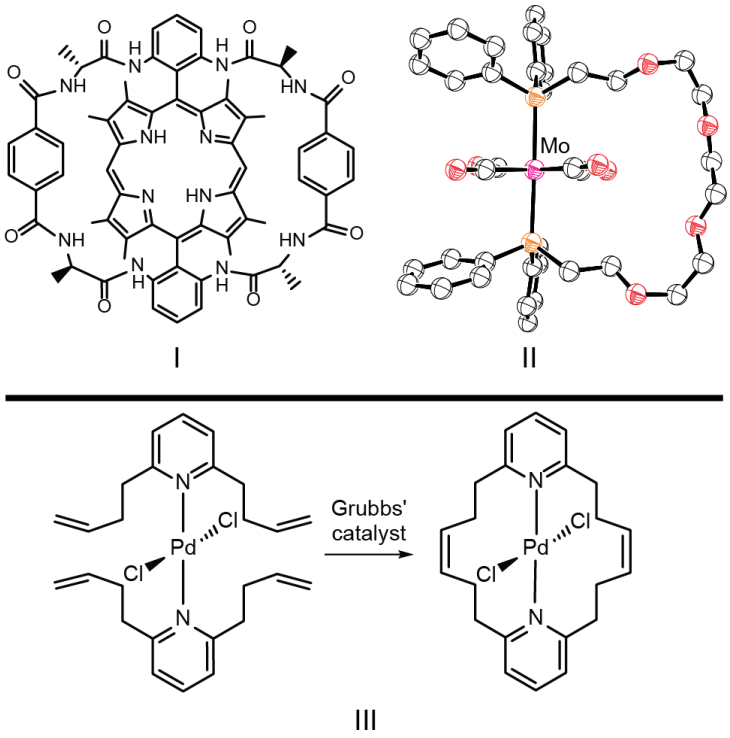

I II III

Figure 1-3. Rose type ″gyroscope″ porphyrin. (**I**) Thermal ellipsoid plot of Gray's molybdenum *trans*-spanning diphosphine complex. (**II**) Ring closing metathesis of Lambert's *trans*-spanning diphosphine palladium chloride complex. (**III**)

The next appearance of the term "gyroscope" comes with Gray and coworkers in 1994 and the synthesis of the *trans*-spanning diphosphine molybdenum complex in Figure 1-3 (**II**).[11] This represents the first example of a metalla-crown ether with *trans*-coordinated phosphorus donors. In order to be considered a molecular rotor, complexes must contain a rotator and a stator. Unlike the "gyroscope" porphyrins of Rose, where no portion of the complex could function as a rotator, the molybdenum complex can unmistakably be considered a molecular rotor.

Lambert published the synthesis of a palladium complex which is the product of a two-fold ring closing metathesis reaction illustrated in Figure 1-3 (**III**). Representing

the next phase in the evolution of the molecular gyroscope, this work represents the first application of alkene metathesis in the synthesis of a *trans*-spanning chelate ligand. Prior to this point, no attempts had been made to provide a strict definition for a molecular gyroscope. Thus, this complex is not referred to as a "molecular gyroscope," but it provides an important chemical precedent to *our* molecular gyroscopes.[12]

More recent and influential contributors to the world of molecular gyroscopes are the Garcia-Garibay and Setaka groups.[8,13] Portions of their work will be detailed in later sections.

1.4 Gladysz type molecular gyroscopes

In 2000, the Gladysz group began to study alkene metathesis in metal coordination spheres.[14,15] The initial stages of our endeavor involved developing routes to complexes that can be regarded as "insulated molecular wires"[16-17] and then branched out to what we refer to as molecular gyroscopes.

At the outset of our investigation into the syntheses of molecular gyroscopes, it was important to define the framework within which the ideal gyroscope could be produced. A set of properties was conceived that was thought to lead to molecules that would best approximate macroscopic gyroscopes. These properties were:[5]

(1) There should be a functional axis of rotation which allows an interior domain of the molecule (the rotator) to rotate independently of an exterior domain (the stator).

(2) The exterior domain should sterically shield and optimally encase the rotator with ″spokes″, as with toy and real-world gyroscopes.

(3) They should closely model the connectivity and symmetry of a toy gyroscope which is generally D_{nh}.

A molecular gyroscope meeting solely the formerly defined framework would rotate with Brownian (random) motion, i.e. unidirectional rotation is not guaranteed. Thus it would fall short of a true molecular level imitation of real world gyroscopes.[18] Exploiting the interaction of a dipole moment and an electric field, a dipole inserted on the rotator could then be oriented or unidirectionally driven.[9] The latter feature would address the question of how to more accurately mimic the physics of real world gyroscopes.[5,18]

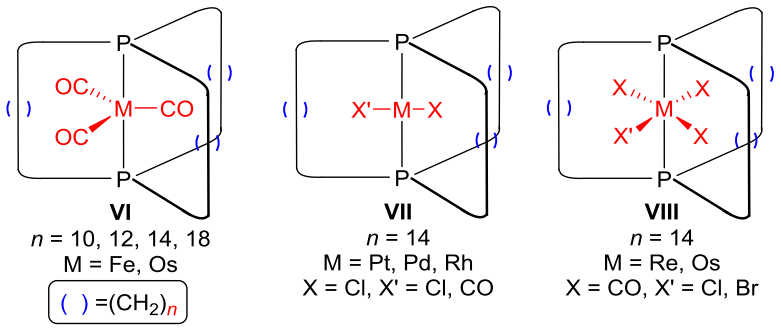

Figure 1-4. Gyroscope like complexes of the Gladysz group based upon *trans*-spanning diphosphines with $(CH_2)_n$ linkers.

The Gladysz group established that phosphine ligands containing a $(CH_2)_mCH{=}CH_2$ substituent occupying *trans* positions in various metal complexes could undergo alkene metathesis and subsequent hydrogenation to afford molecular

gyroscopes of the general formula *trans*-$ML_y(P((CH_2)_n)_3P)$, where M = Pt, Pd,[20] Fe,[21] Os,[22] Rh,[23,24] and Re[25] and *n* = the number of methylene carbons in the spokes. Three coordination environments investigated by the Gladysz group are depicted in Figure 1-4. The trigonal bipyramidal Fe and Os systems are represented by **VI**,[22] the square planar coordination with Pt, Pd, and Rh by **VII**,[20,23,24] and the octahedral environment employed with Os and Re[22,25] by **VIII**.

1.5 Aim of this work

At the outset of this dissertation, preliminary results of the trigonal bipyramidal iron gyroscope like complexes had been reported with *trans*-diphosphine ligands. Section 2 will expand upon the chemistry already reported.

An important question is whether this methodology could be extended to complexes with a different ligand set, more specifically, extension to other group 15 elements. Thus, Section 3 will describe the syntheses of arsenic analogs of complexes in Section 2. Such complexes were sought with a goal of expanding the "clearance to rotate" within the methylene spokes. Due to the larger covalent radius of arsenic, this "clearance" should be greater; therefore, the barrier to rotation for the rotator would be decreased. Rotation is probed by variable temperature $^{13}C\{^1H\}$ NMR spectroscopy and several barriers are reported.

As previously discussed, the incorporation of a dipole moment on the rotator would allow for potential rotational control. In Sections 2 and 3, substitution reactions at

the rotator with NO^+ BF_4^- are reported; however, neutral complexes would have advantages for sustained unidirectional rotation. Sections 4 and 5 will discuss strategies for obtaining molecular gyroscopes equipped with these types of rotators. Section 4 will focus on the synthesis of iron tricarbonyl complexes, and sequential carbonyl ligand substitutions by nitrosyl, halide, or pseudohalide ligands to afford substituted acyclic gyroscope precursors of the formula *trans*-Fe(CO)(NO)(X)(P((CH$_2$)$_m$CH=CH$_2$)$_3$)$_2$ (X = Br, Cl, I, CN, m = 4-8).

Section 5 will investigate the effectiveness of carrying out ring closing metathesis reactions with the acyclic complexes from Section 4 and the direct substitution of tricarbonyl gyroscope like compounds from Section 2 to yield complexes with the formula *trans*-Fe(CO)(NO)(X)(P((CH$_2$)$_n$)$_3$P) (X = Br, Cl, I, CN).

2. GYROSCOPE LIKE COMPLEXES BASED UPON DIBRIGEHEAD DIPHOSPHINE CAGES THAT ARE ACCESSED BY THREE FOLD INTRAMOLECULAR RING CLOSING METATHESES AND ENCASE $FE(CO)_3$, $FE(CO)_2(NO)^+$ AND $FE(CO)_3(H)^+$ ROTATORS*

2.1 Introduction

Molecular rotors[7] represent a large class of compounds with a variety of potentially practical functions.[26-28,8,13] They are often analyzed in the context of a rotator and a "stationary" stator. All motion is relative, so the latter is taken as the component with the greater moment of inertia.[7] There has been particular interest in developing molecular rotors that can structurally or functionally mimic various attributes of macroscopic gyroscopes.[8,13,20-25,29,30] The latter can be used to sense and/or maintain the orientations of diverse objects, with three representative examples that span more than a century of technology being torpedo warheads, space stations, and the displays associated with mobile phones.[6]

Some efforts involving molecular gyroscopes have been directed at engineering assemblies in which one or more components can exhibit rotation in the solid state, such as the "amphidynamic crystals" designed by Garcia-Garibay.[8b] Others have been concerned with rotation in solution or at solid/liquid interfaces, including ordered arrays

---

*Reprinted with permission from Lang, G. M; Shima, T.; Wang, L.; Cluff, K. J.; Hampel, F.; Blümel, J.; Gladysz, J. A. *J. Am. Chem. Soc*. **2016**, *138*, DOI: 10.1021/jacs.6b03178.

constructed by mounting rotors on surfaces.[31] Importantly, all of the physics embodied in macroscopic gyroscopes[18] for example, the conservation of angular momentum remains applicable at the molecular level,[7] thus setting the stage for the ultimate degree of miniaturization.

As shown in Scheme 2-1, we have discovered that three fold intramolecular ring closing metatheses of *trans* bis(phosphine) complexes of the type **I** can be effected in surprisingly high yields. This methodology has been applied to trigonal bipyramidal, square planar, and octahedral complexes, as detailed in a series of papers.[20-25,29] Subsequent hydrogenations afford adducts of cage like macrocyclic dibridgehead diphosphines (**II**). These are reminiscent of a common type of macroscopic gyroscope in which the ML_y moiety substitutes for a flywheel.

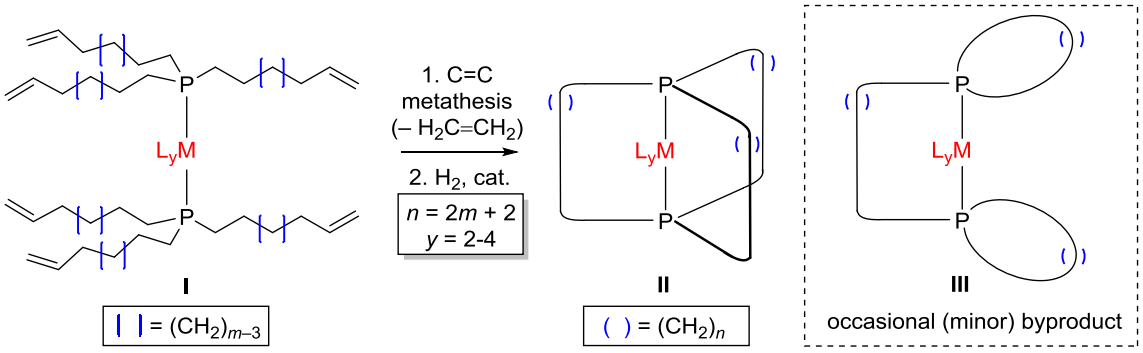

Scheme 2-1. General synthetic approach to gyroscope like complexes of different coordination geometries.

In some cases, an alternative product derived from a combination of *inter*ligand and *intra*ligand metatheses has been detected (**III**), but is rarely the major species.[20b,22]

Depending upon the relative sizes of the macrocycles and the ligands L_y in **II**, rotation of the ML_y moiety may be possible. Interestingly, ligand substitutions can often be carried out in such environments,[20,23-25,22a] allowing the rotational barriers to be fine tuned. The ML_y fragments can also be excised from the dibridgehead diphosphines under appropriate conditions.[20,24b] Furthermore, square planar palladium and rhodium systems can be effective catalyst precursors for carbon carbon bond forming reactions.[24b]

In this section, we return to the iron tricarbonyl systems disclosed in the initial communication,[21] and provide complete details of their (1) syntheses, (2) substitution and addition reactions, (3) solid-state structures, and (4) rotational properties in solution and solid state, as well as a variety of other phenomena. Together with the accompanying analyses, these data provide much new insight regarding the design and optimization of ML_y based molecular gyroscopes. The syntheses of the requisite starting materials, trans-$Fe(CO)_3(P((CH_2)_mCH{=}CH_2)_3)_2$ (**2**; *m* = **a**, 4; **b**, 5; **c**, 6; **e**, 8) have been detailed earlier.[32]

2.2 Results

2.2.1 Syntheses of title complexes

As shown in Scheme 2-2, a 0.0075 M CH_2Cl_2 solution of **2a** was refluxed with Grubbs' catalyst.[34a] The loading, 13 mol%, represented 4 mol% per new C=C linkage. Workup afforded a homogeneous white solid in 60% yield. Aliquots from the reaction

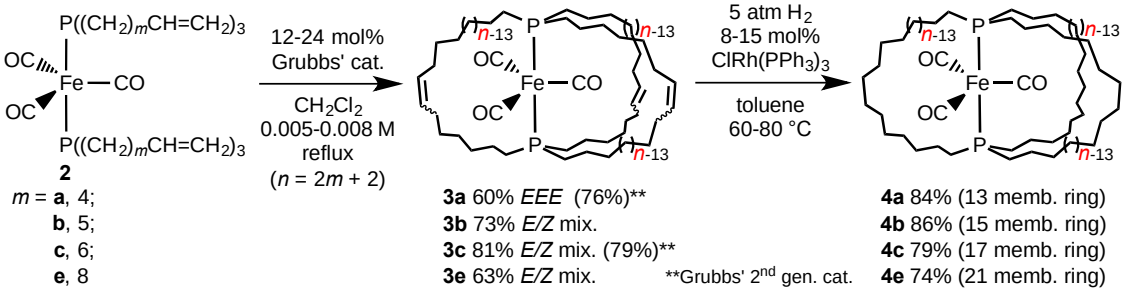

Scheme 2-2. Syntheses of gyroscope like iron tricarbonyl compounds.

mixture were periodically assayed by ^{31}P NMR, and showed two intermediates, presumed to be monocyclic and bicyclic species. The chemical shifts moved progressively downfield as **2a** was converted to the product (64.2, 67.9, 75.0, 84.7 ppm, C_6D_6).

The new complex and all others isolated below were characterized by IR and NMR (^1H, ^{13}C, ^{31}P) spectroscopy, and in most cases microanalyses and mass spectrometry. The mass spectrum exhibited an ion consistent with a three-fold intramolecular metathesis product, and no peaks of higher mass. A ^{13}C NMR spectrum (C_6D_6) indicated a highly symmetric product, with a single Fe***C***O signal coupled to both

phosphorus atoms (213.9 ppm, t, $^2J_{CP}$ = 28.1 Hz), a single ***C***=***C*** signal (132.0 ppm), and four ***C***H_2 signals (24.3 to 33.4 ppm). Hence, the new complex was assigned the gyroscope like structure *E,E,E*-**3a** depicted in Scheme 2-2, with three thirteen membered rings containing *E* C=C linkages, as verified crystallographically below.

A toluene solution of *E,E,E*-**3a** was then treated with H_2 (5 atm) in the presence of Wilkinson's catalyst ($ClRh(PPh_3)_3$; 15 mol%) at 80 °C. Workup gave the hydrogenation product $Fe(CO)_3(P((CH_2)_{10})_3P)$ (**4a**) as a white solid in 84% yield. The ^{13}C NMR spectrum (C_6D_6) exhibited one Fe***C***O signal (216.4 ppm, t, $^2J_{CP}$ = 28.0 Hz) and five ***C***H_2 signals (21.2 to 29.1 ppm), consistent with the idealized molecular symmetry (D_{3h}). When aliquots from the reaction mixture were assayed by ^{31}P NMR, two intermediates, presumed to be diolefinic and monoolefinic species, were detected. The chemical shifts moved progressively upfield as *E,E,E*-**3a** was converted to **4a** (84.7, 81.1, 78.1, 75.5 ppm, C_6D_6). Complexes *E,E,E*-**3a** and **4a** were moderately air sensitive, but showed no mass loss at temperatures less than 300 °C (TGA).

The generality of this sequence was tested with **2b**,**c**,**e** (Scheme 2-2), which contain longer methylene segments. Similar metatheses gave **3b**,**c**,**e**, featuring three fifteen, seventeen, and twenty one membered rings, in 63-81% yields. Mass spectra showed molecular ions, and no peaks of higher mass. However, mixtures of *E*/*Z* C=C isomers formed, as evidenced by multiple ^{31}P NMR signals and more complex patterns of C***H***=C***H*** ^1H NMR signals. High *E* selectivities as seen with *E,E,E*-**3a** appear limited to ring closing metatheses that place *trans* P-M-P linkages in thirteen membered rings.[35]

In any event, when **3b**,**c**,**e** were hydrogenated with Wilkinson's catalyst, isomerically homogeneous **4b**,**c**,**e** were obtained in 74-86% yields.

Superior yields are often obtained with advanced generations of Grubbs' catalysts. When **2a**,**c** and Grubbs' second generation catalyst[34b] were similarly reacted, the yield of *E*,*E*,*E*-**3a** increased from 60 to 76%, but that of **3c** was scarcely affected. In efforts with related complexes to date, only one other example has been found where Grubbs' second generation catalyst afforded a significantly higher yield. This case also involved a thirteen membered ringed product.[35]

The spectroscopic properties of **4a-c**,**e** exhibited several trends. The ^{31}P NMR signals shifted ca. 10 ppm upfield as the ring sizes increased, consistent with data for other cyclic organophosphorus compounds.[36] The IR ν_{CO} values of the complexes with the two smaller ring sizes (**4a**,**b**; 1841, 1853 cm^{-1}) were at lower frequencies than the others (**4c**,**e**; 1861, 1859 cm^{-1}). However, the ^{13}C NMR chemical shifts and $^{2}J_{CP}$ values for the ***C***O signals fell into narrow ranges (216.4, 215.5, 215.6, 215.7 ppm, C_6D_6; 27.5, 28.4, 29.0, 28.0 Hz). The P***C***H$_2$, PCH$_2$***C***H$_2$, and PCH$_2$CH$_2$***C***H$_2$ signals were *apparent* doublets of doublets (30.1-32.0 ppm, $^{1}J_{CP}$ = 14.7-15.0, 11.7-12.1 Hz),[37] singlets (21.2-24.3 ppm), and virtual triplets (29.1-31.6 ppm, $^{3}J_{CP}$ = 5.3-7.2 Hz),[37] respectively, as confirmed by ^{1}H,^{1}H COSY and ^{1}H,^{13}C HSQC experiments.[38]

2.2.2 Molecular structures

In order to help analyze the steric environments within the diphosphine cages, structural data for the preceding compounds were sought. Accordingly, crystals of the benzene and mesitylene solvates *E,E,E*-**3a**·C_6H_6 and *E,E,E*-**3a**·2(1,3,5-$C_6H_3(CH_3)_3$), as well as non-solvated **4c**, were grown. X-ray data were collected and the structures were solved as summarized in the experimental section and crystallography section.

Thermal ellipsoid representations of two representative complexes, *E,E,E*-**3a**·C_6H_6 and **4c**, are presented in Figure 2-1. Complex *E,E,E*-**3a**·C_6H_6 exhibited a three fold symmetry axis coincident with the P-Fe-P linkage, and (in a perpendicular plane) three two fold symmetry axes coincident with each Fe-C-O linkage (see Figure 2-1; point group D_3). The C_3 axis also passed through the centroid of the benzene solvate. Complex **4c** exhibited a C_2 axis coincident with the Fe-C1-O1 linkage, and *E,E,E*-**3a**·2(1,3,5-$C_6H_3(CH_3)_3$) was of analogous symmetry. In all complexes, the substituents along the P-Fe-P axes (CH_2/CO/CH_2) adopted staggered conformations (Figure 2-1, left). Crystallographic distances of greatest interest are summarized in Table 2-1. The bond lengths and angles about iron are close to those of other *trans* bis(phosphine) iron tricarbonyl complexes.[39]

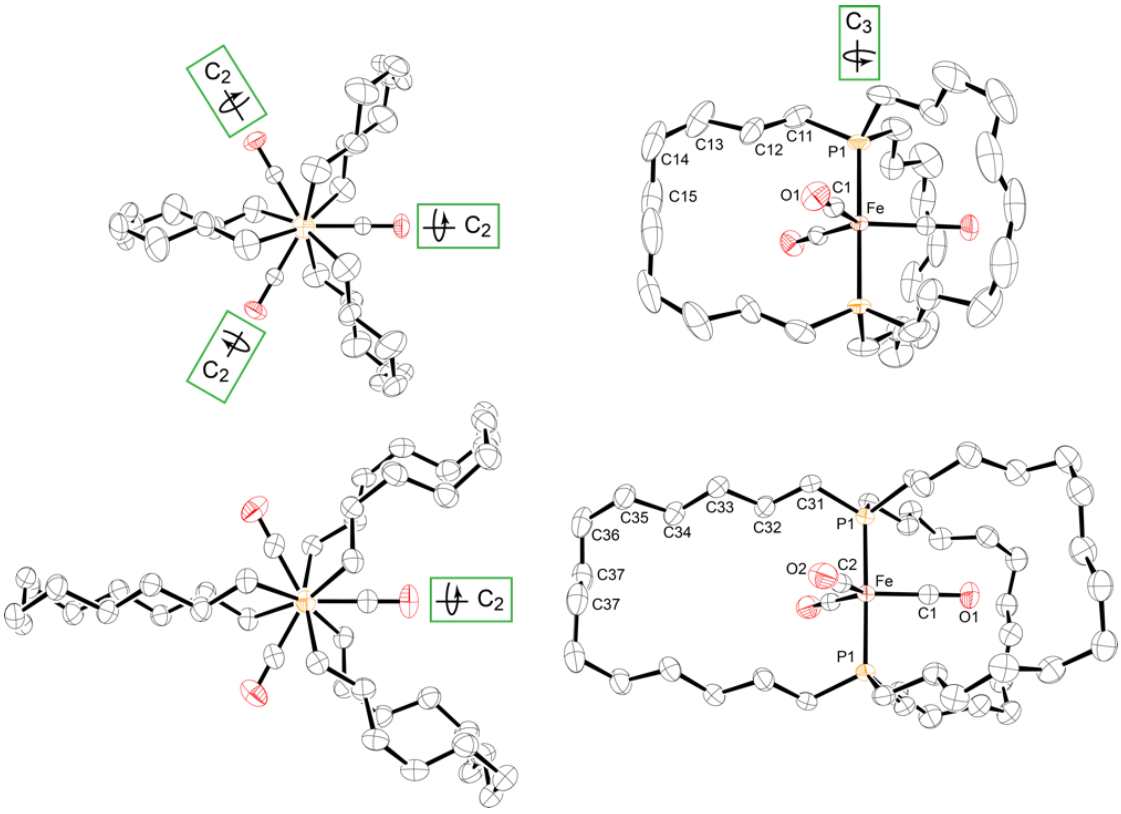

Figure 2-1. Molecular structures of *E,E,E*-**3a**·C_6H_6 (top) and **4c** (bottom) with solvate molecules and hydrogen atoms omitted and attendant symmetry axes depicted. *Crystal structures were obtained by Dr. Leyong Wang and Dr. Takinora Shima, but all figures and analyses were done by the author.

Table 2-1. Intramolecular and intermolecular distances involving rotator and stator atoms in gyroscope like complexes (Å), and selected bond and torsion angles (°).

Complex	*E,E,E*-**3a**·C_6H_6	*E,E,E*-**3a**·2(1,3,5-$C_6H_3(CH_3)_3$)	**4c**
Fe-P[a]	2.190	2.202	2.206
FeCO[a]	2.929	2.928	2.927
radius of rotator[b]	4.45	4.45	4.45
Fe-C_a[c]	5.34	5.32	7.46
Fe-C'_a[c]	5.34	5.33	6.64
Fe-C_b[c]	5.34	5.33	6.64
Fe-C'_b[c]	5.34	5.32	7.46
Fe-C_c[c]	5.35	5.31	7.86
Fe-C'_c[c]	5.35	5.31	7.86
Fe-C_{distal}–vdW[d]	3.64	3.61	4.94
Fe-$C_{distal'}$–vdW[e]	3.65	3.63	6.16
Fe-$C_{neighbor}$[f]	5.87	6.10[g]	6.04
Fe-$C_{neighbor}$–vdW[h]	4.17	4.40[g]	4.34
∠ P-Fe-P	180.0	179.8	178.9
P(**C**H_2)$_3$/P(**C**H_2)$_3$[i]	5.94	5.94	6.00
C$_a$P-Fe-P**C**$_a$[j]	6.02	6.06	6.13
C$_b$P-Fe-P**C**$_b$	6.02	6.06	6.13
C$_c$P-Fe-P**C**$_c$	6.02	6.09	6.02
C$_a$P-Fe-P**C**$_b$[k]	6.35	6.26	6.42
C$_b$P-Fe-P**C**$_c$	6.35	6.29	6.36
C$_c$P-Fe-P**C**$_a$	6.35	6.29	6.36
C_a-P-P-C_a[l]	34.3	44.4	38.0
C_b-P-P-C_b	34.3	44.4	38.0
C_c-P-P-C_c	34.5	44.5	38.3
C_a-P-P-C_b[m]	85.7	75.3	82.6
C_b-P-P-C_c	85.6	75.7	81.6
C_c-P-P-C_a	85.6	75.7	81.6

[a]The average distance within the molecule. [b]The FeCO distance plus the van der Waals radius of the oxygen atom (1.52 Å). [c]The distance from iron to the two remote carbon atoms of the three macrocycles (a, b, c; c always contains a C_2 axis) that are closest to the plane of the rotator (Fe-C_{distal}). [d]The shortest of the previous six distances, minus the van der Waals radius of the carbon atom (1.70 Å). [e]The longest of the previous six distances, minus the van der Waals radius of the carbon atom. [f]The distance from iron to the nearest carbon atom of a neighboring gyroscope like or solvate molecule. [g]This distance is for a solvate molecule; it is 0.58 Å further to the nearest carbon atom of another molecule of *E,E,E*-**3a**. [h]The previous entry minus the van der Waals radius of the carbon atom. [i]The distance between planes defined by the three carbon atoms attached to each phosphorus atom (see **VI** in Figure 2-15 below). [j]The distance between the P**C**H_2 carbon atoms of each macrocycle (see **IX** in Figure 2-15). [k]The distance between the P**C**H_2 carbon atoms that most closely flank each CO ligand (from different macrocycles; see **VII** and **VIII** in Figure 2-15). [l]The C-P-P-C torsion angle within the three macrocycles (a, b, c). [m]The C-P-P-C torsion angle involving carbon atoms that most closely flank each CO ligand (from different macrocycles).

Space filling representations of the preceding structures are given in Figure 2-2. It is evident that the $Fe(CO)_3$ moiety of *E,E,E*-**3a** is essentially in a "straight jacket", such that each carbonyl group can only oscillate between two of the *trans* spanning carbon chains, each part of a thirteen membered ring. For more quantitative analyses, the radius of the $Fe(CO)_3$ rotator must be considered. This can be calculated by taking the average iron-oxygen distance[40] and adding the van der Waals (vdW) radius of oxygen.[41,42] As outlined in Table 2-1, the resulting value, 4.45 Å, is compared with the distances between the iron atom and the C=C carbon atoms of the three *trans* spanning linkages (5.343-5.345 Å), which are the atoms closest to the plane of the rotator. The van der Waals radius of a carbon atom[41,42] is then subtracted from the shortest of the six values to give 3.64 Å (see "Fe-C_{distal}–vdW"). This can be taken as a "clearance" for the rotator, somewhat analogous to a "bridge height" on a highway. Obviously, it is impossible for a rotator of radius 4.45 Å to pass underneath a bridge height of 3.64 Å.

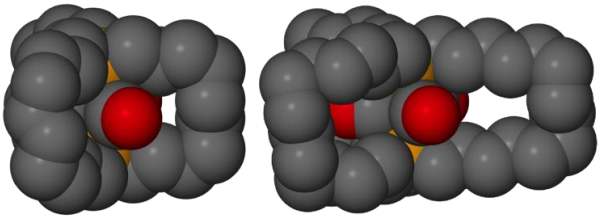

Figure 2-2. Space filling representations of *E,E,E*-**3a**·C_6H_6 (left) and **4c** (right) with solvate molecules and hydrogen atoms omitted.

In contrast to the situation with *E,E,E*-**3a**, space filling representations of **4c** suggest that there is enough room for the $Fe(CO)_3$ moiety to rotate within the three

$P(CH_2)_{14}P$ linkages, each part of a seventeen membered ring. Here, the carbon atoms closest to the plane of the rotator are methylene groups, and their distances from iron span a considerable range (6.64-7.86 Å) due to conformational differences in the macrocycles. When the van der Waals radius of a carbon atom is subtracted from these values, considerable "clearance" remains (4.45 Å vs. 4.94-6.10 Å). Usually, the shortest ("rotation limiting") distance is emphasized; however, other approaches to analyzing these data are possible.[43] Additional aspects of these crystal structures, including properties associated with the lattice, are analyzed below.

2.2.3 Substitutions and oxidations

The symmetries of *E*,*E*,*E*-**3a** and **4a**-**c**,**e** are too high to probe the rate of $Fe(CO)_3$ rotation by conventional solution phase NMR techniques. One of the three *trans* spanning linkages or carbonyl ligands must be differentiated.

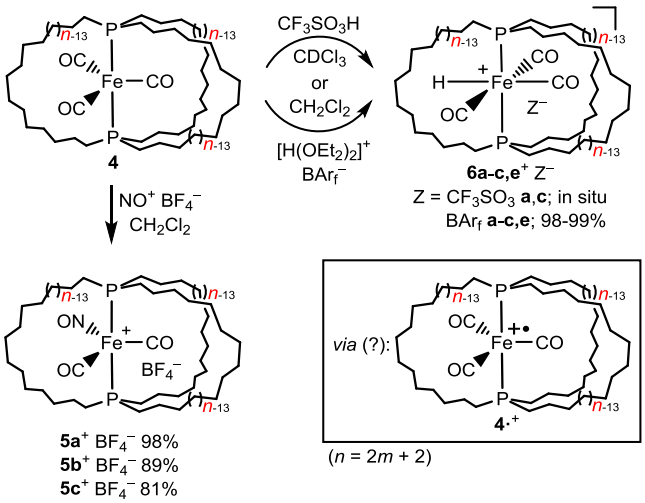

Scheme 2-3. Substitution and addition reactions involving gyroscope like complexes **4**.

It has been shown that reactions of the bis(phosphine) tricarbonyl complexes *trans*-$Fe(CO)_3(PR_3)_2$ and NO^+ Z^- (Z = BF_4, PF_6) give salts of the isoelectronic and isosteric dicarbonyl nitrosyl cations, *trans*-$[Fe(CO)_2(NO)(PR_3)_2]^+$ Z^-, in near quantitative yields.[44] As depicted in Scheme 2-3, reactions of **4a-c** and NO^+ BF_4^- gave the dicarbonyl nitrosyl complexes *trans*-$[Fe(CO)_2(NO)(P((CH_2)_n)_3P)]^+$ BF_4^- (**5a-c**$^+$ BF_4^-) in 81-98% yields after workup.

The IR spectra of **5a-c**$^+$ BF_4^- exhibited two ν_{CO} bands (2023-2030 cm^{-1} m, 1953-1965 cm^{-1} s) and a ν_{NO} band (1752-1764 cm^{-1} s). Ambient temperature ^{13}C NMR spectra of **5a**,**b**$^+$ BF_4^- showed two sets of P(***C***$H_2)_{n/2}$ signals with a ca. 2:1 area ratio, while the spectrum of **5c**$^+$ BF_4^- gave only one set. This indicates, in accord with the expectations from the crystal structures, that $Fe(CO)_2(NO)^+$ rotation is rapid on the

NMR time scale at room temperature for **5c**$^+$ BF_4^- (seventeen membered rings) but slow for **5a**,**b**$^+$ BF_4^- (thirteen and fifteen membered rings; two $(CH_2)_n$ chains occupy interstices between the CO/NO ligands, and the other that between two CO ligands). Importantly, the P***C***H_2CH_2***C***H_2 and ***C***O signals of **5c**$^+$ BF_4^- retain phosphorus couplings, excluding dissociation of the carbon monoxide ligand or phosphorus donor atoms in the mechanisms that render the bridges equivalent.

From a steric standpoint, it is curious that these carbonyl ligand substitutions are not inhibited by the three methylene bridges. In this context, note that NO^+ is a strong one electron oxidant,[45] and that seventeen valence electron metal complexes show enhanced substitution labilities.[46] Thus, cyclic voltammograms of *E,E,E*-**3a** and **4a-c** were recorded under standard conditions in CH_2Cl_2. As summarized in Table 2-2, all exhibited appreciably reversible one electron oxidations with i_c/i_a values of 0.89 to 0.95. For **4a** through **4c**, the E° values monotonically decreased from 0.406 to 0.314 V (vs. ferrocene at 0.46 V). This indicates thermodynamically more favorable oxidations, or phosphine ligands that are progressively more σ donating and/or less π accepting. Since under similar conditions the $NO^+/{\cdot}NO$ couple has a redox potential of 1.00 V,[45c] quantitative generation of the radical cations **4a-c**$^{\cdot+}$ (Scheme 2-3) is possible.

Table 2-2. Cyclic voltammetry data for iron tricarbonyl complexes.[a]

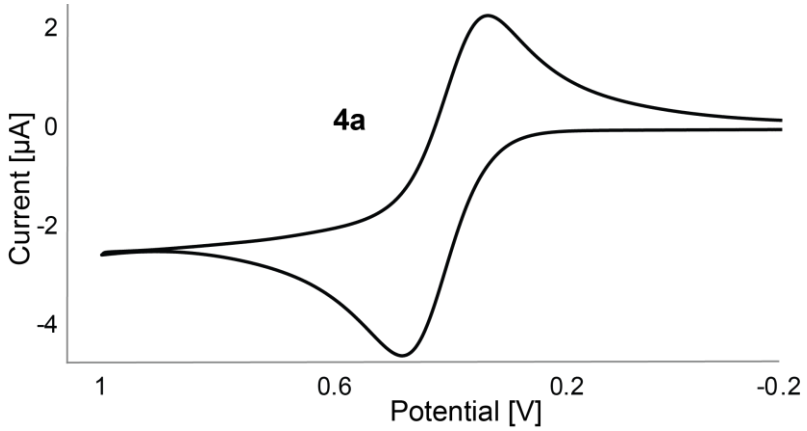

complex	$E_{p,a}$ [V]	$E_{p,c}$ [V]	$E°$ [V]	ΔE [mV]	i_c/i_a
E,*E*,*E*-**3a**	0.342	0.215	0.279	127	0.950
4a	0.477	0.335	0.406	142	0.918
4b	0.438	0.209	0.324	229	0.887
4c	0.461	0.166	0.314	295	0.921

[a]Conditions: 0.0010 M in 0.10 M Bu_4N^+ PF_6^-/CH_2Cl_2, 22 °C ± 1 °C; Pt working and auxiliary electrodes, Ag/AgCl pseudoreference; scan rate, 200 mV/s (data were similar at 100 and 150 mV/s); ferrocene = 0.46 V. All scans were continued to –1.0 V but no additional features were observed.

2.2.4 Protonations

Additional derivatives of lower symmetry were sought. Iron complexes of the formula *trans*-$Fe(CO)_3(PR_3)_2$ have been protonated by a variety of strong acids (HZ), affording octahedral cationic hydride complexes *mer*,*trans*-$[Fe(CO)_3(H)(PR_3)_2]^+$ Z^-.[47] As shown in Schemes 2-3 and 2-4, **4a**,**c** and *E*,*E*,*E*-**3a** were combined with CF_3SO_3H in $CDCl_3$ in NMR tubes. The hydride complexes *mer*,*trans*-$[Fe(CO)_3(H)(P((CH_2)_n)_3P)]$ $CF_3SO_3^-$ (**6a**,**c**$^+$ $CF_3SO_3^-$) and *E*,*E*,*E*-*mer*,*trans*-$[Fe(CO)_3(H)(P((CH_2)_4CH{=}CH(CH_2)_4)_3P)]^+$ $CF_3SO_3^-$ (*E*,*E*,*E*-**7a**$^+$ $CF_3SO_3^-$) formed in

quantitative yields, as evidenced by diagnostic ^{1}H NMR signals (–9.41 to –9.46 ppm, t, $^{2}J_{HP}$ = 21.4 to 29.4 Hz). However, workups of these triflate salts did not give solid products.

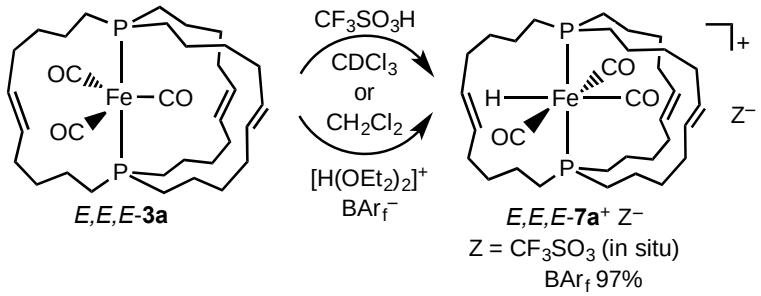

Scheme 2-4. Protonation of *E,E,E*-**3a**.

Thus, larger scale reactions were conducted with **4a**-**c**,**e** or *E,E,E*-**3a** and the protic oxonium salt $[H(OEt_2)_2]^+$ BAr_f^- (BAr_f^- = $B(3,5\text{-}C_6H_3(CF_3)_2)_4^-$).[48] Workups gave the hydride complexes **6a**-**c**,**e**$^+$ BAr_f^- and *E,E,E*-**7a**$^+$ BAr_f^- in 97-99% yields as powders or gums. Interestingly, the $^{2}J_{HP}$ values associated with the Fe***H*** ^{1}H NMR signals increased with macrocycle size (22.1-22.7, 27.0, 30.2, 32.2 Hz). As seen for **4a**-**c**,**e**, the ^{31}P NMR signals of **6a**-**c**,**e**$^+$ BAr_f^- shifted upfield as the ring sizes increased (Δppm ca. 17). In accord with literature precedent,[47] three IR ν_{CO} bands were observed, with the intensities decreasing with increasing frequency.[49] All bands were at higher frequencies than those of the neutral precursors.

The ambient temperature ^{13}C NMR spectra of **6a**$^+$ Z^- (Z = CF_3SO_3, BAr_f) and **7a**$^+$ $CF_3SO_3^-$, which have thirteen membered rings, exhibited two sets of P(***C***$H_2)_4$***C***

signals (all 2:1). This indicates, analogously to the case with the nitrosyl complex **5a**$^+$ BF_4^-, that $Fe(CO)_3(H)^+$ rotation is slow on the NMR time scale. The complexes **6b**$^+$ BAr_f^- and **6c**$^+$ Z^-, which have fifteen or seventeen membered rings, showed only a single set of ***C***H_2 signals, suggesting rapid rotation. Importantly, the hydride ^{1}H NMR signals retained phosphorus couplings (t, $^2J_{HP}$ = 28-29 Hz), indicating that the hydride and phosphorus donor atoms remain bound during the process that renders the bridges equivalent. Similarly, the CO signals retained phosphorus couplings (t, $^2J_{CP}$ = 15-20 Hz).

2.2.5 Lattice analyses

The relationships between molecular rotors in crystal lattices are of interest from a variety of standpoints. In the case of **4c**, the molecules pack in well-defined layers with all P-Fe-P axes parallel, as shown in Figure 2-3 (top). Between adjacent and all subsequent layers, the P-Fe-P axes are offset. Within a layer, the molecules exhibit two orientations, as shown in Figure 2-3 (bottom). One carbonyl oxygen atom of each rotator "points" at the "middle" or "innermost" CH_2CH_2 linkage of a seventeen membered ring of an adjacent molecule. The other two carbonyl oxygen atoms are directed more towards the centers of seventeen membered rings of adjacent molecules.

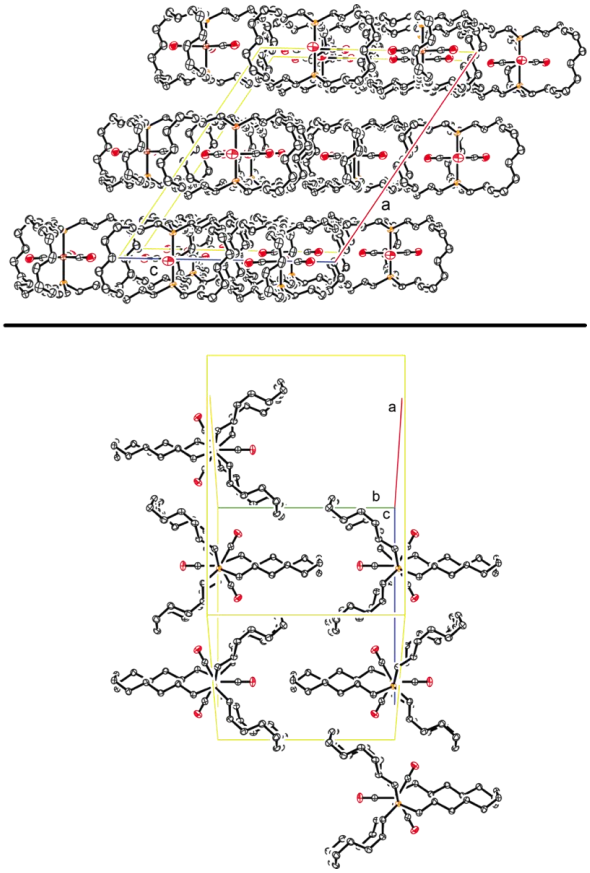

Figure 2-3. The crystal lattice of 4c as viewed along (top) and perpendicular (bottom) to the b axis; Fe = ●; O = ●.

As shown in Figure 2-4, the solvate *E*,*E*,*E*-**3a**·C_6H_6 packs in stacks in which the benzene molecules are sandwiched between the P-Fe-P axes. Within each stack, the rotators and stators of adjacent molecules are antiparallel. The individual molecules in adjacent stacks are offset, with the P-Fe-P units somewhat higher or lower (Figure 4). Hence, there is no layering as observed with **4c**. However, all of the P-Fe-P axes remain parallel. The lattice of *E*,*E*,*E*-**3a**·2(1,3,5-$C_6H_3(CH_3)_3$), depicted in Figure 2-5, is somewhat more complex. The mesitylene solvent molecules are π stacked in pairs

(vertical separation 3.9 Å), and do not sandwich individual iron complexes as in *E*,*E*,*E*-**3a**·C_6H_6.

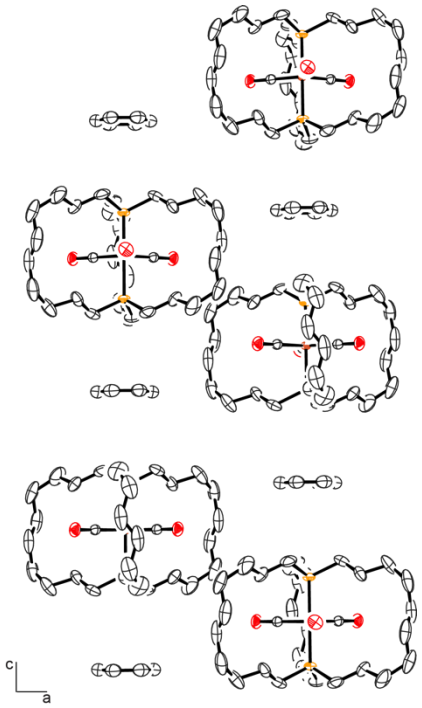

Figure 2-4. The crystal lattice of *E*,*E*,*E*-**3a**·C_6H_6 as viewed along the b axis.

An important issue regarding the viabilities of such crystalline iron complexes as molecular gyroscopes involves the distances of neighboring molecules from the rotators. Of particular interest are cases where the distances from the iron atom of one molecule to the nearest non-hydrogen atoms of neighboring molecules (adjusted for the van der Waals radii of the nearest atoms) are *greater* than the radius of the rotator. These would be the most promising candidates for rotation in the solid state. Relevant data, derived from the crystal structures, are presented in Table 2-1 (see "Fe-$C_{neighbor}$–vdW").

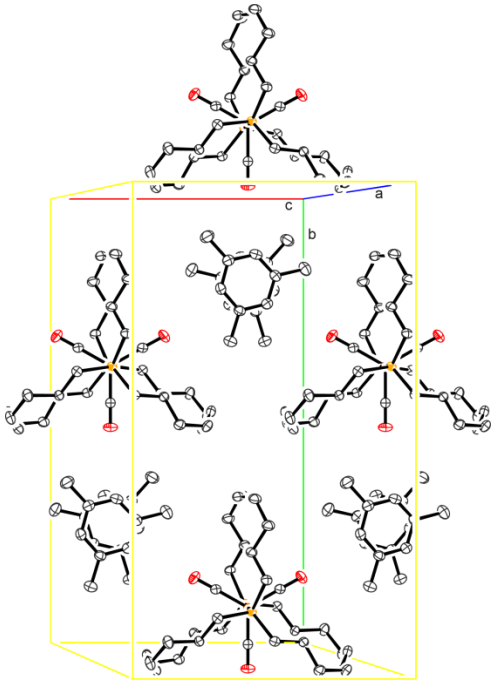

Figure 2-5. Packing in the crystal lattice of *E*,*E*,*E*-**3a**·2(1,3,5-$C_6H_3(CH_3)_3$) as viewed along the P-Fe-P bond.

Importantly, the distances are quite close in **4c** (4.34 Å vs. 4.45 Å rotator radius). However, as shown in Figure 2-6, this atom is considerably removed from the plane of the rotator. The next nearest atom, which is only slightly removed from the rotator plane, allows for more clearance (4.53 Å after vdW correction). The comparisons are similarly auspicious for the solvates of *E*,*E*,*E*-**3a**, but the rotators therein are constrained by the shorter $P(CH_2)_4CH{=}CH(CH_2)_4P$ bridges (see "Fe-C_{distal}–vdW").

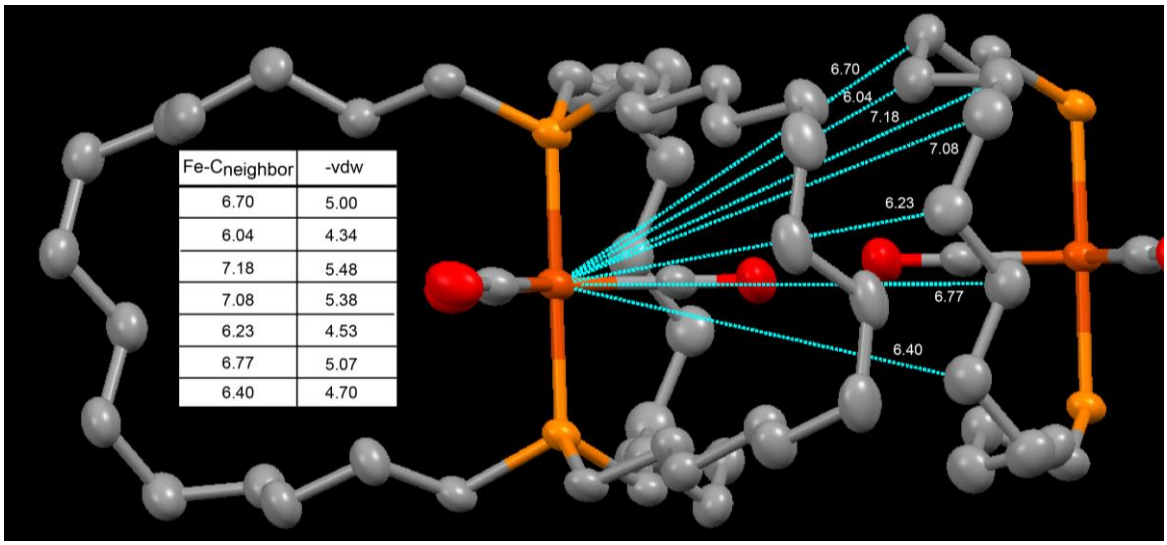

Figure 2-6. Distances from the iron atom of crystalline **4c** to the nearest atoms of a neighboring molecule.

2.2.6 Variable temperature and solid state NMR experiments

As shown in Figure 2-7 (left), ^{13}C NMR spectra of **5c**$^{+}$ BF_4^{-} were recorded in $CDFCl_2$[50] at progressively lower temperatures (–10 to –80 °C). The chemical shifts of the P***C***H_2***C***H_2***C***H_2 carbon atoms remained roughly constant (Δδ 0.3-0.6 ppm), while some of the others varied much more (Δδ 1.3-2.1 ppm). This suggests that the methylene groups that are not anchored as closely to the phosphorus atoms can sample conformations with greater chemical shift differences, the differential entropies of which in turn lead to more pronounced temperature dependencies. In any event, many peaks broadened, and the PCH_2***C***H_2 signal (green) eventually decoalesced in a reasonably well defined manner (two peaks, ca. 2:1 area ratio). The line shapes were simulated using gNMR (red)[51] and the rate constants extrapolated at each temperature.

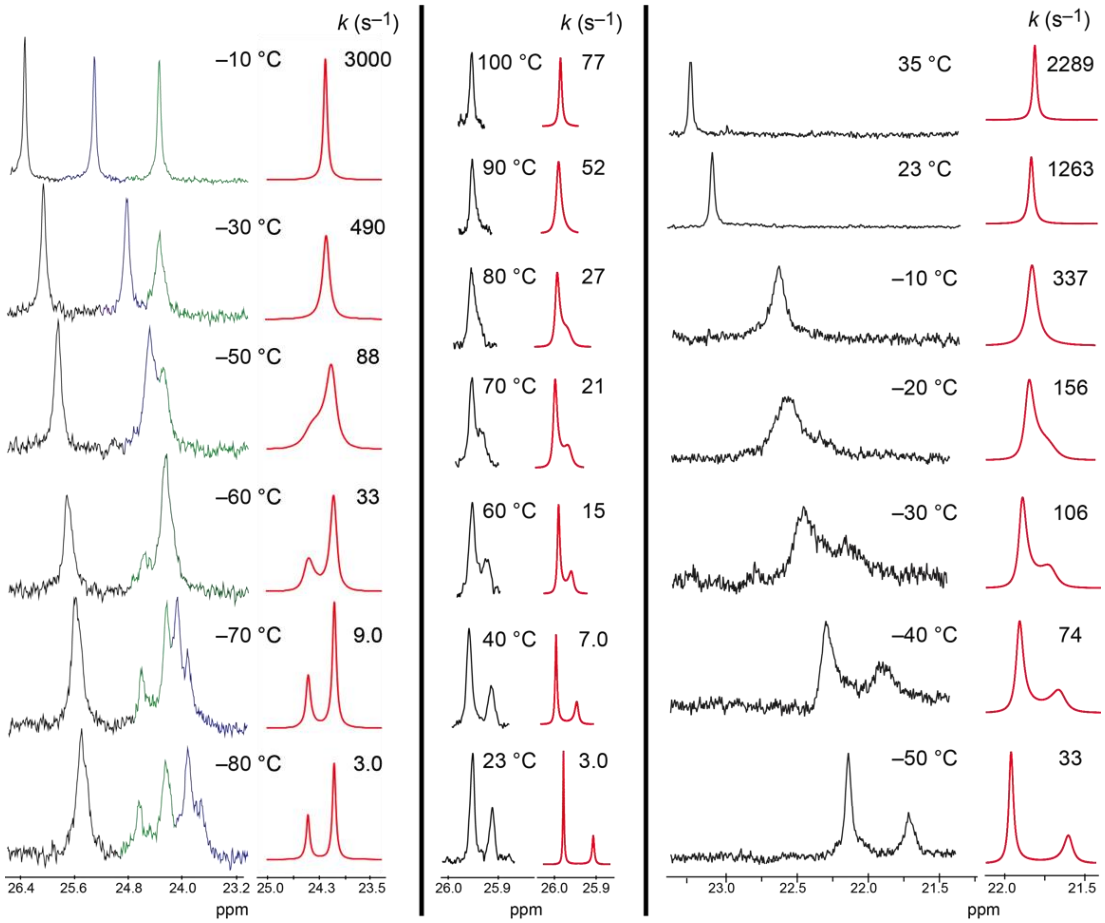

Figure 2-7. Partial ^{13}C NMR spectra of **5c**$^{+}$ BF_4^- ($CDFCl_2$, left), **5b**$^{+}$ BF_4^- (C_6D_5Cl, middle), and **6b**$^{+}$ BAr_f^- (CD_2Cl_2, right) as a function of temperature. Each spectrum is paired with simulated line shapes for the signals of interest (red).

An Eyring plot using these rate constants (Figure 2-8) gave $\Delta H^{\ddagger}$ and $\Delta S^{\ddagger}$ values of 9.5 kcal/mol and –6.5 eu for the process rendering the CH_2 signals equivalent. This was attributed to rotation of the $Fe(CO)_2(NO)^+$ moiety, as detailed further in the discussion section.

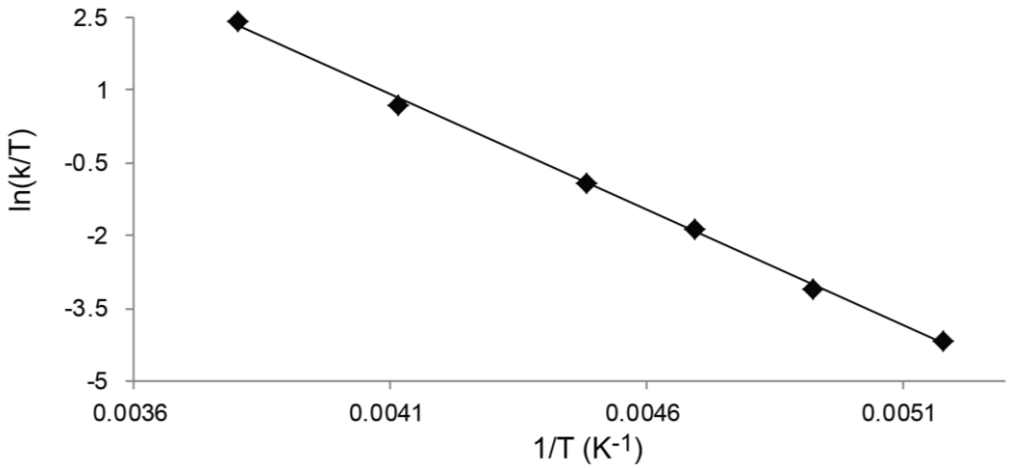

Figure 2-8. Eyring plot involving rate constants for the process that renders the $(CH_2)_{14}$ bridges of **5c**$^+$ BF_4^- equivalent ($Fe(CO)_2(NO)^+$ rotation by 240°).

Next, ^{13}C NMR spectra of **5b**$^+$ BF_4^-, which features smaller fifteen membered rings, were recorded in C_6D_5Cl at progressively higher temperatures (23 to 100 °C). All of the ***C***H_2 signals broadened, and as depicted in Figure 2-7 (middle), two (ca. 2:1 area ratio; $P(CH_2)_{n'}$***C***H_2, $n' \geq 3$) exhibited a well defined coalescence at 80 °C. The data were treated as for **5c**$^+$ BF_4^-, with an Eyring plot (Figure 2-9) giving $\Delta H^{\ddagger}$ and $\Delta S^{\ddagger}$ values of 8.3 kcal/mol and –28.4 eu. This corresponds to a $\Delta G^{\ddagger}_{298K}$ value of 16.7 kcal/mol, which as expected is a considerably higher barrier than that of **5c**$^+$ BF_4^- (11.4 kcal/mol). Additional aspects of the activation parameters are analyzed in the discussion section.

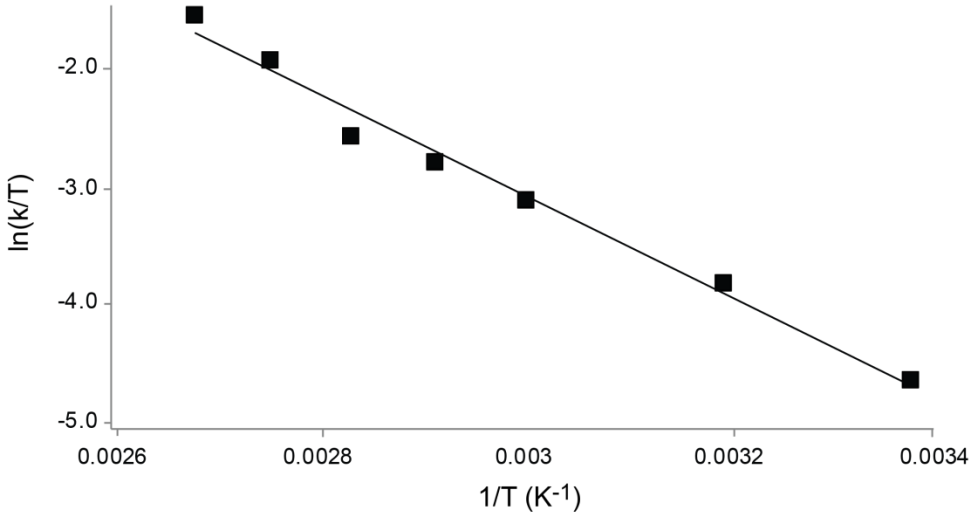

Figure 2-9. Eyring plot involving rate constants for the process that renders the $(CH_2)_{14}$ bridges of **5b**$^+$ BF_4^- equivalent $(Fe(CO)_2(NO)^+$ rotation by 240°).

Finally, ^{13}C NMR spectra of **6b**$^+$ BAr_f^-, which features a tetrasubstituted rotator, were recorded in CD_2Cl_2 at progressively lower temperatures (35 to –50 °C). As depicted in Figure 2-7 (right), the $PCH_2\boldsymbol{C}H_2$ signal broadened and then decoalesced into two peaks (ca. 2:1 area ratio). A similar treatment of these data (Figure 2-10) gave $\Delta H^{\ddagger}$ and $\Delta S^{\ddagger}$ values of 6.1 kcal/mol and –23.5 eu for the process that renders the CH_2 signals equivalent (discussion section). This corresponds to a $\Delta G^{\ddagger}_{298K}$ value of 13.0 kcal/mol.

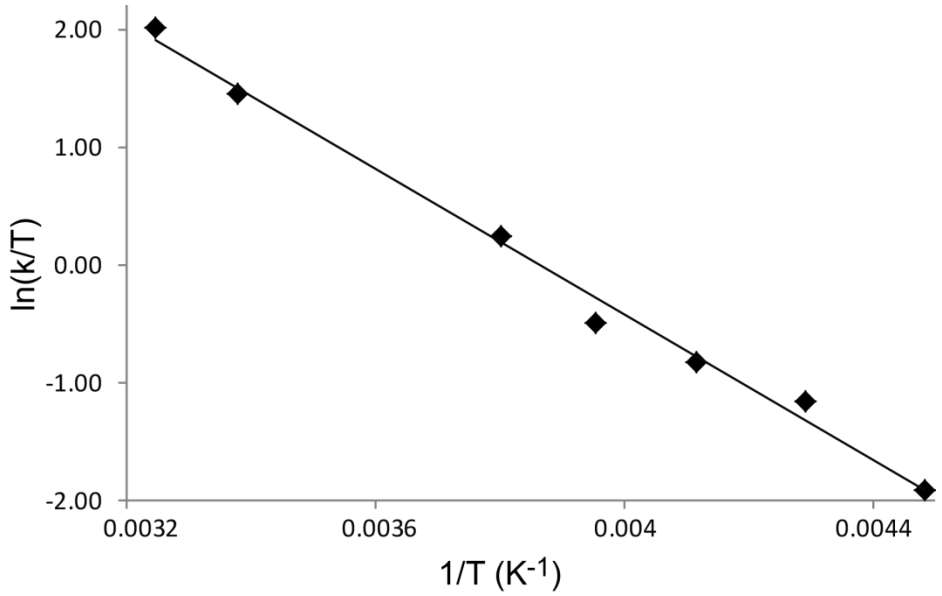

Figure 2-10. Eyring plot involving rate constants for the process that renders the $(CH_2)_{14}$ bridges of **6b**$^+$ BAr_f^-equivalent $(Fe(CO)_3(H)^+$ rotation by 330°).

Rotational barriers were probed in the solid state[52] using polycrystalline **4c**. A ^{13}C CP/ MAS (cross polarization, magic angle spinning) NMR spectrum was recorded at ambient temperature (25 °C), as depicted in Figure 2-11. As expected, the $(CH_2)_{14}$ signals overlapped, and did not show a large Chemical Shift Anisotropy (CSA)[53,54] when the rotational speed was 7 kHz. However, the CO ^{13}C signal, which was visible at 214.4 ppm, exhibited the characteristic large carbonyl CSA[53-55] with the parameters[56] δ_{11} = 367.2, δ_{22} = 352.1, and δ_{33} = –76.2 ppm, and a span[54] δ_{11} - δ_{33} of 443.4 ppm.[56] The residual linewidth of the CO signal was only 76 Hz, and the line was highly symmetric with no indication of a signal splitting or shoulder. In view of the unit cell of **4c** (Figure 2-3), multiple isotropic signals, representing the different orientations of the CO groups with respect to the external magnetic field, would have been expected for a

static $Fe(CO)_3$ moiety. Since the ^{13}C CP/MAS spectrum exhibited only one narrow line for all the CO ligands, it can be concluded that the $Fe(CO)_3$ unit is rotating rapidly about the P-Fe-P axis within the $(CH_2)_{14}$ linkages. The shape and linewidth of the isotropic line of the CO signal did not change upon heating or cooling the sample from 95 °C to –60 °C. Hence, rotation is rapid over the entire temperature range.

In contrast, the CO signal of polycrystalline **4a** exhibited a much broader isotropic line with a width of 231 Hz. The unsymmetric shape of the signal indicates the presence of several slightly different isotropic lines which speaks for a static $Fe(CO)_3$ unit in the solid state.

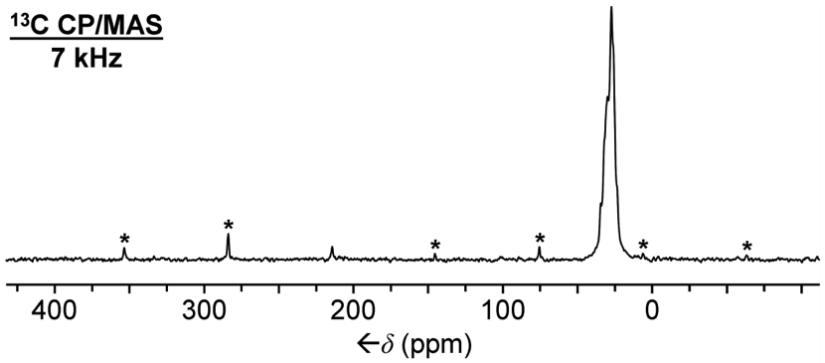

Figure 2-11. ^{13}C CP/MAS NMR spectrum of polycrystalline **4c**; asterisks denote rotational sidebands of the CO signal.

As shown in Figure 2-12, ^{31}P CP/MAS NMR spectra of polycrystalline **4c** were recorded under static conditions (wideline spectrum, bottom), and at 4 and 7 kHz rotational frequencies. A signal with an isotropic chemical shift of 72.1 ppm exhibited a CSA characteristic of gyroscope like molecules with $Fe(CO)_3$ rotators[57] with the

parameters[56] δ_{11} = 130.4, δ_{22} = 117.4, and δ_{33} = –31.4 ppm, and a span[54] δ_{11} - δ_{33} of 161.8 ppm.[56] The residual linewidth of the isotropic signal was only 141 Hz; however, the resonance appeared slightly unsymmetric. A negative linebroadening factor revealed the presence of two overlapping signals with nearly identical chemical shifts. This is in accord with the crystal lattice of **4c** (Figure 2-3), which shows that there are two magnetically inequivalent phosphorus nuclei in the unit cell.

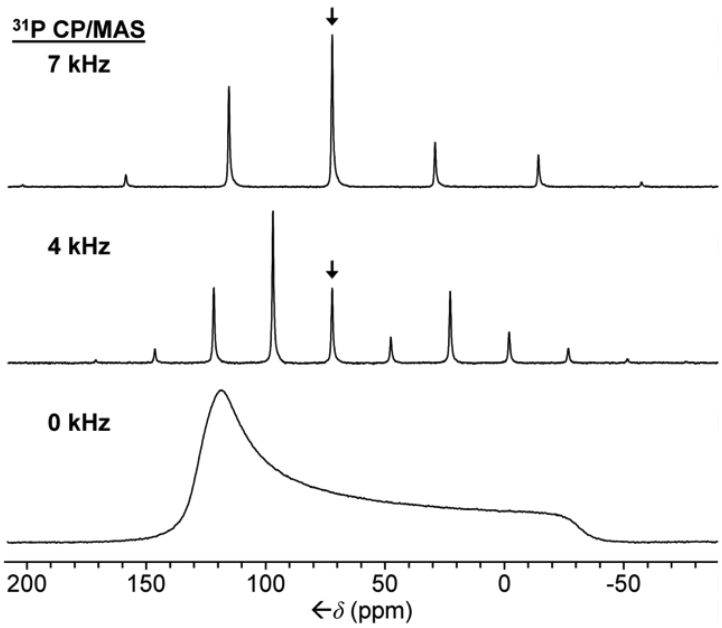

Figure 2-12. ^{31}P CP/MAS NMR spectra of **4c** at the indicated rotational speeds; the arrows denote the isotropic lines.

2.3 Discussion

2.3.1 Syntheses

Scheme 2-2 establishes that trigonal bipyramidal gyroscope like complexes with iron tricarbonyl rotators are easily accessed via three fold intramolecular ring closing metatheses involving *trans* phosphine ligands of the formula $P((CH_2)_mCH=CH_2)_3$ with $m \geq 4$. The overall yields for the metathesis/hydrogenation sequences range from 47 to 64%. These are distinctly higher than for educts with square planar or octahedral coordination geometries,[22,25] which require values of $m \geq 6$ and are presumed to give higher fractions of oligomeric or polymeric products. Furthermore, with some square planar complexes,[20] minor amounts of byproducts with the connectivity **III** (Scheme 2-1) can be observed. For a few of the octahedral complexes, these dominate.[22]

These differences are likely associated with the conformational energy minima of the precursors. For the tricarbonyl complexes **2a**-**c**,**e**, one would expect the $(CH_2)_mCH=CH_2$ substituents on each phosphorus atom to be staggered with respect to the CO ligands on iron, as shown in **IV** in Figure 2-13. This preorganizes the educt for *intra*molecular and *inter*ligand metathesis. Once one macrocycle has been generated, the reduced P-Fe-P conformational mobility should further favor *intra*molecular over *inter*molecular metathesis. However, there is no marked "cooperativity", as each successive macrocyclization can be observed by ^{31}P NMR (see above).

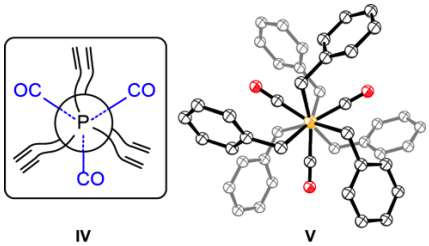

IV V

Figure 2-13. Newman type projection (**IV**) showing the conformational "preorganization" for three fold *intra*molecular and *inter*ligand C=C metathesis in **2a-c**,**e**, and a crystal structure of a bis(tribenzylphosphine) analog (**V**).

We were unable to crystallize any of the complexes corresponding to **IV**. However, the crystal structure of a bis(tribenzylphosphine) analog, depicted in Figure 2-13 (**V**), has been reported.[39] This clearly exhibits staggered relationships between the phosphorus and iron substituents. These orientations are largely retained in the crystalline gyroscope like complexes (Figure 2-1). In any case, square planar and octahedral educts do not provide analogous conformational templates, as illustrated elsewhere.[20b,22a] Thus, yields for the metathesis/hydrogenation sequences are lower, and products with thirteen and fifteen membered rings cannot be accessed at all. Furthermore, the greater number of rotator substituents in the octahedral precursors can impede *inter*ligand metathesis, increasing the relative amounts of byproducts **III**.[22]

In general, internal olefins are much less reactive towards chain carrying ruthenium alkylidene catalysts than terminal olefins.[9] For this and other reasons, we consider the ring closing metatheses of **2a-c**,**e** to be under kinetic control. Insightful recent studies have described methods for minimizing oligomeric byproducts.[59] Thus, it may prove possible to further increase the yields in Scheme 2-2. Indeed, in a previous

paper involving *di*macrocyclic complexes with P-Pt-P linkages, we were able to vary the ratios of monomeric/oligomeric products by carrying out metatheses at different concentrations using Grubbs' second generation catalyst.[35]

As noted above, only in the case of *E,E,E*-**3a** was the ring closing metathesis highly stereoselective. Interestingly, ring closing metatheses of other complexes with *trans* $H_2C{=}CH(CH_2)_4P\text{-}M\text{-}P(CH_2)_4CH{=}CH_2$ linkages give exclusively *E* C=C isomers, at least within the limits of detection.[15,35] In this context, note that an *E* CC=CC segment spans a carbon-carbon distance of 3.9 Å, whereas a *Z* segment extends only 3.15 Å.[60] Hence, despite the higher strain energy associated with *E* CC=CC moieties in smaller carbocyclic rings, this stereochemistry provides more "rope" for bridging a fixed distance, and may be the more stable isomer in the absence of transannular interactions or other destabilizing features. Indeed, for an olefinic fourteen membered lactone synthesized using Grubbs' second generation catalyst, a 12:1 *E*/*Z* ratio has been reported, close to the 19:1 equilibrium value derived computationally.[61]

2.3.2 Reactions of gyroscope like complexes

The cage like diphosphine ligands in *E,E,E*-**3a** and **4a-c**,**e** would not be expected to significantly hinder the protonations in Schemes 2-3 and 2-4. However, the substitution of a CO ligand by the cation of NO^+ BF_4^- is another matter. As noted above, NO^+ is a strong one electron oxidant,[45] and the generation of the seventeen valence electron radical cations $\mathbf{4}^{\cdot+}$ BF_4^- (Scheme 2-3) is thermodynamically downhill.

Although such species are substitution labile,[46] we suggest it is more probable – at least for the larger ring sizes – that the resulting ·NO radical covalently binds to give the eighteen valence electron octahedral species $\mathbf{8}^{+}$ BF_4^{-} shown in Scheme 2-5. The nitrogen lone pair associated with the bent nitrosyl ligand would then serve as an internal nucleophile for displacing a carbonyl ligand.

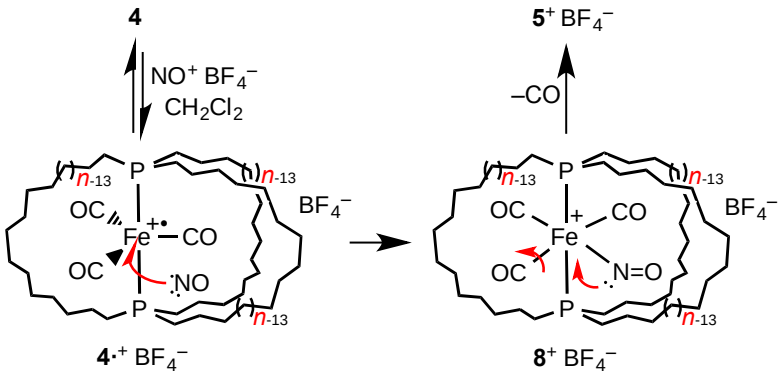

Scheme 2-5. One possible mechanism for the substitution of CO by NO^{+} in **4**.

Given the extensive chemistry of iron carbonyl complexes, there are many possible reactions that could be carried out with the products in Schemes 2-4. Some negative results not treated in the results section are briefly summarized here. First, attempts to replace one or more of the CO ligands in *E*,*E*,*E*-**3a** by the ligand-based C=C linkages were unsuccessful, either under photochemical conditions (450 W ultraviolet lamp through quartz; sun lamp through Pyrex) or using chemical agents such as Me_3N^{+}-O^{-}.[47] When the reaction of **4c** and Me_3N^{+}-O^{-} was monitored by ^{31}P NMR, a new signal

could be detected, but subsequent additions of potential ligands did not give tractable products.

Well defined reactions of methyl iodide and *trans*-$Fe(CO)_3(PMe_3)_2$ have been reported,[63] but **4c** gave no conversion under comparable conditions over a ten day period. Although MeLi readily adds to $Fe(CO)_5$ in ether at –60 °C,[64] no reaction was detected when **4c** and MeLi were combined in THF-d_8 at 66 °C, as assayed by NMR (^{31}P, ^{1}H, ^{13}C; 1-24 h). The cationic complex $\mathbf{5c}^+$ BF_4^- should be more electrophilic. However, no reaction took place when a CD_2Cl_2 solution of $\mathbf{5c}^+$ BF_4^- was treated with the strong hydride donor K(*sec*-Bu)$_3$BH or the formyl complex (η^5-C_5H_5)Re(PPh_3)(NO)(CHO).[65,66] Since analogous results were obtained with *trans*-$[Fe(CO)_2(NO)(P((CH_2)_mCH{=}CH_2)_3)_2]^+$ BF_4^-,[32] which lacks the cage like diphosphine ligand, this cannot be attributed to a steric effect.

2.3.3 Rotator and stator dimensions

Figure 2-14 provides a graphical representation of some of the metrical data in Table 2-1. The radii of the $Fe(CO)_3$ rotators (4.45 Å) are easily calculated as described above.[25] However, the interior dimensions of the stator are more challenging to define. As is evident from the many crystallographically characterized gyroscope like complexes,[20,24,25,22a] and **4c** in this section, the macrocycles can sample many conformations and do not necessarily extend to an equal extent from the metal center.

Thus, per Figure 2-14, we consider the two carbon atoms in <u>each</u> *trans* spanning linkage that lie nearest to the plane of the rotator.

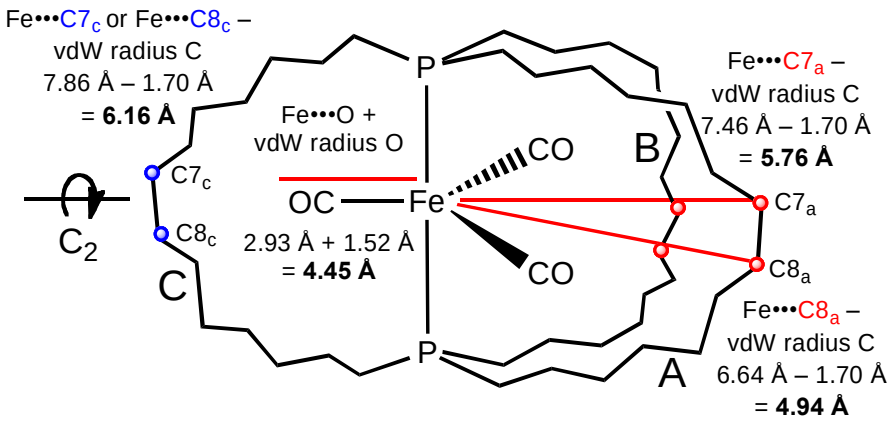

Figure 2-14. Spatial relationships involving the iron atom, rotator, and $(CH_2)_{14}$ bridges in **4c**; see text and Table 2-1 (vdW = van der Waals; A/B/C refer to the macrocycle labels in Table 2-1).

For the complexes in this section, these are the "innermost" CH_2CH_2 or CH=CH segments. In contrast, in other complexes the macrocycle conformations are not necessarily symmetric with respect to the plane of the rotator, such that the "in plane" CH_2CH_2 segments can become biased towards one phosphorus terminus.[20,24,25,22a] In any event, we commonly focus on the shortest of the six iron-carbon distances. After subtraction of the van der Waals radius of carbon, this gives the most conservative estimate of the void space or "horizontal clearance". However, it could be argued that average values would provide better comparisons between complexes in solution.

Empirically, we find that when the radius of the rotator is less than or approximately equal to the horizontal clearance, rotation is rapid in solution at room

temperature on the NMR time scale. We note in passing that this treatment neglects the hydrogen atoms associated with the *trans* spanning linkages. However, it is often found that the sizes of hydrogen atoms are negligible when evaluating the feasibility of dynamic processes from space filling models.

Importantly, the void space within the diphosphine cage is three dimensional, and the "vertical" or "top/bottom" clearance also affects rotational barriers. Figure 2-15 focuses on the spatial relationship between the CO ligands and the C-P-Fe-P-C linkages. One obvious reference point is the distance between the planes defined by the three carbon atoms attached to each phosphorus atom, which are constrained to be parallel by virtue of the C_2 symmetry axes noted above (5.94-6.00 Å per Table 2-1 and **VI** in Figure 2-15). Another would be the distances between the P***C***H_2 carbon atoms within each macrocycle – i.e., those with the smallest C-P--P-C torsion angles (see **IX** in Figure 2-15). As would be expected from the diagonal relationships of the atoms with respect to the P-Fe-P vectors, the distances are slightly greater than the plane-plane separations, and in **4c** range from 6.02 Å to 6.13 Å (Table 2-1). From either reference point, subtraction of the van der Waals radii of two carbon atoms gives a vertical clearance (2.62 Å to 2.73 Å for **4c**). The distances between the P***C***H_2 carbon atoms that most closely flank each CO ligand in the crystal can also be considered (**VII** and **VIII** in Figure 2-15). Since these involve different macrocycles, they are somewhat greater (6.36-6.42 Å for **4c**).

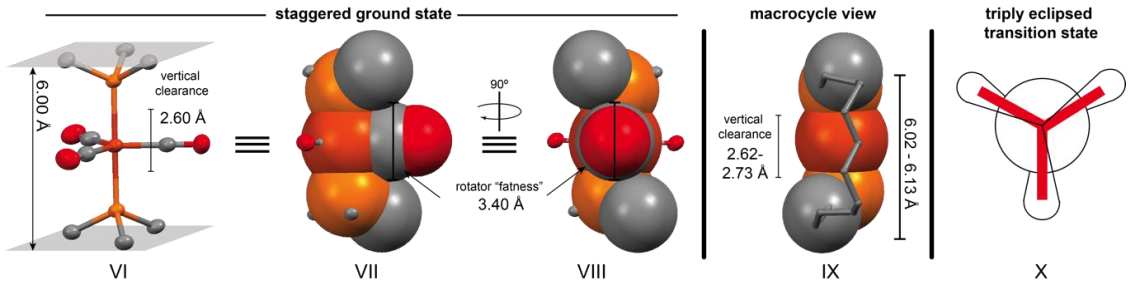

Figure 2-15. Steric relationships between atoms in **4c** relevant to "vertical clearance" of the rotator. **VI**: separation of planes defined by the P*C*H$_2$ carbon atoms. **VII** and **VIII**: as in **VI**, but with selected atoms at van der Waals radii (e.g., the P*C*H$_2$ carbon atoms that most closely flank a CO ligand, which are from different macrocycles). **IX**: relationship of the two P*C*H$_2$ carbon atoms within a macrocycle. **X**: Newman type projection of transition state in which all three CO ligands pass between P*C*H$_2$ carbon atoms belonging to the same macrocycle.

What counts now in the vertical dimension is not the radius of the rotator, but its "fatness", which is best approximated by the van der Waals diameter of the ligating carbon, 3.40 Å. This is somewhat greater than the distance between the flanking P***C***H$_2$ carbon atoms in the crystal, minus their van der Waals radii (6.36-6.42 Å – 2(1.70 Å) or 2.96-3.02Å for **4c**; see **VII** and **VIII**). In the transition state **X**, the three CO ligands are positioned between P***C***H$_2$ carbon atoms of the type in **IX**, with narrower clearances (2.62-2.73 Å for **4c**). This squeeze can to some extent be ameliorated by concurrent conformational changes within the macrocycles. These would for example expand key torsion angles and/or increase rotator/stator clearances. Regardless, this analysis shows that there is the potential to significantly lower rotational barriers by increasing the distance between the metal and the bridgehead donor atoms that anchor the cage like ligand. Some opportunities are detailed below.

2.3.4 Rotational barriers

As represented by **X** in Figure 2-15, the transition state for rotator rotation in trigonal bipyramidal gyroscope like complexes entails a three fold eclipsing interaction. As illustrated in Figure 2-16 and elsewhere,[20b,22a] the corresponding transition states for octahedral or square planar gyroscope like complexes involve only a single eclipsing interaction. For this and other reasons, these barriers are much lower, as long as the ligands on the rotators have approximately the same sizes (CO ~ Cl ~ CH_3). Although activation parameters are not yet available, it has been possible to bound the barrier for $Rh(CO)_2I$ rotation as substantially greater than that of Rh(CO)(I).[24a]

The variable temperature NMR data in Figure 2-7 allow rotational barriers to be calculated for the dicarbonyl nitrosyl complexes **5b**,**c**$^+$ BF_4^-. The $\Delta G^{\ddagger}_{298K}$ values, 16.7 and 11.4 kcal/mol, respectively, exhibit the expected decrease with increased macrocycle size. The cations of these salts are viewed as isoelectronic and isosteric surrogates for the tricarbonyl complexes **4b**,**c**, which are presumed to have very similar barriers.

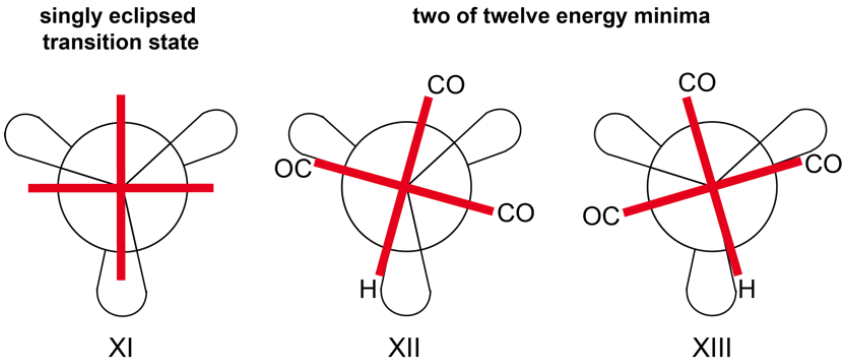

Figure 2-16. Selected rotator conformations in octahedral gyroscope like complexes such as **6b**$^+$ BAr_f^-.

The negative $\Delta S^{\ddagger}$ values (–28.4 and –6.5 eu) are consistent with the loss of entropy that would be anticipated from the three fold eclipsing interaction in **X** and correlated changes in the macrocycle conformations to alleviate the interactions diagrammed in Figure 2-15. However, the $\Delta H^{\ddagger}$ values counterintuitively increase with increased macrocycle size (8.3 and 9.5 kcal/mol). In this context, note that the $\Delta S^{\ddagger}$ values also increase (become less negative). This logically follows from the much higher degree of correlated conformational changes that would be required for the three CO ligands to pass through the smaller macrocycles in **5b**$^+$ BF_4^- as opposed to **5c**$^+$ BF_4^-. Thus, at least for this pair of complexes, there is appreciable enthalpy-entropy compensation.[67] One consequence is an isokinetic temperature of –217 °C (56 K), but under experimentally relevant conditions, $Fe(CO)_2(NO)^+$ rotation is always faster in **5c**$^+$ BF_4^-.

In order to render the signals of all three $P(CH_2)_n\boldsymbol{C}H_2$ carbon atoms of **5b**,**c**$^+$ BF_4^- equivalent, the $Fe(CO)_2(NO)^+$ moieties must rotate by 240° (all $\boldsymbol{C}H_2$ groups need to exchange between CO/NO and CO/CO environments). In the case of **5c**$^+$ BF_4^-, the rate constant for this process can be extrapolated from the Eyring plot (Figure 2-8) as 25,600 s^{-1} (Hz) at 25 °C. When this is scaled to 360°, it represents a rate equivalent to 1,000,000 rpm at room temperature. However, $Fe(CO)_2(NO)^+$ rotation is not unidirectional but Brownian, a topic further treated in the final section.

Solid-state NMR data can supply information on the rotational barriers of the more symmetric tricarbonyl complexes **4a**-**c**,**e**. Interestingly, since only a single symmetric CP/MAS CO ^{13}C NMR signal with a narrow linewidth is observed with crystalline **4c**, the barrier to $Fe(CO)_3$ rotation appears to be lower than that for $Fe(CO)_2(NO)^+$ rotation in **5c**$^+$ BF_4^- in solution. This is supported by the CP/MAS data for **4a**, which shows two overlapping CO signals. Thus, **4c** affords amphidynamic crystals, with the rotator able to navigate past atoms of neighboring molecules in the solid state and surmount the intramolecular van der Waals interactions diagrammed in Figure 2-15. A DSC analysis of **4c** revealed a melting exotherm (160 °C), but no other phase transitions down to –100 °C. In contrast, **4b**, which should have a higher barrier to $Fe(CO)_3$ rotation, exhibited a second phase transition at a lower temperature than the melting endotherm (–1 °C vs. 231 °C).

As noted above, the transition state for rotation of the rotator in analogous octahedral gyroscope like complexes features only a single eclipsing interaction, as shown in **XI** in Figure 2-16. Thus, it is not surprising that **6b**$^+$ BAr_f^- exhibits a lower rotational barrier than **5b**$^+$ BF_4^-, given the equal macrocycle sizes ($\Delta G^{\ddagger}_{298K}$ 13.0 vs. 16.7 kcal/mol). However, additional subtle points merit emphasis. For example, in view of the symmetry of **6b**$^+$ BAr_f^- (see representative rotamer **XII**), three sets of CH_2 signals would be expected (1:1:1) as opposed to the two observed (2:1). Several rhodium complexes behave similarly, all of which feature a single small ligand on the rotator that is able to rapidly pass through a macrocycle on the NMR time scale.[23,24] In the case of

6b^{+} BAr_f^{-}, the barrier for the hydride ligand passing through a macrocycle would be expected to be much lower than those for a CO ligand. Thus, the interconversion of the pseudomirror image rotamers **XII** and **XIII** could remain rapid at the low temperature limit in Figure 2-7, resulting in two sets of CH_2 signals. As more fully analyzed elsewhere,[22a,72] such complexes exhibit twelve maxima (and minima) as the rotator is rotated through 360°; in order for a CH_2 group to sample all environments, the rotator must traverse 330°.

In these contexts, the contributions of other research groups merit emphasis. First, Setaka has utilized three fold intramolecular ring closing metatheses to access a number of systems that feature an arene rotator with two silicon substituents connected by three polymethylene bridges.[13] Representative examples are shown in Scheme 2-6. He has determined a variety of rotational barriers by NMR, both in solution (**XV-Bc**,**d** using variable temperature EXSY ^{13}C NMR spectra)[13a,d] and the solid state (**XV-Aa**,**c**,**e** using ^{2}H NMR spectra).[13c] Paralleling our observations, the solid-state barriers are quite low (E_a 6.6-9.0 kcal/mol), despite van der Waals interactions between the rotator and stator. Kono has also probed these barriers computationally.[68]

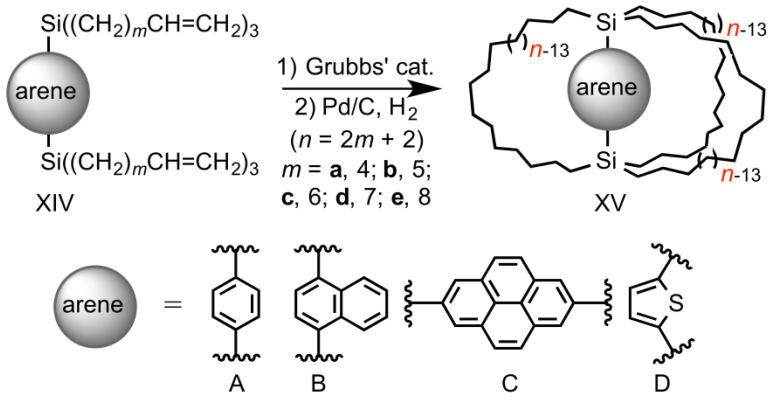

Scheme 2-6. Organosilicon gyroscope like compounds prepared by the Setaka group.

Garcia-Garibay has used other synthetic methods to access carbocyclic analogs of **XV**, and versions with ether containing polymethylene segments.[69] He has determined rotational barriers in the solid state for a variety of *p*-phenylene or diadamantane rotators suspended between two bulky (triarylmethyl)ethynyl or steroidal endgroups, using ^{2}H NMR and variable temperature ^{13}C CP/MAS NMR.[8a,c,70]

2.3.5 Towards molecular gyroscopes

With either macroscopic or molecular gyroscopes, the minimization of friction is an important operational consideration. Towards this end, the analyses presented above point to a number of ways that the stators in **4**, **5**$^{+}$ BF_4^{-}, and **6**$^{+}$ Z^{-} can be further optimized. Perhaps the most obvious would be to substitute the iron-phosphorus bonds by iron-arsenic or osmium-phosphorus bonds. Since these involve heavier elements, they should be 3-5% longer,[22a,71] leading to more "vertical" clearance for the rotator (Figure 2-15). Unfortunately, we have not yet been able to prepare osmium analogs of **5c**$^{+}$ BF_4^{-},

although analogs of **4c** are readily available.[22a] Arsenic analogs will be described in a forthcoming publication.[72] Another strategy, reminiscent of a theme in Garcia-Garibay's efforts, would involve *trans* alkynyl ligands that would space the atoms that anchor the polymethylene chains further from the metal.

With regard to the horizontal dimension of the stator, the incorporation of rigid units such as *p*-phenylene (C_6H_4) or polyynediyl (-(C≡C)$_r$-) moieties near the anchoring heteroatom might enforce a minimum extension for each macrocycle. Rigid units in any position will also reduce conformational degrees of freedom, and possibly lead to less negative $\Delta S^{\ddagger}$ values (lower $\Delta G^{\ddagger}$ values). In terms of optimizing the rotator, hydride ligands are particularly svelte.[28f] With a rotator of formula M(H)$_y$, barriers might be probed in solution by lowering the symmetry of the stator.

In all of the phenomena described above, the rotators are equally capable of motion in clockwise and counterclockwise directions. However, true gyroscopic properties are only realized in the limit of unidirectional rotation.[7,18] Although an extended discussion of this subject is beyond the scope of this section, the most common strategies involve a dipolar rotator, such that rotation can be driven by a rotating electric field of appropriate frequency.[7,9] While the complexes **5**$^+$ BF_4^- and **6**$^+$ Z^- fulfill this criterion, they are not ideal in that they are salts, and the counter anion will interact with any rotating dipole, increasing the barrier. Accordingly, in a later section related neutral complexes will be described that preserve the dipolar rotator.[73]

In summary, this study illustrates the remarkable ease by which iron tricarbonyl based gyroscope like complexes can be assembled, and the quite low rotational barriers that can be achieved in solution and the solid state without extensive optimization. Subsequent reports will describe systems that have the potential to give still lower barriers through appropriate modifications to both the rotators and stators.

2.4 Experimental section

General data: all reactions were conducted under N_2 (or H_2) atmospheres. Chemicals were treated as follows: THF and toluene, distilled from Na/benzophenone; CH_2Cl_2, distilled from CaH_2 (for reactions) or simple distillation (chromatography); hexanes, ether, acetone, and methanol, simple distillation; C_6D_6, $CDCl_3$, acetone-d_6, Grubbs' catalyst (Strem), Grubbs' second generation catalyst (ABCR), $ClRh(PPh_3)_3$ (Strem), CF_3SO_3H (Fluka), NO^+ BF_4^- (Fluka), SiO_2 (Silicycle), celite (EMD), and neutral Al_2O_3 (Macherey-Nagel), used as received. The $[H(OEt_2)_2]^+$ BAr_f^- and $CDFCl_2$ were synthesized by literature procedures.[48,50,]

^1H, $^{13}C\{^1H\}$, and $^{31}P\{^1H\}$ NMR spectra were recorded on standard 400-500 MHz spectrometers at ambient probe temperature unless noted and referenced as follows (δ, ppm): ^1H, residual internal C_6D_5H (7.15), acetone-d_5 (2.05), $CHCl_3$ (7.26), $CDCl_2H$ (5.32), or $CHFCl_2$ (7.47); ^{13}C, internal C_6D_6 (128.0), acetone-d_6 (29.9), $CDCl_3$ (77.0), CD_2Cl_2 (53.8), or $CDFCl_2$ (104.2); ^{31}P, external H_3PO_4 (0.00). ^{13}C and ^{31}P solid-state

NMR spectra were measured on a Bruker Avance 400 widebore spectrometer equipped with a 2.5 mm multinuclear MAS probehead and ZrO_2 rotors. For ^{13}C and ^{31}P CP/MAS measurements, ^{1}H high-power decoupling was applied with contact times of 5 and 2 ms, respectively. $NH_4H_2PO_4$ was used to establish the ^{31}P Hartmann-Hahn matching condition and as an external chemical shift standard ($\delta(^{31}P)$ = +0.81 ppm). For ^{13}C CP/MAS measurements, adamantane served as Hartmann-Hahn matching and external chemical shift standard ($\delta(^{13}C)$ = 38.52 ppm). The recycle delay was 3 s for the ^{13}C and 5 s for the ^{31}P CP/MAS spectra. Linebroadening factors of 50 Hz were applied for all MAS spectra and 200 Hz for the ^{31}P wideline spectrum. The number of transients collected was 64 for the ^{31}P CP/MAS spectra, 256 for the wideline spectrum, and 7500 for the ^{13}C CP/MAS spectrum. The ^{31}P and ^{13}C CSA parameters were obtained from the MAS spectra and wideline spectrum using the program dmfit.[56]

IR spectra were recorded on ASI React-IR 1000 and a Shimadzu IRAffinity-1 spectrometer with a Pike MIRacle ATR system (diamond/ZnSe crystal). Mass spectra data were recorded on a Micromass Zabspec instrument. Melting points were determined on an Electrothermal IA 9100 apparatus or a Stanford Research Systems (SRS) MPA100 (Opti-Melt) automated device. Microanalyses were conducted in house (Carlo Erba EA1110 instrument) or by Atlantic Microlab. DSC and TGA data were obtained with a Mettler-Toledo DSC-821 instrument.[74]

***trans*-$Fe(CO)_3(P((CH_2)_4CH=CH(CH_2)_4)_3P)$ (3a). (A)** A Schlenk flask was charged with **2a**, *trans*-$Fe(CO)_3(P((CH_2)_4CH=CH_2)_3)_2$ (0.262 g, 0.374 mmol),[32a]

CH_2Cl_2 (50 mL; the resulting solution is 0.0075 M in **2a**), and Grubbs' catalyst (ca. half of 0.040 g, 0.049 mmol, 13 mol%), and fitted with a condenser. The solution was refluxed. After 19 h, the remaining catalyst was added. After another 20 h, the solvent was removed by oil pump vacuum. The residue was filtered through neutral alumina (2.5 × 2.5 cm) using 2:1 v/v hexane/CH_2Cl_2. The solvent was removed from the filtrate by oil pump vacuum to give *E,E,E*-**3a** as a white solid (0.139 g, 0.226 mmol, 60%), mp 213-216 °C (capillary).[75] TGA: onset of mass loss, 303 °C (T_e).[74] Anal. Calcd. for $C_{33}H_{54}FeO_3P_2$ (616.58): C 64.31, H 8.78; found: C 64.79, H 9.00, **(B)** Complex **2a** (0.198 g, 0.283 mmol), CH_2Cl_2 (50 mL; the resulting solution is 0.0057 M in **2a**), and Grubbs' second generation catalyst (0.026 g, 0.031 mmol, 10 mol%) were similarly combined. The solution was refluxed. After 20 h, the remaining catalyst was added. After another 17 h, the solvent was removed by oil pump vacuum. The residue was filtered through neutral alumina (2.5 × 5.0 cm) using 2:1 v/v hexane/CH_2Cl_2. The solvent was removed from the filtrate by oil pump vacuum to give *E,E,E*-**3a** as a white solid (0.132 g, 0.214 mmol, 76%).

NMR (C_6D_6, δ in ppm):[38] ^{1}H (400 MHz) 5.49 (m, 6H, C***H***=), 2.15 (m, 12H, C***H***$_2$CH=), 1.79 (m, 12H, PC***H***$_2$), 1.49 (m, 24H, C***H***$_2$); ^{13}C{^{1}H} (100 MHz) 213.9 (t, $^2J_{CP}$ = 28.0 Hz, ***C***O), 132.0 (s, ***C***H=), 33.4 (s, ***C***H$_2$CH=), 31.0 (virtual t, $^3J_{CP}$, $^5J_{CP'}$ = 7.0 Hz,[37] PCH$_2$CH$_2$***C***H$_2$), 30.1 (dd, $^1J_{CP}$, $^3J_{CP'}$ = 14.0, 12.0 Hz,[37] P***C***H$_2$), 24.3 (s, PCH$_2$***C***H$_2$); ^{31}P{^{1}H} (162 MHz) 84.7 (s). ($CDCl_3$, δ in ppm):[38] ^{1}H (500 MHz) 5.30 (m,

6H, C***H***=), 2.12-1.99 (m, 12H, C***H***$_2$CH=), 1.81-1.55 (m, 24H, PC***H***$_2$ and C***H***$_2$), 1.54-1.37 (m, 12H, C***H***$_2$); $^{13}C\{^1H\}$ (126 MHz) 213.6 (t, $^2J_{CP}$ = 28.0 Hz, ***C***O), 131.8 (s, ***C***H=), 33.0 (s, ***C***H$_2$CH=), 30.7 (virtual t, $^3J_{CP}$, $^5J_{CP'}$ = 7.0 Hz,[37] PCH$_2$CH$_2$***C***H$_2$), 30.0 (dd, $^1J_{CP}$, $^3J_{CP'}$ = 15.5, 11.5 Hz,[37] P***C***H$_2$), 24.1 (s, PCH$_2$***C***H$_2$); $^{31}P\{^1H\}$ (202 MHz) 84.0 (s).

IR (cm^{-1}, powder film): 2926 w, 2849 w, 1853 s (ν_{CO}), 1436 w, 961 w, 718 w, 645 s. MS:[76] 616 (**3a**$^+$, 20%), 561 ([**3a**-2CO]$^+$, 50%), 532 ([**3a**-3CO]$^+$, 100%).

***trans*-Fe(CO)$_3$(P((CH$_2$)$_5$CH=CH(CH$_2$)$_5$)$_3$P) (3b)**. Complex **2b**, *trans*-Fe(CO)$_3$(P((CH$_2$)$_5$CH=CH$_2$)$_3$)$_2$, (0.320 g, 0.408 mmol),[32a] CH$_2$Cl$_2$ (50 mL; the resulting solution is 0.0082 M in **2b**), and Grubbs' catalyst (0.040 g, 0.049 mmol, 12 mol%) were combined in a procedure analogous to that for **3a**. The solution was refluxed. After 20 h, the remaining catalyst was added. After another 24 h, the solvent was removed by oil pump vacuum. The residue was filtered through neutral alumina (2.5 × 4.0 cm) using 2:1 v/v hexane/CH$_2$Cl$_2$. The solvent was removed from the filtrate by oil pump vacuum to give **3b** as a waxy solid (0.208 g, 0.297 mmol, 73%, mixture of *E/Z* isomers). Anal. Calcd. for C$_{39}$H$_{66}$FeO$_3$P$_2$ (700.75): C 66.88, H 9.43; found: C 66.96, H 9.84.

NMR (C$_6$D$_6$, δ in ppm): ^1H (400 MHz) 5.69-5.54 (m, 6H, C***H***=), 2.33-2.30 (m, 8H, C***H***$_2$), 1.79-1.33 (m, 52H, C***H***$_2$); $^{31}P\{^1H\}$ (162 MHz) 69.8 (s, 44%), 68.5 (s, 39%), 67.4 (s, 13%), 66.1 (s, 4%).

IR (cm^{-1}, powder film): 3002 w, 2921 m, 2852 m, 1852 s (ν_{CO}), 1445 m, 1412 m, 1048 w, 1030 w, 969 m, 726 m. MS:[76] 700 (**3b**$^+$, 50%), 617 ([**3b**-3CO]$^+$, 100%).

***trans*-Fe(CO)$_3$(P((CH$_2$)$_6$CH=CH(CH$_2$)$_6$)$_3$P) (3c)**. **(A)** Complex **2c**, *trans*-Fe(CO)$_3$(P((CH$_2$)$_6$CH=CH$_2$)$_3$)$_2$, (0.223 g, 0.257 mmol),[32a] CH_2Cl_2 (50 mL; the resulting solution is 0.0051 M in **2c**), and Grubbs' catalyst (0.040 g, 0.049 mmol, 19 mol%) were combined in a procedure analogous to that for **3a**. The solution was refluxed. After 18 h, the remaining catalyst was added. After another 20 h, the solvent was removed by oil pump vacuum. The residue was filtered through neutral alumina (2.5 × 2.5 cm) using 2:1 v/v hexane/CH_2Cl_2. The solvent was removed from the filtrate by oil pump vacuum to give **3c** as a white solid (0.169 g, 0.208 mmol, 81%, mixture of *E/Z* isomers), mp 155-160 °C (capillary). Anal. Calcd. for $C_{45}H_{78}FeO_3P_2$ (784.91): C 68.90, H 9.95; found: C 69.24, H 10.33. **(B)** Complex **2c** (0.318 g, 0.366 mmol), CH_2Cl_2 (50 mL; the resulting solution is 0.0073 M in **2c**), and Grubbs' second generation catalyst (0.036 g, 0.0424 mmol, 12 mol%), were similarly combined. The solution was refluxed. After 19 h, the remaining catalyst was added. After another 20 h, the solvent was removed by oil pump vacuum. The residue was filtered through neutral alumina (2.5 × 5.0 cm) using 2:1 v/v hexane/CH_2Cl_2. The solvent was removed from the filtrate by oil pump vacuum to give **3c** as a white solid (0.226 g, 0.288 mmol, 79%, mixture of *E/Z* isomers).

NMR (C_6D_6, δ in ppm):[38] ^{1}H (400 MHz) 5.48 (m, 2H, C***H***=), 5.35 (m, 4H, C***H***=), 2.06 (m, 12H, C***H***$_2$), 1.78-1.69 (m, 20H, C***H***$_2$), 1.42 (m, 40H, C***H***$_2$); ^{13}C{^{1}H}

(100 MHz) (major isomer only) 215.1 (t, $^{2}J_{CP}$ = 28.3 Hz, ***C***O), 131.5 (s, ***C***H=), 32.9 (s, ***C***H_2), 31.9 (virtual t, $^{3}J_{CP}$, $^{5}J_{CP'}$ = 6.8 Hz,[37] PCH_2CH_2***C***H_2), 31.6 (dd, $^{1}J_{CP}$, $^{3}J_{CP'}$ = 15.2, 12.0 Hz,[37] P***C***H_2), 29.3 (s, ***C***H_2), 29.2 (s, ***C***H_2), 25.3 (s, PCH_2***C***H_2); $^{31}P\{^{1}H\}$ (162 MHz) 71.3 (s, 84%), 70.4 (s, 16%).

IR (cm^{-1}, powder film): 2926 m, 2853 m, 1930 m, 1861 s (ν_{CO}), 1459 w, 1440 w, 1409 w, 961 m, 672 m. MS:[62] 784 (**3c**$^{+}$, 10%), 700 ([**3c**-3CO]$^{+}$, 100%).

***trans*-Fe(CO)$_3$(P((CH$_2$)$_8$CH=CH(CH$_2$)$_8$)$_3$P) (3e)**. Complex **2e**, *trans*-$Fe(CO)_3(P((CH_2)_8CH=CH_2)_3)_2$ (0.259 g, 0.250 mmol),[32a] CH_2Cl_2 (50 mL; the resulting solution is 0.0050 M in **2e**), and Grubbs' catalyst (0.050 g, 0.049 mmol, 24 mol%) were combined in a procedure analogous to that for **3a**. The solution was refluxed. After 18 h, the remaining catalyst was added. After another 21 h, the solvent was removed by oil pump vacuum. A ^{1}H NMR spectrum of the residue (0.163 g) showed some residual terminal olefin. Grubbs' catalyst (0.031 g, 0.038 mmol, 15 mol%) and CH_2Cl_2 (50 mL) were added and the solution was refluxed. After 20 h, the solvent was removed by oil pump vacuum. The residue was filtered through neutral alumina (2.5 × 4.0 cm) using 2:1 v/v hexane/CH_2Cl_2. The solvent was removed from the filtrate by oil pump vacuum to give **3e** as a waxy solid (0.149 g, 0.157 mmol, 63%, mixture of *E/Z* isomers).

NMR (C_6D_6, δ in ppm): ^{1}H (400 MHz) 5.56-5.36 (m, 6H, C***H***=), 2.08 (m, 10H, C***H***$_2$), 1.76 (m, 21H, C***H***$_2$), 1.44-1.36 (m, 65H, C***H***$_2$); $^{31}P\{^{1}H\}$ (162 MHz) 69.3 (s, 62%), 69.0 (s, 30%), 68.6 (s, 8%).

***trans*-Fe(CO)$_3$(P((CH$_2$)$_{10}$)$_3$P) (4a)**. A Fischer-Porter bottle was charged with *E,E,E*-**3a** (0.215 g, 0.349 mmol), ClRh(PPh$_3$)$_3$ (0.050 g, 0.054 mmol, 15 mol%), toluene (10 mL), and H_2 (5 atm). The solution was stirred at 80 °C. After 48 h, the solvent was removed by oil pump vacuum. The residue was filtered through neutral alumina (2.5 × 5.0 cm) using 2:1 v/v hexane/CH_2Cl_2. The solvent was removed from the filtrate by oil pump vacuum to give **4a** as a white solid (0.183 g, 0.294 mmol, 84%), mp 165-170 °C (capillary). DSC ($T_i/T_e/T_p/T_c/T_f$):[74] 131.0/150.0/ 174.3/182.4/185.7 °C (melting endotherm). TGA: onset of mass loss, 346 °C (T_e). Anal. Calcd. for $C_{33}H_{60}FeO_3P_2$ (622.63): C 63.99, H 9.65; found: C 64.38, H 9.77.

NMR (C_6D_6, δ in ppm):[38] ^{1}H (400 MHz) 1.68 (m, 12H, PC*H*$_2$), 1.59-1.54 (m, 48H, C*H*$_2$); ^{13}C{^{1}H} (100 MHz) 216.4 (t, $^2J_{CP}$ = 27.5 Hz, ***C***O), 30.1 (dd, $^1J_{CP}$, $^3J_{CP'}$ = 15.0, 11.7 Hz,[37] P***C***H$_2$), 29.1 (virtual t, $^3J_{CP}$, $^5J_{CP'}$ = 5.3 Hz,[37] PCH$_2$CH$_2$***C***H$_2$), 27.5 (s, ***C***H$_2$), 25.7 (s, ***C***H$_2$), 21.2 (s, PCH$_2$***C***H$_2$); ^{31}P{^{1}H} (162 MHz) 75.5 (s).

IR (cm^{-1}, powder film): 2922 w, 2853 w, 1841 s (ν_{CO}), 1455 w, 1413 w, 718 w, 691 w. MS:[76] 622 (**4a**$^+$, 50%), 539 ([**4a**-3CO]$^+$, 100%).

***trans*-Fe(CO)$_3$(P((CH$_2$)$_{12}$)$_3$P) (4b)**. Complex **3b** (0.246 g, 0.352 mmol), ClRh(PPh$_3$)$_3$ (0.026 g, 0.028 mmol, 8 mol%), toluene (10 mL), and H_2 (5 atm) were combined in a procedure analogous to that for **4a**. A similar reaction (70 °C, 68 h) and workup gave **4b** as a white solid (0.214 g, 0.303 mmol, 86%), mp 220-225 °C (capillary). DSC ($T_i/T_e/T_p/T_c/T_f$):[74] –21.2/–1.4/10.1/13.7/ 20.0 °C (endotherm);

218.7/231.3/250.0/270.0/283.5 °C (melting endotherm). TGA: onset of mass loss, 334 °C (T_e). Anal. Calcd. for $C_{39}H_{72}FeO_3P_2$ (706.79): C 66.31, H 10.20; found: C 66.22, H 10.36.

NMR (C_6D_6, δ in ppm):[38] ^{1}H (400 MHz) 1.80-1.70 (m, 14H, C***H***$_2$), 1.65-1.60 (m, 8H, C***H***$_2$), 1.48-1.43 (m, 50H, C***H***$_2$); ^{13}C{^{1}H} (100 MHz) 215.5 (t, $^2J_{CP}$ = 28.4 Hz, ***C***O), 32.0 (dd, $^1J_{CP}$, $^3J_{CP'}$ = 14.7, 12.1 Hz,[37] P***C***H$_2$), 29.9 (virtual t, $^3J_{CP}$, $^5J_{CP'}$ = 7.2 Hz,[37] PCH$_2$CH$_2$***C***H$_2$), 27.8 (s, ***C***H$_2$), 27.5 (s, ***C***H$_2$), 26.3 (s, ***C***H$_2$), 22.9 (s, PCH$_2$***C***H$_2$); ^{31}P{^{1}H} (162 MHz) 67.5 (s).

IR (cm^{-1}, powder film): 2926 m, 2853 m, 1853 s (ν_{CO}), 1459 w, 1413 w, 803 w, 741 w, 641 s. MS:[76] 706 (**4b**$^+$, 20%), 622 ([**4b**-3CO]$^+$, 100%).

***trans*-Fe(CO)$_3$(P((CH$_2$)$_{14}$)$_3$P) (4c)**. Complex **3c** (0.164 g, 0.209 mmol), ClRh(PPh$_3$)$_3$ (0.025 g, 0.027 mmol, 13 mol%), toluene (10 mL), and H_2 (5 atm) were combined in a procedure analogous to that for **4a**. A similar reaction (60 °C, 72 h) and workup gave **4c** as a white solid (0.130 g, 0.165 mmol, 79%), mp 163-168 °C (capillary). DSC ($T_i/T_e/T_p/T_c/T_f$):[74] 128.2/157.9/ 173.6/177.2/181.8 °C (melting endotherm; no other phase transitions, –100 to 150 °C). TGA: onset of mass loss, 341 °C (T_e). Anal. Calcd. for $C_{45}H_{84}FeO_3P_2$ (790.96): C 68.33, H 10.71; found: C 68.05, H 10.90.

NMR (C_6D_6, δ in ppm):[38] ^{1}H (400 MHz) 1.75 (m, 24H, PC***H***$_2$ and PCH$_2$C***H***$_2$), 1.45-1.41 (m, 60H, C***H***$_2$); ^{13}C{^{1}H} (100 MHz) 215.6 (t, $^2J_{CP}$ = 29.0 Hz, ***C***O), 31.6 (dd,

$^{1}J_{CP}$, $^{3}J_{CP'}$ = 15.1, 11.7 Hz,[37] P***C***H_2), 31.0 (virtual t, $^{3}J_{CP}$, $^{5}J_{CP'}$ = 6.6 Hz,[37] PCH_2PCH_2***C***H_2), 28.2 (s, ***C***H_2), 28.0 (s, ***C***H_2), 27.1 (s, ***C***H_2), 26.5 (s, ***C***H_2), 24.0 (s, PCH_2***C***H_2); $^{31}P\{^{1}H\}$ (162 MHz) 66.9 (s).

IR (cm^{-1}, powder film): 2926 m, 2856 m, 1861 s (ν_{CO}), 1459 w, 737 w, 645 m. MS:[76] 790 (**4c**$^{+}$, 20%), 736 ([**4c**-2CO]$^{+}$, 30%), 706 ([**4c**-3CO]$^{+}$, 100%).

***trans*-Fe(CO)$_3$(P((CH$_2$)$_{18}$)$_3$P)** (**4e**). Complex **3e** (0.149 g, 0.157 mmol), $ClRh(PPh_3)_3$ (0.096 g, 0.103 mmol, 10 mol%), toluene (10 mL), and H_2 (5 atm) were combined in a procedure analogous to that for **4a**. A similar reaction (65 °C, 72 h), alumina filtration (2.5 × 5.0 cm, 3:1 v/v hexane/CH_2Cl_2), and workup gave **4e** as a colorless oil, which became a waxy solid after an additional week (0.738 g, 0.770 mmol, 74%). Anal. Calcd for $C_{57}H_{108}FeO_3P_2$ (875.12): C 71.37, H 11.37; found: C 71.95, H 10.94.[77]

NMR (C_6D_6, δ in ppm):[38] ^{1}H (400 MHz) 1.76 (m, 24H, PC***H***$_2$ and PCH_2C***H***$_2$), 1.41-1.34 (m, 84H, C***H***$_2$); $^{13}C\{^{1}H\}$ (100 MHz) 215.7 (t, $^{2}J_{CP}$ = 28.0 Hz, ***C***O), 31.6 (virtual t, $^{3}J_{CP}$, $^{5}J_{CP'}$ = 6.1 Hz,[37] PCH_2CH_2***C***H_2) 31.2 (dd, $^{1}J_{CP}$, $^{3}J_{CP'}$ = 14.9, 12.1 Hz,[37] P***C***H_2), 29.4 (s, ***C***H_2), 29.2 (s, ***C***H_2), 28.8 (s, ***C***H_2), 28.3 (s, ***C***H_2), 28.1 (s, ***C***H_2), 27.5 (s, ***C***H_2), 24.3 (s, PCH_2***C***H_2); $^{31}P\{^{1}H\}$ (162 MHz) 66.0 (s).

IR (cm^{-1}, oil film): 2922 m, 2850 m, 1859 s (ν_{CO}), 1460 w, 740 w, 642 m.

***trans*-[Fe(CO)$_2$(NO)(P((CH$_2$)$_{10}$)$_3$P)]$^{+}$ BF$_4^{-}$ (5a^{+} BF_4^{-})**. A Schlenk flask was charged with **4a** (0.123 g, 0.198 mmol) and CH_2Cl_2 (8 mL). Then NO^{+} BF_4^{-} (0.0325 g,

0.278 mmol) was added with stirring. After 15 h, the solvent was removed by oil pump vacuum. The residue was extracted with acetone and the extract was filtered through a Celite plug over sintered glass. The solvent was removed by oil pump vacuum and the residue was triturated under ether. The ether was decanted and the residue dried by oil pump vacuum to give **5a**$^+$ BF_4^- as a yellow solid (0.138 g, 0.194 mmol, 98%), mp 206-208 °C (capillary). Anal. Calcd. for $C_{32}H_{60}BF_4FeNO_3P_2$ (711.43): C 54.04, H 8.44, N 1.97; found: C 52.39, H 8.71, N 1.85.[77]

NMR ($CDCl_3$, δ in ppm):[38] ^{1}H (400 MHz) 2.27-2.10 (m, 12H, PC***H***$_2$), 1.65-1.58 (m, 18H, C***H***$_2$), 1.47-1.27 (m, 30H, C***H***$_2$); $^{13}C\{^1H\}$ (100 MHz) 208.7 (t, $^2J_{CP}$ = 25.1 Hz, ***C***O), 28.3 (virtual t, $^3J_{CP}$, $^5J_{CP'}$ = 5.3 Hz,[37] 2PCH$_2$CH$_2$***C***H$_2$), 27.9-27.6 (overlapping virtual t/m, 1PCH$_2$CH$_2$***C***H$_2$, 2P***C***H$_2$, 1P***C***H$_2$), 26.8 and 26.7 (2s, 1***C***H$_2$ and 2***C***H$_2$), 25.0 and 24.2 (2s, 2***C***H$_2$ and 1***C***H$_2$), 22.3 and 21.4 (2s, 1PCH$_2$***C***H$_2$ and 2PCH$_2$***C***H$_2$); $^{31}P\{^1H\}$ (162 MHz) 67.0 (s).

IR (cm^{-1}, powder film): 2926 m, 2856 w, 2023 m (ν_{CO}), 1953 s (ν_{CO}), 1752 s (ν_{NO}), 1459 w, 1413 w, 1046 s, 714 m, 637 s. MS:[76] 625 (**5a**$^+$, 50%), 597 ([**5a**-CO]$^+$, 20%), 569 ([**5a**-2CO]$^+$, 100%).

***trans*-[Fe(CO)$_2$(NO)(P((CH$_2$)$_{12}$)$_3$P)]$^+$ BF$_4^-$ (5b**$^+$ BF_4^-**)**. Complex **4b** (0.0840 g, 0.119 mmol), CH_2Cl_2 (5 mL), and NO^+ BF_4^- (0.0230 g, 0.197 mmol) were combined in a procedure analogous to that for **5a**$^+$ BF_4^-. An identical workup gave **5b**$^+$ BF_4^- as a

yellow solid (0.0845 g, 0.106 mmol, 89%), mp 204-206 °C (capillary). Anal. Calcd. for $C_{38}H_{72}BF_4FeNO_3P_2$ (795.59): C 57.39, H 9.06, N 1.76; found: C 57.43, H 9.43, N 1.50.

NMR ($CDCl_3$, δ in ppm):[38] ^1H (400 MHz) 2.26 (m, 12H, PC***H***$_2$), 1.57 (m, 20H, C***H***$_2$), 1.41-1.28 (m, 40H, C***H***$_2$); $^{13}C\{^1H\}$ (100 MHz) 207.5 (t, $^2J_{CP}$ = 24.8 Hz, ***C***O), 29.5-28.6 (overlapping virtual t/m, 2PCH$_2$CH$_2$***C***H$_2$, 1PCH$_2$CH$_2$***C***H$_2$, 2P***C***H$_2$ and 1P***C***H$_2$), 27.1 and 27.0 (2s, 2***C***H$_2$ and 1***C***H$_2$), 26.8 and 26.6 (2s, 2***C***H$_2$ and 1***C***H$_2$), 25.8 and 25.7 (2s, 2***C***H$_2$ and 1***C***H$_2$), 23.2 and 23.0 (2s, 1PCH$_2$***C***H$_2$ and 2PCH$_2$***C***H$_2$); $^{31}P\{^1H\}$ (162 MHz) 57.5 (s).

VT-NMR: (C_6D_5Cl, δ in ppm):[38] ^1H (500 MHz, 40 °C) 2.42-2.22 (m, 12H, PC***H***$_2$), 1.66-1.52 (m, 20H, C***H***$_2$), 1.49-1.33 (m, 40H, C***H***$_2$); $^{13}C\{^1H\}$ (125 MHz, 40 °C; Figure 2-7) 207.8 (t, $^2J_{CP}$ = 25.0 Hz, ***C***O), 29.2 (virtual t, $^3J_{CP}$, $^5J_{CP'}$ = 7.5 Hz,[37] PCH$_2$CH$_2$***C***H$_2$), 28.4 (m, P***C***H$_2$), 27.22 and 27.17 (2s, 2***C***H$_2$ and 1***C***H$_2$), 27.0 and 26.9 (2s, 2***C***H$_2$ and 1***C***H$_2$), 26.1 and 26.0 (2s, 2***C***H$_2$ and 1***C***H$_2$), 23.2 and 22.9 (2s, 1PCH$_2$***C***H$_2$ and 2PCH$_2$***C***H$_2$); $^{13}C\{^1H\}$ (125 MHz, 100 °C; Figure 2-7) 207.9 (t, $^2J_{CP}$ = 25.0 Hz, ***C***O), 29.15 (virtual t, $^3J_{CP}$, $^5J_{CP'}$ = 7.5 Hz,[37] PCH$_2$CH$_2$***C***H$_2$), 28.8 (br m, P***C***H$_2$), 27.3 (s, ***C***H$_2$), 27.2 (s, ***C***H$_2$), 26.4 (s, ***C***H$_2$), 23.3 and 23.1 (2s, 1PCH$_2$***C***H$_2$ and 2PCH$_2$***C***H$_2$).

IR (cm^{-1}, powder film): 2926 m, 2856 w, 2026 m (ν_{CO}), 1965 s (ν_{CO}), 1764 s (ν_{NO}), 1459 w, 1413 w, 1046 s, 633 m. MS:[76] 708 (**5b**$^+$, 50%), 652 ([**5b**-2CO]$^+$, 100%).

***trans*-[Fe(CO)$_2$(NO)(P((CH$_2$)$_{14}$)$_3$P)]$^+$ BF$_4^-$ (5c$^+$ BF$_4^-$)**. Complex **4c** (0.0730 g, 0.0924 mmol), CH_2Cl_2 (5 mL), and NO^+ BF_4^- (0.0190 g, 0.163 mmol) were combined in a procedure analogous to that for **5a**$^+$ BF_4^-. An identical workup gave **5c**$^+$ BF_4^- as a yellow solid (0.0657 g, 0.0748 mmol, 81%), mp 168-170 °C (capillary). Anal. Calcd. for $C_{44}H_{84}BF_4FeNO_3P_2$ (879.76): C 60.10, H 9.56, N 1.59; found: C 58.64, H 9.51, N 1.53.[77]

NMR (acetone-d_6, δ in ppm):[38] ^{1}H (400 MHz) 2.42 (m, 12H, PC***H***$_2$), 1.66-1.56 (m, 24H, PCH$_2$C***H***$_2$ and PCH$_2$CH$_2$C***H***$_2$), 1.36-1.31 (m, 48H, C***H***$_2$); ^{13}C{^{1}H} (100 MHz) 208.2 (t, $^2J_{CP}$ = 25.3 Hz, ***C***O), 30.7 (virtual t, $^3J_{CP}$, $^5J_{CP'}$ = 7.6 Hz,[37] PCH$_2$CH$_2$***C***H$_2$), 28.7 (dd,[37] $^1J_{CP}$, $^3J_{CP'}$ = 15.4, 13.5 Hz, P***C***H$_2$), 28.2 (s, ***C***H$_2$), 28.0 (s, ***C***H$_2$), 27.2 (s, ***C***H$_2$), 26.6 (s, ***C***H$_2$), 24.6 (s, PCH$_2$***C***H$_2$); ^{31}P{^{1}H} (162 MHz) 56.8 (s).

VT-NMR: ($CDFCl_2$, δ in ppm):[23] ^{1}H (400 MHz, –10 °C) 1.93 (m, 12H, PC***H***$_2$), 1.25 (m, 24H, PCH$_2$C***H***$_2$ and PCH$_2$CH$_2$C***H***$_2$), 1.07-1.00 (m, 48H, C***H***$_2$); ^{13}C{^{1}H} (100 MHz, –10 °C; Figure 2-7) 207.3 (t, $^2J_{CP}$ = 25.0 Hz, ***C***O), 30.3 (virtual t, $^3J_{CP}$, $^5J_{CP'}$ = 7.1 Hz,[37] PCH$_2$CH$_2$***C***H$_2$), 28.2 (dd,[37] $^1J_{CP}$, $^3J_{CP'}$ = 14.9, 14.1 Hz, P***C***H$_2$), 27.6 (s, ***C***H$_2$), 27.3 (s, ***C***H$_2$), 26.3 (s, ***C***H$_2$), 25.3 (s, ***C***H$_2$), 24.3 (s, PCH$_2$***C***H$_2$); ^{31}P{^{1}H} (162 MHz, –10 °C) 57.2 (s); ^{13}C{^{1}H} (100 MHz, –80 °C; Figure 2-7) 206.5 (t, $^2J_{CP}$ = 23.0 Hz, ***C***O), 30.1 (m, PCH$_2$CH$_2$***C***H$_2$), 27.6 (m (sh), P***C***H$_2$), 27.3 (s, ***C***H$_2$), 26.9 (s, ***C***H$_2$), 25.4 (s, ***C***H$_2$), 24.6 and 24.2 (2s, 1***C***H$_2$ and 2***C***H$_2$), 23.9 and 23.7 (2s, 2***C***H$_2$ and 1***C***H$_2$).

IR (cm^{-1}, powder film): 2926 m, 2856 m, 2030 m (ν_{CO}), 1965 s (ν_{CO}), 1764 s (ν_{NO}), 1459 w, 1413 w, 1054 s, 726 m, 633 s. MS:[76] 793 (**5c**$^+$, 30%), 737 ([**5c**-2CO]$^+$, 100%).

***mer,trans*-[Fe(CO)$_3$(H)(P((CH$_2$)$_{10}$)$_3$P)]$^+$ BAr$_f^-$ (6a$^+$ BAr$_f^-$).** A Schlenk flask was charged with **4a** (0.0250 g, 0.0402 mmol), CH_2Cl_2 (8.0 mL), and $[H(OEt_2)_2]^+$ BAr_f^- (0.041 g, 0.040 mmol) with stirring. After 24 h, the solvent was removed by oil pump vacuum. The residue was washed with hexane and dried by oil pump vacuum to give **6a**$^+$ BAr_f^- as an off white powder (0.059 g, 0.040 mmol, 99%), mp 162-167 °C (capillary; greenish liquid). Anal. Calcd. for $C_{65}H_{73}BF_{24}FeO_3P_2$ (1486.86): C 52.51, H 4.95; found: C 52.37, H 5.04.

NMR (CD_2Cl_2, δ in ppm):[38] ^{1}H (500 MHz) 7.74-7.70 (m, 8H, C$_6$***H***$_3$ *o* to B), 7.58-7.53 (m, 4H, C$_6$***H***$_3$ *p* to B), 2.05-1.81 (m, 12H, C***H***$_2$), 1.70-1.22 (m, 48H, C***H***$_2$), –9.44 (t, $^2J_{PH}$ = 22.17 Hz, 1H, Fe***H***); ^{13}C{^{1}H} (125 MHz) 206.8 (t, $^2J_{CP}$ = 20.7 Hz, ***C***O *trans* to ***H***), 206.0 (t, $^2J_{CP}$ = 20.7 Hz, ***C***O *cis* to ***H***), 162.2 (q, $^1J_{BC}$ = 50 Hz, ***C***$_6$H$_3$ *i* to B), 135.3 (s, ***C***$_6$H$_3$ *o* to B), 129.3 (q, $^2J_{CF}$ = 31 Hz, ***C***$_6$H$_3$ *m* to B), 123.6 (q, $^1J_{CF}$ = 272 Hz, ***C***F$_3$), 117.9 (s, ***C***$_6$H$_3$ *p* to B), 28.7 (dd, $^1J_{CP}$, $^3J_{CP'}$ = 15.1 Hz, 15.0 Hz,[37] 2P***C***H$_2$) and 28.0 (dd, $^1J_{CP}$, $^3J_{CP'}$ = 15.1 Hz, 15.0 Hz,[22] 1P***C***H$_2$), 28.6-28.4 (overlapping virtual t, $^3J_{CP}$, $^5J_{CP'}$ = 5.8 Hz,[37] PCH$_2$CH$_2$***C***H$_2$), 26.8 and 26.5 (2s, 2***C***H$_2$ and 1***C***H$_2$), 26.2 and

25.4 (2s, 1***C***H_2 and 2***C***H_2), 22.1 and 20.5 (2s, 1PCH_2***C***H_2 and 2PCH_2***C***H_2); $^{31}P\{^1H\}$ (202 MHz) 59.7 (s).

IR (cm^{-1}, powder film): 2933 w, 2860 w, 2059 w (ν_{CO}), 2007 m (ν_{CO}), 1992 s (ν_{CO}), 1608 w, 1458 w, 1352 s, 1273 s.

***mer,trans*-[Fe(CO)$_3$(H)(P((CH$_2$)$_{12}$)$_3$P)]$^+$ BAr$_f^-$ (6b$^+$ BAr$_f^-$)**. Complex **4b** (0.0250 g, 0.0354 mmol), CH_2Cl_2 (8.0 mL), and $[H(OEt_2)_2]^+$ BAr_f^- (0.036 g, 0.035 mmol) were combined in a procedure analogous to that for **6a**$^+$ BAr_f^-. An identical workup gave **6b**$^+$ BAr_f^- as an off white powder (0.055 g, 0.035 mmol, 99%), mp 161-165 °C (capillary; greenish liquid). Anal. Calcd. for $C_{71}H_{85}BF_{24}FeO_3P_2$ (1571.02): C 54.28, H 5.45; found: C 54.15, H 5.46.

NMR (CD_2Cl_2, δ in ppm):[38] ^1H (500 MHz) 7.75-7.69 (m, 8H, C_6***H***$_3$ *o* to B), 7.58-7.54 (m, 4H, C_6***H***$_3$ *p* to B), 1.99-1.87 (m, 12H, C***H***$_2$), 1.60-1.49 (m, 24H, C***H***$_2$), 1.47-1.40 (m, 12H, C***H***$_2$), 1.38-1.29 (m, 24H, C***H***$_2$), –9.45 (t, $^2J_{PH}$ = 27.1 Hz, 1H, Fe***H***); $^{13}C\{^1H\}$ (125 MHz) 206.8-206.2 (overlapping triplets, ***C***O), 162.2 (q, $^1J_{BC}$ = 50 Hz, ***C***$_6H_3$ *i* to B), 135.2 (s, ***C***$_6H_3$ *o* to B), 129.3 (q, $^2J_{CF}$ = 31 Hz, ***C***$_6H_3$ *m* to B), 123.6 (q, $^1J_{CF}$ = 272 Hz, ***C***F_3), 117.9 (s, ***C***$_6H_3$ *p* to B), 30.8 (virtual t, $^1J_{CP}$, $^3J_{CP'}$ = 15.4 Hz,[37] P***C***H_2), 29.2 (virtual t, $^3J_{CP}$, $^5J_{CP'}$ = 7.2 Hz,[37] PCH_2CH_2***C***H_2), 27.5 (s, ***C***H_2), 27.2 (s, ***C***H_2), 26.7 (s, ***C***H_2), 23.2 (s, PCH_2***C***H_2); $^{31}P\{^1H\}$ (202 MHz) 49.9 (s).

VT-NMR: (CD_2Cl_2, δ in ppm):[38] ^{1}H (500 MHz, 35 °C; Figure 2-7) 7.76-7.71 (m, 8H, $C_6\boldsymbol{H}_3$ *o* to B), 7.60-7.55 (m, 4H, $C_6\boldsymbol{H}_3$ *p* to B), 1.98-1.85 (m, 12H, C$\boldsymbol{H}_2$), 1.63-1.50 (m, 24H, C$\boldsymbol{H}_2$), 1.49-1.41 (m, 12H, C$\boldsymbol{H}_2$), 1.40-1.25 (m, 24H, C$\boldsymbol{H}_2$), –9.44 (t, $^2J_{PH}$ = 27.1 Hz, 1H, Fe***H***); $^{13}C\{^1H\}$ (126 MHz, 35 °C; Figure 2-7) 206.8-206.2 (overlapping triplets, ***C***O), 162.2 (q, $^1J_{BC}$ = 50 Hz, $\boldsymbol{C}_6H_3$ *i* to B), 135.3 (s, $\boldsymbol{C}_6H_3$ *o* to B), 129.4 (q, $^2J_{CF}$ = 31 Hz, $\boldsymbol{C}_6H_3$ *m* to B), 125.1 (q, $^1J_{CF}$ = 272 Hz, ***C***F_3), 117.9 (s, $\boldsymbol{C}_6H_3$ *p* to B), 31.0 (virtual t, $^1J_{CP}$, $^3J_{CP'}$ = 15.2 Hz,[37] P***C***H_2), 29.4 (virtual t, $^3J_{CP}$, $^5J_{CP'}$ = 7.0 Hz,[37] $PCH_2CH_2\boldsymbol{C}H_2$), 27.7 (s, ***C***$H_2$), 27.3 (s, ***C***$H_2$), 26.8 (s, ***C***$H_2$), 23.4 (s, $PCH_2\boldsymbol{C}H_2$); $^{13}C\{^1H\}$ (126 MHz, –50 °C; Figure 2-7) 206.8-206.2 (unresolved m, ***C***O), 161.6 (q, $^1J_{BC}$ = 50 Hz, $\boldsymbol{C}_6H_3$ *i* to B), 134.5 (s, $\boldsymbol{C}_6H_3$ *o* to B), 128.4 (q, $^2J_{CF}$ = 31 Hz, $\boldsymbol{C}_6H_3$ *m* to B), 124.3 (q, $^1J_{CF}$ = 272 Hz, ***C***F_3), 117.4 (s, $\boldsymbol{C}_6H_3$ *p* to B), 29.9 and 29.1 (2 × unresolved m, 2P***C***H_2 and 1P***C***H_2), 28.4 and 27.8 (2 × unresolved m, $2PCH_2CH_2\boldsymbol{C}H_2$ and $1PCH_2CH_2\boldsymbol{C}H_2$), 26.8 and 26.11 (2s, 2***C***H_2 and 1***C***H_2), 26.3 and 26.0 (2s, 2***C***H_2 and 1***C***H_2), 25.8 and 25.1 (2s, 2***C***H_2 and 1***C***H_2), 22.2 and 21.8 (s, 2s, 2 $PCH_2\boldsymbol{C}H_2$ and $1PCH_2\boldsymbol{C}H_2$)

IR (cm^{-1}, powder film): 2931 w, 2860 w, 2073 w (ν_{CO}), 2025 m (ν_{CO}), 1998 s (ν_{CO}), 1610 w, 1458 w, 1352 s, 1275 s, 1157 s, 1120, s, 887 m, 713 s, 680 m, 669 m.

***mer,trans*-[Fe(CO)$_3$(H)(P((CH$_2$)$_{14}$)$_3$P)]$^+$ BAr$_f^-$ (6c$^+$ BAr$_f^-$)**. Complex **4c** (0.0250 g, 0.0316 mmol), CH_2Cl_2 (8.0 mL), and $[H(OEt_2)_2]^+$ BAr_f^- (0.032 g, 0.032

mmol) were combined in a procedure analogous to that for **6a**$^+$ BAr_f^-. An identical workup gave **6c**$^+$ BAr_f^- as an off white powder (0.051 g, 0.031 mmol, 98%), mp 185-188 °C (capillary; greenish liquid). Anal. Calcd. for $C_{77}H_{97}BF_{24}FeO_3P_2$ (1655.18): C 55.91, H 5.85; found: C 55.26, H 5.76.[77]

NMR (CD_2Cl_2, δ in ppm):[38] ^{1}H (500 MHz) 7.75-7.70 (m, 8H, $C_6\boldsymbol{H}_3$ *o* to B), 7.60-7.55 (m, 4H, $C_6\boldsymbol{H}_3$ *p* to B), 2.00-1.88 (m, 12H, C$\boldsymbol{H}_2$), 1.60-1.45 (m, 24H, C$\boldsymbol{H}_2$), 1.44-1.24 (m, 48H, C$\boldsymbol{H}_2$), –9.45 (t, $^2J_{PH}$ = 30.2 Hz, 1H, Fe***H***); ^{13}C{^{1}H} (125 MHz) 206.8 (t, $^2J_{CP}$ = 21.1 Hz, ***C***O *cis* to ***H***), 206.0 (t, $^2J_{CP}$ = 15.0 Hz, ***C***O *trans* to ***H***), 162.2 (q, $^1J_{BC}$ = 50 Hz, $\boldsymbol{C}_6H_3$ *i* to B), 135.3 (s, $\boldsymbol{C}_6H_3$ *o* to B), 129.3 (q, $^2J_{CF}$ = 31 Hz, $\boldsymbol{C}_6H_3$ *m* to B), 125.4 (q, $^1J_{CF}$ = 272 Hz, ***C***F_3), 117.9 (s, $\boldsymbol{C}_6H_3$ *p* to B), 30.13 (virtual t, $^1J_{CP}$, $^3J_{CP'}$ = 15.1 Hz,[37] P***C***H_2), 30.08 (overlapping virtual t, $^3J_{CP}$, $^5J_{CP'}$ = 5.5 Hz,[37] $PCH_2CH_2\boldsymbol{C}H_2$), 27.9 (s, ***C***$H_2$), 27.7 (s, ***C***$H_2$), 27.28 (s, ***C***$H_2$), 27.26 (s, ***C***$H_2$), 23.9 (s, $PCH_2\boldsymbol{C}H_2$); ^{31}P{^{1}H} (202 MHz) 46.9 (s).

IR (cm^{-1}, powder film): 2931 w, 2858 w, 2081 w (ν_{CO}), 2031 m (ν_{CO}), 2015 s (ν_{CO}), 1608 w, 1352 s, 1276 s.

***mer,trans*-[Fe(CO)$_3$(H)(P((CH$_2$)$_{18}$)$_3$P)]$^+$ BAr$_f^-$ (6e$^+$ BAr_f^-)**. Complex **4e** (0.0250 g, 0.0261 mmol), CH_2Cl_2 (8.0 mL), and $[H(OEt_2)_2]^+$ BAr_f^- (0.026 g, 0.026 mmol) were combined in a procedure analogous to that for **6a**$^+$ BAr_f^-. An identical

workup gave **6e**$^+$ BAr_f^- as a yellow gum (0.046 g, 0.026 mmol, 99%). Anal. Calcd. for $C_{89}H_{121}BF_{24}FeO_3P_2$ (1823.51): C 58.62, H 6.69; found: C 59.26, H 6.83.[77]

NMR (CD_2Cl_2, δ in ppm):[38] ^{1}H (500 MHz) 7.76-7.72 (m, 8H, $C_6\boldsymbol{H}_3$ *o* to B), 7.59-7.57 (m, 4H, $C_6\boldsymbol{H}_3$ *p* to B), 2.01-1.89 (m, 12H, C$\boldsymbol{H}_2$), 1.61-1.45 (m, 24H, C$\boldsymbol{H}_2$), 1.43-1.24 (m, 72H, C$\boldsymbol{H}_2$), –9.48 (t, $^2J_{PH}$ = 32.2 Hz, 1H, Fe***H***); ^{13}C{^{1}H} (125 MHz) 207.0 (t, $^2J_{CP}$ = 22.1 Hz, ***C***O *cis* to ***H***), 206.0 (t, $^2J_{CP}$ = 13.6 Hz, ***C***O *trans* to ***H***), 162.2 (q, $^1J_{BC}$ = 55 Hz, $\boldsymbol{C}_6H_3$ *i* to B), 135.3 (s, $\boldsymbol{C}_6H_3$ *o* to B), 129.4 (q, $^2J_{CF}$ = 33 Hz, $\boldsymbol{C}_6H_3$ *m* to B), 125.1 (q, $^1J_{CF}$ = 273 Hz, $\boldsymbol{C}F_3$), 117.9 (s, $\boldsymbol{C}_6H_3$ *p* to B), 30.7 (virtual t, $^3J_{CP}$, $^5J_{CP'}$ = 6.9 Hz,[37] $PCH_2CH_2\boldsymbol{C}H_2$), 29.3 (virtual t, $^1J_{CP}$, $^3J_{CP'}$ = 14.7 Hz,[37] P$\boldsymbol{C}H_2$), 28.8 (s, $\boldsymbol{C}H_2$), 28.7 (s, $\boldsymbol{C}H_2$), 28.6 (s, $\boldsymbol{C}H_2$), 28.56 (s, $\boldsymbol{C}H_2$), 28.3 (s, $\boldsymbol{C}H_2$), 28.2 (s, $\boldsymbol{C}H_2$), 23.9 (s, $PCH_2\boldsymbol{C}H_2$); ^{31}P{^{1}H} (202 MHz) 43.4 (s).

IR (cm^{-1}, oil film): 2927 w, 2856 w, 2081 w (ν_{CO}), 2025 m (ν_{CO}), 2009 s (ν_{CO}), 1608 w, 1440 w, 1352 s, 1273 s.

***mer,trans*-[Fe(CO)$_3$(H)(P((CH$_2$)$_4$CH=CH(CH$_2$)$_4$))$_3$P)]$^+$ BAr$_f^-$ (7a$^+$ BAr_f^-).** Complex *E,E,E*-**3a** (0.0250 g, 0.0405 mmol), CH_2Cl_2 (8.0 mL), and $[H(OEt_2)_2]^+$ BAr_f^- (0.041 g, 0.041 mmol) were combined in a procedure analogous to that for **6a**$^+$ BAr_f^-. An identical workup gave *E,E,E*-**7a**$^+$ BAr_f^- as an off white powder (0.058 g, 0.039 mmol, 97%), mp 156-158 °C (capillary; greenish liquid). Anal. Calcd. for $C_{65}H_{67}BF_{24}FeO_3P_2$ (1480.81): C 52.76, H 4.50; found: C 52.96, H 4.78.

NMR (CD_2Cl_2, δ in ppm):[38] ^{1}H (500 MHz) 7.77-7.71 (m, 8H, $C_6\boldsymbol{H}_3$ *o* to B), 7.60-7.57 (m, 4H, $C_6\boldsymbol{H}_3$ *p* to B), 5.48-5.44 (m, 2H, C***H***=C***H***), 5.33-5.30 (m, 4H, C***H***=C***H***), 2.17-2.07 (m, 12H, C$\boldsymbol{H}_2$), 2.00-1.79 (m, 12H, C$\boldsymbol{H}_2$), 1.72-1.45 (m, 30H, C$\boldsymbol{H}_2$), –9.40 (t, $^2J_{PH}$ = 22.1 Hz, 1H, Fe***H***); ^{13}C{^{1}H} (125 MHz) 206.3-205.8 (overlapping triplets, ***C***O), 162.1 (q, $^1J_{BC}$ = 50 Hz, $\boldsymbol{C}_6H_3$ *i* to B), 135.2 (s, $\boldsymbol{C}_6H_3$ *o* to B), 132.6 (s, 2***C***H_2=), 131.9 (s, 1***C***H_2=), 129.2 (q, $^2J_{CF}$ = 31 Hz, $\boldsymbol{C}_6H_3$ *m* to B), 125.0 (q, $^1J_{CF}$ = 272 Hz, ***C***F_3), 117.9 (s, $\boldsymbol{C}_6H_3$ *p* to B), 33.1 (s, 2***C***H_2CH=), 31.2 (s, 1***C***H_2CH=), 30.0 (virtual t, $^3J_{CP}$, $^5J_{CP'}$ = 7.6 Hz,[37] 2PCH_2CH_2***C***H_2), 29.7 (virtual t, $^3J_{CP}$, $^5J_{CP'}$ = 5.2 Hz,[37] 1PCH_2CH_2***C***H_2), 29.1 (dd, $^1J_{CP}$, $^3J_{CP'}$ = 15.7, 14.5 Hz,[37] 2P***C***H_2), 27.3 (dd, $^1J_{CP}$, $^3J_{CP'}$ = 15.3, 14.1 Hz,[37] 1P***C***H_2), 25.6 (s, 2PCH_2***C***H_2), 22.5 (s, 1PCH_2***C***H_2); ^{31}P{^{1}H} (202 MHz) 66.4 (s).

IR (cm^{-1}, powder film): 2933 w, 2858 w, 2067 w (ν_{CO}), 2015 m (ν_{CO}), 2000 s (ν_{CO}), 1610 w, 1440 w, 1352 s, 1273 s.

6a$^+$ $CF_3SO_3^-$. A 5 mm NMR tube was charged with **4a** (0.002 g, 0.003 mmol), $CDCl_3$ (0.5 mL) and CF_3SO_3H (0.001 mL, 0.01 mmol). NMR spectra showed the quantitative generation of **6a**$^+$ $CF_3SO_3^-$ ($CDCl_3$, δ in ppm):[38] ^{1}H (400 MHz) 2.17-1.92 (m, 12H, C$\boldsymbol{H}_2$), 1.58-1.40 (s, 48H, C$\boldsymbol{H}_2$), –9.41 (t, $^2J_{HP}$ = 21.4 Hz, 1H, Fe***H***); ^{13}C{^{1}H} (100 MHz) 206.7 (t, $^2J_{CP}$ = 21.1 Hz, ***C***O), 28.5-28.2 and 27.7 (overlapping m/virtual t, $^3J_{CP}$, $^5J_{CP'}$ = 14.0 Hz,[37] 2P***C***H_2CH_2***C***H_2 and 1P***C***H_2CH_2***C***H_2), 26.6 and 26.3 (2s, 2***C***H_2

and 1***C***H_2), 26.0 and 25.2 (2s, 1***C***H_2 and 2***C***H_2), 21.9 and 20.2 (2s, 2PCH_2***C***H_2 and 1PCH_2***C***H_2); $^{31}P\{^1H\}$ (162 MHz) 60.5 (s).

6c$^+$ $CF_3SO_3^-$. A 5 mm NMR tube was charged with **4c** (0.0066 g, 0.0084 mmol), $CDCl_3$ (0.5 mL) and CF_3SO_3H (0.001 mL, 0.01 mmol). NMR spectra showed the quantitative generation of **6c**$^+$ $CF_3SO_3^-$ ($CDCl_3$, δ in ppm): [38] ^1H (400 MHz) 2.00 (m, 12H, PC***H***$_2$), 1.54 (m, 24H, PCH_2C***H***$_2$C***H***$_2$), 1.35-1.30 (m, 48H, C***H***$_2$), –9.46 (t, $^2J_{HP}$ = 29.4 Hz, 1H, Fe***H***); $^{13}C\{^1H\}$ (100 MHz) 206.7 (s, ***C***O), 29.9-29.3 (overlapping virtual t/m, P***C***H_2CH_2***C***H_2), 27.7 (s, ***C***H_2), 27.5 (s, ***C***H_2), 27.1 (s, ***C***H_2), 27.0 (s, ***C***H_2), 23.8 (s, PCH_2C***H***$_2$); $^{31}P\{^1H\}$ (162 MHz) 47.5 (s).

7a$^+$ $CF_3SO_3^-$. A 5 mm NMR tube was charged with *E*,*E*,*E*-**3a** (<0.010 g), $CDCl_3$ (0.4 mL), and CF_3SO_3H (0.001 mL, 0.01 mmol). NMR spectra showed the quantitative generation of *(E,E,E)*-**7a**$^+$ $CF_3SO_3^-$ ($CDCl_3$, δ in ppm): [38] ^1H (400 MHz) 5.43 (m, 2H, C***H***=), 5.27 (m, 4H, C***H***=), 2.11-1.94 (m, 24H, C***H***$_2$), 1.55 (m, 24H, C***H***$_2$), –9.42 (t, $^2J_{HP}$ = 21.8 Hz, 1H, Fe***H***); $^{13}C\{^1H\}$ (100 MHz) 206.4 (unresolved m, ***C***O), 132.5 and 131.9 (2s, 4***C***H= and 2***C***H=), 33.2 and 31.3 (2s, 2***C***H_2 and 1***C***H_2), 30.0 and 29.7 (2 virtual t, $^3J_{CP}$, $^5J_{CP'}$ = 7.8 and 5.2 Hz,[37] 2PCH_2CH_2***C***H_2 and 1PCH_2CH_2***C***H_2), 28.7 and 26.8 (2 virtual t, $^1J_{CP}$, $^3J_{CP'}$ = 14.6 and 15.3 Hz,[37] 2P***C***H_2 and 1P***C***H_2), 25.5 and 22.4 (2s, 2 PCH_2***C***H_2 and 1 PCH_2***C***H_2); $^{31}P\{^1H\}$ (162 MHz) 67.0 (s).

Cyclic voltammetry: a BAS*i*Epsilon Electrochemical Workstation (Cell Stand C3) with the program Epsilon EC (version 2.13.77) was employed. Samples were

prepared under N_2 and data were recorded as described in Table 2-2 (ferrocene added after each measurement).

2.5 Crystallography

A. Complex **4c** was suspended in methanol and warmed. THF was added until the sample was homogeneous. After one day at room temperature, colorless prisms were obtained. Data were collected as outlined in Table 2-3. Cell parameters were obtained from 10 frames using a 10° scan and refined with 10223 reflections. Lorentz, polarization, and absorption corrections were applied.[78] The space group was determined from systematic absences and subsequent least-squares refinement. The structure was solved by direct methods. The parameters were refined with all data by full-matrix-least-squares on F^2 using SHELXL-97.[79] Non-hydrogen atoms were refined with anisotropic thermal parameters. The hydrogen atoms were fixed in idealized positions using a riding model. Scattering factors were taken from literature.[80] **B**. A solution of *E,E,E*-**3a** in hexane/benzene (2 mL, 1:1 v/v) was kept in a freezer (–20 °C). After one day, a colorless prism was obtained, which upon warming to room temperature turned white. Data were collected as outlined in Table 2-3. Cell parameters were obtained from 10 images using a 10° scan and refined with 3060 reflections. Using Olex2,[81] the structure was solved with SHELXS[79] by direct methods and refined with SHELXL[79] using least squares minimization. The space group was determined by systematic absences and intensity statistics. Non-hydrogen atoms were refined with

anisotropic thermal parameters. The hydrogen atoms were fixed in idealized position using a riding model. Scattering factors were taken from literature.[80] **C**. A white prism of *E,E,E*-**3a**·2(1,3,5-$C_6H_3(CH_3)_3$) was analogously obtained from *E,E,E*-**3a** (0.150 g) using hexane/mesitylene. The structure was solved by an identical series of procedures (cell parameters from 10 images using a 10° scan and refined with 8529 reflections).

Table 2-3. Summary of crystallographic data.[a]

Complex	*E,E,E*-**3a**·C_6H_6	*E,E,E*-**3a**·2(1,3,5-$C_6H_3(CH_3)_3$)	**4c**
empirical formula	$C_{33}H_{54}FeO_3P_2 \cdot C_6H_6$	$C_{33}H_{54}FeO_3P_2 \cdot 2(C_9H_{12})$	$C_{45}H_{84}FeO_3P_2$
formula weight	694.66	856.92	790.91
crystal system	Trigonal	Monoclinic	Monoclinic
space group	R-3c	C 2/c	C 2/c
unit cell dimensions			
a [Å]	15.835(2)	13.0820(3)	21.5104(8)
b [Å]	15.835(2)	23.0562(9)	13.9765(6)
c [Å]	27.470(6)	17.1097(6)	18.3436(8)
α [°]	90	90	90
β [°]	90	106.467(2)	122.839(2)
γ [°]	120	90	90
volume [$Å^3$]	5965(2)	4949.0(3)	4633.5(3)
Z	6	4	4
ρ_{calcd} [Mg/m^3]	1.160	1.150	1.134
μ [mm^{-1}]	0.492	0.408	0.430
F(000)	2244.0	1856.0	1736
crystal size [mm^3]	0.35 × 0.3 × 0.25	0.15 × 0.15 × 0.1	0.35 × 0.15 × 0.10
range for data collection	5.146 to 55.044	4.318 to 50.102	2.25 to 27.49
index ranges	$-20 \le h \le 17$	$-15 \le h \le 15$	$-27 \le h \le 27$
	$-16 \le k \le 20$	$-27 \le k \le 27$	$-17 \le k \le 18$
	$-28 \le l \le 34$	$-20 \le l \le 20$	$-23 \le l \le 23$
reflections collected	3060	8529	10223
independent reflections	1337 [R(int) = 0.0326]	4369 [R(int) = 0.0288]	5304 [R(int) = 0.0478]
max. and min. transmission	0.8597 and 0.8113	0.9604 to 0.9414	0.9583 and 0.8642
data/restraints/parameters	1337 / 0 / 71	4369 / 0 / 262	5304 / 0 / 232
goodness-of-fit on F^2	1.085	1.030	1.001
final R indices [I>2σ(I)]	R_1 = 0.0527, wR_2 = 0.1115	R_1 = 0.0336, wR_2 = 0.0799	R_1 = 0.0428, wR_2 = 0.0907
R indices (all data)	R_1 = 0.0800, wR_2 = 0.1214	R_1 = 0.0540, wR_2 = 0.0875	R_1 = 0.0889, wR_2 = 0.1036
largest diff. peak & hole [e $Å^{-3}$]	0.29 and –0.19	0.26 and –0.23	0.241 and –0.306

[a]data common to all structures: T = 173.15 K; λ = 0.71073 Å; diffractometer = Nonius KappaCCD

3. SYNTHESES, REACTIVITY, STRUCTURES, AND DYNAMIC PROPERTIES OF GYROSCOPE LIKE IRON CARBONYL COMPLEXES BASED UPON DIBRIGEHEAD DIARSINE CAGES

3.1 Introduction

Gyroscopes are not normally items that one goes shopping for, but they are ubiquitous albeit hidden partners in everyone's daily lives. As preserved in historic video footage,[82] Steve Jobs unveiled the iPhone 4 against the backdrop of a classical mechanical gyroscope (the actual in phone gyroscope that controls the screen orientation and other functions has an advanced generation design). In view of their many technological applications[6] and the ever increasing emphasis in consumer, industrial, or military devices on miniaturization, several groups have undertaken long term quests for molecular gyroscopes.[2,8,13,28f,83,84] All of these involve assemblies consisting of a "rotator" and "stator",[7] the former being akin to the flywheel of the classical gyroscope.

Our research group has undertaken extensive investigations of dibridgehead diphosphine complexes of the type **I** (Scheme 3-1).[20-25,29,30,84,85] These are accessed in surprisingly high yields via three fold intramolecular ring closing metatheses of bis(phosphine) complexes of the formula *trans*-$ML_y(P((CH_2)_mCH=CH_2)_3)_2$. Both the lengths of the methylene chains that connect the two phosphorus atoms and the sizes of the ancillary ligands (L_y) are easily varied. Many performance characteristics of gyroscopes are maximized when rotational friction or barriers are minimized. Several

barriers to ML_y rotation in **I** have been quantified by NMR,[21,85] and others have been bounded. It can be estimated that some are lower than 6 kcal/mol (25 °C to –100 °C).[20a,b,22a,23,24a,25]

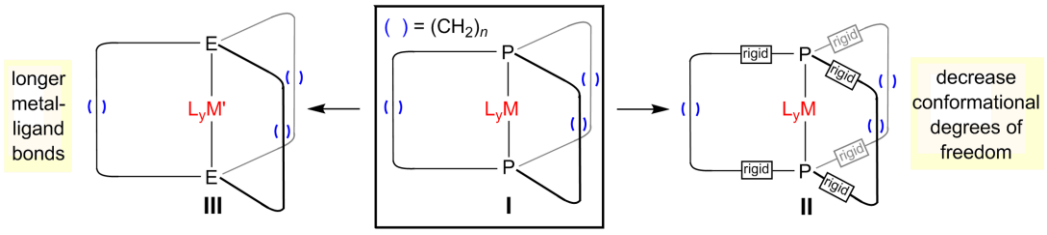

Scheme 3-1. Strategies for minimizing ML_y rotational barriers in gyroscope like complexes.

In previous studies, we have discussed various factors that may allow rotational barriers to be further minimized.[85,22a] One is the replacement of portions of the methylene chains with rigid groups, such that a minimum "horizontal" extension of the macrocycles is guaranteed, as exemplified in **II** (Scheme 3-1). This would disfavor conformations that collapse a macrocycle inwards about the ML_y substituents, decreasing the free space available for their rotation. Another is to increase the "vertical clearance" by replacing atoms on the axis of rotation with those that make longer bonds. This could involve the metal and/or the donor atom, with both possibilities illustrated in **III**.

Accordingly, we became interested in preparing analogs of **I** based upon dibridgehead diarsines as opposed to diphosphines. Bonds between metals and triorganoarsines are typically 4% longer than those involving triorganophosphines,[71] a

difference further manifested in various types of radii associated with atoms.[41] Since rotational barriers have been determined for species **I** with $Fe(CO)_3$, $Fe(CO)_2(NO)^+$, and $Fe(CO)_3(H)^+$ rotators (n = 12, 14),[21,85] it was decided to target analogous iron carbonyl diarsine complexes. In this section, we report on the synthesis and reactivity of these complexes, and their solid state structures and dynamic properties.

3.2 Results

3.2.1 Syntheses of title compounds

Trialkylarsines are often prepared by reactions of Grignard reagents and arsenic trichloride, $AsCl_3$.[86] Accordingly, α,ω-bromoalkenes $Br(CH_2)_mCH=CH_2$ (m = 4, **a**; 5, **b**; 6, **c**) were obtained from commercial sources or prepared as described previously[87,88] and converted to Grignard reagents $BrMg(CH_2)_mCH=CH_2$, which were standardized.[89] As shown in Scheme 3-2, subsequent additions of $AsCl_3$ (0.29-0.31 equiv, 0 °C) gave the new trialkyl arsines $As((CH_2)_mCH=CH_2)_3$ (**1a-c**) as colorless oils in 58-70% yields after silica gel filtration. These compounds and all other new species isolated below were characterized by NMR (^1H, $^{13}C\{^1H\}$) and in most cases microanalysis, as detailed in the experimental section. The iron carbonyl complexes were additionally characterized by IR spectroscopy.

Benzylideneacetone iron tricarbonyl, $(BDA)Fe(CO)_3$,[90] has been employed as a precursor to bis(arsine) iron tricarbonyl complexes *trans*-$Fe(CO)_3(AsR_3)_2$.[91] Thus, as

depicted in Scheme 3-2, THF solutions of (BDA)Fe(CO)$_3$ and the arsines **1a-c** (2.1 equiv) were combined. Chromatographic workups afforded the target bis(arsine) complexes *trans*-Fe(CO)$_3$(As((CH$_2$)$_m$CH=CH$_2$)$_3$)$_2$ (**2a-c**) as moderately air sensitive yellow-orange oils in 66-70% yields. Key spectroscopic data are summarized in Table 3-1.

Table 3-1. Selected NMR and IR data for the new iron arsine complexes.

Complex	$^{13}C\{^{1}H\}$[a]				^{1}H[a]	IR (cm^{-1})[b]	
	$AsCH_2$	$AsCH_2CH_2$	$AsCH_2CH_2CH_2$	CO	Fe*H*	ν_{CO}	ν_{NO}
2a	27.3	24.1	30.8	215.7	-	1851 (s)	-
2b	27.3	24.3	31.0	215.7	-	1853 (s)	-
2c	27.4	24.5	31.5	215.9	-	1855 (s)	-
3a	26.8	24.4	30.8	214.3	-	1851 (s)	-
3b	25.7	23.6	28.5	215.4	-	1849 (s)	-
3c	28.9	25.3	31.7	214.9	-	1859 (s)	-
4a	27.0	22.5	29.2	216.0	-	1842 (s)	-
4b	27.6	23.3	30.0	215.5	-	1847 (s)	-
4c	28.1	24.3	31.0	215.5	-	1859 (s)	-
5a^{+} BF_4^{-}	26.4/26.2	23.3/22.9	28.7/28.3	208.6	-	2017 (s) 1951 (s)	1753 (s)
5b^{+} BF_4^{-}	27.1	23.9	29.3	207.6	-	2019 (s) 1959 (s)	1755 (s)
5c^{+} BF_4^{-}	29.0	25.3	30.9	207.3	-	2021 (s) 1961 (s)	1757 (s)
6a^{+} BAr_f^{-}	26.63/26.56	23.2/22.3	28.9/28.3	207.6, 206.5	–9.4	2065 (w) 2015 (m) 1998 (s)	-
6b^{+} BAr_f^{-}	27.4	23.8	29.3	206.38, 206.36	–9.5	2069 (w) 2021 (m) 1996 (s)	-
6c^{+} BAr_f^{-}	27.9	24.4	30.0	206.5, 205.9	–9.6	2073 (w)[c] 2021 (m) 2004 (s)	-

[a]NMR spectra (δ /ppm) were recorded in $CDCl_3$ at ambient probe temperatures. [b]Oil (**2a**-**b**) or powder (other complexes) film.

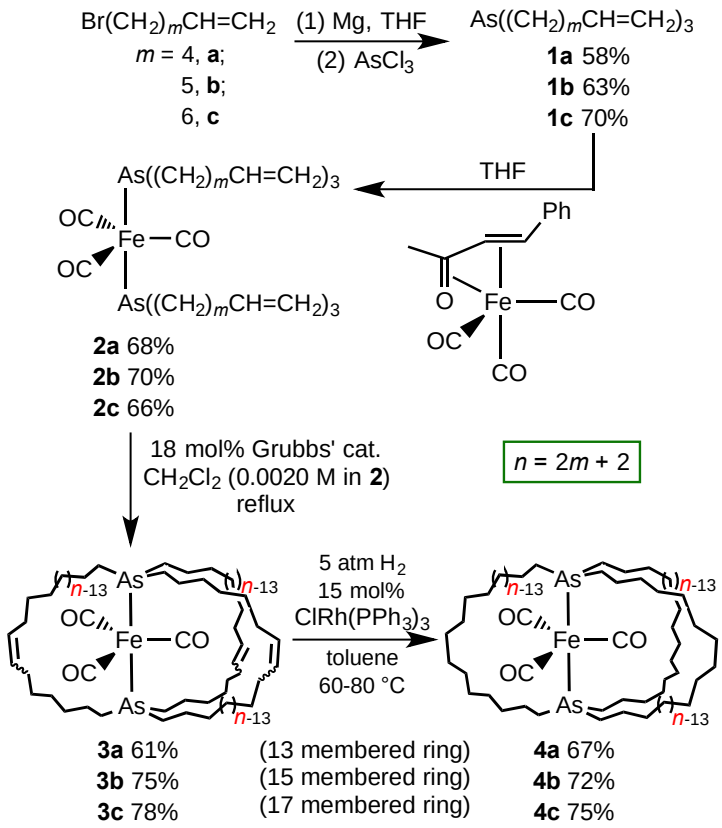

Scheme 3-2. Syntheses of gyroscope like dibridgehead diarsine iron tricarbonyl complexes.

Consistent with precedent for related iron tricarbonyl complexes, **2a-c** exhibited a single strong IR ν_{CO} band (1851-1855 cm^{-1}).[91] The $AsCH_2CH_2CH_2$ ^1H and ^{13}C NMR signals were assigned via 2D spectra. First the $AsC\boldsymbol{H}_2C\boldsymbol{H}_2C\boldsymbol{H}_2$ ^1H NMR signals of **2a**,**c** were identified via $^1H,^1H$ COSY experiments, as exemplified for the latter complex in Figure 3-1. The $As\boldsymbol{C}H_2\boldsymbol{C}H_2\boldsymbol{C}H_2$ ^{13}C signals were then established by $^1H,^{13}C$ HSQC experiments as illustrated in Figure 2.

As shown in Scheme 3-2, ring closing metatheses of **2a-c** were carried out using

Grubbs' catalyst (first generation; 18 mol% or 6 mol%/new C=C, added in portions) in dilute refluxing CH_2Cl_2 to minimize *inter*molecular condensations. After 48 h, aliquots were analyzed by ^1H NMR ($CDCl_3$). As depicted in Figure 3-3, the terminal alkene signals (5.73-5.89/4.88-5.08 ppm, C***H***=C***H***$_2$) could no longer be detected, and peaks for internal C***H***=C***H*** linkages could be observed (5.22-5.52 ppm). Chromatographic workups afforded *trans*-$Fe(CO)_3(As((CH_2)_mCH{=}CH(CH_2)_m)_3As)$ (**3a-c**) as moderately air stable light yellow solids in 61-78% yields. Four C=C isomers are possible (*EEE*, *EEZ*, *EZZ*, *ZZZ*), and **3b**,**c** exhibited multiple ^1H and ^{13}C ***CH*=*CH*** NMR signals. However, **3a** was homogenous, and based upon the diphosphine analog,[21,85] as well as the stereochemistry of ring closing metatheses of other complexes with *trans*-$(H_2C{=}CH)(CH_2)_4PMP(CH_2)_4(CH{=}CH_2)$ linkages,[15,35] was assigned as the *E*,*E*,*E* isomer.

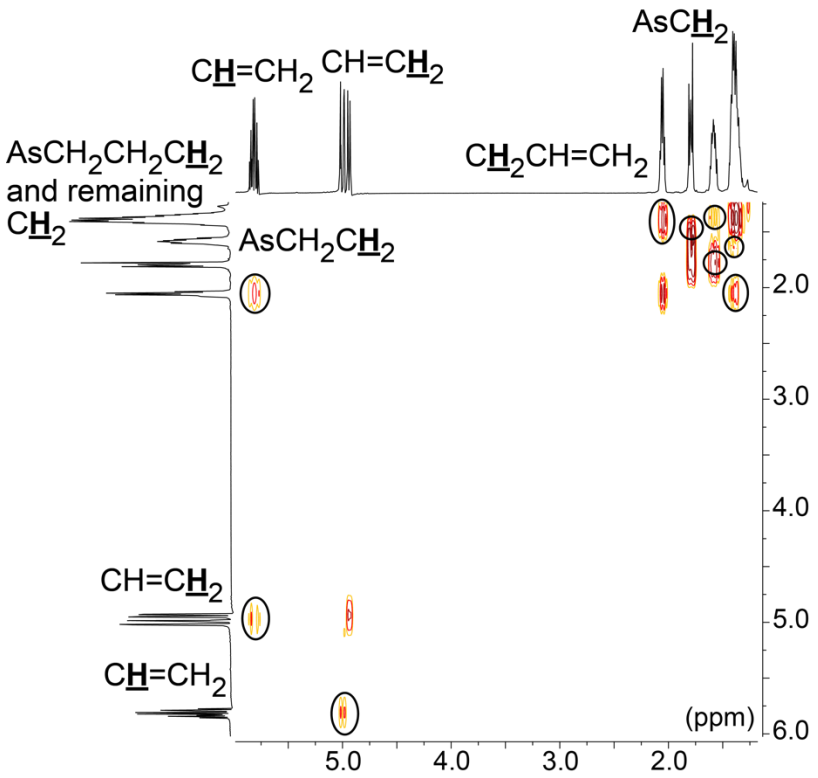

Figure 3-1. $^{1}H,^{1}H$ COSY NMR spectrum of **2c** and attendant signal assignments.

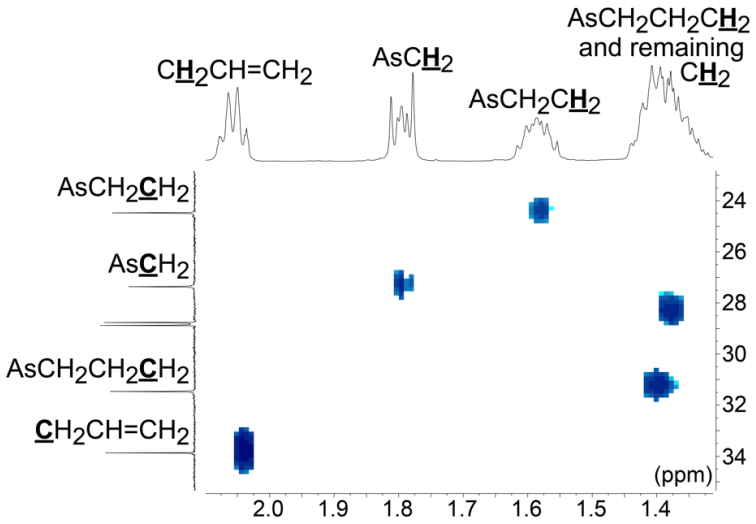

Figure 3-2. $^{1}H,^{13}C\{^{1}H\}$ HSQC NMR spectrum of **2c** and attendant signal assignments.

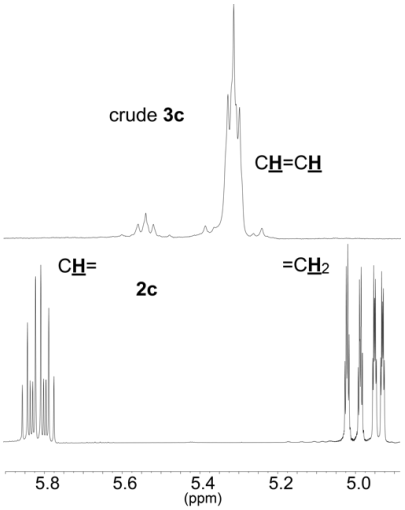

Figure 3-3. ^{1}H NMR spectra (=C***H*** region) of **2c** (bottom) and the crude ring closing metathesis product **3c** (top).

As shown in Scheme 3-2, toluene solutions of **3a-c** and Wilkinson's catalyst ($ClRh(PPh_3)_3$; 15 mol% or 5 mol%/C=C) were treated with H_2 (5 atm, 60-80 °C, 48-72 h). Chromatographic workups afforded the gyroscope like complexes *trans*-$Fe(CO)_3(As((CH_2)_n)_3As)$ (**4a-c**; $n = 2m+2$) of idealized D_{3h} symmetry as off white solids in 67-75% yields. A DSC analysis of **4c** revealed a melting endotherm (160 °C), but no other phase transitions down to –150 °C. In contrast, **4a,b** exhibited second phase transitions at temperatures considerably lower than their melting endotherms (**4a**, 87 °C vs. 133 °C; **4b**, –52 °C vs. 123 °C).

The IR spectra of **4a-c** (Table 3-1) exhibited a single strong ν_{CO} band of progressively increasing frequency (1842 to 1859 cm^{-1}). The $^{13}C\{^{1}H\}$ NMR spectra showed one Fe***C***O signal (215.5-216.0 ppm, $CDCl_3$). As illustrated in Figure 3-4, the As***C***H_2***C***H_2***C***H_2 signals shifted progressively downfield. The assignments for **4a**,**c** (and

E,E,E-**3a**) were made using 2D NMR experiments analogous to those depicted in Figures 3-1 and 3-2.

3.2.2 Reactions

The symmetries of **4a**-**c** are too high for rotational barriers to be measured by typical solution phase variable temperature NMR methods. One obvious remedy is to replace a carbonyl ligand by an isoelectronic and isosteric counterpart, such as a nitrosyl (NO^+) cation. Indeed, bis(arsine) complexes *trans*-$Fe(CO)_3(AsR_3)_2$ have been shown to react with nitrosonium salts NO^+ Z^- to yield cationic dicarbonyl nitrosyl complexes of the formula $[Fe(CO)_2(NO)((AsR_3)_2)]^+$ Z^-.[92] Neutral analogs with thiocarbonyl (CS) ligands would also likely have been easily accessible,[93] but were not pursued due to the larger size of sulfur vs. oxygen.[41]

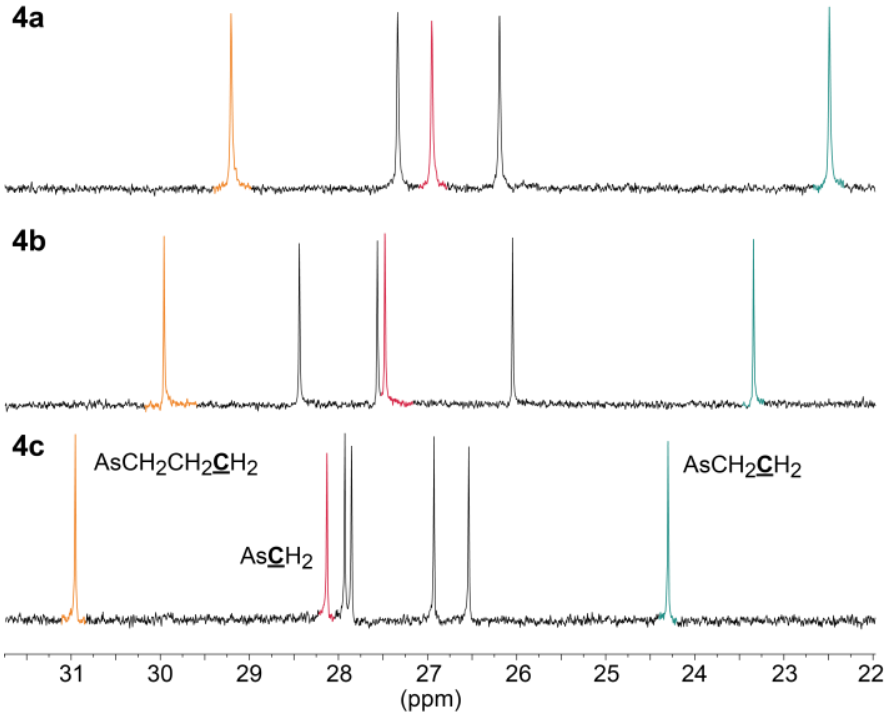

Figure 3-4. Methylene carbon regions of the $^{13}C\{^1H\}$ NMR spectra of **4a-c** (red = As***C***H_2; blue = $AsCH_2$***C***H_2; orange = $AsCH_2CH_2$***C***H_2).

Thus, CH_2Cl_2 solutions of **4a-c** were treated with solid NO^+ BF_4^- (1.2 equiv) as shown in Scheme 3-3. Workups gave the target complexes *trans*-$[Fe(CO)_2(NO)(As((CH_2)_n)_3As)]^+$ BF_4^- (**5a-c**$^+$ BF_4^-) as moderately air sensitive yellow solids in 89-95% yields. The IR spectra of **5a-c**$^+$ BF_4^- (Table 3-1) exhibited weak (2017-2021 cm^{-1}) and strong (1951-1961 cm^{-1}) ν_{CO} bands, as well as a strong ν_{NO} band at lower frequency (1753-1757 cm^{-1}). As was seen with **3a-c** and **4a-c**, the lowest frequencies were found with the smallest macrocycle (**5a**$^+$ BF_4^-).

The $^{13}C\{^1H\}$ NMR spectra of **5a-c**$^+$ BF_4^- exhibited a single ***C***O signal (~207 ppm, $CDCl_3$), upfield from those of **4a-c** (~216 ppm). That of **5a**$^+$ BF_4^- gave two sets of

$As(CH_2)_{n/2}$ signals (2:1 ratio), one for the two methylene chains occupying interstices between CO/NO ligands, and one for the methylene chain occupying the unique interstice between CO/CO ligands (see **IV**, Scheme 3-3). In contrast, those of **5b**,$\mathbf{c}^+$ BF_4^- gave only one set of $As(CH_2)_{n/2}$ signals. This indicates that, in accord with analogous diphosphine complexes,[21,85] $Fe(CO)_2(NO)^+$ rotation is rapid on the NMR time scale at room temperature for **5b**,$\mathbf{c}^+$ BF_4^-, but slow for $\mathbf{5a}^+$ BF_4^-.

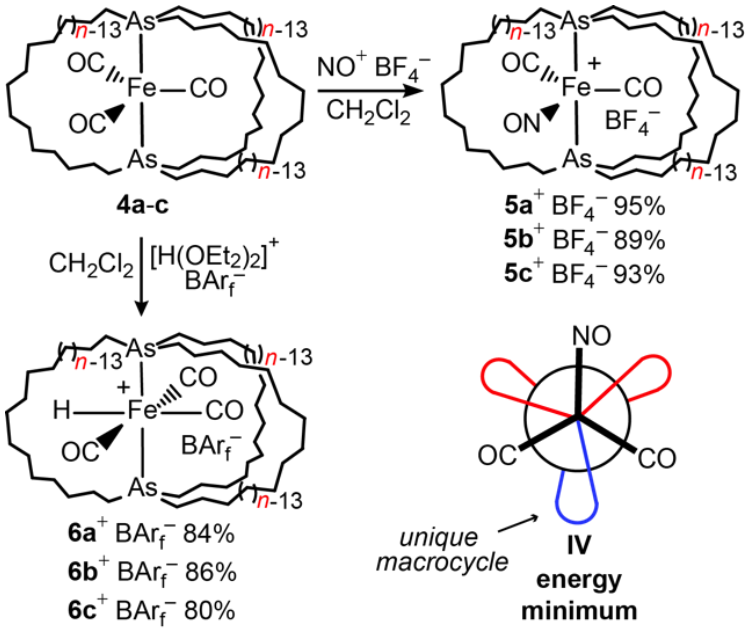

Scheme 3-3. Symmetry lowering reactions of **4a-c**.

Additional derivatives of lower symmetry were sought. The diphosphine analogs of **4a-c**[21,85] as well as related complexes[47] have been protonated by a variety of strong acids to give cationic octahedral tricarbonyl hydride complexes. Thus, **4a-c** and the

oxonium salt $[H(OEt_2)_2]^+$ BAr_f^- (BAr_f^- = $B(3,5\text{-}C_6H_3(CF_3)_2)_4^-$) were combined in CH_2Cl_2.[48] Workups gave the corresponding hydride complexes *mer,trans*-$[Fe(CO)_3(H)(As((CH_2)_n)_3As)]^+$ BAr_f^- (**6a-c**$^+$ BAr_f^-) in 80-84% yields as off white solids.

As summarized in Table 3-1, **6a-c**$^+$ BAr_f^- exhibited three IR ν_{CO} bands, with the intensities increasing with decreasing frequency: one weak (2065-2073 cm^{-1}), one medium (2015-2021 cm^{-1}), and one strong (1996-2004 cm^{-1}).[49] As was seen with the other complexes, the smallest macrocycle (**6a**$^+$ BAr_f^-) generally gave the lowest frequency absorption. The ^1H NMR spectra showed characteristic hydride ligand signals at –9.4 to –9.6 ppm ($CDCl_3$).

The room temperature $^{13}C\{^1H\}$ NMR spectrum of **6a**$^+$ BAr_f^- gave, like that of **5a**$^+$ BF_4^-, two sets of $As(CH_2)_{n/2}$ signals (2:1 ratio). Although this indicates that full $Fe(CO)_3(H)^+$ rotation is slow on the NMR time scale at room temperature, it also requires some dynamic behavior, as otherwise three sets of signals would have been present; these subtleties are analyzed in the discussion section. In contrast, **6b**,**c**$^+$ BAr_f^- gave a single set of methylene signals under analogous conditions. Complexes **6a-c**$^+$ BAr_f^- also exhibited two Fe***C***O signals with a ca. 2:1 area ratio (206.4-206.5, 205.9-207.6), corresponding to the groups *cis* and *trans* to the hydride ligand.

In order to probe the redox behavior of **4a-c**, cyclic voltammograms were recorded under standard conditions in CH_2Cl_2. As summarized in Table 3-2, one

electron oxidations with appreciable reversibilities were observed, as reflected by i_c/i_a values of 0.999 to 0.809. The E° values monotonically decreased from 0.348 to 0.247 V (vs. ferrocene at 0.46 V) with increasing macrocycle size. Under similar conditions, the $NO^+/\cdot NO$ couple has a redox potential of 1.00 V.[45c] Hence, the generation of radical cations derived from **4a-c** (**4a-c**$^{\cdot+}$) during the nitrosations in Scheme 3-3 would be exergonic.

Table 3-2. Cyclic voltammetry data for gyroscope like iron tricarbonyl complexes.[a]

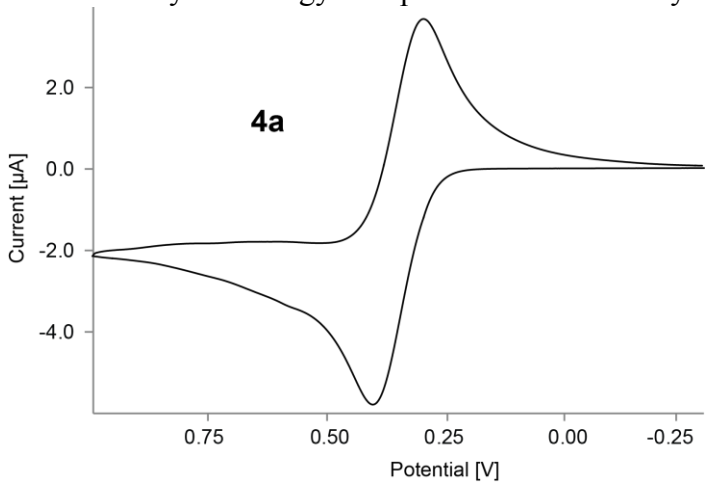

complex	$E_{p,a}$ [V]	$E_{p,c}$ [V]	$E°$ [V]	ΔE [mV]	i_c/i_a
4a	0.402	0.294	0.348	108	0.999
4b	0.400	0.161	0.281	239	0.983
4c	0.311	0.183	0.247	128	0.809

[a]Conditions: 0.0010 M in 0.10 M Bu_4N^+ PF_6^-/CH_2Cl_2, 22 °C ± 1 °C; Pt working and auxiliary electrodes, Ag/AgCl pseudoreference; scan rate, 200 mV/s (data were similar at 100 and 150 mV/s); ferrocene = 0.46 V. All scans were continued to –1.0 V but no additional features were observed.

3.2.3 Molecular structures: primary data

In order to better analyze the steric environments experienced by the rotators within the diarsine cages, crystal structures were sought of as many complexes as possible. Crystals of the tricarbonyl complexes **4a**-**c** and the dicarbonyl nitrosyl complex **5b**$^{+}$ BF_4^- (or solvates thereof) could be grown. X-ray data were collected and the structures were solved as described in the crystallography section. Key metrical parameters are given in Table 3-3.

Table 3-3. Intramolecular and intermolecular distances involving rotator and stator atoms in gyroscope like complexes (Å), and selected bond and torsion angles (°).

Complex	**4a** ·0.5C_6H_{14}	**4b**	**4c**	**5b**$^+$ BF_4^-·2CH_2Cl_2	
				Fe1	**Fe2**
Fe-As[a]	2.30	2.31	2.30	2.36	2.36
FeCO[a]	2.92	2.92	2.93	2.90[b]	2.90[b]
radius of rotator[c]	4.44	4.44	4.45	4.42	4.42
Fe-C_a[d]	5.30	5.76	7.93	6.59	7.14
Fe-C'_a[d]	5.28	5.83	7.93	6.58	6.89
Fe-C_b[d]	5.54	5.62	7.54	6.29	6.66
Fe-C'_b[d]	5.16	5.67	6.71	6.21	6.72
Fe-C_c[d]	4.68	6.35	7.54	6.08	6.34
Fe-C'_c[d]	5.28	6.38	6.71	6.17	6.61
Fe-C_{distal}–vdW[e]	2.98	3.92	5.01	4.38	4.64
Fe-C_{distal}–vdW[f]	3.84	4.68	6.23	4.89	5.44
Fe-$C_{neighbor}$[g]	5.76	6.13	6.01	5.86[h]	5.44[i]
Fe-$C_{neighbor}$–vdW[j]	4.06	4.43	4.31	4.16	3.74
∠ As-Fe-As	178.0	178.2	179.3	178.1	178.22
As($\underline{C}H_2$)$_3$/As($\underline{C}H_2$)$_3$[k]	6.21	6.38	6.29	6.28	6.31
$\underline{C}_a$As-Fe-As$\underline{C}_a$[l]	6.14	6.45	6.32	6.36	6.42
$\underline{C}_b$As-Fe-As$\underline{C}_b$	6.33	6.54	6.43	6.19	6.58
$\underline{C}_c$As-Fe-As$\underline{C}_c$	6.35	6.64	6.43	6.32	6.53
$\underline{C}_a$As-Fe-As$\underline{C}_b$[m]	6.65	6.68	6.71	6.91	6.55
$\underline{C}_b$As-Fe-As$\underline{C}_c$	6.90	6.76	6.72	6.92	6.71
$\underline{C}_c$As-Fe-As$\underline{C}_a$	6.55	6.65	6.71	6.95	6.57
C_a-As-As-C_a[n]	37.6	44.1	37.7	10.9	49.5
C_b-As-As-C_b	38.7	45.6	36.1	10.0	55.4
C_c-As-As-C_c	38.6	56.8	36.1	9.5	54.7
C_a-As-As-C_b[o]	81.6	71.8	83.1	107.3	68.0
C_b-As-As-C_c	112.8	74.5	84.3	110.2	64.2
C_c-As-As-C_a	127.9	67.1	83.1	112.1	68.2
<[As-Fe-As + As-Fe-As][p]	78.4	[q]	[q]	58.3	58.3
<[$Fe(CO)_3$][p]	78.9	[q]	[q]	54.5	54.5

[a]The average distance within the molecule. [b]This represents the average of two FeCO and one FeNO distances, as the carbon and nitrogen atoms could not be distinguished crystallographically. [c]The FeCO distance plus the van der Waals radius of the oxygen atom (1.52 Å). [d]The distance from iron to the two remote carbon atoms of the three macrocycles (a, b, c; the labels are arbitrary except for **4c**, for which c contains the C_2 axis) that are closest to the plane of the rotator (Fe-C_{distal}). [e]The shortest of the previous six distances, minus the van der Waals radius of the carbon atom (1.70 Å). [f]The longest of the previous six distances, minus the van der Waals radius of the carbon atom. [g]The distance from iron to the nearest carbon atom of a neighboring gyroscope like molecule. [h]There is a shorter contact of 5.79 Å involving the chlorine atom of a solvate molecule. [i]There is a shorter contact of 5.39 Å involving a fluorine atom of the BF_4^- anion. [j]The previous entry minus the van der Waals radius of the carbon atom. [k]The distance between planes defined by the three carbon atoms attached to each arsenic atom, taken at the centroid of the three carbon atoms. [l]The distance between the As$\underline{C}H_2$ carbon atoms of each macrocycle. [m]The distance between the As$\underline{C}H_2$ carbon atoms that most closely flank each CO ligand. [n]The C-As-As-C torsion angle within the three macrocycles (a, b, c). [o]The C-As-As-C torsion angle involving carbon atoms that most closely flank each CO ligand (from different macrocycles). [p]Planes used for angle calculations between sets of molecules with parallel As-Fe-As axis. [q]All of the As-Fe-As axes in the lattice are parallel.

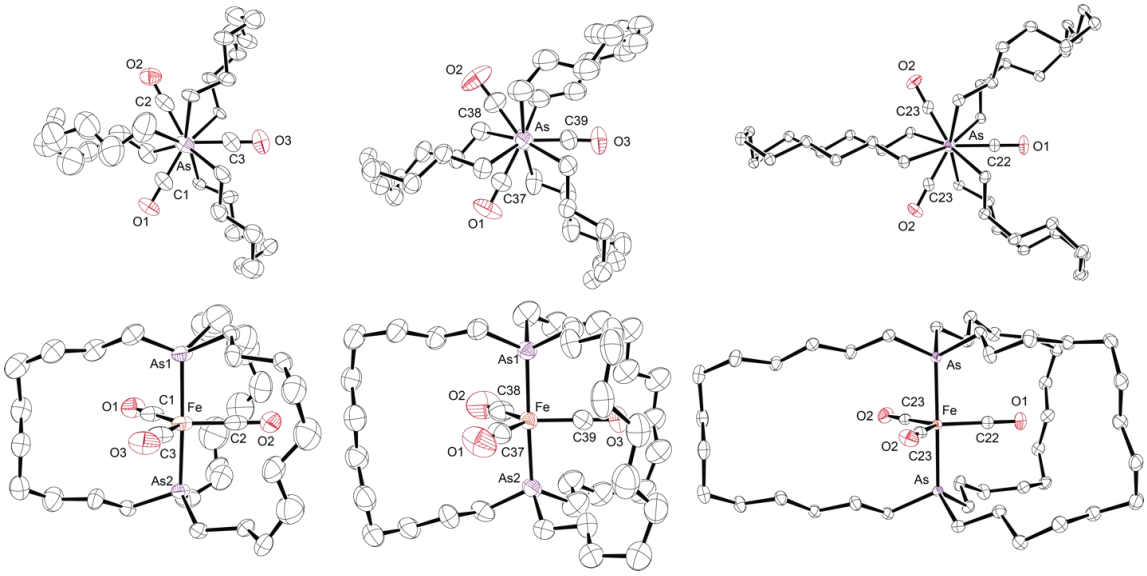

Figure 3-5. Thermal ellipsoid plots (50% probability) of the dominant conformations of **4a-c** (left to right; hexane hemisolvate of **4a** omitted).

Thermal ellipsoid representations of **4a-c** are provided in Figure 3-5. Many of the methylene chains of **4a**,**b** were disordered, and only the dominant conformations are depicted (52:48 and 72:28 occupancy ratios). With **4c**, a C_2 axis passed through one of the Fe-C-O linkages, as seen earlier for the diphosphine analog, which crystallized with an identical conformation.[21,85] The iron-arsenic bonds in **4c** were 4.0% longer than the iron-phosphorus bonds in the analog (2.2954(3) Å vs. 2.2056(5) Å). However, the volume of the unit cell of **4c** was only 0.7% greater (4666.5(10) $Å^3$ vs. 4633.5(3) $Å^3$; space group and *Z* identical).

The crystal structure of $\mathbf{5b}^+$ BF_4^- exhibited two independent molecules in the unit cell (denoted Fe1 and Fe2), both of which are depicted in Figure 3-6. They differed in the macrocycle conformations – i.e., the gauche/anti sequencing of successive four atom units. In both cations, the CO/NO ligands were positionally disordered, so the atom

labels are arbitrary. It has not yet proved possible to crystallize any of the analogous nitrosyl cations in the diphosphine series.

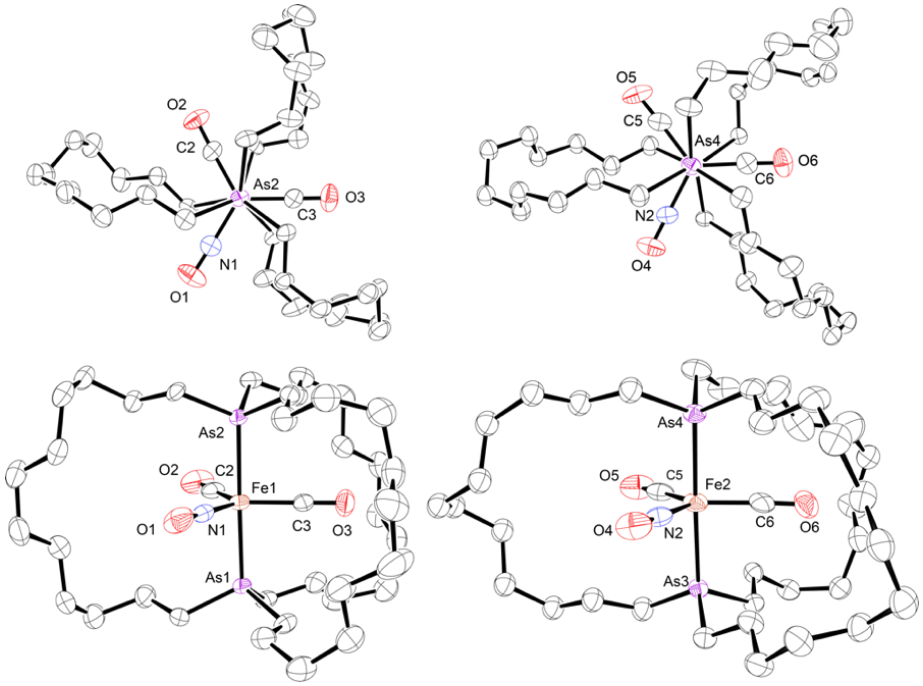

Figure 3-6. Thermal ellipsoid plots (50% probability) of the cations of the two independent molecules of **5b**$^{+}$ BF_4^{-}·$2CH_2Cl_2$ in the unit cell (left, Fe1; right, Fe2).

In **4c**, the substituents along the As-Fe-As axes (CH_2/CO/CH_2) adopted approximately staggered conformations, with C-As--As-C torsion angles of 36.1-37.7° (for carbon atoms from the same macrocycle; Table 3-3). The torsion angles in **4a** were similar (37.6-38.7°), but increased somewhat in **4b** (44.1-56.8°). Interestingly, in one cation of **5b**$^{+}$ BF_4^{-} (Fe1), the corresponding angles decreased to 9-11°, making for nearly eclipsed As-CH_2 linkages. This limit, which has never been approached in diphosphine analogs, is perhaps facilitated by the longer iron-arsenic bonds.

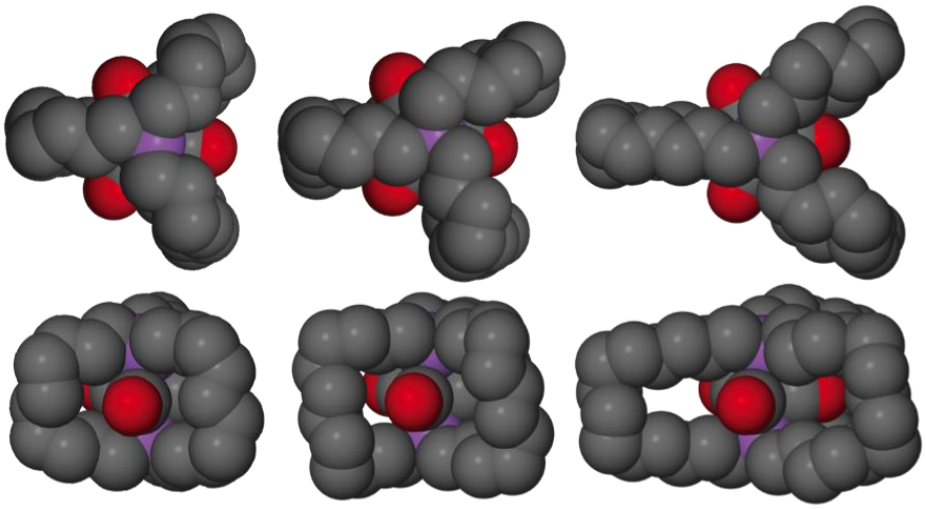

Figure 3-7. Space filling representations of **4a-c** (left to right): side view (bottom) and view along the As-Fe-As axis (top) with solvate molecules and hydrogen atoms omitted.

Space filling representations of **4a-c** are provided in Figure 3-7. When space filling models are used to gauge the feasibility of dynamic processes in organic molecules, it is often found that the hydrogen atoms can be neglected. Thus, **4c** would seem to be an auspicious case for $Fe(CO)_3$ rotation, and **4a** inauspicious. However, Figure 3-8 shows that the apparent interior space within the diarsine cages decreases significantly when the hydrogen atoms are included. It also hints at a slightly more spacious interior domain for $\mathbf{5b}^+$ BF_4^- as compared to **4b**, despite identical macrocycle sizes (further analyses below).

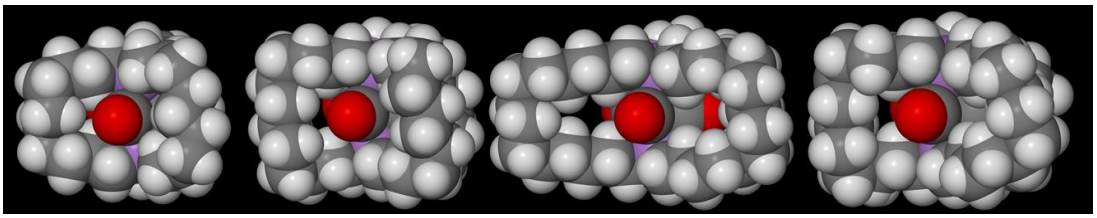

Figure 3-8. Space filling representations of **4a-c** and **5b**$^{+}$ BF_4^- (left to right) with hydrogen atoms included and any solvate molecules and anions omitted.

No direct structural comparisons of bis(phosphine) and bis(arsine) iron tricarbonyl complexes have heretofore been reported.[71] However, the bis(triphenylphosphine) adduct *trans*-$Fe(CO)_3(PPh_3)_2$ (**7**) has been structurally characterized.[94] Thus, the bis(triphenylarsine) analog *trans*-$Fe(CO)_3(AsPh_3)_2$ (**8**) was prepared by a literature procedure[91] and crystallized as described in the experimental section. The structure was determined analogously to the other complexes. As shown in Figure 3-9, the conformations of **7** and **8** are quite similar, despite different solvation levels and space groups. The iron-arsenic bonds in **8** (2.287(8) Å) are 3.1% longer than the iron-phosphorus bonds in **7** (2.218(1) Å). The CH_2/CO/CH_2 substituents along the As-Fe-As axis of **8** are nearly perfectly staggered, resulting in C-As--As-C torsion angles of 8.0-11.5°.

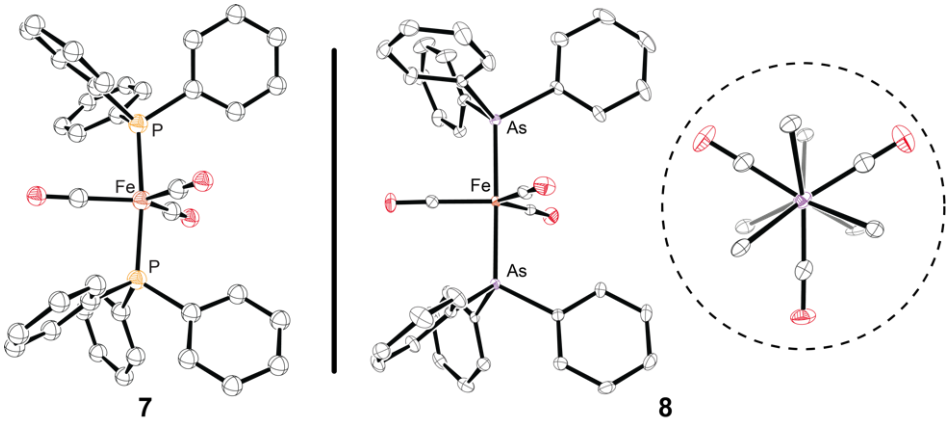

Figure 3-9. Thermal ellipsoid plots (50% probability) of *trans*-$Fe(CO)_3(PPh_3)_2$ (**7**; left) and *trans*-$Fe(CO)_3(AsPh_3)_2$ (**8**; middle/full view and right/Newman type projection down the As-Fe-As axis).

3.2.4 Molecular structures: derived quantities

How can one conceptualize the void space available to the rotators within the gyroscope cages in the preceding structures? The semiquantitative treatment in Figure 3-10 has been developed in previous work in this series.[85,20b,22a] The initial step is to determine the radius of the rotator. This is calculated by taking the average iron-oxygen distance[40] and adding the van der Waals radius of oxygen (1.52 Å).[41] The resulting values for **4a-c** and **5b**$^+$ BF_4^- are given in Table 3-3 and as expected span a narrow range (4.42 Å to 4.45 Å).

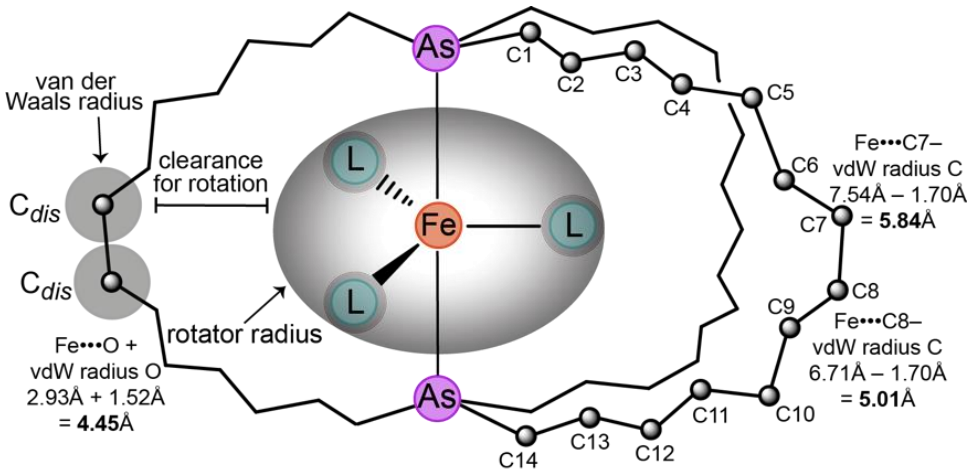

Figure 3-10. Spatial relationships involving the iron atom, CO ligands, and $(CH_2)_{14}$ bridges in **4c** (see text and Table 3-3; vdW = van der Waals).

The next step is to calculate the "horizontal clearance" available to the rotator. One first determines the distances from the iron atom to the remote carbon atoms of the three methylene chains. For an $As(CH_2)_{14}As$ linkage, the remote carbon atoms would (in the absence of a distorted macrocycle conformation) be C7 and C8. The van der Waals radius of carbon (1.70 Å) is then subtracted from these two distances.[41] We have usually employed the shortest of the six values thus calculated (see Fe-C_{distal}-vdW, Table 3-3).[43] For **4c**, this is 5.01 Å – which is significantly greater than the radius of the rotator (4.45 Å). However, one could argue for an alternative approach, in which the average of the six values is employed to better account for the conformational mobility of the macrocycles (this yields a greater clearance).

In the case of **4a**, the horizontal clearance is much less than the radius of the rotator (2.98 Å vs. 4.44 Å). This suggests a prohibitive barrier to $Fe(CO)_3$ rotation, and is in accord with the NMR data described above and below. With **4b** and **5b**$^+$ BF_4^-,

which share the same macrocycle size, the horizontal clearances are >10% greater for the latter (**4b**: 3.92 Å; **5b**$^{+}$ BF_4^{-}: 4.38 Å/ Fe1, 4.64 Å/Fe2). While a rationale is not obvious at this time, the solvate molecules and counter anion abut the methylene chains of the cationic complex. When the distances to all six remote carbon atoms are averaged, the values increase, and exceed the radius of the rotator in both independent molecules of **5b**$^{+}$ BF_4^{-} (4.62 Å and 5.03 Å; **4b**, 4.24 Å).

3.2.5 Lattice analyses

The crystal lattices of the preceding complexes have been analyzed with respect to the rotator of one molecule and the nearest non-hydrogen atoms of neighboring molecules. Specifically, the distances from iron to these nearest atoms were calculated and the van der Waals radius of latter (carbon unless noted) subtracted. The resulting intermolecular clearances are denoted Fe-$C_{neighbor}$–vdW and are summarized in Table 3-3. Of special significance are complexes where these values are greater than the radius of the rotator. Such systems would show the most promise for amphidynamic behavior[8a,b] – i.e., rotation in the solid state.

With **4b**,**c**, the intermolecular clearances are quite similar (4.43/4.31 Å) and comparable to the radii of the rotators (4.44/4.45 Å). However, as shown in Figure 3-11, the nearest carbon atom of a neighboring molecule of **4c** (C11) is considerably removed from the plane of the rotator. The next nearest carbon atom (C14) lies much closer to the plane of the rotator, and provides a somewhat greater clearance (4.48 Å vs. 4.31 Å).

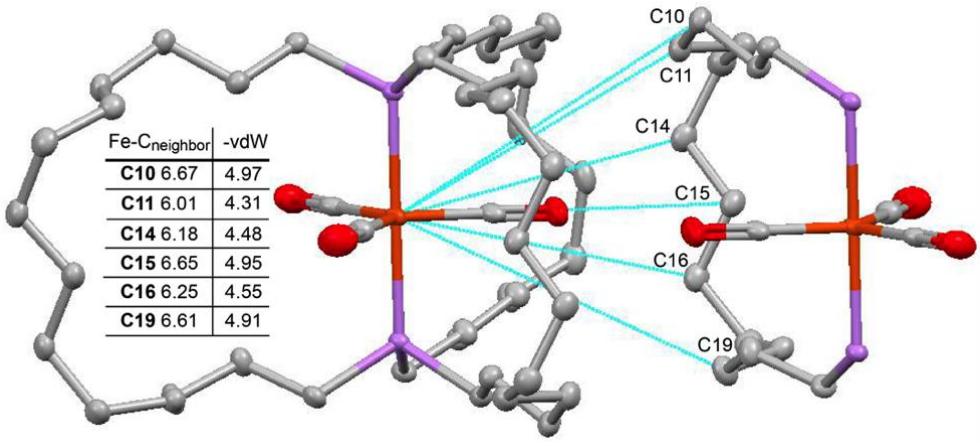

Fe-$C_{neighbor}$	-vdW
C10 6.67	4.97
C11 6.01	4.31
C14 6.18	4.48
C15 6.65	4.95
C16 6.25	4.55
C19 6.61	4.91

Figure 3-11. Distances from the iron atom of crystalline **4c** to the six nearest atoms of a neighboring molecule.

With **4a**, the clearance is ca. 10% less than the radius of the rotator (4.06 Å vs. 4.44 Å), although rotation in this complex is prohibited by the lengths of the methylene chains alone. The two independent molecules of **5b**$^{+}$ BF_4^- also exhibit clearances that are less than the radius of the rotator (4.16 and 3.74 Å vs. 4.42 Å). Furthermore, there are additional short contacts involving a chlorine atom of a solvate molecule and a fluorine atom of the BF_4^- anion (5.70/5.39 Å or 4.04/3.92 Å after subtracting the van der Waals radius of chlorine/fluorine).

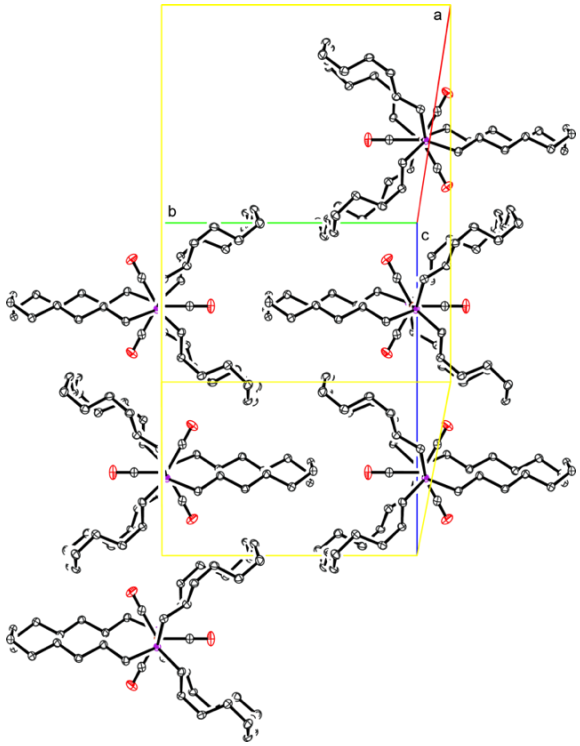

Figure 3-12. The crystal lattice of 4c viewed with the As-Fe-As axes perpendicular to the plane of the paper.

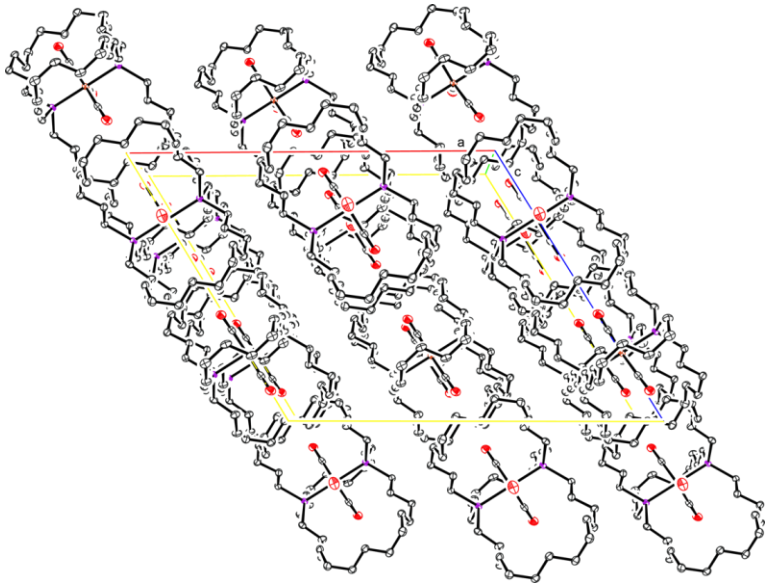

Figure 3-13. The crystal lattice of **4c** viewed along the b axis.

As shown in Figures 3-12 and 3-13, the molecules in the crystal lattice of **4c** pack in well-defined layers with the As-Fe-As axes parallel. Between the layers, the As-Fe-As axes are slightly offset. Within a layer, the molecules exhibit two orientations (Figure 3-12). One carbonyl oxygen atom of each rotator is directed towards the middle CH_2-CH_2 linkage of a seventeen membered macrocycle of an adjacent molecule. The other two are directed more towards the center of a macrocycle of an adjacent molecule. This packing motif is identical with that of the diphosphine analog reported previously.[21,85]

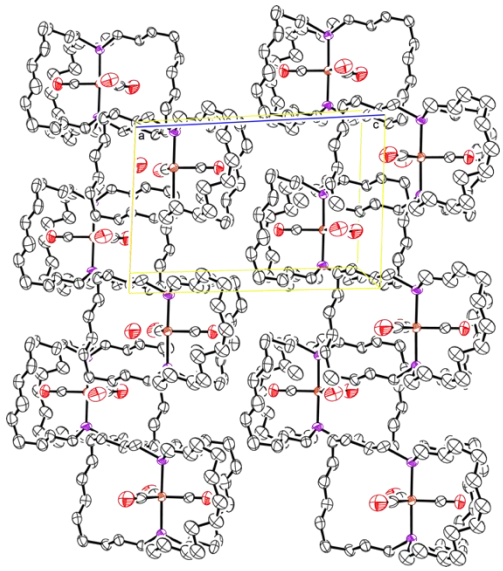

Figure 3-14. The crystal lattice of **4b** viewed along the b axis.

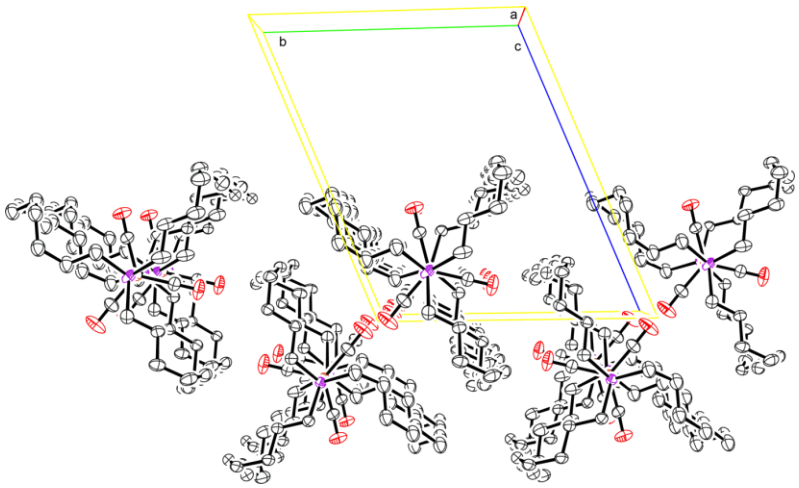

Figure 3-15. The crystal lattice of **4b** viewed along the a axis.

As shown in Figure 3-14, the lattice of **4b** exhibits stacks of molecules, all of which have parallel As-Fe-As axes. The molecules in adjacent stacks are vertically offset from each other. When the stacks are viewed from above (see Figure 3-15), the rotators are eclipsed within a stack and orient antiparallel with respect to adjacent stacks. In contrast to **4b**,**c**, the lattice of **4a** features two sets of molecules with parallel As-Fe-As axes, but with non-parallel relationships between the sets. The planes defined by grouping axes from each set intersect with an angle of 78.4°. As depicted in Figure 3-16, each set of independent cations in the lattice of $\mathbf{5b}^{+}$ BF_4^{-} exhibits parallel As-Fe-As axes. However, there is again a non-parallel relationship between the two sets, with a 58.3° angle between the planes of the axes.

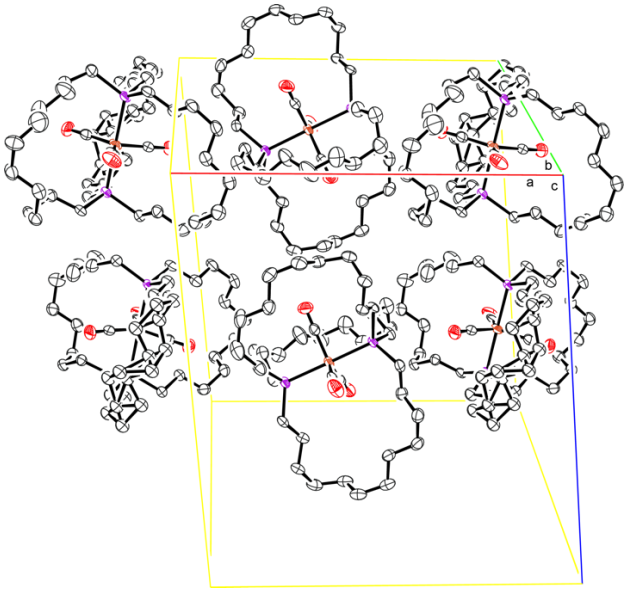

Figure 3-16. The crystal lattice of **5b**$^{+}$ BF_4^{-} viewed along the b axis with solvate molecules and anions omitted.

3.2.6 Rotational barriers

The less symmetrical nitrosyl and hydride complexes **5a-c**$^{+}$ BF_4^{-} and **6a-c**$^{+}$ BAr_f^{-} were probed by variable temperature $^{13}C\{^{1}H\}$ NMR. As shown in Figures 3-17 and in Appendix A, spectra of **5b**$^{+}$ BF_4^{-} were recorded in CD_2Cl_2 at progressively lower temperatures (35 °C to –60 °C). As documented for the diphosphine analogs,[21,85] the chemical shifts of most methylene carbon signals were temperature dependent. This presumably reflects changes in relative populations of macrocycle conformations (each distinguished by a unique set of chemical shifts) as a result of differential entropies.

Table 3-4. Activation parameters for $Fe(CO)_2(NO)^+$ or $Fe(CO)_3(H)^+$ rotation as determined by variable temperature NMR.

Complex	$\Delta H^{\ddagger}$ (kcal/mol)	$\Delta S^{\ddagger}$ (eu)	$\Delta G^{\ddagger}_{298K}$ (kcal/mol)	$\Delta G^{\ddagger}_{383K}$ (kcal/mol)
5a$^+$ BF_4^-	-	-	-	>19.4
5b$^+$ BF_4^-	7.7	–22.1	14.2	16.2
5b-P$_2$ $^+$ BF_4^- [a]	8.3	–28.4	16.7	19.2
5c-P$_2$ $^+$ BF_4^- [a]	9.5	–6.5	11.4	11.9
6a$^+$ BAr_f^-	-	-	-	>18.9
6b$^+$ BAr_f^-	5.4	–22.7	12.2	14.1
6b-P$_2$ $^+$ BAr_f^- [a] [a]	6.1	–23.5	13.0	15.1

[a] P_2 denotes the diphosphine analog.[8]

The $AsCH_2\boldsymbol{C}H_2$ signal broadened and decoalesced as depicted in Figure 3-17 (left; additional signals are shown in Appendix A). The line shapes were simulated using gNMR[51] (red traces) and the rate constants determined at each temperature. An Eyring plot utilizing these rate constants (Figure 3-18, blue) afforded $\Delta H^{\ddagger}$, $\Delta S^{\ddagger}$, and $\Delta G^{\ddagger}_{298K}$ values of 7.7 kcal/mol, –22.1 eu, and 14.2 kcal/mol (Table 3-4) for the process rendering the CH_2 signals equivalent. In analogous studies of the diphosphine analogs, mechanisms involving ligand dissociation were considered, but could be excluded based upon phosphorus coupling and other criteria.[21,85] Hence, signal coalescence was attributed to rotation of the $Fe(CO)_2(NO)^+$ moiety of **5b**$^+$ BF_4^-. As noted above, the horizontal clearance available to the rotator in crystalline **5b**$^+$ BF_4^- (Fe-C_{distal}–vdW,

Table 3-3; 4.38-4.64 Å) is comparable to the radius of the rotator (4.42 Å).

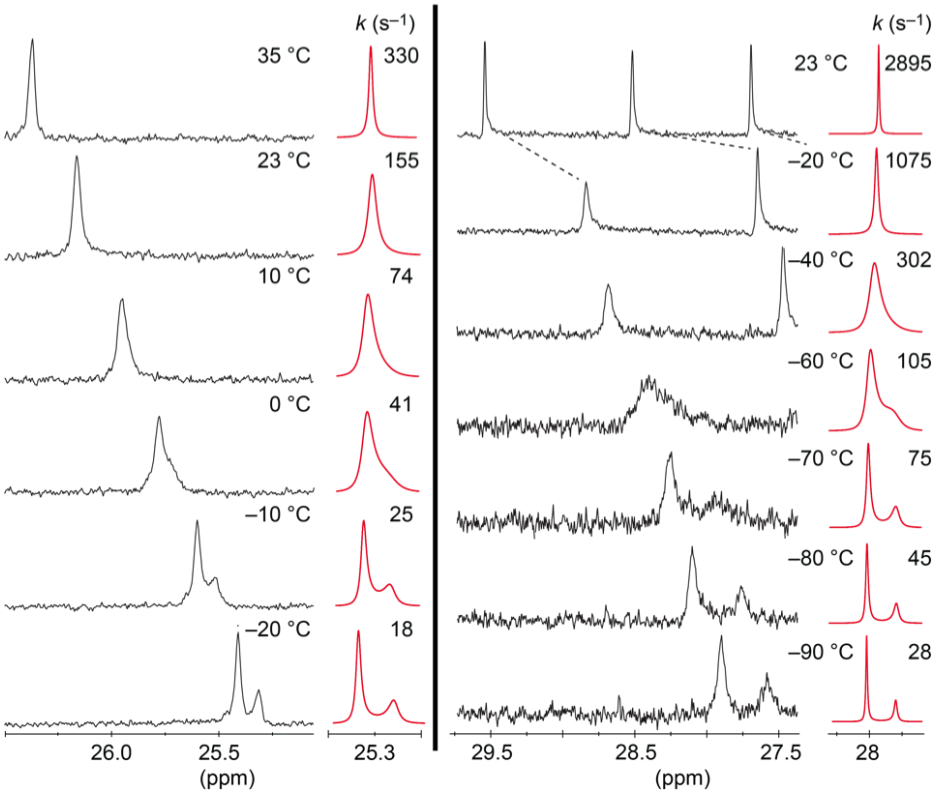

Figure 3-17. Partial $^{13}C\{^{1}H\}$ NMR spectra of **5b**$^{+}$ BF_4^- (CD_2Cl_2, left) and **6b**$^{+}$ BAr_f^- (CD_2Cl_2, right) as a function of temperature. Each spectrum is paired with simulated line shapes for the signals of interest (red).

A similar experiment was conducted with the octahedral hydride complex **6b**$^{+}$ BAr_f^- (Figures 3-17 and Appendix A), The $AsCH_2CH_2\boldsymbol{C}H_2$ signal (among others) decoalesced, and an analogous treatment of the data gave $\Delta H^{\ddagger}$, $\Delta S^{\ddagger}$, and $\Delta G^{\ddagger}_{298K}$ values of 5.4 kcal/mol, –22.7 eu, and 12.2 kcal/mol, as summarized in Table 3-4. Based upon additional results involving the diphosphine analogs,[85] the coalescence was attributed to

rotation of the $Fe(CO)_3(H)^+$ moiety.

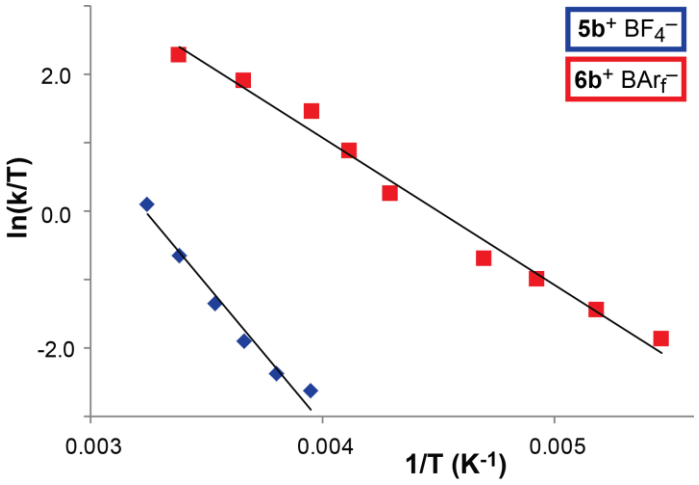

Figure 3-18. Eyring plots involving rate constants for the process that renders the $(CH_2)_{12}$ bridges of **5b**$^+$ BF_4^- and **6b**$^+$ BAr_f^- equivalent.

Solutions of the larger macrocycles **5c**$^+$ BF_4^- and **6c**$^+$ BAr_f^- (CD_2Cl_2) were similarly cooled to –90 °C or below ($CDFCl_2$[50]). As exemplified in Appendix A, only line broadening (substantial in $CDFCl_2$) was observed. Hence, the rotational barriers for these complexes must be much lower than those of **5b**$^+$ BF_4^- and **6b**$^+$ BAr_f^-, as would be intuitively expected.

The smaller macrocycles **5a**$^+$ BF_4^- and **6a**$^+$ BAr_f^- both exhibited two sets of As($\boldsymbol{C}H_2)_{n/2}$ ^{13}C NMR signals at room temperature, as exemplified for the former in Figure 3-19 (CD_2Cl_2) and further illustrated in Appendix A. Solutions of C_6D_5Cl were warmed to 110 °C, but no coalescence was observed. As can be easily derived (see SI), this allows lower limits of 19.4 kcal/mol and 18.9 kcal/mol ($\Delta G^{\ddagger}_{383K}$) to be set for the

rotational barriers. These are summarized in Table 3-4, together with $\Delta G^{\ddagger}_{383K}$ values for the other complexes.

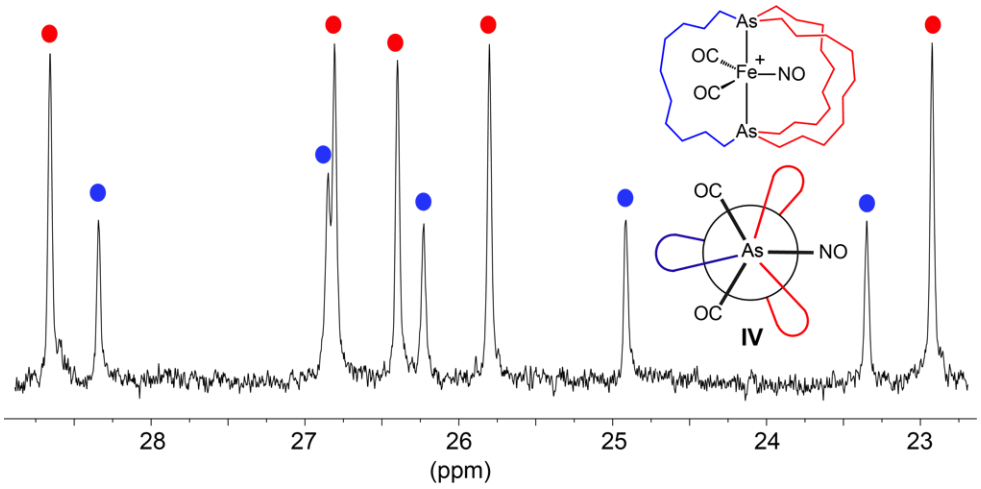

Figure 3-19. Partial $^{13}C\{^{1}H\}$ NMR spectrum of **5a**$^{+}$ BF_4^- (CD_2Cl_2) illustrating the two sets of methylene carbon signals in a ca. 2:1 ratio.

3.3 Discussion

3.3.1 Syntheses and reactions of gyroscope like complexes

Scheme 3-2 establishes that trigonal bipyramidal gyroscope like iron tricarbonyl complexes with dibridgehead diarsine stators (**4a-c**) can be accessed similarly to the diphosphine analogs reported earlier.[21,85] The overall yields are comparable (41-59% vs. 50-64%), and higher than those obtained via ring closing metatheses of related square planar and octahedral complexes.[20,22-25] This has been attributed to a conformational preference for staggered alkyl/CO/alkyl As-Fe-As or P-Fe-P substituents in precursors of the type **2a-c**.[21,85] This enforces a *syn* relationship between the $(CH_2)_mCH{=}CH_2$ groups

that must react with each other, as can easily be visualized with the arsenic-carbon bonds in the crystal structure of the model bis(arsine) complex **8** (right view, Figure 3-9).

The nitrosylations and protonations to give the cationic complexes **5a-c**$^+$ BF_4^- and **6a-c**$^+$ BAr_f^- also have abundant precedent with the diphosphine analogs, as well as other iron complexes. The former reaction is believed to involve an initial electron transfer to give the cation radical **4a-c**$^{\cdot+}$ BF_4^- and radical ·NO. As diagrammed earlier,[85] there are several possible ways that this radical pair could collapse to give the product. Table 3-2 shows that **4a-c** are 0.043-0.067 V easier to oxidize than the corresponding diphosphines ($E°$ 0.406, 0.324, 0.314 V).[85] The electrochemistry of *trans*-$Fe(CO)_3(AsPh_3)_2$ (**8**), *trans*-$Fe(CO)_3(PPh_3)_2$ (**7**) and the tetracarbonyl analogs has previously been studied.[95] These arsine complexes are also more easily oxidized than their phosphine counterparts. Furthermore, at platinum electrodes, the gyroscope like complexes **4a-c** give much more reversible couples than **8**.

Various electronic effects appear to be correlated to the macrocycle size. For example, **4c** is ca. 0.1 V thermodynamically easier to oxidize than the smaller macrocycle **4a**. This suggests that the diarsine ligand in the former is a stronger σ donor and/or a weaker π acceptor. On the other hand, as noted above and summarized in Table 3-1, the smaller macrocycles (**4a**, **5a**$^+$ BF_4^-, **6a**$^+$ BAr_f^-) consistently exhibit the lower ν_{CO} and ν_{NO} values. Since this would imply the opposite electronic trend (smaller macrocycle stronger σ donor and/or weaker π acceptor), we tentatively ascribe this to a steric effect of the smaller cages on the vibrational frequencies.

3.3.2 Rotational barriers

All rotational barriers that have been determined or bounded for the dibridgehead diarsine complexes in this section or the diphosphine analogs are summarized in Table 3- 4. The barriers are always lower for the diarsine complexes. There are no significant differences in the "horizontal clearances" associated with the diarsine and diphosphine complexes. Hence, the reduced barriers can be attributed to enhanced "vertical clearances" arising from the longer iron-arsenic vs. -phosphorus bonds, in accord with our original thesis (Scheme 3-1).

Complexes **4a-c** and **5a-c**$^{+}$ BF_4^- are characterized by *three* fold rotational barriers, with three energy maxima and three energy minima as the rotators move through 360°. In the transition states, which can be represented by **X** in Figure 3-20, the three ligands on the rotators simultaneously pass through the three macrocycles. In analyzing the difference between **5b**$^{+}$ BF_4^- and the diphosphine analog, what counts is the "fatness" of the ligands on the rotators. This would be *twice* the van der Waals *radius* of the largest atom. Both carbon and nitrogen atoms have greater van der Waals radii than oxygen atoms (1.70 Å and 1.55 Å vs. 1.52 Å). When both CO and NO ligands are present, the former will be "fatness determining" (3.40 Å vs. 3.10 Å diameters).

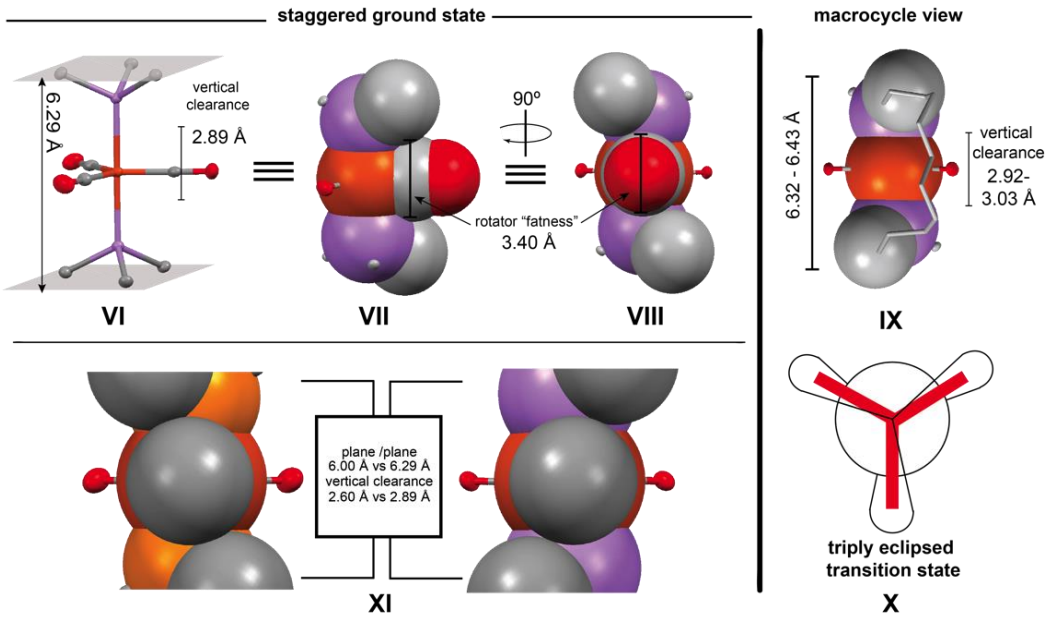

Figure 3-20. Crystallography derived relationships between atoms in **4c** relevant to vertical clearance of the rotator. **VI**: separation of planes defined by the As***C***H_2 carbon atoms. **VII** and **VIII**: as in **VI**, but with selected atoms at van der Waals radii (e.g., the As***C***H_2 carbon atoms that most closely flank a CO ligand, which are from different macrocycles). **IX**: relationship of the two As*C*H_2 carbon atoms within a macrocycle. **X**: Newman type projection of transition state in which all three CO ligands pass between As***C***H_2 carbon atoms from the same macrocycle. **XI**: comparison of van der Waals interactions in crystalline **4c** (right) with those in the diphosphine analog (left, orange atoms).

In order to best visualize these trends, we focus on the diarsine and diphosphine complexes with the most comparable crystallographic data, as opposed to two for which barriers have actually been quantified. This would be the tricarbonyl complex **4c** and the diphosphine analog, in which the macrocycles adopt identical solid state conformations (see Figure 3-5). In Figure 3-20, the spatial relationships between the CO ligands and C-As-Fe-As-C linkages of **4c** are examined. First, planes that contain the three methylene carbon atoms on each donor atom are defined. As shown in **VI**, these are parallel and

separated by 6.29 Å, vs. 6.00 Å in the diphosphine analog. When the van der Waals radii of two carbon atoms are subtracted, vertical clearances of 2.89 Å and 2.60 Å are obtained.

The distances between the $AsCH_2$ carbon atoms within each macrocycle can also be considered. These are the moieties through which the rotating ligands must "squeeze" (**X**), and one perspective is provided in **IX**. The $AsCH_2/AsCH_2$ distances range from 6.32 Å to 6.43 Å, as compared to 6.02 Å to 6.13 Å in the diphosphine analog. These are slightly greater than the plane-plane separations, as would be expected since the vectors that connect the atoms are not perpendicular to the plane. When the van der Waals radii of two carbon atoms are subtracted, a vertical clearance of 2.92-3.03 Å (**4c**) is obtained.

This analysis can be repeated using the $AsCH_2$ carbon atoms that most closely flank each CO ligand in the crystal. As can be gleaned from the top perspectives in Figure 3-5, these arise from different macrocycles, and are represented in **VII** and **VIII** (Figure 3-20). The carbon-carbon distances here are somewhat greater: 6.71-6.72 Å vs. 6.42-6.46 Å for the diphosphine analog. Of course, these do not represent transition states, but rather the minima in the crystal, meaning that all of the atoms have defined positions. Thus, a portion of **VIII** is expanded in Figure 3-20, and presented side by side with the diphosphine analog for a direct visual comparison (see **XI**). A discerning eye will detect slightly more congestion in the latter.

As noted above, there are some subtleties that attend the rotation of the $Fe(CO)_3H^+$ moieties in the octahedral hydride complexes **6a-c**$^+$ BAr_f^-. First, these constitute twelve fold rotational barriers, with twelve maxima and twelve minima as the

$Fe(CO)_3H^+$ units move through 360°. All minima are depicted in Figure 3-21 (**XII-XXIII**). The corresponding maxima differ by 15° and feature a single eclipsing interaction, as exemplified by **XXIV-XXVI** in Figure 3-21. There have been extensive studies of rotational processes in organic molecules, and it is well known that higher order barriers tend to have much lower activation energies than lower order barriers (for substituents of comparable sizes).[96] Key factors in this trend are as follows: (1) there are fewer eclipsing interactions in the transition states of systems with higher order barriers (e.g., three for **X** in Figure 3-20 vs. one for **XXIV-XXVI** in Figure 3-21); (2) there is additional ground state strain in systems with higher order barriers (e.g., two ligands are nearly eclipsed with the macrocycles in **XII-XXIII**, per the 15° idealized torsion angles). Taken together, these factors compress the energy differences between maxima and minima in systems with higher order barriers.

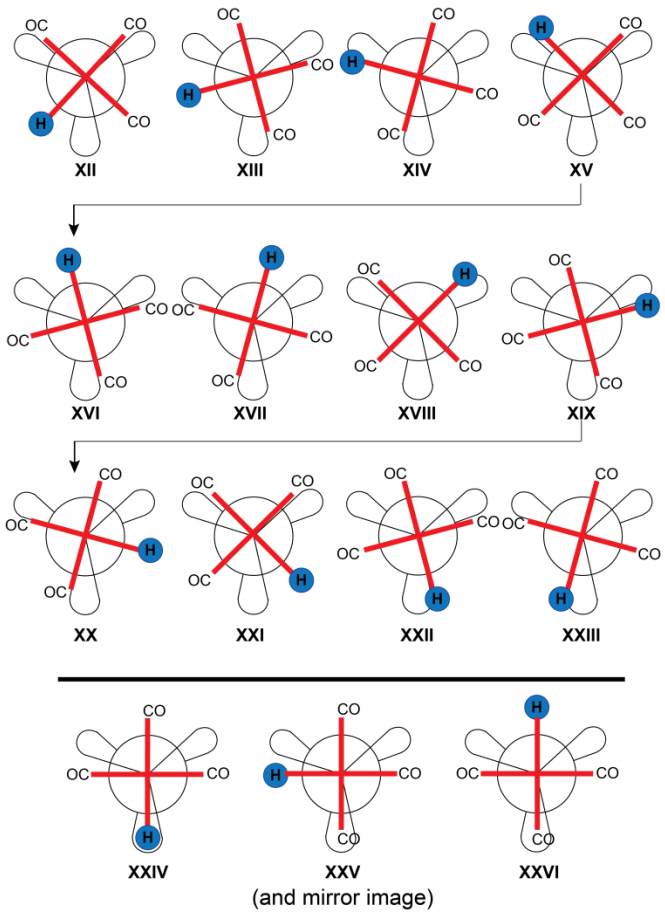

Figure 3-21. Newman type projections of energy minima as the $Fe(CO_3H^+$ moieties in **6a-c**$^+$ BAr_f^- are rotated through 360° (**XII-XXIII**), and three types of energy maxima (**XXIV**, **XXV**, **XXVI**).

Thus, it is intuitively plausible that **6b**$^+$ BAr_f^- and the diphosphine analog exhibit lower rotational barriers than **5b**$^+$ BF_4^- and the diphosphine analog (Table 3-4, $\Delta G^{\ddagger}_{298K}$: 12.2 and 13.0 kcal/mol vs. 14.2 and 16.7 kcal/mol). A further issue involves the number of sets of $As(CH_2)_{n/2}$ ^{13}C NMR signals observed at the low temperature limits for **6a**,**b**$^+$ BAr_f^-. Given the symmetries of the individual minima **XII-XXIII**, three

(1:1:1) might have been expected, as opposed to the two (2:1) that were found. This is easily rationalized by considering any of several pairs of structures equivalent to the pseudo mirror images **XIV** and **XV**. In order for these to interconvert, only a small hydride ligand need pass through a macrocycle (see **XXIV**) – a process that should have a much lower barrier than for a CO ligand (see **XXV** or **XXVI**). Accordingly, the former remains fast on the NMR time scale at the low temperature limit. Similar phenomena have been observed with square planar gyroscope like complexes that are substituted with one large and one small ligand.[20c,23,24] Also, the 1:1:1 signal pattern has been observed in octahedral gyroscope like complexes with larger ligand sets.[24a,73]

Several related matters merit a brief discussion. First, the negative $\Delta S^{\ddagger}$ values for $Fe(CO)_2(NO)^+$ or $Fe(CO)_3(H)^+$ rotation in **5b**$^+$ BF_4^- and **6b**$^+$ BAr_f^- (Table 3-4: –22.1 to –22.7 eu) are consistent with correlated changes in macrocycle conformations necessary to minimize the steric repulsion associated with the eclipsing interactions in the transition states **X** and **XXIV** (Figures 3-20 and 3-21). Second, in order to render the methylene ^{13}C NMR signals of **5b**$^+$ BF_4^- equivalent, the $Fe(CO)_2(NO)^+$ moiety need only rotate by 240° (all ***C***H_2 groups must exchange between CO/NO and CO/CO environments). In contrast, the analogous coalescence with **6b**$^+$ BAr_f^- requires that $Fe(CO)_3(H)^+$ undergo a 330° rotation (from **XII** to **XXIII**, Figure 3-21). Thus, the corresponding rate constants refer to differing arcs, and in neither case a full 360° turn. This distinction can be important in calculating other quantities, such as angular momentum, upon which many properties of gyroscopes depend.[18] Finally, preliminary

^{13}C CP/MAS measurements with **4c** show that the $Fe(CO)_3$ moiety undergoes rapid rotation in the solid state, as previously noted for the diphosphine analog.[97] These data will be incorporated into a more detailed study that includes new complexes that will be described in a subsequent report.[73]

3.3.3 Pursuit of molecular gyroscopes

The preceding data have shown that when the iron-phosphorus bonds in gyroscope like molecules of the type **I** (Scheme 3-1) are replaced by iron-arsenic bonds, the rotational barriers of the rotators are significantly reduced (Table 3-4). This can be ascribed to the 3-4% increase in bond lengths, as exemplified by an arsenic/arsenic separation of 4.59 Å in **4c**, as compared to a phosphorus/phosphorus separation of 4.41 Å in the diphosphine analog.

However, analyses of space filling representations (Figures 3-7 and 3-21) show that considerable van der Waals interactions continue to attend rotation of the rotators in seventeen membered macrocycles such as **4c** and **5c**$^+$ BF_4^-. These are of course are more pronounced in the smaller macrocycles. The interactions arise mainly from the $As(CH_2)_3$ moieties. Clearly, donor atoms that afford still longer bonds would be beneficial. In this context, iron carbonyl complexes with stibine[98-100] or bismuthine[101] ligands have crystallographically characterized. The iron-antimony bonds are 8% longer than the iron-phosphorus bonds of related complexes, and the iron-bismuth bonds are 3% longer yet.[100]

As noted in a previous paper,[22a] osmium-phosphorus bonds are typically 3-5% longer than iron-phosphorus bonds. Thus, increasing the sizes of both the metal and the donor atoms promises a substantial reduction in barriers. It has proved possible to prepare osmium/phosphorus analogs of **4c** and **6c**$^{+}$ BAr_f^{-} (both of which have been crystallographically characterized),[22a] and the route could likely be adapted to diarsine and distibine analogs. However, the route is not amenable to smaller macrocycles, and efforts to effect CO/NO^{+} substitution have been unsuccessful.

The analyses accompanying Figure 3-21 focus upon the benefits of increasing the order of the rotational barrier. However, the most productive way to apply this strategy is likely with square planar complexes, which have six fold rotational barriers, and efforts along these lines are in progress. One reason that no quantitative data are available to date is that the rotational barriers in solution for the most easily accessible complexes have proved too low to measure by the NMR techniques described above.[20,23,24]

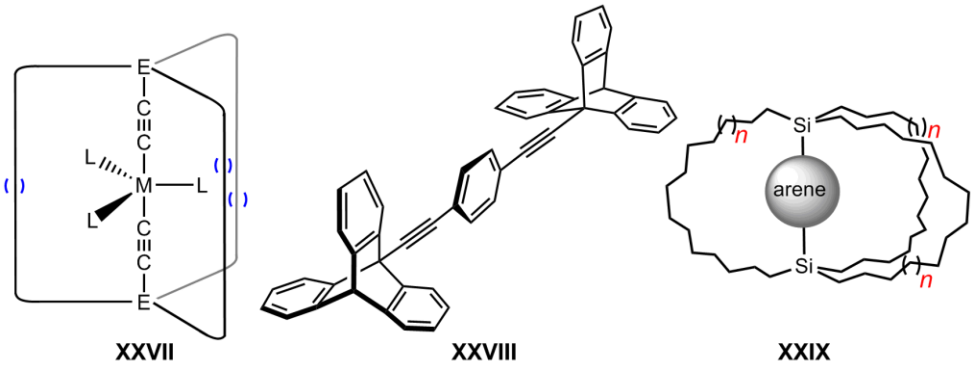

XXVII **XXVIII** **XXIX**

Figure 3-22. Possible metal based gyroscope like complexes containing alkynyl ligands (**XXVII**), and previously synthesized molecular rotors from other groups incorporating C≡C moieties or heavy atoms (**XXVIII**, **XXIX**).

Game changing results might be realized with gyroscope like complexes containing two *trans* C≡C-E(CH_2R)$_3$ ligands, as exemplified by **XXVII** in Figure 3-22. Here, the svelte alkynyl linkages should sterically insulate the rotator from the four atom E(CH_2)$_3$ moieties, as well as the methylene chains that define the stator. The judicious incorporation of rigid groups, such as in **II** (Scheme 3-1), could also further minimize interactions. This strategy takes a page from the work of Garcia-Garibay, who has insulated many types of rotators and stators with C≡C moieties.[8] A representative system in shown in **XXVIII**.[8a,b] Setaka has also incorporated heavier atoms into stator/rotator junctions, as illustrated by the disilicon systems **XXIX**.[13]

Under the conditions of our NMR experiments (e.g., Figure 3-17), the iron carbonyl moieties are rotating in both clockwise and counterclockwise directions. However, the direction sensing properties of classical mechanical gyroscopes require (dominant) rotation in a single direction.[18] Hence, this challenge must be met before any

of the types of molecules described in this section can exhibit gyroscopic properties. A number of strategies have been advanced.[7] The most popular requires that a dipole moment be introduced on the rotator. Thus, the cationic complexes **5a-c**$^+$ BF_4^- and **6a-c**$^+$ BAr_f^- qualify, but not **4a-c**. Dipoles can of course be manipulated by external electric fields, and it has been proposed that unidirectional rotation can be driven by rotating electric fields. Computational studies have defined the optimum rotational frequency to be applied for a given rotational barrier.[7]

Nonetheless, **5a-c**$^+$ BF_4^- and **6a-c**$^+$ BAr_f^- are not ideal candidates for molecular gyroscopes, as the anions will energetically interact with any rotating dipoles, increasing the barrier. Hence, the next sections in this series will examine neutral iron carbonyl complexes with dipolar rotators, several of which possess excellent clearances for rotator rotation both in solution and the solid state.[73] Importantly, the strategy embodied in **II** in Scheme 3-1 has so far only been lightly bought into play, as exemplified by the incorporation of *p*-phenylene (*p*-C_6H_4) units into the stators.[23] Hence, we remain highly optimistic that very "low friction" gyroscope like molecular rotors can be engineered, and ultimately elaborated into working devices.

3.4 Experimental section

General data: all reactions were conducted under N_2 or H_2 atmospheres. Chemicals were treated as follows: CH_2Cl_2, THF, toluene, ether, and hexanes, dried and

degassed using a Glass Contour solvent purification system; $CDCl_3$, CD_2Cl_2, C_6D_5Cl (3 × Cambridge Isotope Laboratories), Mg turnings (Alfa Aesar), $Br(CH_2)_mCH=CH_2$ (m = 4, 5; Oakwood Chemical), dibromoethane (99%, Aldrich), $AsCl_3$ (Aldrich), Grubbs' catalyst ($Ru(=CHPh)(PCy_3)_2(Cl)_2$; Strem), $ClRh(PPh_3)_3$ (Strem), NO^+ BF_4^- (Alfa Aesar, 98%), NH_4Cl (Fisher Scientific), CF_3SO_3H (Fluka), SiO_2 (Silicycle, 40-63 μm, 230-400 mesh), neutral Al_2O_3 (Macherey-Nagel), celite (EMD), used as received. $Br(CH_2)_6CH=CH_2$, $(BDA)Fe(CO)_3$, and $[H(OEt_2)_2]^+$ BAr_f^- were synthesized by literature procedures.[87,88,90,48]

^1H and $^{13}C\{^1H\}$ NMR spectra were recorded on a 500 MHz spectrometer at ambient probe temperatures unless otherwise noted and referenced as follows (δ, ppm): ^1H, residual internal $CHCl_3$ (7.26), $CDHCl_2$ (5.32), or C_6D_4HCl (7.14); ^{13}C, $CDCl_3$ (77.0), CD_2Cl_2 (53.84), or C_6D_5Cl (134.19). IR spectra were recorded using a Shimadzu IRAffinity-1 spectrometer with a Pike MIRacle ATR system (diamond/ZnSe crystal). Microanalyses were conducted by Atlantic Microlab.

$As((CH_2)_4CH=CH_2)_3$ (1a). A Schlenk flask was charged with magnesium turnings (0.820 g, 33.8 mmol), THF (40 mL), and 1,2-dibromoethane (0.30 mL, 3.5 mmol), and was cooled to 0 °C. Then $Br(CH_2)_4CH=CH_2$ (5.616 g, 34.4 mmol) was added dropwise with stirring over 0.5 h. After 1 h, the cooling bath was removed. After 16 h, the remaining magnesium was removed by filtration. Following a standard protocol,[89] an aliquot of the filtrate was used to determine the concentration of the

Grignard reagent $BrMg(CH_2)_4CH=CH_2$. The filtrate was cooled to 0 °C, and $AsCl_3$ (1.808 g, 9.98 mmol; 0.29 equiv) in THF (10 mL) was added dropwise with stirring over 0.5 h. The cooling bath was removed. After 15 h, the mixture was cooled to 0 °C and aqueous NH_4Cl (10 mL) was added dropwise with stirring over 12 min. After 1 h, the cooling bath was removed. After 1 h, the aqueous phase was removed via syringe. The solvent was removed from the organic phase by oil pump vacuum, and CH_2Cl_2 (20 mL) was added. The solution was passed through a short pad of silica (2.5 × 2.5 cm), which was washed with CH_2Cl_2 (75 mL). The solvent was removed from the filtrate by oil pump vacuum to give **1a** as a colorless oil (1.878 g, 5.79 mmol, 58%). Anal. Calcd. For $C_{18}H_{33}As$ (324.38): C 66.65, H 10.25; found: C 66.72, H 10.17.

NMR ($CDCl_3$, δ in ppm): ^1H (500 MHz) 5.80 (ddt, $^3J_{HHtrans}$ = 17.2 Hz, $^3J_{HHcis}$ = 10.7 Hz, $^3J_{HH}$ = 6.9 Hz, 3H, C***H***=), 5.05-4.89 (m, 6H, =C***H***$_2$), 2.13-1.99 (m, 6H, C***H***$_2$CH=CH_2), 1.54-1.33 (m, 18H, remaining C***H***$_2$); $^{13}C\{^1H\}$ (125 MHz) 138.9 (s, ***C***H=), 114.5 (s, =***C***H_2), 33.6 (s, ***C***H_2CH=CH_2), 31.2 (s, $AsCH_2CH_2$***C***H_2), 26.5 (s, As***C***H_2), 25.1 (s, $AsCH_2$***C***H_2).

As((CH$_2$)$_5$CH=CH$_2$)$_3$ (1b). Magnesium turnings (0.978 g, 40.3 mmol), THF (40 mL), 1,2-dibromoethane (0.30 mL, 3.5 mmol), and $Br(CH_2)_5CH=CH_2$ (4.698 g, 26.5 mmol), $AsCl_3$ (1.489 g, 8.22 mmol; 0.31 equiv), and THF (10 mL) were combined in a procedure analogous to that for **1a**, An identical workup gave **1b** as a colorless oil (1.898 g, 5.18 mmol, 63%). Anal. Calcd. For $C_{21}H_{39}As$ (366.46): C 68.83, H 10.73; found: C 69.13, H 10.64.

NMR ($CDCl_3$, δ in ppm): ^{1}H (500 MHz) 5.81 (ddt, $^3J_{HH}$*trans* = 17.2 Hz, $^3J_{HH}$*cis* = 10.8 Hz, $^3J_{HH}$ = 7.3 Hz, 3H, C***H***=), 5.04-4.89 (m, 6H, =C***H***$_2$), 2.10-1.99 (m, 6H, C***H***$_2$CH=CH$_2$), 1.50-1.31 (m, 24H, remaining C***H***$_2$); ^{13}C{^{1}H} (125 MHz) 139.2 (s, ***C***H=), 114.4 (s, =***C***H$_2$), 33.9 (s, ***C***H$_2$CH=CH$_2$), 31.6 (s, AsCH$_2$CH$_2$***C***H$_2$), 28.8 (s, ***C***H$_2$), 26.9 (s, As***C***H$_2$), 25.3 (s, AsCH$_2$***C***H$_2$).

As((CH$_2$)$_6$CH=CH$_2$)$_3$ (1c). Magnesium turnings (0.913 g, 37.6 mmol), THF (40 mL), 1,2-dibromoethane (0.30 mL, 3.5 mmol), Br(CH$_2$)$_6$CH=CH$_2$ (5.916 g, 31.0 mmol),[19,20] $AsCl_3$ (1.630 g, 8.99 mmol; 0.29 equiv), and THF (10 mL) were combined in a procedure analogous to that for **1a**. An identical workup gave **1c** as a colorless oil (2.571 g, 6.29 mmol, 70%). Anal. Calcd. for $C_{24}H_{45}As$ (408.54): C 70.56, H 11.10; found: C 70.70, H 11.30.

NMR ($CDCl_3$, δ in ppm): ^{1}H (500 MHz) 5.81 (ddt, $^3J_{HH}$*trans* = 17.4 Hz, $^3J_{HH}$*cis* = 10.1 Hz, $^3J_{HH}$ = 6.9 Hz, 3H, C***H***=), 5.03-4.91 (m, 6H, =C***H***$_2$), 2.11-1.98 (m, 6H, C***H***$_2$CH=CH$_2$), 1.50-1.25 (m, 30H, remaining C***H***$_2$); ^{13}C{^{1}H} (125 MHz) 139.3 (s, ***C***H=), 114.3 (s, =***C***H$_2$), 34.0 (s, ***C***H$_2$CH=CH$_2$), 32.0 (s, AsCH$_2$CH$_2$***C***H$_2$), 29.0 (s, ***C***H$_2$), 28.98 (s, ***C***H$_2$), 27.0 (s, As***C***H$_2$), 25.3 (s, AsCH$_2$***C***H$_2$).

***trans*-Fe(CO)$_3$(As((CH$_2$)$_4$CH=CH$_2$)$_3$)$_2$ (2a)**. A Schlenk flask was charged with (BDA)Fe(CO)$_3$ (0.861 g, 3.01 mmol),[90] THF (30 mL), and **1a** (2.050 g, 6.32 mmol) with stirring. The red solution turned yellow-orange. After 15 h, the solvent was removed by oil pump vacuum. The residue was chromatographed on a silica gel column

(1.5 × 20 cm) using hexanes and then 2:1 v/v hexanes/CH_2Cl_2. The solvent was removed from the product containing fractions by oil pump vacuum to give **2a** as a yellow oil (1.614 g, 2.05 mmol, 68%). Anal. Calcd. for $C_{39}H_{66}As_2FeO_3$ (788.63): C 59.40, H 8.44; found: C 59.44, H 8.29.

NMR ($CDCl_3$, δ in ppm): ^{1}H (500 MHz) 5.82 (ddt, $^3J_{HH}$*trans* = 17.0 Hz, $^3J_{HH}$*cis* = 10.1 Hz, $^3J_{HH}$ = 6.6 Hz, 6H, C***H***=), 5.08-4.92 (m, 12H, =C***H***$_2$), 2.16-2.05 (m, 12H, C***H***$_2$CH=CH$_2$), 1.85-1.78 (m, 12H, AsC***H***$_2$), 1.67-1.58 (m, 12H, AsCH$_2$C***H***$_2$), 1.56-1.45 (m, 12H, AsCH$_2$CH$_2$C*H*$_2$); ^{13}C{^{1}H} (125 MHz) 215.7 (s, ***C***O), 138.7 (s, ***C***H=), 114.7 (s, =***C***H$_2$), 33.4 (s, ***C***H$_2$CH=CH$_2$), 30.8 (s, AsCH$_2$CH$_2$***C***H$_2$), 27.3 (s, As***C***H$_2$), 24.1 (s, AsCH$_2$***C***H$_2$).

IR (oil film, cm^{-1}): 2924 (w), 2854 (w), 1851 (s, ν_{CO}), 1639 (w), 1444 (w), 1413 (w), 989 (w), 908 (w), 715 (w), 634 (s).

***trans*-Fe(CO)$_3$(As((CH$_2$)$_5$CH=CH$_2$)$_3$)$_2$ (2b)**. (BDA)Fe(CO)$_3$ (0.366 g, 1.28 mmol),[90] THF (30 mL), and **1b** (0.985 g, 2.69 mmol) were combined in a procedure analogous to that for **2a**. An identical workup gave **2b** as a yellow oil (0.785 g, 0.899 mmol, 70%). Anal. Calcd. for $C_{45}H_{78}As_2FeO_3$ (872.79): C 61.93, H 9.01; found: C 62.23, H 9.12.

NMR ($CDCl_3$, δ in ppm): ^{1}H (500 MHz) 5.81 (ddt, $^3J_{HH}$*trans* = 17.0 Hz, $^3J_{HH}$*cis* = 10.5 Hz, $^3J_{HH}$ = 6.6 Hz, 6H, C***H***=), 5.05-4.91 (m, 12H, =C***H***$_2$), 2.13-2.01 (m, 12H, C***H***$_2$CH=CH$_2$), 1.86-1.77 (m, 12H, AsC***H***$_2$), 1.65-1.55 (m, 12H, AsCH$_2$C***H***$_2$), 1.49-1.37

(m, 24H, remaining C***H***$_2$); ^{13}C{^{1}H} (125 MHz) 215.8 (s, ***C***O), 139.0 (s, ***C***H=), 114.5 (s, =***C***H$_2$), 33.7 (s, ***C***H$_2$CH=CH$_2$), 31.0 (s, AsCH$_2$CH$_2$***C***H$_2$), 28.5 (s, ***C***H$_2$), 27.3 (s, As***C***H$_2$), 24.3 (s, AsCH$_2$***C***H$_2$).

IR (oil film, cm^{-1}): 2926 (w), 2854 (w), 1853 (s, ν_{CO}), 1640 (w), 1413 (w), 991 (w), 906 (m), 713 (w), 642 (s).

***trans*-Fe(CO)$_3$(As((CH$_2$)$_6$CH=CH$_2$)$_3$)$_2$ (2c)**. (BDA)Fe(CO)$_3$ (0.683 g, 2.39 mmol),[90] THF (30 mL), and **1c** (2.050 g, 5.02 mmol) were combined in a procedure analogous to that for **2a**. An identical workup gave **2c** as a yellow oil (1.514 g, 1.58 mmol, 66%). Anal. Calcd. for $C_{51}H_{90}As_2FeO_3$ (956.95): C 64.01, H 9.48; found: C 64.25, H 9.42.

NMR ($CDCl_3$, δ in ppm): ^{1}H (500 MHz) 5.81 (ddt, $^3J_{HH\textit{trans}}$ = 17.1 Hz, $^3J_{HH\textit{cis}}$ = 10.3 Hz, $^3J_{HH}$ = 6.6 Hz, 6H, C***H***=), 5.06-4.88 (m, 12H, =C***H***$_2$), 2.10-2.00 (m, 12H, C***H***$_2$CH=CH$_2$), 1.84-1.75 (m, 12H, AsC***H***$_2$), 1.63-1.52 (m, 12H, AsCH$_2$C***H***$_2$), 1.45-1.29 (m, 36H, remaining C***H***$_2$); ^{13}C{^{1}H} (125 MHz) 215.9 (s, ***C***O), 139.2 (s, ***C***H=), 114.4 (s, =***C***H$_2$), 33.9 (s, ***C***H$_2$CH=CH$_2$), 31.5 (s, AsCH$_2$CH$_2$***C***H$_2$), 28.9 (s, ***C***H$_2$), 28.8 (s, ***C***H$_2$), 27.4 (s, As***C***H$_2$), 24.5 (s, AsCH$_2$***C***H$_2$).

IR (powder film, cm^{-1}): 2926 (w), 2854 (w), 1855 (s, ν_{CO}), 1640 (w), 1413 (w), 991 (w), 906 (w), 723 (w), 642 (s).

***trans*-Fe(CO)$_3$(As((CH$_2$)$_4$CH=CH(CH$_2$)$_4$)$_3$As) (3a)**. A Schlenk flask was charged with **2a** (1.159 g, 1.47 mmol) and CH_2Cl_2 (734 mL; the resulting solution is

0.0020 M in **2a**), and fitted with a condenser. A solution of Grubbs' catalyst (ca. half of 0.218 g (0.265 mmol, 18 mol%) in 10 mL of CH_2Cl_2) was added dropwise over 5 min. The sample was refluxed. After 18 h, the remaining catalyst was added. After another 16 h, the solvent was removed by oil pump vacuum. The residue was filtered through neutral alumina (2.5 × 5 cm) using 2:1 v/v hexanes/CH_2Cl_2. The solvent was removed from the filtrate by oil pump vacuum to give *E,E,E*-**3a** as a pale yellow solid (0.632 g, 0.897 mmol, 61%), mp 208-212 °C (capillary). Anal. Calcd. for $C_{33}H_{54}As_2FeO_3$ (704.48): C 56.26, H 7.73; found: C 56.54, H 7.60.

NMR ($CDCl_3$, δ in ppm): ^{1}H (500 MHz) 5.36-5.35 (m, 6H, C***H***=), 2.12-1.98 (m, 12H, AsC$\boldsymbol{H}_2$), 1.78-1.60 (m, 24H, AsCH$_2$C$\boldsymbol{H}_2$), 1.56-1.41 (m, 12H, AsCH$_2$CH$_2$C$\boldsymbol{H}_2$); ^{13}C{^{1}H} (125 MHz) 214.3 (s, ***C***O), 131.5 (s, ***C***H=), 32.8 (s, ***C***H$_2$CH=), 30.8 (s, AsCH$_2$CH$_2$***C***H$_2$), 26.8 (s, As***C***H$_2$), 24.4 (s, AsCH$_2$***C***H$_2$).

IR (powder film, cm^{-1}): 2920 (m), 2848 (w), 1851 (s, ν_{CO}), 1456 (w), 1409 (w), 962 (m), 707 (w), 636 (s).

***trans*-Fe(CO)$_3$(As((CH$_2$)$_5$CH=CH(CH$_2$)$_5$)$_3$As) (3b)**. Complex **2b** (0.773 g, 0.886 mmol), CH_2Cl_2 (443 mL; the resulting solution is 0.0020 M in **2b**), and Grubbs' catalyst (0.131 g (0.159 mmol, 18 mol%) in 10 mL of CH_2Cl_2) were combined in a procedure analogous to that for **3a**. An identical workup gave **3b** as a pale yellow solid (0.525 g, 0.665 mmol, 75%, mixture of *E*/*Z* isomers), mp 160-164 °C (capillary).

NMR ($CDCl_3$, δ in ppm): ^{1}H (500 MHz) 5.52-5.32 (m, 6H, C***H***=), 2.19-2.08 (m, 12H, C$\boldsymbol{H}_2$CH=), 1.85-1.59 (m, 24H, AsC$\boldsymbol{H}_2$ and AsCH$_2$C$\boldsymbol{H}_2$), 1.52-1.38 (m, 24H,

$AsCH_2CH_2C\boldsymbol{H}_2$ and remaining $C\boldsymbol{H}_2$); $^{13}C\{^1H\}$ (125 MHz; major isomer only) 215.4 (s, ***C***O), 130.1 (s, ***C***H=), 29.9 (s, $\boldsymbol{C}H_2CH$=), 28.5 (s, $AsCH_2CH_2\boldsymbol{C}H_2$), 28.1 (s, $\boldsymbol{C}H_2$), 25.7 (s, $\boldsymbol{C}H_2$), 23.6 (s, $AsCH_2\boldsymbol{C}H_2$).

IR (powder film, cm^{-1}): 2920 (m), 2850 (w), 1849 (s, ν_{CO}), 1446 (w), 1022 (w), 802 (m), 709 (w), 634 (s).

***trans*-Fe(CO)$_3$(As((CH$_2$)$_6$CH=CH(CH$_2$)$_6$)$_3$As) (3c)**. Complex **2c** (1.512 g, 1.58 mmol), CH_2Cl_2 (790 mL; the resulting solution is 0.0020 M in **2c**), and Grubbs' catalyst (0.234 g (0.284 mmol, 18 mol%) in 10 mL of CH_2Cl_2) were combined in a procedure analogous to that for **3a**. An identical workup gave **3c** as a pale yellow solid (1.075 g, 1.23 mmol, 78%, mixture of *E*/*Z* isomers), mp 159-162 °C (capillary). Anal. Calcd. for $C_{45}H_{78}As_2FeO_3$ (872.80): C 61.93, H 9.01; found: C 61.15, H 9.08.[77]

NMR ($CDCl_3$, δ in ppm): ^1H (500 MHz) 5.40-5.22 (m, 6H, C***H***=), 2.05-1.95 (m, 12H, $\boldsymbol{H}_2CH$=), 1.77-1.71 (m, 12H, As$\boldsymbol{C}H_2$), 1.67-1.56 (m, 12H, $AsCH_2\boldsymbol{C}H_2$), 1.45-1.22 (m, 36H, $AsCH_2CH_2C\boldsymbol{H}_2$ and remaining CH_2); $^{13}C\{^1H\}$ (125 MHz; major isomer only) 214.9 (s, ***C***O), 131.1 (s, ***C***H=), 32.5 (s, $\boldsymbol{C}H_2CH$=CH_2), 31.7 (s, $AsCH_2CH_2\boldsymbol{C}H_2$), 28.9 (s, $\boldsymbol{C}H_2$), 28.6 (s, $\boldsymbol{C}H_2$), 27.8 (s, $\boldsymbol{C}H_2$), 25.3 (s, $AsCH_2\boldsymbol{C}H_2$).

IR (powder film, cm^{-1}): 2920 (s), 2848 (m), 1859 (s, ν_{CO}), 1454 (w), 964 (w), 804 (m), 709 (w), 634 (s).

***trans*-Fe(CO)$_3$(As((CH$_2$)$_{10}$)$_3$As) (4a)**. A Fischer-Porter bottle was charged with *E,E,E*-**3a** (0.586 g, 0.832 mmol), $ClRh(PPh_3)_3$ (0.100 g, 0.108 mmol, 15 mol%), toluene

(20 mL), and H_2 (5 atm). The solution was stirred at 80 °C. After 2 d, the solvent was removed by oil pump vacuum. The residue was filtered through neutral alumina (2.5 × 5.0 cm) using 2:1 v/v hexanes/CH_2Cl_2. The solvent was removed from the filtrate by oil pump vacuum to give **4a** as a pale yellow solid (0.396 g, 0.558 mmol, 67%), mp 139-145 °C (capillary). DSC ($T_i/T_e/T_p/T_c/T_f$):[74] 66.3/ 87.0/104.0/114.5/124.0 °C (endotherm); 126.0/132.8/140.3/146.5/151.2 °C (melting endotherm). Anal. Calcd. for $C_{33}H_{60}As_2FeO_3$ (710.53): C 55.78, H 8.51; found: C 55.86, H 8.52.

NMR ($CDCl_3$, δ in ppm): ^{1}H (500 MHz) 1.82-1.77 (m, 12H, AsC***H***$_2$), 1.73-1.65 (m, 12H, AsCH$_2$C***H***$_2$), 1.55-1.48 (m, 12H, AsCH$_2$CH$_2$C***H***$_2$), 1.44-1.34 (m, 24H, remaining C***H***$_2$); ^{13}C{^{1}H} (125 MHz) 216.0 (s, ***C***O), 29.2 (s, AsCH$_2$CH$_2$***C***H$_2$), 27.3 (s, ***C***H$_2$), 27.0 (s, As***C***H$_2$), 26.2 (s, ***C***H$_2$), 22.5 (s, AsCH$_2$***C***H$_2$).

IR (powder film, cm^{-1}): 2920 (w), 2850 (w), 1842 (s, ν_{CO}), 1454 (w), 1411 (w), 1259 (w), 1016 (w), 802 (m), 796 (s), 707 (w), 634 (s).

***trans*-Fe(CO)$_3$(As((CH$_2$)$_{12}$)$_3$As) (4b)**. Complex **3b** (0.754 g, 0.956 mmol), ClRh(PPh$_3$)$_3$ (0.133 g, 0.143 mmol, 15 mol%), toluene (30 mL), and H_2 (5 atm) were combined in a procedure similar to that for **3a** (70 °C, 64 h). An identical workup gave **4b** as a pale yellow solid (0.547 g, 0.688 mmol, 72%), mp 171-175 °C (capillary). DSC ($T_i/T_e/T_p/T_c/T_f$):[74] –65.0/–52.2/–40.5/–35.8/–20.5 °C (endotherm); 109.0/123.2/133.7/141.7/162.7 °C (melting endotherm). Anal. Calcd. for $C_{39}H_{72}As_2FeO_3$ (794.69): C 58.94, H 9.13; found: C 59.04, H 8.99.

NMR ($CDCl_3$, δ in ppm): ^{1}H (500 MHz) 1.79-1.72 (m, 12H, AsC***H***$_2$), 1.68-1.60 (m, 12H, $AsCH_2C$***H***$_2$), 1.47-1.40 (m, 12H, $AsCH_2CH_2C$***H***$_2$), 1.40-1.26 (m, 36H, remaining C***H***$_2$); ^{13}C{^{1}H} (125 MHz) 215.5 (s, ***C***O), 30.0 (s, $AsCH_2CH_2$***C***H_2), 28.4 (s, ***C***H_2), 27.6 (s, As***C***H_2), 27.5 (s, ***C***H_2), 26.1 (s, ***C***H_2), 23.3 (s, $AsCH_2$***C***H_2).

IR (powder film, cm^{-1}): 2922 (w), 2850 (w), 1847 (s, ν_{CO}), 1456 (w), 1410 (w), 707 (w), 634 (s).

trans-Fe(CO)$_3$(As((CH$_2$)$_{14}$)$_3$As) (4c). Complex **3c** (1.075 g, 1.23 mmol), $ClRh(PPh_3)_3$ (0.171 g, 0.195 mmol, 15 mol%), toluene (20 mL), and H_2 (5 atm) were combined in a procedure similar to that for **3a** (60 °C, 72 h). An identical workup gave **4c** as a pale yellow solid (0.812 g, 0.924 mmol, 75%), mp 162-166 °C (capillary). DSC ($T_i/T_e/T_p/T_c/T_f$):[74] 121.0/150.5/160.5/163.5/ 164.2 °C (melting endotherm). Anal. Calcd. for $C_{45}H_{84}As_2FeO_3$ (878.85): C 61.50, H 9.63; found: C 61.32, H 9.66.

NMR ($CDCl_3$, δ in ppm): ^{1}H (500 MHz) 1.80-1.73 (m, 12H, AsC***H***$_2$), 1.66-1.57 (m, 12H, $AsCH_2C$***H***$_2$), 1.44-1.36 (m, 12H, $AsCH_2CH_2C$***H***$_2$), 1.36-1.26 (m, 48H, remaining C***H***$_2$); ^{13}C{^{1}H} (125 MHz) 215.5 (s, ***C***O), 31.0 (s, $AsCH_2CH_2$***C***H_2), 28.1 (s, As***C***H_2), 27.93 (s, ***C***H_2), 27.85 (s, ***C***H_2), 26.9 (s, ***C***H_2), 26.5 (s, ***C***H_2), 24.3 (s, $AsCH_2$***C***H_2).

IR (powder film, cm^{-1}): 2924 (m), 2852 (w), 1855 (s, ν_{CO}), 1556 (w), 711 (w), 634 (m).

***trans*-[Fe(CO)$_2$(NO)(As((CH$_2$)$_{10}$)$_3$As)]$^+$ BF$_4^-$ (5a$^+$ BF$_4^-$)**. A Schlenk flask was

charged with **4a** (0.092 g, 0.129 mmol) and CH_2Cl_2 (30 mL). Solid NO^+ BF_4^- (0.018 g, 0.155 mmol) was added with stirring. After 15 h, the pale yellow mixture had turned orange. The solvent was removed by oil pump vacuum and CH_2Cl_2 (15 mL) was added. The mixture was filtered through a short plug of celite (2.5 × 2.5 cm), which was washed with CH_2Cl_2 (25 mL). The solvent was removed from the filtrate by oil pump vacuum to give **5a**$^+$ BF_4^- as a yellow solid (0.098 g, 0.123 mmol, 95%), mp 176-179 °C (capillary). Anal. Calcd. for $C_{32}H_{60}As_2BF_4FeNO_3$ (799.33): C 48.08, H 7.57; found: C 48.04, H 7.72.

NMR ($CDCl_3$, δ in ppm): ^{1}H (500 MHz) 2.42-2.30 (s, 12H, AsC***H***$_2$), 1.61-1.45 (m, 12H, $AsCH_2C$***H***$_2$), 1.39-1.21 (m, 36H, $AsCH_2CH_2C$***H***$_2$ and remaining C*H*$_2$); ^{13}C{^{1}H} (125 MHz) 208.6 (s, ***C***O), 28.7 and 28.3 (2s, $2AsCH_2CH_2$***C***H_2 and $1AsCH_2CH_2$***C***H_2), 26.9 and 26.8 (2s, 1***C***H_2 and 2***C***H_2), 26.4 and 26.2 (2s, 2As***C***H_2 and 1$AsCH_2$), 25.8 and 24.9 (2s, 2***C***H_2 and 1***C***H_2), 23.3 and 22.9 (2s, $1AsCH_2$***C***H_2 and $2AsCH_2$***C***H_2).

IR (powder film, cm^{-1}): 2926 (m), 2854 (w), 2017 (w, ν_{CO}), 1951 (s, ν_{CO}), 1753 (s, ν_{NO}), 1456 (w), 1417(w), 1055 (s), 711 (w), 634 (s).

***trans*-[Fe(CO)$_2$(NO)(As((CH$_2$)$_{12}$)$_3$As)]$^+$ BF$_4^-$ (5b$^+$ BF$_4^-$)**. Complex **4b** (0.030 g, 0.037 mmol), CH_2Cl_2 (30 mL), and NO^+ BF_4^- (0.005 g, 0.045 mmol) were combined in a procedure similar to that for **5a**$^+$ BF_4 (18 h). A comparable workup (washing with 30 mL CH_2Cl_2) gave **5b**$^+$ BF_4^- as a yellow solid (0.029 g, 0.033 mmol, 89%), mp 157-

161 °C (capillary). Anal. Calcd. for $C_{38}H_{72}As_2BF_4FeNO_3$ (883.49): C 51.66, H 8.21; found: C 51.36, H 8.07.

NMR ($CDCl_3$, δ in ppm): ^1H (500 MHz) 2.42-2.27 (m, 12H, AsC$\boldsymbol{H}_2$), 1.67-1.49 (m, 24H, $AsCH_2C\boldsymbol{H}_2$), 1.47-1.35 (m, 12H, $AsCH_2CH_2C\boldsymbol{H}_2$), 1.34-1.20 (m, 24H, remaining C$\boldsymbol{H}_2$); $^{13}C\{^1H\}$ (125 MHz) 207.6 (s, ***C***O), 29.3 (s, $AsCH_2CH_2\boldsymbol{C}H_2$), 27.4 (s, ***C***$H_2$), 27.11 (s, As***C***$H_2$), 27.05 (s, ***C***$H_2$), 25.9 (s, ***C***$H_2$), 23.9 (s, $AsCH_2\boldsymbol{C}H_2$).

IR (powder film, cm^{-1}): 2924 (m), 2854 (w), 2019 (w, ν_{CO}), 1959 (s, ν_{CO}), 1755 (s, ν_{NO}), 1458 (w), 1417(w), 1056 (s), 711 (w), 634 (s).

***trans*-[Fe(CO)$_2$(NO)(As((CH$_2$)$_{14}$)$_3$As)]$^+$ BF$_4^-$ (5c$^+$ BF$_4^-$)**. Complex **4c** (0.051 g, 0.059 mmol), CH_2Cl_2 (30 mL), and NO^+ BF_4^- (0.008 g, 0.071 mmol) were combined in a procedure analogous to that for **5a**$^+$ BF_4. An identical workup gave **5c**$^+$ BF_4^- as a yellow solid (0.053 g, 0.054 mmol, 93%), mp 120-124 °C (capillary). Anal. Calcd. for $C_{44}H_{84}As_2BF_4FeNO_3$ (967.65): C 54.62, H 8.75; found: C 54.35, H 8.80.

NMR ($CDCl_3$, δ in ppm): ^1H (500 MHz) 2.40-2.32 (m, 12H, AsC$\boldsymbol{H}_2$), 1.61-1.46 (m, 24H, $AsCH_2C\boldsymbol{H}_2$ and $AsCH_2CH_2C\boldsymbol{H}_2$), 1.38-1.24 (m, 48H, remaining C$\boldsymbol{H}_2$); $^{13}C\{^1H\}$ (125 MHz) 207.3 (s, ***C***O), 30.9 (s, $AsCH_2CH_2\boldsymbol{C}H_2$), 29.0 (s, As***C***$H_2$), 27.8 (s, ***C***$H_2$), 27.5 (s, ***C***$H_2$), 26.8 (s, ***C***$H_2$), 26.2 (s, ***C***$H_2$), 25.3 (s, $AsCH_2\boldsymbol{C}H_2$).

IR (powder film, cm^{-1}): 2924 (m), 2854 (w), 2021 (w, ν_{CO}), 1961 (s, ν_{CO}), 1757 (s, ν_{NO}), 1456 (w), 1417(w), 1051 (s), 715 (w), 634 (s).

***mer,trans*-[Fe(CO)$_3$(H)(As((CH$_2$)$_{10}$)$_3$As)]$^+$ BAr$_f^-$ (6a$^+$ BAr$_f^-$)**. A Schlenk

flask was charged with **4a** (0.065 g, 0.091 mmol), CH_2Cl_2 (10 mL), and $[H(OEt_2)_2]^+$ BAr_f^- (0.093 g, 0.092 mmol)[48] with stirring. After 18 h, the solution was filtered through a syringe filter and the solvent removed by oil pump vacuum. The residue was washed with hexanes and dried by oil pump vacuum to give **6a**$^+$ BAr_f^- as an off white solid (0.123 g, 0.077 mmol, 84%), mp 175-177 °C (capillary). Anal. Calcd. for $C_{65}H_{93}As_2BF_{24}FeO_3$ (1594.92): C 49.58, H 4.67; found C 49.54, H 4.75.

NMR ($CDCl_3$, δ in ppm): ^{1}H (500 MHz) 7.73-7.69 (m, 8H, $C_6\boldsymbol{H}_3$ *o* to B), 7.55-7.50 (m, 4H, $C_6\boldsymbol{H}_3$ *p* to B), 2.14-1.95 (m, 12H, As$C\boldsymbol{H}_2$), 1.68-1.60 (m, 12H, $AsCH_2C\boldsymbol{H}_2$), 1.59-1.30 (m, 36H, $AsCH_2CH_2C\boldsymbol{H}_2$ and remaining $C\boldsymbol{H}_2$), –9.37 (s, 1H, Fe*H*); $^{13}C\{^1H\}$ (125 MHz) 207.6 (s, ***C***O *trans* to H), 206.5 (s, ***C***O *cis* to H),[102] 161.8 (q, $^1J_{BC}$ = 49.9 Hz, $\boldsymbol{C}_6H_3$ *i* to B), 134.9 (s, $\boldsymbol{C}_6H_3$ *o* to B), 129.0 (q, $^2J_{CF}$ = 30.5 Hz, $\boldsymbol{C}_6H_3$ *m* to B), 124.7 (q, $^1J_{CF}$ = 272.5 Hz, $\boldsymbol{C}F_3$), 117.6 (s, $\boldsymbol{C}_6H_3$ *p* to B), 28.9 and 28.3 (2s, $2AsCH_2CH_2\boldsymbol{C}H_2$ and $1AsCH_2CH_2\boldsymbol{C}H_2$), 26.80 and 26.77 (2s, $2\boldsymbol{C}H_2$ and $1\boldsymbol{C}H_2$), 26.6 and 26.56 (2s, $2As\boldsymbol{C}H_2$ and $1As\boldsymbol{C}H_2$), 26.5 and 25.9 (2s, $1\boldsymbol{C}H_2$ and $2\boldsymbol{C}H_2$), 23.2 and 22.3 (2s, $2AsCH_2\boldsymbol{C}H_2$ and $1AsCH_2\boldsymbol{C}H_2$).

IR (powder film, cm^{-1}): 2933 (m), 2858 (m), 2065 (w, ν_{CO}), 2015 (m, ν_{CO}), 1998 (s, ν_{CO}), 1352 (w), 1274 (s), 1163 (s), 885 (m), 839 (m), 713 (s), 685 (s), 669 (s).

***mer,trans*-$[Fe(CO)_3(H)(As((CH_2)_{12})_3As)]^+$ BAr_f^- (6b$^+$ BAr_f^-)**. Complex **4b** (0.101 g, 0.127 mmol), CH_2Cl_2 (10 mL), and $[H(OEt_2)_2]^+$ BAr_f^- (0.128 g, 0.127

mmol)[48] were combined in a procedure analogous to that for **6a**$^+$ BAr_f^-. An identical workup gave **6b**$^+$ BAr_f^- as an off white solid (0.183 g, 0.109 mmol, 86%), mp 147-149 °C (capillary). Anal. Calcd. for $C_{71}H_{105}As_2BF_{24}FeO_3$ (1679.1): C 51.44, H 5.11; found C 52.09, H 5.21.[77]

NMR ($CDCl_3$, δ in ppm): ^{1}H (500 MHz) 7.76-7.64 (m, 8H, $C_6\boldsymbol{H}_3$ *o* to B), 7.59-7.47 (m, 4H, $C_6\boldsymbol{H}_3$ *p* to B), 2.08-1.94 (m, 12H, As$C\boldsymbol{H}_2$), 1.61-1.53 (m, 12H, $AsCH_2C\boldsymbol{H}_2$), 1.51-1.44 (m, 12H, $AsCH_2CH_2C\boldsymbol{H}_2$), 1.43-1.37 (m, 12H, $C\boldsymbol{H}_2$), 1.34-1.25 (m, 24H, remaining $C\boldsymbol{H}_2$), –9.49 (s, 1H, Fe***H***); $^{13}C\{^1H\}$ (125 MHz) 206.38 (s, ***C***O *cis* to H),[102] 206.36 (s, ***C***O *trans* to H), 161.8 (q, $^1J_{BC}$ = 49.9 Hz, $\boldsymbol{C}_6H_3$ *i* to B), 134.9 (s, $\boldsymbol{C}_6H_3$ *o* to B), 129.0 (q, $^2J_{CF}$ = 30.5 Hz, $\boldsymbol{C}_6H_3$ *m* to B), 124.7 (q, $^1J_{CF}$ = 272.5 Hz, $\boldsymbol{C}F_3$), 117.6 (s, $\boldsymbol{C}_6H_3$ *p* to B), 29.3 (s, $AsCH_2CH_2\boldsymbol{C}H_2$), 28.3 (s, As$\boldsymbol{C}H_2$), 27.4 (s, $\boldsymbol{C}H_2$), 26.9 (s, $\boldsymbol{C}H_2$), 26.4 (s, $\boldsymbol{C}H_2$), 23.8 (s, $AsCH_2\boldsymbol{C}H_2$).

IR (powder film, cm^{-1}): 2931 (m), 2860 (m), 2069 (w, ν_{CO}), 2021 (m, ν_{CO}), 1996 (s, ν_{CO}), 1352 (w), 1274 (s), 1157 (s), 1145 (s), 887 (m), 839 (m), 713 (s), 685 (s), 669 (s).

***mer,trans*-[Fe(CO)$_3$(H)(As((CH$_2$)$_{14}$)$_3$As)]$^+$ BAr$_f^-$ (6c$^+$ BAr_f^-).** Complex **4c** (0.068 g, 0.077 mmol), CH_2Cl_2 (10 mL), and $[H(OEt_2)_2]^+$ BAr_f^- (0.078 g, 0.077 mmol)[48] were combined in a procedure analogous to that for **6a**$^+$ BAr_f^-. An identical workup gave **6c**$^+$ BAr_f^- as an off white solid (0.108 g, 0.061 mmol, 80%), mp 183-189

°C (capillary). Anal. Calcd. for $C_{77}H_{117}As_2BF_{24}FeO_3$ (1763.24): C 53.09, H 5.55; found C 53.01, H 5.66.

NMR ($CDCl_3$, δ in ppm): ^{1}H (500 MHz) 7.73-7.67 (m, 8H, $C_6\boldsymbol{H}_3$ *o* to B), 7.55-7.51 (m, 4H, $C_6\boldsymbol{H}_3$ *p* to B), 2.08-1.95 (m, 12H, $AsC\boldsymbol{H}_2$), 1.60-1.50 (m, 12H, $AsCH_2C\boldsymbol{H}_2$), 1.51-1.41 (m, 12H, $AsCH_2CH_2C\boldsymbol{H}_2$), 1.42-1.23 (m, 48H, remaining $C\boldsymbol{H}_2$), –9.60 (s, 1H, Fe***H***); $^{13}C\{^1H\}$ (125 MHz) 206.5 (s, ***C***O *cis* to H),[102] 205.9 (s, ***C***O *trans* to H), 161.8 (q, $^1J_{BC}$ = 49.9 Hz, $\boldsymbol{C}_6H_3$ *i* to B), 134.9 (s, $\boldsymbol{C}_6H_3$ *o* to B), 129.0 (q, $^2J_{CF}$ = 30.5 Hz, $\boldsymbol{C}_6H_3$ *m* to B), 124.7 (q, $^1J_{CF}$ = 272.5 Hz, $\boldsymbol{C}F_3$), 117.6 (s, $\boldsymbol{C}_6H_3$ *p* to B), 30.0 (s, $AsCH_2CH_2\boldsymbol{C}H_2$), 27.9 (s, $As\boldsymbol{C}H_2$), 27.7 (s, $\boldsymbol{C}H_2$), 27.4 (s, $\boldsymbol{C}H_2$), 27.06 (s, $\boldsymbol{C}H_2$), 27.04 (s, $\boldsymbol{C}H_2$), 24.4 (s, $AsCH_2\boldsymbol{C}H_2$).

IR (powder film, cm^{-1}): 2929 (m), 2856 (m), 2073 (w, ν_{CO}), 2021 (m, ν_{CO}), 2004 (s, ν_{CO}), 1352 (w), 1273 (s), 1163 (s), 1139 (s), 887 (m), 839 (m), 711 (s), 683 (s), 667 (s).

Cyclic voltammetry: a BAS*i* Epsilon Electrochemical Workstation (Cell Stand C3) with the program Epsilon EC (version 2.13.77) was employed. Samples were prepared under N_2 and data were recorded as described in Table 3-2 (ferrocene added after each measurement).

3.5 Crystallography

A. A saturated hexanes solution of **4a** was kept at –40 °C. After 2 d, data were

collected on one of the yellow prisms as outlined in Table 3-5. Cell parameters were obtained from 60 data frames taken at widths of 0.5° and refined with 43321 reflections. Integrated intensity information for each reflection was obtained by reduction of the data frames with the program APEX2.[103] Data were corrected for Lorentz and polarization factors, and using SADABS[104] for absorption and crystal decay effects. The structure, a hemisolvate **4a**·0.5C_6H_{14}, was solved by direct methods using SHELXTL/XS.[79] Hydrogen atoms were placed in idealized positions and refined using a riding model. All non-hydrogen atoms were refined with anisotropic thermal parameters. All methylene chains (C1A–C30A) were disordered over two positions, which refined to a 52:48 occupancy ratio. Restraints were used to keep the metrical parameters meaningful. The absence of additional symmetry and voids were confirmed using PLATON (ADDSYM).[105] The structure was refined (weighted least squares refinement on F^2) to convergence.[79,81] **B.** A saturated pentane solution of **4b** was kept at –40 °C. After 2 d, data were collected on one of the yellow prisms as outlined in Table 3-5. Cell parameters were obtained from 60 data frames taken at widths of 0.5° and refined with 38299 reflections. Integrated intensity information for each reflection was obtained by reduction of the data frames with the program APEX2.[103] Data were corrected for Lorentz and polarization factors and using SADABS[104] for absorption and crystal decay effects. The structure was solved by direct methods using SHELXTL/XS.[79] Hydrogen atoms were placed in idealized positions and refined using a riding model. All non-hydrogen atoms were refined with anisotropic thermal parameters. The carbon atoms

C24-C36 were disordered over two positions and refined to a 72:28 occupancy ratio. Restraints were used to keep the metrical parameters meaningful. The structure was refined (weighted least squares refinement on F^2) to convergence.[79,81] **C**. A saturated pentane solution of **4c** was kept at –40 °C. After 2 d, data were collected on one of the yellow prisms as outlined in Table 3-5. Cell parameters were obtained from 60 frames using a 0.5° scan and refined with 28637 reflections. Integrated intensity information for each reflection was obtained by reduction of the data frames with the program APEX2.[103] Data were corrected for Lorentz and polarization factors, and using SADABS[104] for absorption and crystal decay effects. The structure was solved by direct methods using SHELXTL/XS.[79] Hydrogen atoms were placed in idealized positions and refined using a riding model. All non-hydrogen atoms were refined with anisotropic thermal parameters. The structure was refined (weighted least squares refinement on F^2) to convergence.[79] **D.** A concentrated CH_2Cl_2 solution of **5b**$^+$ BF_4^- was layered with hexanes and kept at –40 °C. After 14 d, data were collected on one of the orange needles as outlined in Table 3-5. Cell parameters were obtained from 60 data frames taken at widths of 0.5° and refined with 154913 reflections. Integrated intensity information for each reflection was obtained by reduction of the data frames with the program APEX2.[103] Data were corrected for Lorentz and polarization factors, and using SADABS[104] for absorption and crystal decay effects. The structure was solved by direct methods using SHELXTL/XS.[79] Hydrogen atoms were placed in idealized positions and refined using a riding model. All non-hydrogen atoms were refined with anisotropic

thermal parameters. Each unit cell contained two independent molecules and four CH_2Cl_2 solvate molecules. A methylene chain in one of the molecules was disordered, which was modeled with strong restraints and constraints including EADP[79] and refined to a 55:45 occupancy ratio. Due to positional disorder, the NO ligand could not be distinguished from the CO ligands. Their occupancy was restrained with SUMP.[79] Restraints were used to keep the metrical parameters meaningful. The structure was refined (weighted least squares refinement on F^2) to convergence.[79,81] The absence of additional symmetry and voids were confirmed using PLATON (ADDSYM).[105] **E.** A saturated CH_2Cl_2 solution of **8**[91] was kept at –40 °C. After 2 d, data were collected on one of the yellow prisms as outlined in Table 3-5. Cell parameters were obtained from 60 data frames taken at widths of 0.5° and refined with 29982 reflections. Integrated intensity information for each reflection was obtained by reduction of the data frames with the program APEX2.[103] Data were corrected for Lorentz and polarization factors, and using SADABS[104] for absorption and crystal decay effects. The structure, the solvate **8**·3CH_2Cl_2, was solved by direct methods using SHELXTL/XS.[79] Hydrogen atoms were placed in idealized positions and refined using a riding model. All non-hydrogen atoms were refined with anisotropic thermal parameters. One CH_2Cl_2 molecule was disordered over two positions and refined to a 58:42 occupancy ratio. Restraints were used to keep the metrical parameters meaningful. The structure was refined (weighted least squares refinement on F^2) to convergence.[79,81] Absence of additional symmetry and voids were confirmed using PLATON (ADDSYM).[105]

Table 3-5. Summary of crystallographic data.[a]

	4a· 0.5 C_6H_{14}	**4b**	**4c**
empirical formula	$C_{36}H_{67}As_2FeO_3$	$C_{39}H_{72}As_2FeO_3$	$C_{45}H_{84}As_2FeO_3$
formula weight	753.58	794.66	878.81
crystal system	Monoclinic	Triclinic	Monoclinic
space group	$P2_1/c$	P-1	C 2/c
unit cell dimensions			
a[Å]	11.382(2)	10.404(4)	21.438(3)
b[Å]	11.874(2)	13.506(6)	13.9810(17)
c[Å]	28.009(5)	16.155(7)	18.227(2)
	90	111.501(5)	90
β [°]	94.913(2)	92.520(5)	121.3260(10)
γ [°]	90	97.421(6)	90
volume [$Å^3$]	3771.8(13)	2084.2(15)	4666.5(10)
Z	4	2	4
ϱcalcd[Mg/m^3]	1.327	1.266	1.251
μ [mm^{-1}]	2.172	1.969	1.766
F(000)	1596	844	1880
crystal size [mm^3]	0.24 × 0.06 × 0.04	0.35 × 0.20 × 0.06	0.30 × 0.10 × 0.10
range for data collection	1.796 to 27.575	2.29 to 27.50	1.83 to 29.52
index ranges	$-14 \le h \le 14$ $-15 \le k \le 15$ $-36 \le l \le 36$	$-13 \le h \le 13$ $-17 \le k \le 17$ $-20 \le l \le 20$	$-29 \le h \le 28$ $-18 \le k \le 18$ $-24 \le l \le 24$
reflections collected	43321	38299	28637
independent reflections	8719 [R(int) = 0.0499]	9447 [R(int) = 0.0525]	6200 [R(int) = 0.0312]
max. and min. transmission	0.7456 and 0.5904	0.8910 to 0.5457	0.8432 to 0.6194
data/restraints/parameters	8719 / 1395 / 651	9447 / 73 / 371	6200 / 0 / 232
goodness-of-fit on F^2	1.043	1.077	1.008
final R indices [I>2σ(I)]	$R_1 = 0.0526$, $wR_2 = 0.1328$	$R_1 = 0.0557$, $wR_2 = 0.1433$	$R_1 = 0.0257$, $wR_2 = 0.0571$
R indices (all data)	$R_1 = 0.0795$, $wR_2 = 0.1477$	$R_1 = 0.0764$, $wR_2 = 0.1560$	$R_1 = 0.0377$, $wR_2 = 0.0610$
largest diff. peak & hole [e $Å^{-3}$]	1.015 and –0.730	1.940 and –2.437	0.392 and –0.276

[a]data common to all structures: $T = 110.0$ K; λ = 0.71073 Å; diffractometer = Bruker APEX2.

Table 3-5. continued.

	5b^{+} BF_4^{-}·2CH_2Cl_2	**8**·3CH_2Cl_2
empirical formula	$C_{40}H_{76}As_2BCl_4F_4FeNO_3$	$C_{42}H_{36}As_2Cl_6FeO_3$
formula weight	1053.31	1007.10
crystal system	Monoclinic	Monoclinic
space group	$P2_1/c$	$P2_1/c$
unit cell dimensions		
a[Å]	18.013(2)	11.670(3)
b[Å]	27.704(4)	15.421(3)
c[Å]	20.486(3)	23.682(5)
α [°]	90	90
β [°]	94.996(2)	98.720(3)
γ [°]	90	90
volume [Å^3]	10184(2)	4212.9(16)
Z	8	4
ϱcalcd[Mg/m^3]	1.374	1.588
μ [mm^{-1}]	1.844	2.336
F(000)	4384	2024
crystal size [mm^3]	0.19 × 0.17 × 0.02	0.57 × 0.37 × 0.36
range for data collection	1.738 to 27.519	1.740 to 27.781
index ranges	$-23 \le h \le 23$ $-35 \le k \le 35$ $-26 \le l \le 26$	$-12 \le h \le 12$ $-16 \le k \le 20$ $-30 \le l \le 30$
reflections collected	154913	29982
independent reflections	23332 [R(int) = 0.0639]	9302 [R(int) = 0.0712]
max. and min. transmission	0.7456 to 0.6007	0.7456 and 0.3300
data/restraints/parameters	23332 / 68 / 977	9302 / 24 / 509
goodness-of-fit on F^2	1.032	1.012
final R indices [I>2σ(I)]	R_1 = 0.0532, wR_2 = 0.1254	R_1 = 0.0517, wR_2 = 0.1142
R indices (all data)	R_1 = 0.0878, wR_2 = 0.1438	R_1 = 0.0894, wR_2 = 0.1285
largest diff. peak & hole [e Å^{-3}]	2.218 and –1.252	1.119 and –0.977

[a] data common to all structures: T = 110.0 K; λ = 0.71073 Å; diffractometer = Bruker APEX2.

4. SYNTHESES OF IRON COMPLEXES OF SYMMETRICAL TRIALKYLPHOSPHINES WITH THREE TERMINAL VINYL GROUPS, $P((CH_2)_mCH=CH_2)_3$*

4.1 Introduction

There has been much recent interest in the development of molecular rotors that structurally or functionally mimic various attributes of macroscopic gyroscopes.[8,20-25,29,30,106] The Gladysz group focused on systems that contain two *trans* disposed phosphorus donor ligands that are tethered by three chains, usually comprised solely of methylene groups. These encase rotors of the formula L_yM as diagrammed in Scheme 1.[20-25] The *trans* complexes of **1** were then subject to alkene metatheses and hydrogenation reactions as shown in Scheme 1.[20,107]

*Reprinted with permission from Lang, G. M.; Skaper, D.; Shima, T.; Otto, M.; Wang, L.; Gladysz, J. A. *Aust. J. Chem*. **2015**, *68*, 1342-1351.

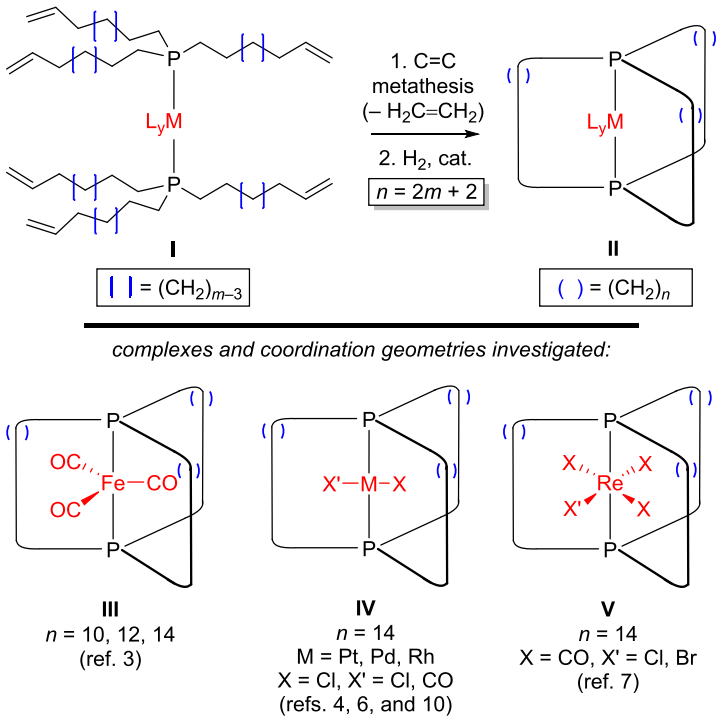

Scheme 4-1. Syntheses of gyroscope like complexes based upon *trans*-spanning diphosphines with $(CH_2)_n$ linkers.

In 2004 the Gladysz group published the synthesis of iron tricarbonyl based gyroscopes of the formula *trans*-$Fe(CO)_3(P((CH_2)_n)_3P)$ (n = 10, 12, 14).[21] Many substituted analogs have since been prepared and will be detailed shortly.[85] These fall into several categories, as one approach to realizing gyroscopic properties is to desymmetrize the $Fe(CO)_3$ rotator, so that it features a dipole moment (the orientation of which can be driven by an electric field).[7,9] Accordingly, this section will describe the syntheses of iron tricarbonyl adducts of **1**, and the sequential substitution by nitrosyl, halide, or pseudohalide ligands. The NMR and IR properties are also carefully defined to identify trends vis-à-vis gyroscope like homologs such as **III** (Scheme 4-1).

4.2 Results

4.2.1 Synthesis of title compounds

Benzylideneacetone iron tricarbonyl, (BDA)Fe(CO)$_3$,[47,90,108] has been shown to be a convenient precursor to diaxially disposed bis(phosphine) iron(0) complexes of the formula *trans*-Fe(CO)$_3$(PR$_3$)$_2$.[47] Accordingly, as depicted in Scheme 4-2, THF solutions of (BDA)Fe(CO)$_3$ and the phosphines **1a-e** (2.2-2.7 equiv)[88] were combined. Chromatographic workups, described in the experimental section, afforded *trans*-Fe(CO)$_3$(P((CH$_2$)$_m$CH=CH$_2$)$_3$)$_2$ **(2a-e)** as moderately air sensitive yellow/orange oils in 60-75% yields. Consistent with literature precedent for related complexes,[47] tricarbonyl adducts **2a-e** exhibited a single strong IR ν_{CO} band (1855-1859 cm^{-1}). As illustrated in Figure 4-1, the CO ^{13}C NMR signals (214-215 ppm) showed phosphorus coupling (t, J = 29 Hz), as did the P$\underline{C}$H$_2$CH$_2\underline{C}$H$_2$ signals. The PCH$_2$CH$_2\underline{C}$H$_2$ signals were well defined virtual triplets (apparent J = 30-31 Hz),[37] whereas the P$\underline{C}$H$_2$ signals were more complex multiplets.

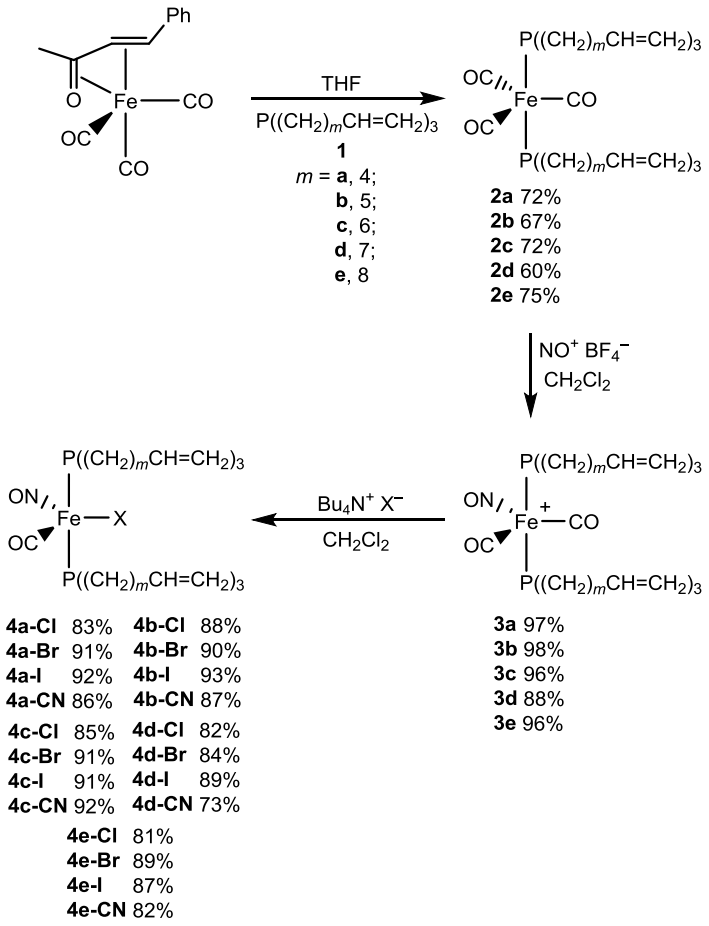

Scheme 4-2. Syntheses of title compounds.

Attention was next turned to substituting the carbonyl ligands. Several species of the type *trans*-$Fe(CO)_3(PR_3)_2$ have been shown to react with nitrosonium salts NO^+ Z^- to yield desymmetrized cationic nitrosyl complexes of the formula $[Fe(CO)_2(NO)((PR_3)_2)]^+$ Z^-.[44] Thus, as depicted in Scheme 4-2, CH_2Cl_2 solutions of **2a-e** were treated with solid NO^+ BF_4^- (1.3-15 equiv). Workups gave the cationic dicarbonyl nitrosyl complexes *trans*-$[Fe(CO)_2(NO)(P((CH_2)_mCH=CH_2)_3)_2]^+$ BF_4^- (**3a-e)**[44b] as moderately air sensitive orange oils in 88-98% yields.

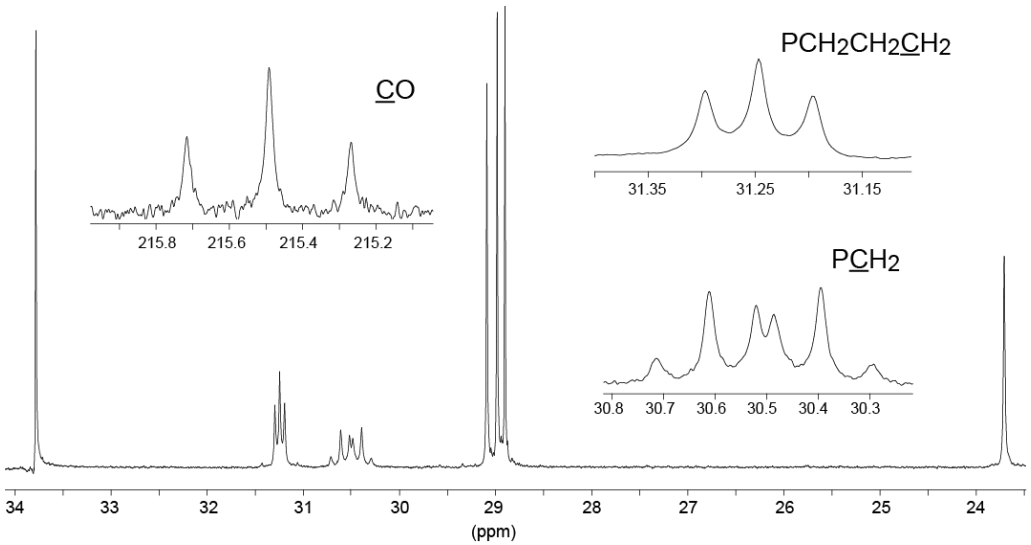

Figure 4-1. The CH_2 and CO regions of the $^{13}C\{^1H\}$ NMR spectrum of **2d** (125 MHz, $CDCl_3$), illustrating the types of phosphorus couplings.

As summarized in Table 4-1, two IR ν_{CO} bands were observed, one weak (2031–2029 cm^{-1}) and one strong (1967 cm^{-1}), as well as a strong ν_{NO} IR band at lower frequency (1768–1766 cm^{-1}). The higher IR ν_{CO} values as compared to **2a-e** are in accord with literature precedent[44] and reflect the superior π accepting ability of the nitrosyl ligand.

Table 4-1. Selected NMR and IR data

Complex	IR [cm^{-1}][a]			$^{31}P\{^1H\}$[b]	$^{13}C\{^1H\}$ (δ/ppm)[b,c]				
	ν_{CO}	ν_{NO}	ν_{CN}	(δ/ppm)	***C***O [$^2J_{PC}$, Hz]	***C***N [$^2J_{PC}$, Hz]	P***C***H_2 [$^1J_{PC}$, Hz]	PCH_2***C***H_2	PCH_2CH_2***C***H_2 [$^3J_{PC}$, Hz]
2a	1855	-	-	63.6	215.6 [28.6]	-	28.8[d]	23.3	31.3 [6.0]
2b	1855	-	-	63.2	215.5 [28.1]	-	28.8	23.6	31.3 [6.0]
2c	1857	-	-	63.0	214.4 [28.6]	-	28.8	23.7	30.0 [6.0]
2d	1857	-	-	63.0	215.7 [28.6]	-	29.2	23.8	31.4 [6.5]
2e	1859	-	-	63.0	215.6 [28.5]	-	29.2	23.7	31.3 [6.5]
3a	2031/1967	1768	-	53.9	207.6 [28.6]	-	27.7	23.3	29.7 [6.5]
3b	2029/1967	1766	-	53.5	207.2 [28.6]	-	27.7	23.8	30.1 [7.0]
3c	2029/1967	1766	-	53.2	207.6 [28.6]	-	27.8	24.0	30.7 [7.0]
3d	2029/1967	1766	-	53.3	207.4 [28.6]	-	27.8	24.0	30.9 [6.5]
3e	2029/1967	1766	-	53.4	208.1 [28.6]	-	27.8	24.1	30.9 [7.0]
4a-Cl	1901	1668	-	47.4	220.9 [37.0]	-	25.6 [12.7]	23.6	30.7 [6.0]
4b-Cl	1901	1668	-	47.4	220.9 [38.0]	-	25.8 [13.0]	24.1	31.1 [7.0]
4c-Cl	1901	1668	-	47.4	221.1 [37.0]	-	25.8 [13.0]	24.2	31.6 [6.3]
4d-Cl	1901	1668	-	47.5	221.2 [37.0]	-	25.9 [13.0]	24.3	31.7 [6.0]
4e-Cl	1901	1668	-	47.3	221.2 [38.0]	-	25.9 [13.0]	24.3	31.7 [6.0]
4a-Br	1901	1672	-	44.6	220.4 [38.0]	-	26.3 [12.5]	23.7	30.6 [6.7]
4b-Br	1903	1672	-	44.1	220.6 [37.0]	-	26.6 [13.0]	24.2	31.0 [6.5]
4c-Br	1903	1674	-	44.2	221.1 [37.0]	-	25.8 [13.0]	24.4	31.6 [6.3]
4d-Br	1903	1674	-	43.4	220.8 [37.0]	-	26.7 [13.0]	24.4	31.6 [6.0]
4e-Br	1903	1674	-	44.3	221.2 [36.0]	-	25.9 [13.0]	24.4	31.7 [6.0]
4a-I	1905	1681	-	41.1	219.9 [36.0]	-	27.4 [12.5]	23.4	30.2 [7.5]

Table 4-1. Continued.

Complex	IR [cm^{-1}][a]			$^{31}P\{^{1}H\}$[b]	$^{13}C\{^{1}H\}$ (δ/ppm)[b,c]				
	ν_{CO}	ν_{NO}	ν_{CN}	(δ/ppm)	***C***O [$^{2}J_{PC}$, Hz]	***C***N [$^{2}J_{PC}$, Hz]	P***C***H_2 [$^{1}J_{PC}$, Hz]	PCH_2***C***H_2	PCH_2CH_2***C***H_2 [$^{3}J_{PC}$, Hz]
4b-I	1905	1681	-	40.1	220.6 [37.0]	-	26.6 [13.0]	24.4	31.0 [6.5]
4c-I	1905	1681	-	40.8	220.5 [35.0]	-	28.2 [13.0]	24.5	31.4 [6.5]
4d-I	1905	1681	-	40.8	220.8 [36.0]	-	26.7 [13.0]	24.6	31.6 [6.0]
4e-I	1905	1681	-	40.6	219.2 [35.0]	-	27.5 [13.0]	24.1	31.4 [6.0]
4a-CN	1913	1697	2096	56.3	220.2 [30.0]	141.9 [42.0]	28.3 [13.0]	23.7	30.6 [7.0]
4b-CN	1913	1699	2096	56.2	220.3 [30.0]	141.7 [42.0]	28.5 [13.7]	24.1	30.9 [6.5]
4c-CN	1915	1699	2096	56.2	220.4 [30.0]	141.7 [42.0]	28.5 [14.0]	24.3	31.4 [6.0]
4d-CN	1915	1699	2096	55.7	218.8 [30.0]	141.9 [42.0]	27.8 [12.7]	24.4	31.2 [6.0]
4e-CN	1915	1699	2096	56.2	220.5 [30.0]	141.8 [42.0]	28.6 [13.0]	24.4	31.7 [6.5]

[a]Oil film. [b]The NMR spectra of **2a-3e** were recorded in $CDCl_3$. The remaining spectra were recorded in C_6D_6. [c]All signals for which *J* values are given correspond to a triplet or an apparent triplet. [d]P$\underline{C}H_2$ signals for **2a-3e** are complex multiplets, so no *J* values are reported.

Cationic dicarbonyl nitrosyl complexes of the type $[Fe(CO)_2(NO)(L_2)]^+ Z^-$ and halide or pseudohalide salts ($M^+/Q^+ X^-$) are known to react to give the monocarbonyl substitution products $Fe(CO)(NO)(X)(L_2)$.[110-113] Thus, as shown in Scheme 4-2, CH_2Cl_2 solutions of **3a-e** and the ammonium salts *n*-$Bu_4N^+ X^-$ (X = Cl, Br, I, or CN) were combined.[114] Chromatographic workups gave the halide or cyanide complexes *trans*-$Fe(CO)(NO)(X)(P((CH_2)_mCH=CH_2)_3)_2$ (**4a-e-X**) as moderately air sensitive red oils in 73-93% yields.

These exhibited a single strong IR ν_{CO} band and a single strong IR ν_{NO} band (1901–1915 and 1668-1699 cm^{-1}, respectively). In accord with literature precedent,[110-112] the frequencies were lower than those of the cationic precursors, and increased in the order X = Cl < Br < I < CN. In the case of the cyanide complexes **4a-e-CN**, a weak IR ν_{CN} band was also observed (2096 cm^{-1}). The CN ^{13}C NMR signals (142 ppm) showed phosphorus coupling (t, $^2J_{CP}$ = 42 Hz).[37]

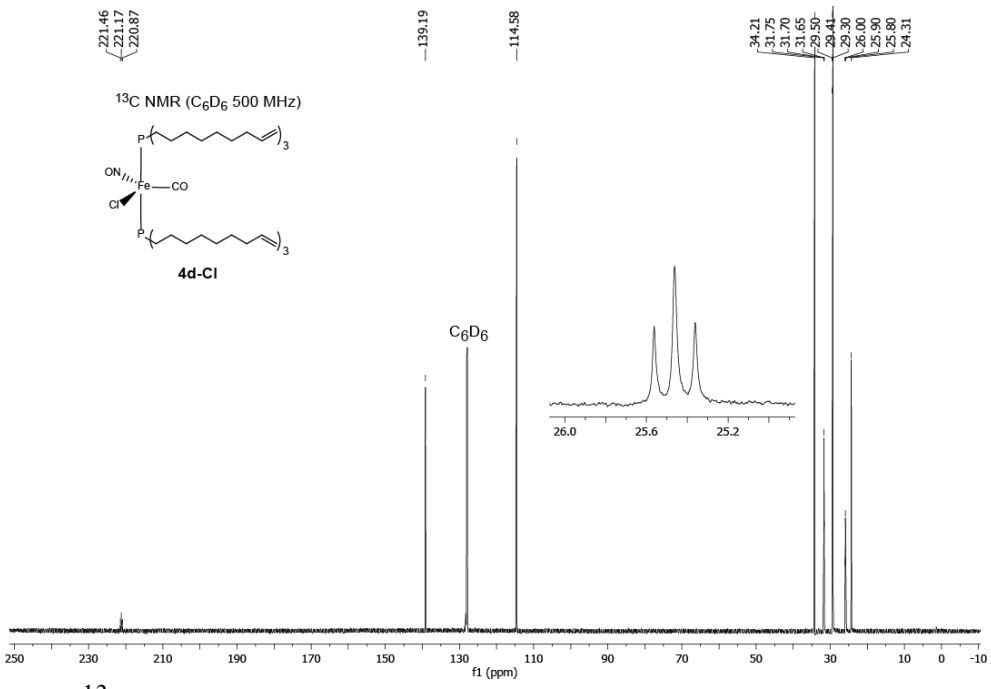

Figure 4-2. ^{13}C NMR spectra of **4d-Cl**.

As mentioned earlier, in the tricarbonyl complexes, the P$\underline{C}H_2$ signals were complicated multiplets; however, in these complexes the $PCH_2CH_2\underline{C}H_2$ and P$\underline{C}H_2$ signals were well defined virtual triplets (apparent J 30.0-31.4 Hz) as shown in Figure 4-2. The $PCH_2CH_2CH_2$ ^{1}H and ^{13}C NMR assignments were confirmed by ^{1}H,^{1}H COSY and ^{1}H,^{13}C HSQC experiments of **4a-Cl** and **4d-Cl** as shown in Figures 4-3 to 4-6.[109]

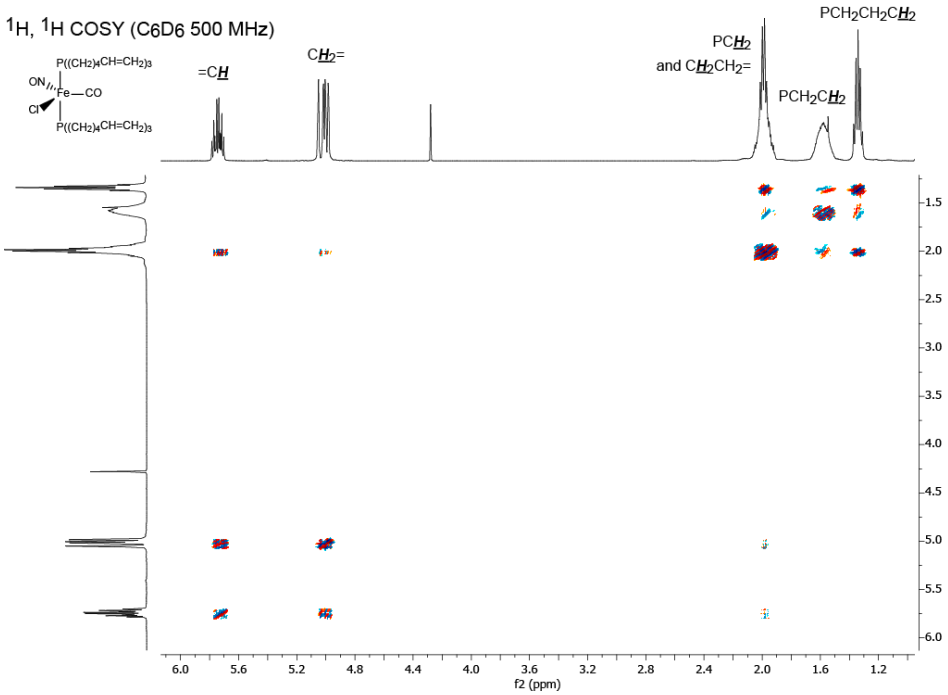

Figure 4-3. $^{1}H,^{1}H$ COSY NMR spectrum (500 MHz) of **4a-Cl** illustrating signal assignments.

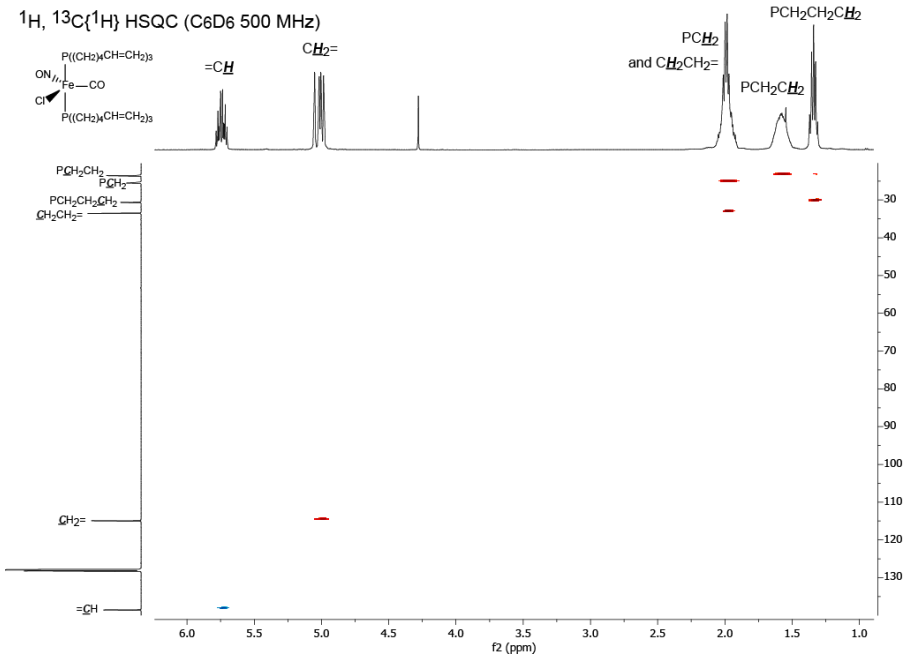

Figure 4-4. $^{1}H,^{13}C\{^{1}H\}$ HSQC NMR spectrum (500 MHz) of **4a-Cl** illustrating signal assignments.

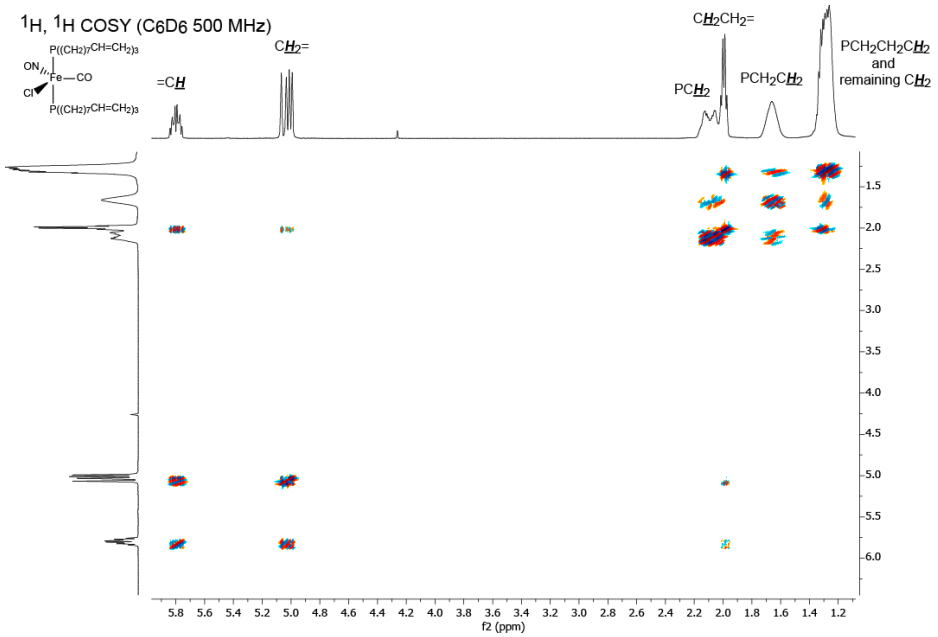

Figure 4-5. $^{1}H,^{1}H$ COSY NMR spectrum (500 MHz) of **4d-Cl** illustrating signal assignments.

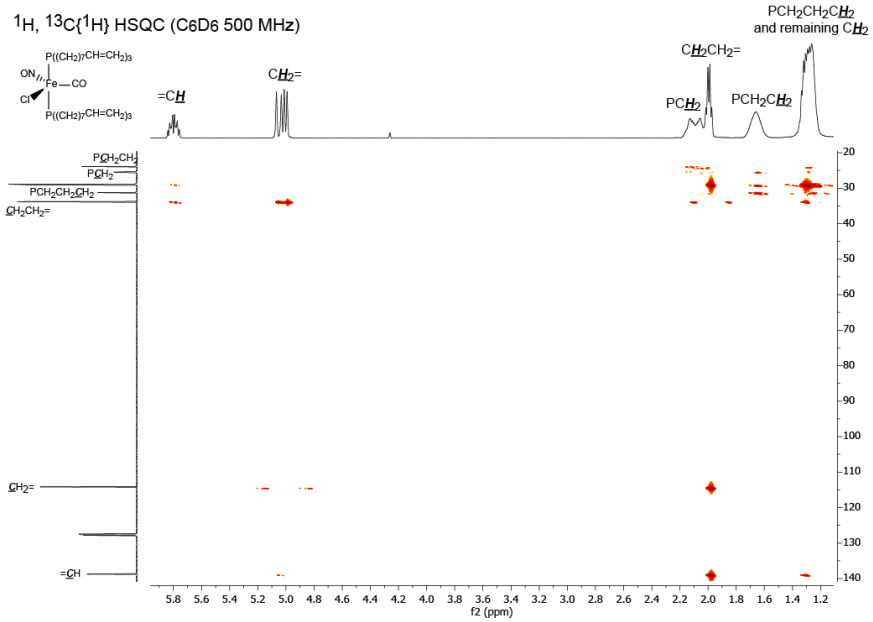

Figure 4-6. $^{1}H,^{13}C\{^{1}H\}$ HSQC NMR spectrum (500 MHz) of **4d-Cl** illustrating signal assignments.

The NMR data in Table 4-1 exhibit several monotonic trends. First, the ^{31}P NMR signals shift progressively upfield upon going from **2a-e** to **3a-e** to **4a-e-Cl** to **4a-e-Br** to

4a-e-I. However, the signals for the cyanide complexes **4a-e-CN** are ca. 3 ppm downfield of those of **3a-e**. The CO ^{13}C NMR signals also shift upfield upon going from **2a-e** to **3a-e**, but those of **4a-e-X** are all downfield of **2a-e**. There are no obvious chemical shift trends within **4a-e-X**, but the $^{2}J_{PC}$ values of the CO signals of the cyanide complexes are less than those of the halides (30 vs. 38-35 Hz). The P$\underline{C}$H$_2$ ^{13}C signals of the halide and cyanide complexes shift slightly downfield in the order X = Cl < Br < I < CN, but the PCH$_2$CH$_2$$\underline{C}H_2$ signals remain essentially constant.

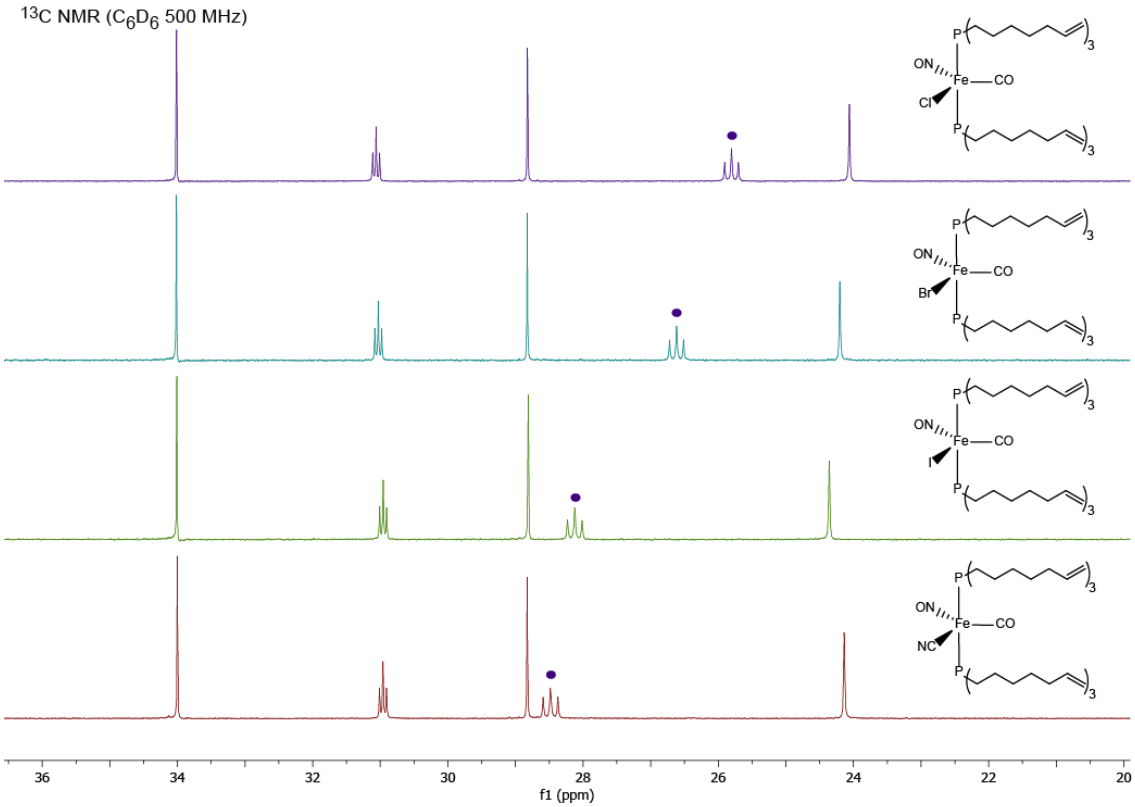

Figure 4-7. CH$_2$ region of the ^{13}C NMR spectra of *trans*-Fe(CO)(NO)(X)(P((CH$_2$)$_5$CH=CH$_2$)$_3$)$_2$ (**4b-Cl**, **Br**, **I**, and **CN**) illustrating the downfield shift of the PCH$_2$CH$_2$***C***H$_2$ signal.

4.2.2 An unexpected impurity

In the course of optimizing the halide substitution reactions, the salts *n*-Bu_4N^+ X^- were added in two fold excesses as solids as opposed to solutions per the experimental section. In these cases, the desired halide complexes **4a-e-X** were accompanied by minor byproducts (**5a-e**) with ^{31}P NMR signals at 40 ppm ($CDCl_3$; 41 ppm in C_6D_6), approximately coincident with those of **4a-e-I** but 4-12 ppm upfield of the other halide and cyanide complexes. The ratios, as assayed by uncorrected NMR integrals, ranged from 98:2 to 85:15. With careful column chromatography, **5a-e** could be separated, but the modified syntheses prevented their formation.

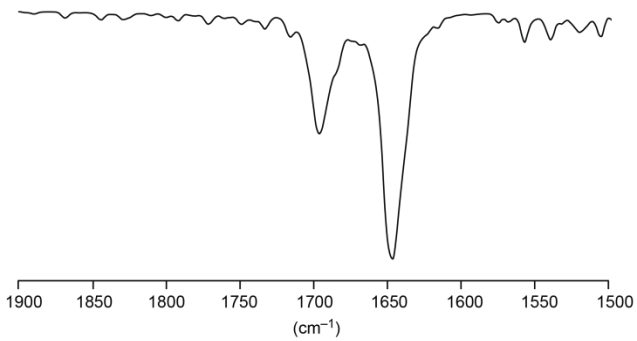

Figure 4-8. Select region of the IR spectrum of **5b**.

The byproducts accompanying **4b-Cl** and **4c-Br** were further characterized by ^1H and ^{13}C NMR and IR spectroscopy. The ^{13}C NMR spectra did not show any CO signals, and the P$\underline{C}H_2$ signals were shifted downfield (29.1 ppm, $CDCl_3$). The IR spectrum did not show any ν_{CO} bands, but two ν_{NO} bands, 1696 (m) and 1647 (s) cm^{-1} appeared to be present. Bitterwolf has reported that the tetrahedral bis(nitrosyl) bis(phosphine) complex

$Fe(NO)_2(P\textit{n}\text{-}Bu_3)_2$ exhibits a ^{31}P NMR signal at 39.46 ppm ($CDCl_3$) and IR ν_{NO} bands at 1696 and 1647 cm^{-1}.[114] Accordingly, **5a-e** were assigned the structures $Fe(NO)_2(P((CH_2)_mCH{=}CH_2)_3)_2$ as shown in Figure 4-9 (**5**).

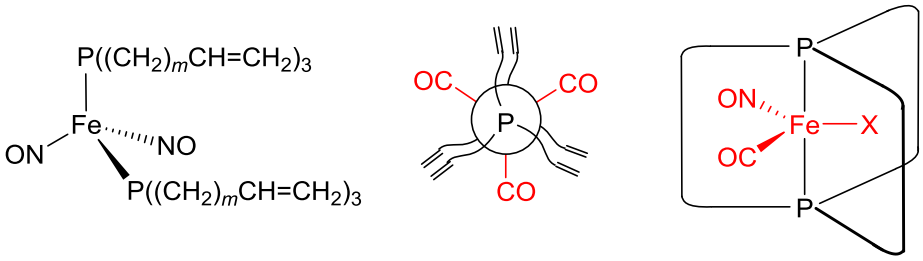

5 **VI** **VII**

Figure 4-9. Additional structures analyzed or discussed.

4.3 Discussion

This study has shown that iron(0) tricarbonyl, dicarbonyl nitrosyl, and carbonyl nitrosyl halide complexes of the general formulae $[Fe(CO)_x(NO)_y(X)_z(P((CH_2)_mCH{=}CH_2)_3)_2]^{n+}$ $n BF_4^-$ ($x/y/z/n$ = 3/0/0/0 (**2**), 2/1/0/1 (**3**), 1/1/1/0 (**4**)) are easily prepared by substitution sequences beginning with the readily available starting material $(BDA)Fe(CO)_3$ (Scheme 4-2).[90] Although all of these complexes proved to be oils, intuitively consistent with the methylene rich phosphine ligands, they could be isolated in good yields. For the endproducts **4a-e-X**, the average overall yield (three steps) is 58%.

Precedent for these transformations was mentioned in passing above, but three reports merit emphasis.[110-113] First, Dolcetti and coworkers reacted cationic dicarbonyl nitrosyl complexes of the formula $[Fe(CO)_2(NO)(PPh_3)_2]^+$ Z^- and sodium salts Na^+ X^-

(X = N_3, SCN, CNO, CN, SeCN) to give PPh_3 analogs of **4a-e-X**.[110] In contrast to our experiences with tri*alkyl*phosphine systems, these were noted as labile in organic solvents. Second, Lalor and coworkers used PPN^+ X^- (PPN = $Ph_3P{\cdots}N{\cdots}PPh_3$; X = Cl, Br) to similarly access the analogous chloride and bromide complexes.[111] Third, Berke and coworkers investigated reactions of iron(II) dichloride dicarbonyl bis(phosphorus donor ligand) complexes *cis*,*cis*,*trans*-$Fe(Cl)_2(CO)_2(L)_2$ with *t*-BuLi and NO^+ BF_4^-.[112] Workups gave analogs of **4a-e-Cl**, *trans*-$Fe(CO)(NO)(Cl)(L)_2$, with L = PEt_3, PMe_3, and $P(OiPr)_3$. The IR spectra of these three groups of complexes show trends similar to those in Table 4-1. However, there are little relevant NMR data, as only Berke reported ^{31}P and ^{13}C spectra.

Besides the preparative objectives, the other main impetus for this study was to establish spectroscopic reference data for precise comparisons with the analogous gyroscope like molecules in Scheme 4-1. One seeks to probe for "cage effects" with respect to both physical and chemical properties. While Table 4-1 provides the necessary baseline IR and NMR values, one remaining challenge would be the determination of a crystal structure, which has so far been thwarted by the oily nature of the products in Scheme 2. A partial rationale for the high yields of gyroscope like complexes that can be derived from **2a-e** involves the likely conformational energy minimum shown in **VI** (Figure 4-9), with mutually staggered $Fe(CO)_3$ and PR_3 fragments. This preorganizes the substrates in favor of *intra*molecular ring closing metatheses, as opposed to *inter*molecular condensations. It would be interesting to see if this feature is present in

the solid state structures of these complexes. Berke was able to obtain a crystal structure of *trans*-Fe(CO)(NO)(Cl)(PEt_3)$_2$, and the L-Fe-P-CH_2 torsion angles varied from 43.8-77.2° and 164.6-176.2°.[112] These two ranges approximate the values associated with idealized gauche (60°) and anti (180°) OC-Fe-P-CH_2 segments in **VI**.

In summary, this work sets the stage for (1) systematic studies of the optimum synthetic routes to iron gyroscope like complexes of the formulae *trans*-[$Fe(CO)_2(NO)(P((CH_2)_m)_3P)]^+$ BF_4^- and *trans*-Fe(CO)(NO)(X)($P((CH_2)_m)_3P$) and (2) the definition of a variety of "cage effects". Will it be advantageous to first carry out alkene metathesis to give the cage compounds, and then effect substitution reactions within the cage, or the other way around, carrying out metatheses using the substituted precursors **3a-e** and **4a-e-X**? These systems are particularly important as they contain a dipole moment in the equatorial plane. This presents an opportunity to orient the rotators using an electric field. Under favorable circumstances, a rotating electric field might be employed to drive rotation, providing a true molecular gyroscope.[7,9]

4.4 Experimental section

General data: all reactions were conducted under dry, inert atmospheres. Chemicals were treated as follows: CH_2Cl_2, THF, and hexanes (Fisher Scientific; reaction and workup solvents), dried and degassed using a Glass Contour solvent purification system; NO^+ BF_4^- (Alfa Aesar, 98%), *n*-Bu_4N^+ X^- (X = Cl or CN, Aldrich,

97-95%; Br, TCI, 99%; I, Alfa Aesar, 98%), C_6D_6, $CDCl_3$ (2 × Cambridge Isotope Laboratories), and silica (Silicycle, 40-63 μm, 230-400 mesh), used as received.

NMR spectra (Varian NMRS 500 MHz instrument) were recorded at ambient probe temperatures and referenced as follows (δ, ppm): ^{1}H, residual internal $CHCl_3$ (7.26) or C_6D_5H (7.16); ^{13}C, internal $CDCl_3$ (77.16) or C_6D_6 (128.06); $^{31}P\{^1H\}$, external H_3PO_4 (0.00). IR spectra were recorded using a Shimadzu IRAffinity-1 spectrometer with a Pike MIRacle ATR system (diamond/ZnSe crystal). Microanalyses were conducted by Atlantic Microlab.

***trans*-Fe(CO)$_3$(P((CH$_2$)$_4$CH=CH$_2$)$_3$)$_2$ (2a).** A Schlenk flask was charged with (BDA)$Fe(CO)_3$ (0.648 g, 2.27 mmol; BDA = benzylideneacetone),[90] THF (30 mL), and **1a** (1.398 g, 4.99 mmol)[88] with stirring. The red solution turned yellow/orange. After 15 h, the solvent was removed by oil pump vacuum. The residue was chromatographed on a silica gel column (1.5 × 20 cm) using hexanes and then 2:1 v/v hexanes/CH_2Cl_2. The solvent was removed from the filtrate by oil pump vacuum to give **2a** as a yellow/orange oil (1.148 g, 1.64 mmol, 72%). Anal. Calcd. for $C_{39}H_{66}FeO_3P_2$ (700.73): C 66.85, H 9.49; found: C 67.13, H 9.55.

NMR (δ, ppm $CDCl_3$):[109] ^{1}H (500 MHz) 5.98-5.69 (ddt, 6H, $^3J_{HH\textit{trans}}$ = 17.0 Hz, $^3J_{HH\textit{cis}}$ = 10.1 Hz, $^3J_{HH}$ = 6.9 Hz, C***H***=), 5.13-4.85 (m, 12H, =C***H***$_2$), 2.23-2.08 (m, 12H, C***H***$_2$CH=), 1.90-1.74 (m, 12H, C***H***$_2$), 1.70-1.46 (m, 24H, PCH_2CH_2C***H***$_2$ and remaining C***H***$_2$); $^{13}C\{^1H\}$ (125 MHz) 215.6 (t, $^2J_{CP}$ = 28.6 Hz, ***C***O), 138.5 (s, ***C***H=),

114.7 (s, =***C***H_2), 33.4 (s, ***C***H_2), 31.3 (virtual t,[37] $^3J_{CP}$ = 6.0 Hz, PCH_2CH_2***C***H_2), 28.8 (virtual m,[37] P***C***H_2), 23.3 (s, PCH_2***C***H_2); $^{31}P\{^1H\}$ (202 MHz) 63.6 (s).

IR (oil film, cm^{-1}): 2927 (w), 2854 (w), 1855 (s, ν_{CO}), 1640 (w), 1413 (w), 989 (w), 906 (w), 725 (w), 642 (s).

***trans*-Fe(CO)$_3$(P((CH$_2$)$_5$CH=CH$_2$)$_3$)$_2$ (2b).** A Schlenk flask was charged with (BDA)$Fe(CO)_3$ (0.403 g, 1.14 mmol)[90], THF (30 mL), and **1b** (1.002 g, 3.11 mmol)[88] with stirring. The red solution turned yellow/orange. After 17 h, the solvent was removed by oil pump vacuum. The residue was chromatographed on a silica gel column (1.5 × 20 cm) using hexanes and then 2:1 v/v hexanes/CH_2Cl_2. The solvent was removed from the filtrate by oil pump vacuum to give **2b** as a yellow/orange oil (0.683 g, 0.870 mmol, 62%). Anal. Calcd. for $C_{45}H_{78}FeO_3P_2$ (784.89): C 68.86, H 10.02; found: C 68.94, H 10.03.

NMR (δ, ppm $CDCl_3$):[109] ^1H (500 MHz) 5.92-5.74 (ddt, 6H, $^3J_{HHtrans}$ = 17.0 Hz, $^3J_{HHcis}$ = 10.3 Hz, $^3J_{HH}$ = 6.9 Hz, C***H***=), 5.09-4.91 (m, 12H, =C***H***$_2$), 2.14-2.03 (m, 12H, C***H***$_2$CH=), 1.85-1.72 (m, 12H, C***H***$_2$), 1.67-1.52 (m, 12H, C***H***$_2$), 1.52-1.38 (m, 24H, PCH_2CH_2C***H***$_2$ and remaining C***H***$_2$); $^{13}C\{^1H\}$ (125 MHz) 215.5 (t, $^2J_{CP}$ = 28.1 Hz, ***C***O), 138.9 (s, ***C***H=), 114.5 (s, =***C***H_2), 33.7 (s, ***C***H_2), 31.3 (virtual t,[37] $^3J_{CP}$ = 6.0 Hz, PCH_2CH_2***C***H_2), 28.8 (virtual m,[37] P***C***H_2), 28.5 (s, ***C***H_2), 23.6 (s, PCH_2***C***H_2); $^{31}P\{^1H\}$ (202 MHz) 63.2 (s) .

IR (oil film, cm^{-1}): 2926 (w), 2854 (w), 1855 (s, ν_{CO}), 1640 (w), 1413 (w), 991

(w), 906 (w), 723 (w), 642 (s).

***trans*-Fe(CO)$_3$(P((CH$_2$)$_6$CH=CH$_2$)$_3$)$_2$ (2c).** A Schlenk flask was charged with (BDA)Fe(CO)$_3$ (0.426 g, 1.49 mmol),[90] THF (30 mL), and **1c** (1.192 g, 3.27 mmol)[88] with stirring. The red solution turned yellow/orange. After 13h, the solvent was removed by oil pump vacuum. The residue was chromatographed on a silica gel column (1.5 × 20 cm) using hexanes and then 2:1 v/v hexanes/CH_2Cl_2. The solvent was removed from the filtrate by oil pump vacuum to give **2c** as a yellow/orange oil (0.930 g, 1.07 mmol, 72%). Anal. Calcd. for $C_{51}H_{90}FeO_3P_2$ (869.05): C 70.48, H 10.44; found: C 70.62, H 10.47.

NMR (δ, ppm $CDCl_3$):[109] ^{1}H (500 MHz) 5.93-5.70 (ddt, 6H, $^3J_{HH\textit{trans}}$ = 17.0 Hz, $^3J_{HH\textit{cis}}$ = 10.3 Hz, $^3J_{HH}$ = 6.9 Hz, C***H***=), 5.07-4.88 (m, 12H, =C***H***$_2$), 2.11-1.99 (m, 12H, C***H***$_2$CH=), 1.83-1.71 (m, 12H, C***H***$_2$), 1.62-1.48 (m, 12H, C***H***$_2$), 1.48-1.29 (m, 36H, PCH$_2$CH$_2$C***H***$_2$ and remaining C***H***$_2$); ^{13}C{^{1}H} (125 MHz) 214.4 (t, $^2J_{CP}$ = 28.6 Hz, ***C***O), 137.9 (s, ***C***H=), 113.2 (s, =***C***H$_2$), 32.7 (s, ***C***H$_2$), 30.0 (virtual t,[37] $^3J_{CP}$ = 6.3 Hz, PCH$_2$CH$_2$***C***H$_2$), 30.4 (virtual m,[37] P***C***H$_2$), 28.85 (s, ***C***H$_2$), 28.79 (s, ***C***H$_2$), 23.7 (s, PCH$_2$***C***H$_2$); ^{31}P{^{1}H} (202 MHz) 63.0 (s).

IR (oil film, cm^{-1}): 2924 (w), 2852 (w), 1857 (s, ν_{CO}), 1640 (w), 1463 (w), 993 (w), 908 (w), 721 (w), 642 (s).

***trans*-Fe(CO)$_3$(P((CH$_2$)$_7$CH=CH$_2$)$_3$)$_2$ (2d).** A Schlenk flask was charged with (BDA)Fe(CO)$_3$ (0.407 g, 1.42 mmol),[90] THF (30 mL), and **1d** (1.470 g, 3.61 mmol)[88]

with stirring. The red solution turned yellow/orange. After 16h, the solvent was removed by oil pump vacuum. The residue was chromatographed on a silica gel column (1.5 × 20 cm) using hexanes and then 2:1 v/v hexanes/CH_2Cl_2. The solvent was removed from the filtrate by oil pump vacuum to give **2d** as a yellow/orange oil (0.814 g, 0.854 mmol, 60%). Anal. Calcd. for $C_{57}H_{102}FeO_3P_2$ (953.21): C 71.82, H 10.79; found: C 71.69, H 10.78.

NMR (δ, ppm $CDCl_3$):[109] ^{1}H (500 MHz) 5.93-5.70 (ddt, 6H, $^3J_{HH\textit{trans}}$ = 17.0 Hz, $^3J_{HH\textit{cis}}$ = 10.1 Hz, $^3J_{HH}$ = 6.9 Hz, C***H***=), 5.07-4.88 (m, 12H, =C***H***$_2$), 2.12-1.99 (m, 12H, C***H***$_2$CH=), 1.83-1.71 (m, 12H, C***H***$_2$), 1.62-1.49 (m, 12H, C***H***$_2$), 1.49-1.29 (m, 48H, PCH_2CH_2C***H***$_2$ and remaining C***H***$_2$); $^{13}C\{^1H\}$ (125 MHz) 215.7 (t, $^2J_{CP}$ = 28.3 Hz, ***C***O), 139.2 (s, ***C***H=), 114.3 (s, =***C***H$_2$), 33.9 (s, ***C***H$_2$), 31.4 (virtual t,[37] $^3J_{CP}$ = 6.5 Hz, PCH_2CH_2***C***H$_2$), 29.2 (virtual m,[37] P***C***H$_2$), 29.2 (s, ***C***H$_2$), 29.1 (s, ***C***H$_2$), 29.0 (s, ***C***H$_2$), 23.8 (s, PCH_2***C***H$_2$); $^{31}P\{^1H\}$ (202 MHz) 63.0 (s).

IR (oil film, cm^{-1}): 2924 (w), 2852 (w), 1857 (s, ν_{CO}), 1640 (w), 1463 (w), 993 (w), 906 (w), 721 (w), 642 (s).

***trans*-Fe(CO)$_3$(P((CH$_2$)$_8$CH=CH$_2$)$_3$)$_2$ (2e).** A Schlenk flask was charged with (BDA)$Fe(CO)_3$ (0.289 g, 1.01 mmol),[90] THF (30 mL), and **1e** (0.998 g, 2.22 mmol)[88] with stirring. The red solution turned yellow/orange. After 15h, the solvent was removed by oil pump vacuum. The residue was chromatographed on a silica gel column (1.5 × 20 cm) using hexanes and then 2:1 v/v hexanes/CH_2Cl_2. The solvent was removed from the

filtrate by oil pump vacuum to give **2e** as a yellow/orange oil (0.790 g, 0.761 mmol, 75%). Anal. Calcd. for $C_{63}H_{114}FeO_3P_2$ (1037.37): C 72.94, H 11.08; found: C 73.20, H 11.12.

NMR (δ, ppm $CDCl_3$):[109] ^{1}H (500 MHz) 5.94-5.75 (ddt, 6H, $^3J_{HH\textit{trans}}$ = 17.0 Hz, $^3J_{HH\textit{cis}}$ = 10.1 Hz, $^3J_{HH}$ = 6.9 Hz, C***H***=), 5.08-4.89 (m, 12H, =C***H***$_2$), 2.12-1.99 (m, 12H, C***H***$_2$CH=), 1.86-1.71 (m, 12H, C***H***$_2$), 1.62-1.51 (m, 12H, C***H***$_2$), 1.46-1.22 (m, 60H, $PCH_2CH_2C\boldsymbol{H}_2$ and remaining C***H***$_2$); $^{13}C\{^1H\}$ (125 MHz) 215.6 (t, $^2J_{CP}$ = 28.5 Hz, ***C***O), 139.2 (s, ***C***H=), 114.1 (s, =***C***H$_2$), 33.8 (s, ***C***H$_2$), 31.3 (virtual t,[37] $^3J_{CP}$ = 6.5 Hz, $PCH_2CH_2\boldsymbol{C}H_2$), 29.2 (virtual m,[37] P***C***H$_2$), 29.4 (s, ***C***H$_2$), 29.2 (s, ***C***H$_2$), 29.1 (s, ***C***H$_2$), 28.9 (s, ***C***H$_2$), 23.7 (s, $PCH_2\boldsymbol{C}H_2$); $^{31}P\{^1H\}$ (202 MHz) 63.0 (s).

IR (oil film, cm^{-1}): 2924 (w), 2852 (w), 1857 (s, ν_{CO}), 1640 (w), 1463 (w), 991 (w), 906 (w), 746 (w), 721 (w), 642 (s).

[*trans*-Fe(CO)$_2$(NO)(P((CH$_2$)$_4$CH=CH$_2$)$_3$)$_2$]$^+$ BF$_4^-$ (3a). A Schlenk flask was charged with **2a** (0.942 g, 1.34 mmol) and CH_2Cl_2 (50 mL). Solid NO^+ BF_4^- (0.225 g, 1.93 mmol) was added with stirring. After 18 h, the solvent was removed by oil pump vacuum. The residue was suspended in CH_2Cl_2 (15 mL) and the mixture was filtered through a syringe filter. The solvent was removed from the filtrate by oil pump vacuum to give **3a** as an orange oil (1.029 g, 1.30 mmol, 97%). Anal. Calcd. for $C_{38}H_{66}FeNO_3P_2BF_4$ (789.53): C 57.81, H 8.43, N 1.77; found: C 57.51, H 8.32; N; 1.67.

NMR (δ, ppm $CDCl_3$):[109] ^1H (500 MHz) 5.82-5.71 (ddt, 6H, $^3J_{HHtrans}$ = 17.0 Hz, $^3J_{HHcis}$ = 10.1 Hz, $^3J_{HH}$ = 6.9 Hz, C***H***=), 5.07-4.95 (m, 12H, =C***H***$_2$), 2.75-2.16 (m, 12H, C***H***$_2$), 2.16-2.09 (m, 2H, C***H***$_2$), 1.65-1.57 (m, 12H, C***H***$_2$), 1.57-1.47 (m, 12H, C***H***$_2$); $^{13}C\{^1H\}$ (125 MHz) 206.8 (t, $^2J_{CP}$ = 28.6 Hz, ***C***O), 137.8 (s, ***C***H=), 115.6 (s, =***C***H$_2$), 33.0 (s, ***C***H$_2$), 29.7 (virtual t,[37] $^3J_{CP}$ = 6.5 Hz, PCH$_2$CH$_2$***C***H$_2$), 27.7 (virtual m,[37] P***C***H$_2$), 23.3 (s, PCH$_2$***C***H$_2$); $^{31}P\{^1H\}$ (202 MHz) 53.9 (s).

IR (oil film, cm^{-1}): 2931 (w), 2862 (w), 2031 (ν_{CO}), 1967 (ν_{CO}), 1768 (ν_{NO}), 1640 (w), 1415 (w), 1267 (w), 1051 (w), 993 (w), 910 (w), 732 (w), 640 (s).

[*trans*-Fe(CO)$_2$(NO)(P((CH$_2$)$_5$CH=CH$_2$)$_3$)$_2$]$^+$ BF$_4^-$ (3b). A Schlenk flask was charged with **2b** (0.992 g, 1.26 mmol) and CH_2Cl_2 (50 mL). Solid NO^+ BF_4^- (0.192 g, 1.65 mmol) was added to the solution with stirring. After 16 h, the solvent was removed by oil pump vacuum. The residue was suspended in a small amount of CH_2Cl_2 (15 mL) and the mixture was filtered through a syringe filter. The solvent was removed from the filtrate by oil pump vacuum to give **3b** as an orange oil (1.084 g, 1.24 mmol, 98%). Anal. Calcd. for $C_{44}H_{78}FeNO_3P_2BF_4$ (873.69): C 60.49, H 9.00, N 1.60; found: C 60.43, H 8.99, N 1.63.

NMR (δ, ppm $CDCl_3$):[109] ^1H (500 MHz) 5.83-5.72 (ddt, 6H, $^3J_{HHtrans}$ = 17.0 Hz, $^3J_{HHcis}$ = 10.1 Hz, $^3J_{HH}$ = 6.9 Hz, C***H***=), 5.02-4.91 (m, 12H, =C***H***$_2$), 2.26-2.15 (m, 12H, C***H***$_2$), 2.09-2.01 (m, 12H, C***H***$_2$), 1.57-1.48 (m, 24H, C***H***$_2$), 1.47-1.40 (m, 12H, C***H***$_2$); $^{13}C\{^1H\}$ (125 MHz) 207.0 (t, $^2J_{CP}$ = 25.1 Hz, ***C***O), 138.3 (s, ***C***H=), 114.8 (s,

=***C***H_2), 33.4 (s, ***C***H_2), 30.1 (virtual t,[37] $^3J_{CP}$ = 7.0 Hz, PCH_2CH_2***C***H_2), 28.3 (s, ***C***H_2), 27.7 (virtual m,[37] P***C***H_2), 23.8 (s, PCH_2***C***H_2); $^{31}P\{^1H\}$ (202 MHz) 53.5 (s).

IR (oil film, cm^{-1}): 2929 (w), 2856 (w), 2029 (ν_{CO}), 1967 (ν_{CO}), 1766 (ν_{NO}), 1640 (w), 1459 (w), 1051 (w), 993 (w), 908 (w), 732 (w), 634 (s).

[*trans*-Fe(CO)$_2$(NO)(P((CH$_2$)$_6$CH=CH$_2$)$_3$)$_2$]$^+$ BF$_4^-$ (3c). A Schlenk flask was charged with **2c** (0.424 g, 0.488 mmol) and CH_2Cl_2 (50 mL). Solid NO^+ BF_4^- (0.086 g, 0.738 mmol) was added to the solution with stirring. After 17 h, the solvent was removed by oil pump vacuum. The residue was suspended in a small amount of CH_2Cl_2 (15 mL) and the mixture was filtered through a syringe filter. The solvent was removed from the filtrate by oil pump vacuum to give **3c** as an orange oil (0.447 g, 0.467 mmol, 96%). Anal. Calcd. for $C_{50}H_{90}FeNO_3P_2BF_4$ (957.85): C 62.70, H 9.47, N 1.46; found: C 62.47, H 9.44, N 1.45.

NMR (δ, ppm $CDCl_3$):[109] ^1H (500 MHz) 5.85-5.72 (ddt, 6H, $^3J_{HH\textit{trans}}$ = 17.0 Hz, $^3J_{HH\textit{cis}}$ = 10.1 Hz, $^3J_{HH}$ = 6.9 Hz, C***H***=), 5.03-4.88 (m, 12H, =C***H***$_2$), 2.25-2.14 (m, 12H, C***H***$_2$), 2.07-2.00 (m, 12H, C***H***$_2$), 1.54-1.45 (m, 24H, C***H***$_2$) 1.41-1.30 (m, 24H, C***H***$_2$); $^{13}C\{^1H\}$ (125 MHz) 207.0 (t, $^2J_{CP}$ = 28.6 Hz, ***C***O), 138.7 (s, ***C***H=), 114.6 (s, =***C***H_2), 33.7 (s, ***C***H_2), 30.6 (virtual t,[37] $^3J_{CP}$ = 7.0 Hz, PCH_2CH_2***C***H_2), 28.6 (s, ***C***H_2), 28.57 (s, ***C***H_2), 27.7 (virtual m,[37] P***C***H_2), 24.0 (s, PCH_2***C***H_2); $^{31}P\{^1H\}$ (202 MHz) 53.2 (s).

IR (oil film, cm^{-1}): 2926 (w), 2854 (w), 2029 (ν_{CO}), 1967 (ν_{CO}), 1766 (ν_{NO}),

1640 (w), 1462 (w), 1053 (w), 993 (w), 906 (w), 723 (w), 634 (s).

[*trans*-$Fe(CO)_2(NO)(P((CH_2)_7CH{=}CH_2)_3)_2]^+$ BF_4^- (3d). A Schlenk flask was charged with **2d** (0.545 g, 0.572 mmol) and CH_2Cl_2 (50 mL). Solid NO^+ BF_4^- (0.101 g, 0.8681 mmol) was added to the solution with stirring. After 19 h, the solvent was removed by oil pump vacuum. The residue was suspended in a small amount of CH_2Cl_2 (15 mL) and the mixture was filtered through a syringe filter. The solvent was removed from the filtrate by oil pump vacuum to give **3d** as an orange oil (0.525 g, 0.503 mmol, 88%). Anal. Calcd. for $C_{56}H_{102}FeNO_3P_2BF_4$ (1042.01): C 64.55, H 9.87, N 1.34; found: C 64.26, H 9.95, N 1.55.

NMR (δ, ppm $CDCl_3$):[109] ^1H (500 MHz) 5.84-5.62 (ddt, 6H, $^3J_{HH\textit{trans}}$ = 17.0 Hz, $^3J_{HH\textit{cis}}$ = 10.1 Hz, $^3J_{HH}$ = 6.9 Hz, C***H***=), 5.09-4.88 (m, 12H, =C$\boldsymbol{H}_2$), 2.28-2.05 (m, 12H, C$\boldsymbol{H}_2$), 1.68-1.42 (m, 48H, C$\boldsymbol{H}_2$); $^{13}C\{^1H\}$ (125 MHz) 207.0 (t, $^2J_{CP}$ = 28.6 Hz, ***C***O), 139.0 (s, ***C***H=), 114.5 (s, =***C***H_2), 33.7 (s, ***C***H_2), 30.9 (virtual t,[37] $^3J_{CP}$ = 6.5 Hz, $PCH_2CH_2\boldsymbol{C}H_2$), 29.1 (s, ***C***$H_2$), 28.93 (s, ***C***$H_2$), 28.89 (s, ***C***$H_2$), 27.8 (virtual m,[37] P***C***H_2), 24.0 (s, $PCH_2\boldsymbol{C}H_2$); $^{31}P\{^1H\}$ (202 MHz) 53.3 (s).

IR (oil film, cm^{-1}): 2924 (w), 2854 (w), 2029 (ν_{CO}), 1967 (ν_{CO}), 1766 (ν_{NO}), 1456 (w), 1053 (w), 964 (w), 908 (w), 725 (w), 634 (s).

[*trans*-$Fe(CO)_2(NO)(P((CH_2)_8CH{=}CH_2)_3)_2]^+$ BF_4^- (3e). A Schlenk flask was charged with **2e** (0.796 g, 0.768 mmol) and CH_2Cl_2 (50 mL). Solid NO^+ BF_4^- (0.130 g, 1.11 mmol) was added to the solution with stirring. After 24 h, the solvent was removed

by oil pump vacuum. The residue was suspended in a small amount of CH_2Cl_2 (15 mL) and the mixture was filtered through a syringe filter. The solvent was removed from the filtrate by oil pump vacuum to give **3e** as an orange oil (0.826 g, 0.734 mmol, 96%). Anal. Calcd. for $C_{62}H_{114}FeNO_3P_2BF_4$ (1126.17): C 66.12, H 10.20, N 1.24; found: C 65.94, H 10.24, N 1.20.

NMR (δ, ppm $CDCl_3$):[109] ^{1}H (500 MHz) 5.87-5.70 (ddt, 6H, $^3J_{HH\textit{trans}}$ = 17.0 Hz, $^3J_{HH\textit{cis}}$ = 10.1 Hz, $^3J_{HH}$ = 6.9 Hz, C***H***=), 5.02-4.91 (m, 12H, =C***H***$_2$), 2.26-2.14 (m, 12H, C***H***$_2$), 2.08-1.98 (m, 12H, C***H***$_2$), 1.57-1.46 (m, 24H, C***H***$_2$) 1.41-1.26 (m, 48H, C***H***$_2$); ^{13}C{^{1}H} (125 MHz) 207.0 (t, $^2J_{CP}$ = 28.6 Hz, ***C***O), 139.1 (s, ***C***H=), 114.4 (s, =***C***H$_2$), 33.9 (s, ***C***H$_2$), 30.9 (virtual t,[37] $^3J_{CP}$ = 7.0 Hz, PCH$_2$CH$_2$***C***H$_2$), 29.3 (s, ***C***H$_2$), 29.2 (s, ***C***H$_2$), 29.1 (s, ***C***H$_2$), 29.0 (s, ***C***H$_2$), 27.8 (virtual m,[37] P***C***H$_2$), 24.1 (s, PCH$_2$***C***H$_2$); ^{31}P{^{1}H} (202 MHz) 53.4 (s).

IR (oil film, cm^{-1}): 2926 (w), 2854 (w), 2029 (ν_{CO}), 1967 (ν_{CO}), 1766 (ν_{NO}), 1456 (w), 1053 (w), 964 (w), 908 (w), 732 (w), 634 (s).

***trans*-Fe(CO)(NO)(Cl)(P((CH$_2$)$_4$CH=CH$_2$)$_3$)$_2$ (4a-Cl).** A Schlenk flask was charged with **3a** (0.313 g, 0.396 mmol) and CH_2Cl_2 (30 mL). Then a solution of $(CH_3(CH_2)_3)_4N^+$ Cl^- (0.143 g, 0.515 mmol) in CH_2Cl_2 (10 mL) was added with stirring. After 16 h, the solvent was removed by oil pump vacuum. The red/brown oil was chromatographed on a silica gel column (1.5 × 20 cm) with hexanes and then hexanes/CH_2Cl_2 (4:1, 3:1, and then 2:1 v/v). The solvent was removed from the red

fraction by oil pump vacuum to give **4a-Cl** as a red oil (0.233 g, 0.329 mmol, 83%). Anal. Calcd. for $C_{37}H_{66}FeClNO_2P_2$ (710.17): C 62.58, H 9.37, N 1.97; found: C 62.80, H 9.50, N 1.98.

NMR (δ, ppm C_6D_6):[109] ^{1}H (500 MHz) 5.88-5.67 (ddt, 6H, $^3J_{HHtrans}$ = 17.0 Hz, $^3J_{HHcis}$ = 10.1 Hz, $^3J_{HH}$ = 6.9 Hz, C***H***=), 5.06-4.94 (m, 12H, =C***H***$_2$), 2.10-1.86 (m, 24H, PC***H***$_2$ and C*H*$_2$CH=CH$_2$), 1.67-1.48 (m, 12H, PCH$_2$C***H***$_2$), 1.39-1.28 (m, 12H, PCH$_2$CH$_2$C***H***$_2$); ^{13}C{^{1}H} (125 MHz) 220.9 (t, $^2J_{CP}$ = 37.1 Hz, ***C***O), 138.6 (s, ***C***H=), 114.9 (s, =***C***H$_2$), 33.6 (s, *C*H$_2$CH=CH$_2$), 30.7 (virtual t,[37] $^3J_{CP}$ = 6.3 Hz, PCH$_2$CH$_2$***C***H$_2$), 25.6 (virtual t,[37] $^1J_{CP}$ = 12.7 Hz, P***C***H$_2$), 23.6 (s, PCH$_2$***C***H$_2$); ^{31}P{^{1}H} (202 MHz) 47.4 (s).

IR (oil film, cm^{-1}): 3076 (w), 2926 (m), 2854 (w), 1901 (ν_{CO}, s), 1668 (ν_{NO}, s), 1639 (m), 1442 (w), 1413 (w), 991 (w), 901 (s), 723 (w).

***trans*-Fe(CO)(NO)(Br)(P((CH$_2$)$_4$CH=CH$_2$)$_3$)$_2$ (4a-Br).** A Schlenk flask was charged with **3a** (0.472 g, 0.598 mmol) and CH_2Cl_2 (25 mL). Then a solution of $(CH_3(CH_2)_3)_4N^+$ Br^- (0.251 g, 0.777 mmol) in CH_2Cl_2 (10 mL) was added with stirring. After 16 h, the solvent was removed by oil pump vacuum. The red/brown oil was chromatographed on a silica gel column (1.5 × 20 cm) with hexanes and then hexanes/CH_2Cl_2 mixtures (4:1 and then 2:1 v/v). The solvent was removed from the red fraction by oil pump vacuum to give **4a-Br** as a red oil (0.411 g, 0.544 mmol, 91%). Anal. Calcd. for $C_{37}H_{66}FeBrNO_2P_2$ (754.62): C 58.89, H 8.82, N 1.86; found: C 58.85,

H 8.93, N 1.92.

NMR (δ, ppm C_6D_6):[109] ^{1}H (500 MHz) 5.78-5.60 (ddt, 6H, $^3J_{HHtrans}$ = 17.0 Hz, $^3J_{HHcis}$ = 10.1 Hz, $^3J_{HH}$ = 6.9 Hz, C***H***=), 5.09-4.95 (m, 12H, =C***H***$_2$), 2.16-1.95 (m, 24H, PC***H***$_2$ and C*H*$_2$CH=CH$_2$), 1.60-1.48 (m, 12H, PCH$_2$C***H***$_2$), 1.35-1.21 (m, 12H, PCH$_2$CH$_2$C*H*$_2$); ^{13}C{^{1}H} (125 MHz) 220.4 (t, $^2J_{CP}$ = 38.0 Hz, ***C***O), 138.5 (s, ***C***H=), 114.9 (s, =***C***H$_2$), 33.6 (s, *C*H$_2$CH=CH$_2$), 30.6 (virtual t,[37] $^3J_{CP}$ = 6.7 Hz, PCH$_2$CH$_2$***C***H$_2$), 26.3 (virtual t,[37] $^1J_{CP}$ = 12.7 Hz, P***C***H$_2$), 23.7 (s, PCH$_2$***C***H$_2$); ^{31}P{^{1}H} (202 MHz) 44.6 (s).

IR (oil film, cm^{-1}): 3076 (w), 2926 (m), 2854 (w), 1903 (ν_{CO}, s), 1674 (ν_{NO}, s), 1639 (m), 1442 (w), 1413 (w), 989 (w), 901 (s).

***trans*-Fe(CO)(NO)(I)(P((CH$_2$)$_4$CH=CH$_2$)$_3$)$_2$ (4a-I).** A Schlenk flask was charged with **3a** (0.263 g, 0.333 mmol) and CH_2Cl_2 (30 mL). Then a solution of $(CH_3(CH_2)_3)_4N^+$ I^- (0.123g, 0.333 mmol) in CH_2Cl_2 (10 mL) was added with stirring. After 16 h, the solvent was removed by oil pump vacuum. The red/brown oil was chromatographed on a silica gel column (1.5 × 20 cm) with hexanes and then hexanes/CH_2Cl_2 mixtures (4:1 and then 2:1 v/v). The solvent was removed from the red fraction by oil pump vacuum to give **4a-I** as a red oil (0.246 g, 0.300 mmol, 92%). Anal. Calcd. for $C_{37}H_{66}FeINO_2P_2$ (801.62): C 55.44, H 8.30, N 1.75; found: C 55.27, H 8.25, N 1.82.

NMR (δ, ppm C_6D_6):[109] ^{1}H (500 MHz) 5.81-5.59 (ddt, 6H, $^3J_{HHtrans}$ = 17.0 Hz,

$^3J_{HHcis}$ = 10.1 Hz, $^3J_{HH}$ = 6.9 Hz, C***H***=), 5.17-4.81 (m, 12H, =C***H***$_2$), 2.25-2.12 (m, 12H, PC***H***$_2$), 2.03-1.95 (m, 12H, C***H***$_2$CH=CH$_2$), 1.72-1.45 (m, 12H, PCH$_2$C***H***$_2$), 1.39-1.28 (m, 12H, PCH$_2$CH$_2$C*H*$_2$); ^{13}C{^{1}H} (125 MHz) 219.9 (t, $^2J_{CP}$ = 36.0 Hz, ***C***O), 138.1 (s, ***C***H=), 114.6 (s, =***C***H$_2$), 33.1 (s, *C*H$_2$CH=CH$_2$), 30.2 (virtual t,[37] $^3J_{CP}$ = 7.5 Hz, PCH$_2$CH$_2$***C***H$_2$), 27.4 (virtual t,[37] $^1J_{CP}$ = 12.7 Hz, P***C***H$_2$), 23.4 (s, PCH$_2$***C***H$_2$); ^{31}P{^{1}H} (202 MHz) 41.1 (s).

IR (oil film, cm^{-1}): 3076 (w), 2926 (m), 2854 (w), 1905 (ν_{CO}, s), 1681 (ν_{NO}, s), 1639 (m), 1436 (w), 1415 (w), 989 (w), 908 (s), 725 (m), 636 (w).

***trans*-Fe(CO)(NO)(CN)(P((CH$_2$)$_4$CH=CH$_2$)$_3$)$_2$ (4a-CN).** A Schlenk flask was charged with **3a** (0.350 g, 0.443 mmol) and CH_2Cl_2 (25 mL). Then a solution of $(CH_3(CH_2)_3)_4N^+$ CN^- (0.119 g, 0.443 mmol) in CH_2Cl_2 (10 mL) was added with stirring. After 16 h, the solvent was removed by oil pump vacuum. The red/brown oil was chromatographed on a silica gel column (1.5 × 20 cm) with a 2:1 v/v mixture of hexanes/CH_2Cl_2 and then CH_2Cl_2. The solvent was removed from the red fraction by oil pump vacuum to give **4a-CN** as a red oil (0.267 g, 0.381 mmol, 86%). Anal. Calcd. for $C_{38}H_{66}FeN_2O_2P_2$ (700.74): C 65.13, H 9.49, N 4.00; found: C 65.37, H 9.55, N 4.19.

NMR (δ, ppm C_6D_6):[109] ^{1}H (500 MHz) 5.85-5.66 (ddt, 6H, $^3J_{HHtrans}$ = 17.0 Hz, $^3J_{HHcis}$ = 10.1 Hz, $^3J_{HH}$ = 6.9 Hz, C***H***=), 5.12-4.93 (m, 12H, =C***H***$_2$), 2.07-1.95 (m, 24H, PC***H***$_2$ and C***H***$_2$CH=CH$_2$), 1.68-1.49 (m, 12H, PCH$_2$C***H***$_2$), 1.40-1.28 (m, 12H, PCH$_2$CH$_2$C*H*$_2$); ^{13}C{^{1}H} (125 MHz) 220.2 (t, $^2J_{CP}$ = 30.0 Hz, ***C***O), 141.9 (t, $^2J_{CP}$ =

42.0 Hz, ***C***N), 138.5 (s, =***C***H), 115.1 (s, =***C***H_2), 33.6 (s, *C*H_2CH=CH_2), 30.6 (virtual t,[37] $^3J_{CP}$ = 7.0 Hz, PCH_2CH_2***C***H_2), 28.3 (virtual t,[37] $^1J_{CP}$ = 12.7 Hz, P***C***H_2), 23.7 (s, PCH_2***C***H_2); $^{31}P\{^1H\}$ (202 MHz) 56.3 (s).

IR (oil film, cm^{-1}): 3076 (w), 2941 (w), 2866 (w), 2096 (ν_{CN}, m), 1913 (ν_{CO}, s), 1697 (ν_{NO}, s), 1639 (m), 1440 (w), 1415 (w), 991 (m), 908 (s), 727 (m), 632 (w), 613 (s).

***trans*-Fe(CO)(NO)(Cl)(P((CH$_2$)$_5$CH=CH$_2$)$_3$)$_2$ (4b-Cl).** A Schlenk flask was charged with **3b** (0.513 g, 0.587 mmol) and CH_2Cl_2 (30 mL). Then a solution of $(CH_3(CH_2)_3)_4N^+$ Cl^- (0.168 g, 0.605 mmol) in CH_2Cl_2 (10 mL) was added with stirring. After 16 h, the solvent was removed by oil pump vacuum. The red/brown oil was chromatographed on a silica gel column (1.5 × 20 cm) with hexanes and then hexanes/CH_2Cl_2 mixtures (4:1, 3:1, and then 2:1, v/v). The solvent was removed from the red fraction by oil pump vacuum to give **4b-Cl** as a red oil (0.410 g, 0.516 mmol, 88%). Anal. Calcd. for $C_{43}H_{78}FeClNO_2P_2$ (794.33): C 65.02, H 9.90, N 1.76; found: C 65.16, H 9.85, N 1.84.

NMR (δ, ppm C_6D_6):[109] ^1H (500 MHz) 5.91-5.66 (ddt, 6H, $^3J_{HH\textit{trans}}$ = 17.0 Hz, $^3J_{HH\textit{cis}}$ = 10.1 Hz, $^3J_{HH}$ = 6.9 Hz, C***H***=), 5.14-4.95 (m, 12H, =C***H***$_2$), 2.07-1.91 (m, 24H, PC***H***$_2$ and C*H*$_2$CH=CH_2), 1.66-1.48 (m, 12H, PCH_2C***H***$_2$), 1.37-1.20 (m, 24H, PCH_2CH_2C***H***$_2$ and remaining C***H***$_2$); $^{13}C\{^1H\}$ (125 MHz) 220.9 (t, $^2J_{CP}$ = 38.0 Hz, ***C***O), 138.9 (s, ***C***H=), 114.8 (s, =***C***H_2), 34.0 (s, ***C***H_2CH=CH_2), 31.1 (virtual t,[37] $^3J_{CP}$ =

7.1 Hz, $PCH_2CH_2\boldsymbol{C}H_2$), 28.8 (s, $\boldsymbol{C}H_2$), 25.8 (virtual t,[37] $^1J_{CP}$ = 13.0 Hz, $P\boldsymbol{C}H_2$), 24.1 (s, $PCH_2\boldsymbol{C}H_2$); $^{31}P\{^1H\}$ (202 MHz) 47.4 (s).

IR (oil film, cm^{-1}): 3076 (w), 2926 (m), 2854 (w), 1901 (ν_{CO}, s), 1668 (ν_{NO}, s), 1641 (m), 1441 (w), 1413 (w), 991 (w), 906 (s), 721 (w).

***trans*-Fe(CO)(NO)(Br)(P((CH$_2$)$_5$CH=CH$_2$)$_3$)$_2$ (4b-Br).** A Schlenk flask was charged with **3b** (0.326 g, 0.373 mmol) and CH_2Cl_2 (25 mL). Then a solution of $(CH_3(CH_2)_3)_4N^+$ Br^- (0.130 g, 0.404 mmol) in CH_2Cl_2 (10 mL) was added with stirring. After 16 h, the solvent was removed by oil pump vacuum. The red/brown oil was chromatographed on a silica gel column (1.5 × 20 cm) with hexanes and then hexanes/CH_2Cl_2 mixtures (4:1 and then 2:1, v/v). The solvent was removed from the red fraction by oil pump vacuum to give **4b-Br** as a red oil (0.282 g, 0.336 mmol, 90%). Anal. Calcd. for $C_{43}H_{78}FeBrNO_2P_2$ (838.78): C 61.57, H 9.37, N 1.67; found: C 61.61, H 9.42, N 1.84.

NMR (δ, ppm C_6D_6):[109] ^1H (500 MHz) 5.94-5.64 (ddt, 6H, $^3J_{HH\textit{trans}}$ = 17.0 Hz, $^3J_{HH\textit{cis}}$ = 10.1 Hz, $^3J_{HH}$ = 6.9 Hz, C***H***=), 5.11-4.93 (m, 12H, =C$\boldsymbol{H}_2$), 2.20-2.03 (m, 12H, C$\boldsymbol{H}_2$), 2.03-1.94 (m, 12H, C$\boldsymbol{H}_2$), 1.71-1.47 (m, 12H, $PCH_2C\boldsymbol{H}_2$), 1.41-1.22 (m, 24H, $PCH_2CH_2C\boldsymbol{H}_2$ and remaining C$\boldsymbol{H}_2$); $^{13}C\{^1H\}$ (125 MHz) 220.6 (t, $^2J_{CP}$ = 37.1 Hz, ***C***O), 138.9 (s, ***C***H=), 114.8 (s, =***C***H_2), 34.0 (s, *C*H_2CH=CH_2), 31.0 (virtual t,[37] $^3J_{CP}$ = 6.5 Hz, $PCH_2CH_2\boldsymbol{C}H_2$), 28.8 (s, $\boldsymbol{C}H_2$), 26.6 (virtual t,[37] $^1J_{CP}$ = 13.0 Hz, $P\boldsymbol{C}H_2$), 24.2 (s, $PCH_2\boldsymbol{C}H_2$); $^{31}P\{^1H\}$ (202 MHz) 44.1 (s).

IR (oil film, cm^{-1}): 3076 (w), 2926 (m), 2854 (w), 1903 (ν_{CO}, s), 1672 (ν_{NO}, s), 1639 (m), 1456 (w), 1413 (w), 991 (m), 906 (s), 721 (m).

***trans*-Fe(CO)(NO)(I)(P((CH$_2$)$_5$CH=CH$_2$)$_3$)$_2$ (4b-I).** A Schlenk flask was charged with **3b** (0.375 g, 0.429 mmol) and CH_2Cl_2 (30 mL). Then a solution of $(CH_3(CH_2)_3)_4N^+ I^-$ (0.168 g, 0.456 mmol) in CH_2Cl_2 (10 mL) was added with stirring. After 16 h, the solvent was removed by oil pump vacuum. The red/brown oil was chromatographed on a silica gel column (1.5 × 20 cm) with hexanes and then hexanes/CH_2Cl_2 mixtures (4:1 and then 2:1, v/v). The solvent was removed from the red fraction by oil pump vacuum to give **4b-I** as a red oil (0.353 g, 0.399 mmol, 93%). Anal. Calcd. for $C_{43}H_{78}FeINO_2P_2$ (885.78): C 58.31, H 8.88, N 1.58; found: C 58.56, H 8.91, N 1.79.

NMR (δ, ppm C_6D_6):[109] ^{1}H (500 MHz) 5.94-5.64 (ddt, 6H, $^3J_{HH\textit{trans}}$ = 17.0 Hz, $^3J_{HH\textit{cis}}$ = 10.1 Hz, $^3J_{HH}$ = 6.9 Hz, C***H***=), 5.11-4.93 (m, 12H, =C***H***$_2$), 2.20-2.03 (m, 12H, PC***H***$_2$), 2.03-1.94 (m, 12H, C***H***$_2$CH=CH$_2$), 1.71-1.47 (m, 12H, PCH$_2$C***H***$_2$), 1.41-1.22 (m, 24H, PCH$_2$CH$_2$C***H***$_2$ and remaining C***H***$_2$); ^{13}C{^{1}H} (125 MHz) 220.5 (t, $^2J_{CP}$ = 36.1 Hz, ***C***O), 138.9 (s, ***C***H=), 114.8 (s, =***C***H$_2$), 34.0 (s, *C*H$_2$CH=CH$_2$), 31.0 (virtual t,[37] $^3J_{CP}$ = 6.5 Hz, PCH$_2$CH$_2$***C***H$_2$), 28.8 (s, ***C***H$_2$), 28.1 (virtual t,[37] $^1J_{CP}$ = 13.1 Hz, P***C***H$_2$), 24.4 (s, PCH$_2$***C***H$_2$); ^{31}P{^{1}H} (202 MHz) 40.9 (s).

IR (oil film, cm^{-1}): 3076 (w), 2924 (s), 2852 (m), 1905 (ν_{CO}, s), 1681 (ν_{NO}, s), 1641 (w), 1458 (w), 1413 (w), 991 (m), 906 (s), 719 (m).

***trans*-Fe(CO)(NO)(CN)(P((CH$_2$)$_5$CH=CH$_2$)$_3$)$_2$ (4b-CN).** A Schlenk flask was charged with **3b** (0.263g, 0.301 mmol) and CH_2Cl_2 (25 mL). Then a solution of $(CH_3(CH_2)_3)_4N^+$ CN^- (0.086 g, 0.320 mmol) in CH_2Cl_2 (10 mL) was added with stirring. After 16 h, the solvent was removed by oil pump vacuum. The red/brown oil was chromatographed on a silica gel column (1.5 × 20 cm) with a 2:1 v/v mixture of hexanes/CH_2Cl_2 and then CH_2Cl_2. The solvent was removed from the red fraction by oil pump vacuum to give **4b-CN** as a red oil (0.205 g, 0.262 mmol, 87%). Anal. Calcd. for $C_{44}H_{78}FeN_2O_2P_2$ (784.89): C 67.33, H 10.02, N 3.57; found: C 67.15, H 10.08, N 3.57.

NMR (δ, ppm C_6D_6):[109] ^{1}H (500 MHz) 5.83-5.70 (ddt, 6H, $^3J_{HH\textit{trans}}$ = 17.0 Hz, $^3J_{HH\textit{cis}}$ = 10.1 Hz, $^3J_{HH}$ = 6.9 Hz, C***H***=), 5.13-4.93 (m, 12H, =C***H***$_2$), 2.08-1.92 (m, 24H, PC***H***$_2$ and C***H***$_2$CH=CH$_2$), 1.68-1.51 (m, 12H, PCH$_2$C***H***$_2$), 1.38-1.24 (m, 24H, PCH$_2$CH$_2$C***H***$_2$ and remaining C***H***$_2$); ^{13}C{^{1}H} (125 MHz) 220.3 (t, $^2J_{CP}$ = 30.5 Hz, ***C***O), 141.7 (t, $^2J_{CP}$ = 42 Hz, ***C***N), 138.9 (s, ***C***H=), 114.8 (s, =***C***H$_2$), 34.0 (s, *C*H$_2$CH=CH$_2$), 30.9 (virtual t,[37] $^3J_{CP}$ = 6.5 Hz, PCH$_2$CH$_2$***C***H$_2$), 28.8 (s, ***C***H$_2$), 28.5 (virtual t,[37] $^1J_{CP}$ = 13.7 Hz, P***C***H$_2$), 24.1 (s, PCH$_2$***C***H$_2$); ^{31}P{^{1}H} (202 MHz) 56.2 (s).

IR (oil film, cm^{-1}): 3076 (w), 2926 (s), 2854 (w), 2096 (ν_{CN}, m), 1913 (ν_{CO}, s), 1699 (ν_{NO}, s), 1639 (m), 1458 (w), 1413 (w), 993 (m), 906 (s), 721 (m), 634 (m), 615 (s).

***trans*-Fe(CO)(NO)(Cl)(P((CH$_2$)$_6$CH=CH$_2$)$_3$)$_2$ (4c-Cl).** A Schlenk flask was charged with **3c** (0.500 g, 0.522 mmol) and CH_2Cl_2 (60 mL). Then a solution of

$(CH_3(CH_2)_3)_4N^+$ Cl^- (0.283 g, 1.04 mmol) in CH_2Cl_2 (10 mL) was added with stirring. After 16 h, the solvent was removed by oil pump vacuum. The red/brown oil was chromatographed on a silica gel column (1.5 × 20 cm) with hexanes and then hexanes/CH_2Cl_2 mixtures (4:1, 3:1, and then 2:1, v/v). The solvent was removed from the red fraction by oil pump vacuum to give **4c-Cl** as a red oil (0.391 g, 0.444 mmol, 85%). Anal. Calcd. for $C_{49}H_{90}FeClNO_2P_2$ (878.49): C 66.99, H 10.33, N 1.59; found: C 67.07, H 10.44, N 1.64.

NMR (δ, ppm C_6D_6):[109] ^{1}H (500 MHz) 5.84-5.73 (ddt, 6H, $^3J_{HHtrans}$ = 17.0 Hz, $^3J_{HHcis}$ = 10.1 Hz, $^3J_{HH}$ = 6.9 Hz, C***H***=), 5.08-4.96 (m, 12H, =C***H***$_2$), 2.11-1.92 (m, 24H, PC***H***$_2$ and C*H*$_2$CH=CH$_2$), 1.70-1.50 (m, 12H, PCH$_2$C***H***$_2$), 1.35-1.21 (m, 36H, PCH$_2$CH$_2$C***H***$_2$ and remaining C***H***$_2$); $^{13}C\{^1H\}$ (125 MHz) 221.1 (t, $^2J_{CP}$ = 37.2 Hz, ***C***O), 139.1 (s, ***C***H=), 114.6 (s, =***C***H$_2$), 34.2 (s, ***C***H$_2$CH=CH$_2$), 31.6 (virtual t,[37] $^3J_{CP}$ = 6.3 Hz, PCH$_2$CH$_2$***C***H$_2$), 29.2 (s, ***C***H$_2$), 29.1 (s, ***C***H$_2$), 25.8 (virtual t,[37] $^1J_{CP}$ = 13.3 Hz, P***C***H$_2$), 24.2 (s, PCH$_2$***C***H$_2$); $^{31}P\{^1H\}$ (202 MHz) 47.4 (s).

IR (oil film, cm^{-1}): 3076 (w), 2924 (m), 2852 (w), 1901 (ν_{CO}, s), 1668 (ν_{NO}, s), 1641 (m), 1458 (w), 1413 (w), 993 (w), 906 (s), 719 (m).

***trans*-Fe(CO)(NO)(Br)(P((CH$_2$)$_6$CH=CH$_2$)$_3$)$_2$ (4c-Br).** A Schlenk flask was charged with **3c** (0.150 g, 0.156 mmol) and CH_2Cl_2 (25 mL). Then a solution of $(CH_3(CH_2)_3)_4N^+$ Br^- (0.101 g, 0.313 mmol) in CH_2Cl_2 (10 mL) was added with stirring. After 16 h, the solvent was removed by oil pump vacuum. The red/brown oil

was chromatographed on a silica gel column (1.5 × 20 cm) with hexanes and then hexanes/CH_2Cl_2 mixtures (4:1 and then 2:1 v/v). The solvent was removed from the red fraction by oil pump vacuum to give **4c-Br** as a red oil (0.130 g, 0.142 mmol, 91%). Anal. Calcd. for $C_{49}H_{90}FeBrNO_2P_2$ (922.94): C 63.77, H 9.83, N 1.52; found: C 63.98, H 9.91, N 1.57.

NMR (δ, ppm C_6D_6):[109] ^{1}H (500 MHz) 5.86-5.74 (ddt, 6H, $^3J_{HHtrans}$ = 17.0 Hz, $^3J_{HHcis}$ = 10.1 Hz, $^3J_{HH}$ = 6.9 Hz, C***H***=), 5.09-4.97 (m, 12H, =C***H***$_2$), 2.22-2.07 (m, 12H, PC***H***$_2$), 2.01-1.95 (m, 12H, C***H***$_2$CH=CH$_2$), 1.70-1.50 (m, 12H, PCH$_2$C***H***$_2$), 1.35-1.21 (m, 36H, PCH$_2$CH$_2$C*H*$_2$ and remaining C***H***$_2$); ^{13}C{^{1}H} (125 MHz) 220.7 (t, $^2J_{CP}$ = 36.9 Hz, ***C***O), 139.1 (s, ***C***H=), 114.7 (s, =***C***H$_2$), 34.2 (s, *C*H$_2$CH=CH$_2$), 31.5 (virtual t,[37] $^3J_{CP}$ = 6.3 Hz, PCH$_2$CH$_2$***C***H$_2$), 29.2 (s, ***C***H$_2$), 29.1 (s, ***C***H$_2$), 26.6 (virtual t,[37] $^1J_{CP}$ = 13.2 Hz, P***C***H$_2$), 24.4 (s, PCH$_2$***C***H$_2$); ^{31}P{^{1}H} (202 MHz) 44.2 (s).

IR (oil film, cm^{-1}): 3076 (w), 2924 (m), 2852 (w), 1903 (ν_{CO}, s), 1674 (ν_{NO}, s), 1639 (m), 1456 (w), 1413 (w), 993 (w), 906 (s), 719 (m).

***trans*-Fe(CO)(NO)(I)(P((CH$_2$)$_6$CH=CH$_2$)$_3$)$_2$ (4c-I).** A Schlenk flask was charged with **3c** (0.500 g, 0.522 mmol) and CH_2Cl_2 (30 mL). Then a solution of $(CH_3(CH_2)_3)_4N^+$ I^- (0.385 g, 1.044 mmol) in CH_2Cl_2 (10 mL) was added with stirring. After 16 h, the solvent was removed by oil pump vacuum. The red/brown oil was chromatographed on a silica gel column (1.5 × 20 cm) with hexanes and then hexanes/CH_2Cl_2 mixtures (4:1 and then 2:1, v/v). The solvent was removed from the red

fraction by oil pump vacuum to give **4c-I** as a red oil (0.465 g, 0.480 mmol, 91%). Anal. Calcd. for $C_{49}H_{90}FeINO_2P_2$ (969.94): C 60.68, H 9.35, N 1.44; found: C 60.78, H 9.39, N 1.51.

NMR (δ, ppm C_6D_6)[109] ^{1}H (500 MHz) 5.85-5.75 (ddt, 6H, $^3J_{HHtrans}$ = 17.0 Hz, $^3J_{HHcis}$ = 10.1 Hz, $^3J_{HH}$ = 6.9 Hz, C***H***=), 5.08-4.99 (m, 12H, =C***H***$_2$), 2.32-2.25 (m, 12H, PC***H***$_2$), 2.02-1.96 (m, 12H, C***H***$_2$CH=CH$_2$), 1.73-1.55 (m, 12H, PCH$_2$C***H***$_2$), 1.37-1.25 (m, 36H, PCH$_2$CH$_2$C***H***$_2$ and remaining C***H***$_2$); ^{13}C{^{1}H} (125 MHz) 220.5 (t, $^2J_{CP}$ = 35.5 Hz, ***C***O), 139.1 (s, ***C***H=), 114.7 (s, =***C***H$_2$), 34.1 (s, *C*H$_2$CH=CH$_2$), 31.4 (virtual t,[37] $^3J_{CP}$ = 6.5 Hz, PCH$_2$CH$_2$***C***H$_2$), 29.2 (s, ***C***H$_2$), 29.0 (s, ***C***H$_2$), 28.2 (virtual t,[37] $^1J_{CP}$ = 13.2 Hz, P***C***H$_2$), 24.5 (s, PCH$_2$***C***H$_2$); ^{31}P{^{1}H} (202 MHz) 40.8 (s).

IR (oil film, cm^{-1}): 3074 (w), 2924 (s), 2852 (m), 1905 (ν_{CO}, s), 1681 (ν_{NO}, s), 1639 (m), 1436 (w), 1413 (w), 993 (m), 906 (s), 719 (m).

***trans*-Fe(CO)(NO)(CN)(P((CH$_2$)$_6$CH=CH$_2$)$_3$)$_2$ (4c-CN).** A Schlenk flask was charged with **3c** (0.150 g, 0.156 mmol) and CH_2Cl_2 (25 mL). Then a solution of $(CH_3(CH_2)_3)_4N^+$ CN^- (0.084 g, 0.312 mmol) in CH_2Cl_2 (10 mL) was added with stirring. After 16 h, the solvent was removed by oil pump vacuum. The red/brown oil was chromatographed on a silica gel column (1.5 × 20 cm) with a 2:1 v/v mixture of hexanes/CH_2Cl_2 and then CH_2Cl_2. The solvent was removed from the red fraction by oil pump vacuum to give **4c-CN** as a red oil (0.124 g, 0.143 mmol, 92%). Anal. Calcd. for $C_{50}H_{90}FeN_2O_2P_2$ (869.05): C 69.10, H 10.44, N 3.22; found: C 69.01, H 10.24, N 3.32.

NMR (δ, ppm C_6D_6):[109] ^{1}H (500 MHz) 5.87-5.73 (ddt, 6H, $^3J_{HH\textit{trans}}$ = 17.0 Hz, $^3J_{HH\textit{cis}}$ = 10.1 Hz, $^3J_{HH}$ = 6.9 Hz, C***H***=), 5.07-4.96 (m, 12H, =C***H***$_2$), 2.11-2.03 (m, 12H, PC***H***$_2$), 2.01-1.95 (m, 12H, C***H***$_2$CH=CH$_2$), 1.68-1.51 (m, 12H, PCH$_2$C***H***$_2$), 1.38-1.24 (m, 36H, PCH$_2$CH$_2$C***H***$_2$ and remaining C***H***$_2$); ^{13}C{^{1}H} (125 MHz) 220.4 (t, $^2J_{CP}$ = 30.2 Hz, ***C***O), 141.8 (t, $^2J_{CP}$ = 42.0 Hz, ***C***N), 139.1 (s, ***C***H=), 114.7 (s, =***C***H$_2$), 34.2 (s, *C*H$_2$CH=CH$_2$), 31.4 (virtual t,[37] $^3J_{CP}$ = 6.5 Hz, PCH$_2$CH$_2$***C***H$_2$), 29.2 (s, ***C***H$_2$), 28.5 (virtual t,[37] $^1J_{CP}$ = 13.5 Hz, P***C***H$_2$), 24.3 (s, PCH$_2$***C***H$_2$); ^{31}P{^{1}H} (202 MHz) 56.2 (s).

IR (oil film, cm^{-1}): 3076 (w), 2924 (s), 2854 (w), 2096 (ν_{CN}, m), 1915 (ν_{CO}, s), 1699 (ν_{NO}, s), 1639 (m), 1440 (w), 1413 (w), 993 (m), 906 (s), 721 (m), 632 (m), 615 (s).

***trans*-Fe(CO)(NO)(Cl)(P((CH$_2$)$_7$CH=CH$_2$)$_3$)$_2$ (4d-Cl).** A Schlenk flask was charged with **3d** (0.125 g, 0.120 mmol) and CH_2Cl_2 (20 mL). Then a solution of $(CH_3(CH_2)_3)_4N^+$ Cl^- (0.085 g, 0.300 mmol) in CH_2Cl_2 (10 mL) was added with stirring. After 16 h, the solvent was removed by oil pump vacuum The red/brown oil was chromatographed on a silica gel column (1.5 × 20 cm) with hexanes and then hexanes/CH_2Cl_2 mixtures (4:1, 3:1, and then 2:1, v/v). The solvent was removed from the red fraction by oil pump vacuum to give **4d-Cl** as a red-brown oil (0.226 g, 0.095 mmol, 82%). Anal. Calcd. for $C_{55}H_{102}FeClNO_2P_2$ (962.65): C 68.62, H 10.68, N 1.46; found: C 68.70, H 10.71, N 1.56.

NMR (δ, ppm C_6D_6):[109] ^{1}H (500 MHz) 5.85-5.74 (ddt, 6H, $^3J_{HH\textit{trans}}$ = 17.0 Hz,

$^3J_{HHcis}$ = 10.1 Hz, $^3J_{HH}$ = 6.9 Hz, C***H***=), 5.08-4.97 (m, 12H, =C***H***$_2$), 2.15-1.94 (m, 24H, PC***H***$_2$ and C*H*$_2$CH=CH$_2$), 1.72-1.52 (m, 12H, PCH$_2$C***H***$_2$), 1.35-1.15 (m, 48H, PCH$_2$CH$_2$C***H***$_2$ and remaining C***H***$_2$); ^{13}C{^{1}H} (125 MHz) 221.2 (t, $^2J_{CP}$ = 37.2 Hz, ***C***O), 139.2 (s, ***C***H=), 114.6 (s, =***C***H$_2$), 34.2 (s, ***C***H$_2$CH=CH$_2$), 31.7 (virtual t,[37] $^3J_{CP}$ = 6.1 Hz, PCH$_2$CH$_2$***C***H$_2$), 29.5 (s, ***C***H$_2$), 29.4 (s, ***C***H$_2$), 29.3 (s, ***C***H$_2$), 25.9 (virtual t,[37] $^1J_{CP}$ = 13.0 Hz, P***C***H$_2$), 24.3 (s, PCH$_2$***C***H$_2$); ^{31}P{^{1}H} (202 MHz) 47.5 (s).

IR (oil film, cm^{-1}): 3074 (w), 2924 (s), 2852 (m), 1901 (ν_{CO}, s), 1681 (ν_{NO}, s), 1639 (m), 1456 (w), 1413 (w), 993 (w), 906 (s), 719 (m).

***trans*-Fe(CO)(NO)(Br)(P((CH$_2$)$_7$CH=CH$_2$)$_3$)$_2$ (4d-Br).** A Schlenk flask was charged with **3d** (0.220 g, 0.211 mmol) and CH_2Cl_2 (25 mL). Then a solution of $(CH_3(CH_2)_3)_4N^+$ Br^- (0.136 g, 0.422 mmol) in CH_2Cl_2 (10 mL) was added with stirring. After 16 h, the solvent was removed by oil pump vacuum. The red/brown oil was chromatographed on a silica gel column (1.5 × 20 cm) with hexanes and then hexanes/CH_2Cl_2 mixtures (4:1 and then 2:1, v/v). The solvent was removed from the red fraction by oil pump vacuum to give **4d-Br** as a red oil (0.178 g, 0.177 mmol, 84%). Anal. Calcd. for $C_{55}H_{102}FeBrNO_2P_2$ (1007.1): C 65.59, H 10.21, N 1.39; found: C 65.80, H 10.20, N 1.43.

NMR (δ, ppm C_6D_6):[109] ^{1}H (500 MHz) 5.85-5.66 (ddt, 6H, $^3J_{HHtrans}$ = 17.0 Hz, $^3J_{HHcis}$ = 10.1 Hz, $^3J_{HH}$ = 6.9 Hz, C***H***=), 5.07-4.96 (m, 12H, =C***H***$_2$), 2.19-2.08 (m, 12H, PC***H***$_2$), 2.02-1.96 (m, 12H, C***H***$_2$CH=CH$_2$), 1.72-1.55 (m, 12H, PCH$_2$C*H*$_2$) 1.35-1.20

(m, 48H, $PCH_2CH_2CH_2$ and remaining C***H***$_2$); $^{13}C\{^1H\}$ (125 MHz) 220.8 (t, $^2J_{CP}$ = 36.1 Hz, ***C***O), 139.2 (s, ***C***H=), 114.6 (s, =***C***H_2), 34.2 (s, *C*$H_2CH=CH_2$), 31.6 (virtual t,[37] $^3J_{CP}$ = 6.2 Hz, PCH_2CH_2***C***H_2), 29.5 (s, ***C***H_2), 29.4 (s, ***C***H_2), 29.3 (s, ***C***H_2), 26.7 (virtual t,[37] $^1J_{CP}$ = 12.7 Hz, P***C***H_2), 24.4 (s, PCH_2***C***H_2); $^{31}P\{^1H\}$ (202 MHz) 43.4 (s).

IR (oil film, cm^{-1}): 3076 (w), 2924 (s), 2852 (m), 1903 (ν_{CO}, s), 1674 (ν_{NO}, s), 1639 (m), 1456 (w), 1413 (w), 993 (m), 906 (s), 719 (m).

***trans*-Fe(CO)(NO)(I)(P((CH$_2$)$_7$CH=CH$_2$)$_3$)$_2$ (4d-I).** A Schlenk flask was charged with **3d** (0.235 g, 0.226 mmol) and CH_2Cl_2 (20 mL). Then a solution of $(CH_3(CH_2)_3)_4N^+$ I^- (0.180 g, 0.452 mmol) in CH_2Cl_2 (10 mL) was added with stirring. After 16 h, the solvent was removed by oil pump vacuum. The red/brown oil was chromatographed on a silica gel column (1.5 × 20 cm) with hexanes and then hexanes/CH_2Cl_2 mixtures (4:1 and then 2:1, v/v). The solvent was removed from the red fraction by oil pump vacuum to give **4d-I** as a red oil (0.212 g, 0.201 mmol, 89%). Anal. Calcd. for $C_{55}H_{102}FeINO_2P_2$ (1054.1): C 62.67, H 9.75, N 1.33; found: C 62.39, H 9.87, N 1.52.

NMR (δ, ppm C_6D_6):[109] ^1H (500 MHz) 5.86-5.75 (ddt, 6H, $^3J_{HH\textit{trans}}$ = 17.0 Hz, $^3J_{HH\textit{cis}}$ = 10.1 Hz, $^3J_{HH}$ = 6.9 Hz, C***H***=), 5.09-4.97 (m, 12H, =C***H***$_2$), 2.34-2.26 (m, 12H, PC***H***$_2$), 2.05-1.97 (m, 12H, C***H***$_2$CH=CH_2), 1.74-1.55 (m, 12H, PCH_2C***H***$_2$), 1.35-1.20 (m, 48H, PCH_2CH_2C***H***$_2$ and remaining C***H***$_2$); $^{13}C\{^1H\}$ (125 MHz) 220.8 (t, $^2J_{CP}$ = 36.1 Hz, ***C***O), 139.2 (s, ***C***H=), 114.6 (s, =***C***H_2), 34.2 (s, *C*$H_2CH=CH_2$), 31.6 (virtual t,[37] $^3J_{CP}$

= 6.0 Hz, $PCH_2CH_2\boldsymbol{C}H_2$), 29.5 (s, $\boldsymbol{C}H_2$), 29.4 (s, $\boldsymbol{C}H_2$), 29.3 (s, $\boldsymbol{C}H_2$), 28.2 (virtual t,[37] $^1J_{CP}$ = 13.1 Hz, $P\boldsymbol{C}H_2$), 24.6 (s, $PCH_2\boldsymbol{C}H_2$); $^{31}P\{^1H\}$ (202 MHz) 40.8 (s).

IR (oil film, cm^{-1}): 3076 (w), 2924 (s), 2852 (m), 1903 (ν_{CO}, s), 1681 (ν_{NO}, s), 1639 (m), 1456 (w), 1413 (w), 993 (m), 906 (s), 719 (m).

***trans*-Fe(CO)(NO)(CN)(P((CH$_2$)$_7$CH=CH$_2$)$_3$)$_2$ (4d-CN).** A Schlenk flask was charged with **3d** (0.125 g, 0.120 mmol) and CH_2Cl_2 (20 mL). Then a solution of $(CH_3(CH_2)_3)_4N^+$ CN^- (0.080 g, 0.300 mmol) in CH_2Cl_2 (10 mL) was added with stirring. After 16 h, the solvent was removed by oil pump vacuum. The red/brown oil was chromatographed on a silica gel column (1.5 × 20 cm) with a 2:1 v/v mixture of hexanes/CH_2Cl_2 and then CH_2Cl_2. The solvent was removed from the red fraction by oil pump vacuum to give **4d-CN** as a red oil (0.083 g, 0.088 mmol, 73%). Anal. Calcd. for $C_{56}H_{102}FeN_2O_2P_2$ (953.21): C 70.56, H 10.79, N 2.94; found: C 70.85, H 10.70, N 2.95.

NMR (δ, ppm C_6D_6):[109] ^1H (500 MHz) 5.88-5.71 (ddt, 6H, $^3J_{HH\textit{trans}}$ = 17.0 Hz, $^3J_{HH\textit{cis}}$ = 10.1 Hz, $^3J_{HH}$ = 6.9 Hz, C***H***=), 5.09-4.99 (m, 12H, =C$\boldsymbol{H}_2$), 2.17-2.08 (m, 12H, PC$\boldsymbol{H}_2$), 2.04-1.98 (m, 12H, C$\boldsymbol{H}_2$CH=CH$_2$), 1.75-1.63 (m, 12H, $PCH_2C\boldsymbol{H}_2$), 1.36-1.22 (m, 48H, $PCH_2CH_2C\boldsymbol{H}_2$ and remaining C$\boldsymbol{H}_2$); $^{13}C\{^1H\}$ (125 MHz) 218.8 (t, $^2J_{CP}$ = 30.1 Hz, ***C***O), 141.9 (t, $^2J_{CP}$ = 42.0 Hz, ***C***N), 139.0 (s, ***C***H=), 114.6 (s, =$\boldsymbol{C}H_2$), 34.2 (s, $CH_2CH=CH_2$), 31.6 (virtual t,[37] $^3J_{CP}$ = 6.1 Hz, $PCH_2CH_2\boldsymbol{C}H_2$), 29.5 (s, $\boldsymbol{C}H_2$), 29.4 (s, $\boldsymbol{C}H_2$), 29.3 (s, $\boldsymbol{C}H_2$), 28.6 (virtual t,[37] $^1J_{CP}$ = 12.7 Hz, $P\boldsymbol{C}H_2$), 24.4 (s, $PCH_2\boldsymbol{C}H_2$);

$^{31}P\{^{1}H\}$ (202 MHz) 55.7 (s).

IR (oil film, cm^{-1}): 3076 (w), 2924 (s), 2852 (m), 2096 (ν_{CN}, m), 1915 (ν_{CO}, s), 1699 (ν_{NO}, s), 1639 (m), 1460 (w), 1413 (w), 993 (m), 906 (s), 719 (m), 613 (s).

***trans*-Fe(CO)(NO)(Cl)(P((CH$_2$)$_8$CH=CH$_2$)$_3$)$_2$ (4e-Cl).** A Schlenk flask was charged with **3e** (0.150 g, 0.133 mmol) and CH_2Cl_2 (25 mL). Then a solution of $(CH_3(CH_2)_3)_4N^+$ Cl^- (0.074 g, 0.266 mmol) in CH_2Cl_2 (10 mL) was added with stirring. After 16h, the solvent was removed by oil pump vacuum. The residue was the chromatographed on a silica gel column (1.5 × 20 cm) with hexanes and then hexanes/CH_2Cl_2 mixtures (4:1, 3:1, and then 2:1, v/v). The solvent was removed from the red fraction by oil pump vacuum to give **4e-Cl** as a red oil (0.113 g, 0.108 mmol, 81%). Anal. Calcd. for $C_{61}H_{114}FeClNO_2P_2$ (1046.81): C 69.99, H 10.98, N 1.34; found: C 70.25, H 11.14, N 1.34.

NMR (δ, ppm C_6D_6):[109] ^{1}H (500 MHz) 5.83-5.72 (ddt, 6H, $^{3}J_{HH\textit{trans}}$ = 17.0 Hz, $^{3}J_{HH\textit{cis}}$ = 10.1 Hz, $^{3}J_{HH}$ = 6.9 Hz, C***H***=), 5.06-4.95 (m, 12H, =C***H***$_2$), 2.15-1.94 (m, 24H, PC***H***$_2$ and C*H*$_2$CH=CH$_2$), 1.70-1.58 (m, 12H, PCH$_2$C***H***$_2$), 1.37-1.19 (m, 60H, PCH$_2$CH$_2$C***H***$_2$ and remaining C***H***$_2$); $^{13}C\{^{1}H\}$ (125 MHz) 221.2 (t, $^{2}J_{CP}$ = 38.1 Hz, ***C***O), 139.2 (s, ***C***H=), 114.6 (s, =***C***H$_2$), 34.3 (s, ***C***H$_2$CH=CH$_2$), 31.7 (virtual t,[37] $^{3}J_{CP}$ = 6.2 Hz, PCH$_2$CH$_2$***C***H$_2$), 29.8 (s, ***C***H$_2$), 29.6 (s, ***C***H$_2$), 29.5 (s, ***C***H$_2$), 29.4 (s, ***C***H$_2$), 25.9 (virtual t,[37] $^{1}J_{CP}$ = 13.1 Hz, P***C***H$_2$), 24.3 (s, PCH$_2$***C***H$_2$); $^{31}P\{^{1}H\}$ (202 MHz) 47.4 (s).

IR (oil film, cm^{-1}): 3076 (w), 2924 (s), 2852 (m), 1901 (ν_{CO}, s), 1668 (ν_{NO}, s),

1639 (m), 1463 (w), 1413 (w), 991 (w), 906 (s), 719 (m).

***trans*-Fe(CO)(NO)(Br)(P((CH$_2$)$_8$CH=CH$_2$)$_3$)$_2$ (4e-Br).** A Schlenk flask was charged with **3e** (0.150 g, 0. 133 mmol) and CH_2Cl_2 (25 mL). Then a solution of $(CH_3(CH_2)_3)_4N^+$ Br^- (0.132 g, 0.412 mmol) in CH_2Cl_2 (10 mL) was added with stirring. After 16 h, the solvent was removed by oil pump vacuum. The red/brown oil was chromatographed on a silica gel column (1.5 × 20 cm) with hexanes and then of hexanes/CH_2Cl_2 mixtures (4:1 and then 2:1, v/v). The solvent was removed from the red fraction by oil pump vacuum to give **4e-Br** as a red oil (0.128 g, 0.118 mmol, 89%). Anal. Calcd. for $C_{61}H_{114}FeBrNO_2P_2$ (1091.26): C 67.14, H 10.53, N 1.28; found: C 67.22, H 10.41, N 1.36.

NMR (δ, ppm C_6D_6):[109] ^{1}H (500 MHz) 5.86-5.72 (ddt, 6H, $^3J_{HH\textit{trans}}$ = 17.0 Hz, $^3J_{HH\textit{cis}}$ = 10.1 Hz, $^3J_{HH}$ = 6.9 Hz, C***H***=), 5.11-4.93 (m, 12H, =C***H***$_2$), 2.25-2.10 (m, 12H, PC***H***$_2$), 2.03-1.98 (m, 12H, C***H***$_2$CH=CH$_2$), 1.76-1.57 (m, 12H, PCH$_2$C*H*$_2$), 1.37-1.21 (m, 60H, PCH$_2$CH$_2$C*H*$_2$ and remaining C***H***$_2$); ^{13}C{^{1}H} (125 MHz) 221.2 (t, $^2J_{CP}$ = 38.0 Hz, ***C***O), 139.2 (s, ***C***H=), 114.6 (s, =***C***H$_2$), 34.3 (s, *C*H$_2$CH=CH$_2$), 31.7 (virtual t,[37] $^3J_{CP}$ = 6.1 Hz, PCH$_2$CH$_2$***C***H$_2$), 29.8 (s, ***C***H$_2$), 29.6 (s, ***C***H$_2$), 29.5 (s, ***C***H$_2$), 29.4 (s, ***C***H$_2$), 26.7 (virtual t,[37] $^1J_{CP}$ = 13.2 Hz, P***C***H$_2$), 24.4 (s, PCH$_2$***C***H$_2$); ^{31}P{^{1}H} (202 MHz) 47.4 (s).

IR (oil film, cm^{-1}): 3076 (w), 2924 (s), 2852 (m), 1901 (ν_{CO}, s), 1668 (ν_{NO}, s), 1639 (m), 1463 (w), 1413 (w), 991 (w), 906 (s), 719 (m).

***trans*-Fe(CO)(NO)(I)(P((CH$_2$)$_8$CH=CH$_2$)$_3$)$_2$ (4e-I).** A Schlenk flask was charged with **3e** (0.150 g, 0.133 mmol) and CH_2Cl_2 (25 mL). Then a solution of $(CH_3(CH_2)_3)_4N^+$ I^- (0.098 g, 0.266 mmol) in CH_2Cl_2 (10 mL) was added with stirring. After 16 h, the solvent was removed by oil pump vacuum. The red/brown oil was chromatographed on a silica gel column (1.5 × 20 cm) with hexanes and then hexanes/CH_2Cl_2 mixtures (4:1 and then 2:1, v/v). The solvent was removed from the red fraction by oil pump vacuum to give **4e-I** as a red oil (0.123 g, 0.108 mmol, 87%). Anal. Calcd. for $C_{61}H_{114}FeINO_2P_2$ (1138.26): C 64.37, H 10.09, N 1.23; found: C 64.33, H 10.07, N 1.34.

NMR (δ, ppm C_6D_6):[109] ^{1}H (500 MHz) 5.87-5.65 (ddt, 6H, $^3J_{HH\textit{trans}}$ = 17.0 Hz, $^3J_{HH\textit{cis}}$ = 10.1 Hz, $^3J_{HH}$ = 6.9 Hz, C***H***=), 5.11-4.95 (m, 12H, =C***H***$_2$), 2.35-2.18 (m, 12H, PC***H***$_2$), 2.02-1.91 (m, 12H, C***H***$_2$CH=CH$_2$), 1.75-1.50 (m, 12H, PCH$_2$C***H***$_2$), 1.39-1.09 (m, 60H, PCH$_2$CH$_2$C***H***$_2$ and remaining C***H***$_2$); ^{13}C{^{1}H} (125 MHz) 219.1 (t, $^2J_{CP}$ = 35.0 Hz, ***C***O), 139.3 (s, ***C***H=), 114.2 (s, =***C***H$_2$), 33.9 (s, *C*H$_2$CH=CH$_2$), 31.3 (virtual t,[37] $^3J_{CP}$ = 6.0 Hz, PCH$_2$CH$_2$***C***H$_2$), 29.4 (s, ***C***H$_2$), 29.3 (s, ***C***H$_2$), 29.2 (s, ***C***H$_2$), 29.0 (s, ***C***H$_2$), 27.5 (virtual t,[37] $^1J_{CP}$ = 13.0 Hz, P***C***H$_2$), 24.1 (s, PCH$_2$***C***H$_2$); ^{31}P{^{1}H} (202 MHz) 40.6 (s).

IR (oil film, cm^{-1}): 3076 (w), 2924 (s), 2852 (m), 1901 (ν_{CO}, s), 1681 (ν_{NO}, s), 1641 (m), 1458 (w), 1413 (w), 991 (w), 906 (s), 719 (m).

***trans*-Fe(CO)(NO)(CN)(P((CH$_2$)$_8$CH=CH$_2$)$_3$)$_2$ (4e-CN).** A Schlenk flask was

charged with **3e** (0.150 g, 0.133 mmol) and CH_2Cl_2 (25 mL). Then a solution of $(CH_3(CH_2)_3)_4N^+$ CN^- (0.071 g, 0.266 mmol) in CH_2Cl_2 (10 mL) was added with stirring. After 16 h, the solvent was removed by oil pump vacuum. The red/brown oil was chromatographed on a silica gel column (1.5 × 20 cm) with a 2:1 v/v mixture of hexanes/CH_2Cl_2 and then CH_2Cl_2. The solvent was removed from the red fraction by oil pump vacuum to give **4e-CN** as a red oil (0.113 g, 0.109 mmol, 82%). Anal. Calcd. for $C_{62}H_{114}FeN_2O_2P_2$ (1037.37): C 71.78, H 11.08, N 2.70; found: C 72.04, H 11.13, N 2.73.

NMR (δ, ppm C_6D_6):[109] ^{1}H (500 MHz) 5.85-5.75 (ddt, 6H, $^3J_{HH\textit{trans}}$ = 17.0 Hz, $^3J_{HH\textit{cis}}$ = 10.1 Hz, $^3J_{HH}$ = 6.9 Hz, C***H***=), 5.09-4.98 (m, 12H, =C***H***$_2$), 2.16-2.10 (m, 12H, PC***H***$_2$), 2.04-1.98 (m, 12H, C***H***$_2$CH=CH$_2$), 1.74-1.63 (m, 12H, PCH$_2$C***H***$_2$), 1.39-1.22 (m, 60H, PCH$_2$CH$_2$C***H***$_2$ and remaining C***H***$_2$); ^{13}C{^{1}H} (125 MHz) 220.5 (t, $^2J_{CP}$ = 30.1 Hz, ***C***O), 141.8 (t, $^2J_{CP}$ = 42.2 Hz, ***C***N), 139.2 (s, ***C***H=), 114.6 (s, =***C***H$_2$), 34.3 (s, *C*H$_2$CH=CH$_2$), 31.7 (virtual t,[37] $^3J_{CP}$ = 6.5 Hz, PCH$_2$CH$_2$***C***H$_2$), 29.8 (s, ***C***H$_2$), 29.7 (s, ***C***H$_2$), 29.5 (s, ***C***H$_2$), 29.4 (s, ***C***H$_2$), 28.6 (virtual t,[37] $^1J_{CP}$ = 13.5 Hz, P***C***H$_2$), 24.4 (s, PCH$_2$***C***H$_2$); ^{31}P{^{1}H} (202 MHz) 56.2 (s).

IR (oil film, cm^{-1}): 3074 (w), 2924 (s), 2852 (m), 2096 (ν_{CN}, m), 1915 (ν_{CO}, s), 1700 (ν_{NO}, s), 1639 (m), 1456 (w), 1413 (w), 991 (m), 906 (s), 721 (m), 613 (s).

[Fe(NO)$_2$(P((CH$_2$)$_m$CH=CH$_2$)$_3$)$_2$] (5a-e). As described in the text, these compounds were encountered as minor byproducts when **3a-e** were treated with large

excesses of solid $(CH_3(CH_2)_3)_4N^+ X^-$. They were isolated via silica gel column (1.5 × 20 cm). The impurity elutes from the column prior to the desired halide product as a brown band with a 4:1 v/v mixture of hexanes/CH_2Cl_2. The solvent was removed from the brown fraction by oil pump vacuum to give **5b** and **5c**.

$Fe(NO)_2P((CH_2)_5CH=CH_2)_3)_2$ (5b).

NMR (δ, ppm $CDCl_3$):[109] ^1H (500 MHz) 5.85-5.75 (ddt, 6H, $^3J_{HHtrans}$ = 17.0 Hz, $^3J_{HHcis}$ = 10.1 Hz, $^3J_{HH}$ = 6.9 Hz, C***H***=), 5.02-4.91 (m, 12H, =C***H***$_2$), 2.09-2.0 (m, 12H, C***H***$_2$), 1.64-1.56 (m, 12H, C***H***$_2$), 1.46-1.27 (m, 36H, C***H***$_2$); $^{13}C\{^1H\}$ (125 MHz) 138.9 (s, ***C***H=), 114.6 (s, =***C***H_2), 33.8 (s, ***C***H_2), 31.2 (virtual t,[37] $^3J_{CP}$ = 6.4 Hz, $PCH_2CH_2\boldsymbol{C}H_2$), 29.1 (virtual m,[37] P***C***H_2), 28.7 (s, ***C***H_2), 24.1(s, ***C***H_2); $^{31}P\{^1H\}$ (202 MHz) 40.2 (s).

$Fe(NO)_2P((CH_2)_6CH=CH_2)_3)_2$ (5c).

NMR (δ, ppm $CDCl_3$):[109] ^1H (500 MHz) 5.85-5.75 (ddt, 6H, $^3J_{HHtrans}$ = 17.0 Hz, $^3J_{HHcis}$ = 10.1 Hz, $^3J_{HH}$ = 6.9 Hz, C***H***=), 5.02-4.91 (m, 12H, =C***H***$_2$), 2.09-2.0 (m, 12H, C***H***$_2$), 1.64-1.56 (m, 12H, C***H***$_2$), 1.46-1.27 (m, 48H, C***H***$_2$); $^{13}C\{^1H\}$ (125 MHz) 139.1 (s, ***C***H=), 114.5 (s, =***C***H_2), 33.9 (s, ***C***H_2), 31.6 (virtual t,[37] $^3J_{CP}$ = 6.4 Hz, $PCH_2CH_2\boldsymbol{C}H_2$), 29.1 (virtual m,[37] P***C***H_2), 29.0 (s, ***C***H_2), 28.9(s, ***C***H_2), 24.1(s, ***C***H_2); $^{31}P\{^1H\}$ (202 MHz) 40.4 (s).

IR (oil film, cm^{-1}): 1696 (ν_{NO}, m), 1647 (ν_{NO}, s).

5. SYNTHESIS, REACTIVITY, AND STRUCTURES OF GYROSCOPE LIKE IRON CARBONYL COMPLEXES BASED UPON DIBRIDGEHEAD DIPHOSPHINE CAGES: POST-METATHESIS VS. PRE-METATHESIS SUBSTITUTION AS ROUTES TO SPECIES WITH NEUTRAL DIPOLAR FE(CO)(NO)(X) ROTORS

5.1 Introduction

As has been extensively documented[6] and surveyed in previous papers in this series,[20-25,29,72,85] gyroscopes are utilized in a multitude of technologies. Older readers may recall the Sperry Rand Corporation, which ceased to exist following a hostile merger that resulted in Unisys (1986),[115] had an earlier incarnation as the Sperry Gyroscope Company.[116] The latter was founded in 1910 and for some time supplied most of the world's torpedo warhead and gyrocompass guidance systems. These days, dedicated "gyroscope companies" appear to be extinct, but their spirit lives on in a small cadre of research groups who seek to realize such devices at a molecular level.[8,13,28f,84] Representative applications for which miniaturization is especially important include drones, virtual reality headsets, mobile phone displays, and flying suits as popularized by Iron Man.[117]

Some candidates for molecular gyroscopes that have been under study in our group are shown in Scheme 5-1 (**II**, **IV**).[29-22a] These consist of a P-M-P axis about which the metal based ligands (e.g., L_y) can rotate; the metal/ligand set is termed the

"rotator". Steric shielding is provided by a cage like *trans* spanning dibridgehead diphosphine or "stator". This is assembled via three fold intramolecular ring closing alkene metathesis. Interestingly, a variety of substitution reactions can subsequently be effected (**II** → **IV**), despite the steric shielding of the metal core.

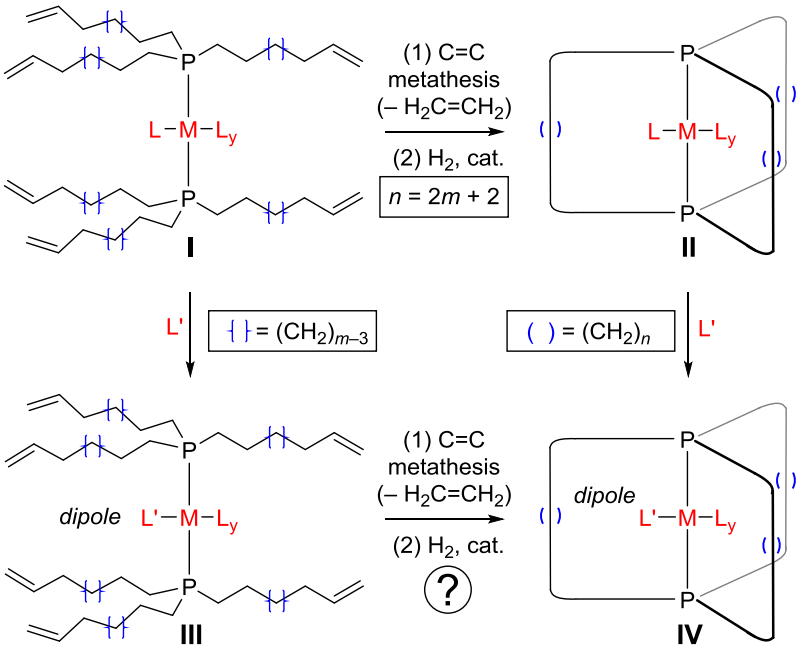

Scheme 5-1. General synthetic approaches to gyroscope like complexes with different substituents on the rotator.

Importantly, all of the physics that underlies the classical mechanical gyroscope[18] – most fundamentally, the conservation of angular momentum – holds at the molecular level.[7] One essential requirement is unidirectional rotation. In contrast, rotations about bonds in molecules are – in accord with microscopic reversibility – bidirectional or Brownian. Hence, this problem must be solved in order to attain

molecular gyroscopes. Of several approaches that have been considered,[7] the most easily conceptualized utilizes electric fields.[9] Electric fields interact with dipoles, and it is a simple matter to prepare gyroscope like complexes in which the rotator possesses a dipole moment (e.g., **IV**). Application of an electric field will orient the dipoles in the sample. The end result is a "molecular compass".[118]

The next level of function would be achieved with a rotating electric field, which could drive the dipole unidirectionally. Indeed, the optimal rotational frequency has already been computed for various rotational barriers.[7] Importantly, if the field rotates too fast, the dipole of the rotator cannot "keep up". For some readers, it may be easier to envision this experiment with some type of "ordered array", such as an ensemble of surface mounted species, or a suitable crystal. Regardless, neutral compounds are preferable to ionic compounds, as any counter ions will interact with the dipoles, and invariably increase the rotational barrier. In fluid environments, counter ions would seek to "follow" the dipole, and in the solid state, the electrostatic potential would increase the energies of some maxima and decrease the energies of some minima.

We have reported iron complexes of the type **II** with $Fe(CO)_3$, $Fe(CO)_2(NO)^+$ and $Fe(CO)_3(H)^+$ rotators and chains of ten to eighteen methylene carbon atoms.[85] The $Fe(CO)_3$ rotators of course lack dipole moments. The others feature dipoles but are accompanied by counter anions. Accordingly, we sought to address two major objectives in this study. First, could the $Fe(CO)_2(NO)^+$ systems be elaborated with anionic (pseudo)halide nucleophiles to neutral Fe(CO)(NO)(X) species? As reported earlier,[32]

the acyclic complexes *trans*-Fe(CO)(NO)(X)(P($(CH_2)_m$CH=CH_2)$_3$)$_2$ are easily accessed in average overall yields of 58% by substitution sequences beginning with the readily available starting material (BDA)Fe$(CO)_3$ and proceeding through Fe$(CO)_2(NO)^+$ species. Second, would the ring closing metatheses to give dibridgehead diphosphine ligands best be carried out before, during, or after the substitution sequences on iron?

In this section, we report a detailed investigation of the aforementioned possibilities as embodied in routes I, II, and III in Scheme 5-2. This graphic also serves to define the sequence of compound numbers. In the course of these efforts, several crystal structures of Fe(CO)(NO)(X) species have been determined that reveal promising properties for molecular gyroscopes. Various observations relating to the rotational barriers associated with the rotators are also described.

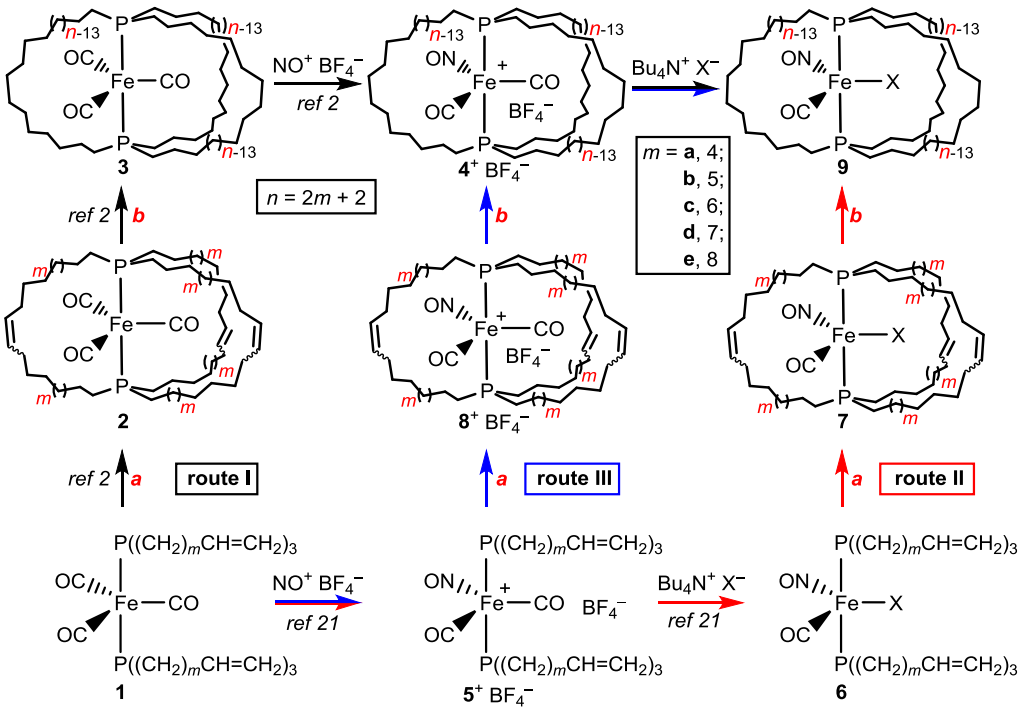

Scheme 5-2. Possible synthetic routes to the title complexes **9**: a, alkene metathesis; b, hydrogenation.

5.2 Results

5.2.1 Syntheses of title complexes

Scheme 5-2 represents a "road map" of the various routes by which neutral gyroscope like complexes with dipolar Fe(CO)(NO)(X) rotators, or *trans*-Fe(CO)(NO)(X)(P((CH$_2$)$_n$)$_3$P) (**9**), can be accessed. The first, route I, employs three steps described in previous papers,[85] followed by substitution of a carbonyl ligand of a cationic dicarbonyl nitrosyl complex *trans*-[Fe(CO)$_2$(NO)(P((CH$_2$)$_n$)$_3$P)]$^+$ BF$_4^-$ (**4**$^+$ BF$_4^-$)[119] by a halide or pseudohalide anion of suitable salt (e.g., M$^+$ X$^-$ or Q$^+$ X$^-$).

Other complexes of the formula *trans*-$[Fe(CO)_2(NO)(L)_2]^+$ Z^- have similarly been converted to halide complexes *trans*-$Fe(CO)(NO)(X)(L)_2$.[110-113]

Thus, as shown in Scheme 5-3, CH_2Cl_2 solutions of $[Fe(CO)_2(NO)(P((CH_2)_{14})_3P)]^+$ BF_4^- (**4c**$^+$ BF_4^-)[85] and the ammonium salts Bu_4N^+ X^- (X = Cl, Br, I, or CN; 1-2 equiv.) were combined. Workups gave the target halide or cyanide complexes *trans*-$Fe(CO)(NO)(X)(P((CH_2)_{14})_3P)$[119] (**9c-Cl**, **-Br**, **-I**, **-CN**) as pale orange solids in 75-83% yields. As summarized in Table 5-1 and the experimental section, these were characterized by IR and NMR (^1H, ^{13}C, ^{31}P) spectroscopy, microanalyses, and mass spectrometry. The IR spectra of **9c-Cl**, **-Br**, **-I**, **-CN** (Table 5-1) exhibited strong ν_{CO} (1905-1917 cm^{-1}) and ν_{NO} (1678-1703 cm^{-1}) bands; that of **9c-CN** furthermore showed a weak ν_{CN} band (2098 cm^{-1}). Consistent with related compounds,[110-113] the frequencies were lower than those of the cationic precursor **4c**$^+$ BF_4^-, and increased in the order X = Cl < Br < I < CN.

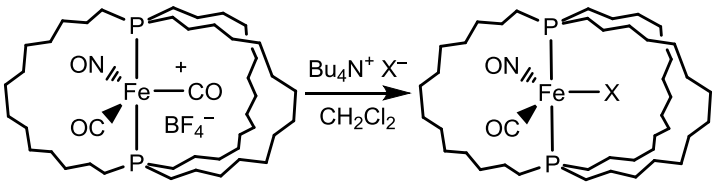

Scheme 5-3. Route I to the title complexes; substitution of the carbonyl ligand by (pseudo)halide nucleophiles following the alkene metathesis/hydrogenation sequence.

The $^{13}C\{^{1}H\}$ NMR spectra ($CDCl_3$) exhibited a single ***C***O signal that was coupled to both phosphorus atoms (218.3-218.9 ppm, t, $^{2}J_{CP}$ = 30.1-37.4 Hz). These were downfield from that of **4c**$^{+}$ BF_4^{-} (208.2 ppm). The ***C***N signal of **9c-CN** (140.7 ppm) was similarly coupled to phosphorus (t, $^{2}J_{CP}$ = 40.6 Hz). The $^{13}C\{^{1}H\}$ NMR spectra of **9c-Cl**, **-Br**, **-CN** gave one set of $P(CH_2)_{n/2}$ signals. The $P\boldsymbol{C}H_2\boldsymbol{C}H_2\boldsymbol{C}H_2$ signals were assigned according to chemical shift and coupling constant trends established earlier for related complexes using 2D NMR experiments.[85] However, the spectrum of **9c-I** was more complicated, and exhibited three sets of peaks for the $P(CH_2)_{n/2}$ signals. This difference is further analyzed below.

Table 5-1. Selected NMR and IR data key gyroscope iron complexes.

Complex	IR [cm^{-1}][a]			$^{31}P\{^{1}H\}$ (δ/ppm)	$^{13}C\{^{1}H\}$ (δ/ppm)[b]				
	ν_{CO}	ν_{NO}	ν_{CN}		***C***O [$^{2}J_{CP}$ Hz]	***C***N [$^{2}J_{CP}$ Hz]	P***C***H_2 [$^{1}J_{CP}$ Hz]	PCH_2***C***H_2	PCH_2CH_2***C***H_2 [$^{3}J_{CP}$ Hz]
3c	1861	-	-	66.9	215.6 [29.0]	-	31.6 [15.1]	24.0	31.0 [6.6]
4c^{+} BF_4^{-}	1965	1764	-	56.8	208.2 [25.3]	-	28.7 [15.4]	24.6	30.7 [7.6]
9c-Cl	1905	1678	-	48.7	218.9 [37.4]	-	26.8 [12.9]	23.5	30.6 [6.5]
9c-Br	1907	1683	-	45.2	218.7 [36.7]	-	26.5 [12.9]	23.2	30.6 [6.1]
9c-I	1911	1691	-	41.7	218.7 [35.5]	-	*c*	24.1/23.8/23.5[c]	30.5/30.2/29.9[c]
9c-CN	1917	1703	2098	58.2	218.3 [30.1]	140.7 [40.6]	29.3 [13.5]	23.8	30.7 [6.9]

[a]Powder film. [b]All signals for which *J* values are given correspond to a triplet or a virtual triplet. [c] The spectrum of **9c-I** exhibited three sets of $P(CH_2)_{n/2}$ signals. The P***C***H_2 signals overlap with other CH_2 signals and could not be assigned.

The apparent $^{1}J_{CP}$ and $^{3}J_{CP}$ values for the P***C***H_2 and PCH_2CH_2***C***H_2 signals were generally lower than those in **4c**$^{+}$ BF_4^- (15.4 /7.6 Hz).[37] The P***C***H_2 signals shifted downfield in the order X = Cl < Br < I ~ CN, but the PCH_2CH_2***C***H_2 and ***C***O signals remained essentially constant. The $^{2}J_{CP}$ values for the ***C***O signals decreased in the series X = Cl/Br/I/CN (37.4, 36.7, 35.9, and 30.1 Hz). The $^{31}P\{^{1}H\}$ NMR signals shifted upfield in the series X = Cl/Br/I (48.7, 45.2, and 41.7 ppm), but that of **9c-CN** was markedly downfield of all of them (58.2 ppm).

As sketched in Scheme 5-2, route II to the title complexes **9** involves ring closing metatheses about the dipolar rotator. Many related gyroscope like complexes possessing halide ligands have been easily accessed via similar metatheses.[10,22a,24,25] Accordingly, as shown in Scheme 5-4, *trans*-Fe(CO)(NO)(X)(P($(CH_2)_6CH=CH_2)_3)_2$ (**6c-Cl**, **Br**, **I**, **CN**)[32,119] were combined with Grubbs' catalyst (first generation; 18 mol% or 6 mol%/new C=C linkage) in dilute refluxing CH_2Cl_2 to minimize *inter*molecular condensations (0.0020 M in **6c-X**). After 24 h, aliquots were analyzed by ^{1}H NMR ($CDCl_3$). Except in the case of **6c-I**, the terminal alkene signals (5.87-5.73/5.09-4.96 ppm, =C***H***/=C***H***$_2$) were no longer detected; for **6c-I**, additional catalyst was required for complete reaction as described in the experimental section.

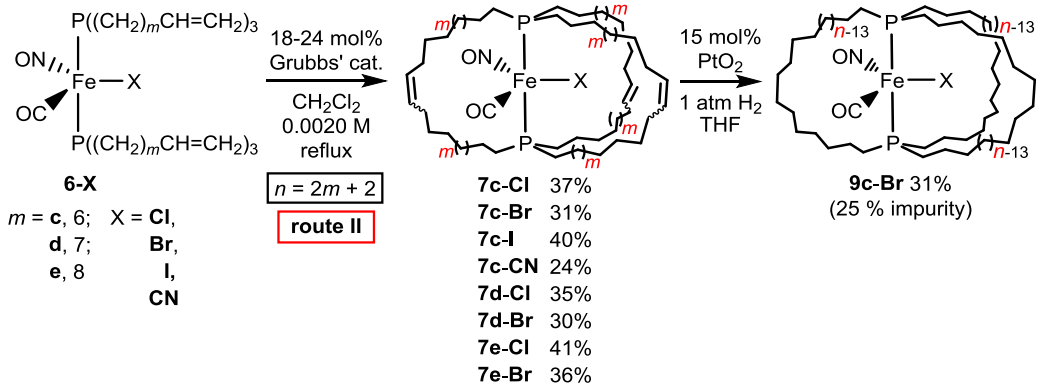

Scheme 5-4. Route II to the title complexes; alkene metathesis after completion of the substitution sequence.

Chromatographic workups afforded *trans*-Fe(CO)(NO)(X)(P((CH$_2$)$_6$CH=CH(CH$_2$)$_6$)$_3$P) (**7c-Cl**, **Br**, **I**, **CN**) as air sensitive red-brown waxy solids in 24-40% yields. The synthesis of **6c-I** was found to be poorly reproducible and the yield of **7c-CN** was consistently low. Thus, further studies were limited to bromide and chloride complexes.

Accordingly, analogous reactions were attempted with *trans*-Fe(CO)(NO)(Cl)(P((CH$_2$)$_m$CH=CH$_2$)$_3$)$_2$ (**6a**,**b**,**d**,**e-Cl**)[119] and Fe(CO)(NO)(Br)(P((CH$_2$)$_m$CH=CH$_2$)$_3$)$_2$ (**6a**,**b**,**d**,**e-Br**).[119] Workups gave *trans*-Fe(CO)(NO)(Cl)(P((CH$_2$)$_m$CH=CH(CH$_2$)$_m$)$_3$P)[119] (**7d**,**e-Cl**) and Fe(CO)(NO)(Br)(P((CH$_2$)$_m$CH=CH(CH$_2$)$_m$)$_3$P)[119] (**7d**,**e-Br**) in 30-41% yields. However, the formation of the smaller macrocycles **7a**,**b-Cl** and **7a**,**b-Br** could not be verified. Data were more consistent with incomplete metatheses, and/or non-gyroscope like products, as further analyzed in the discussion section.

The metathesis products in Scheme 5-4 were characterized by NMR (^{1}H, ^{31}P) spectroscopy. Four C=C isomers are possible (*EEE*, *EEZ*, *EZZ*, *ZZZ*). In no case was there appreciable selectivity, as reflected by the multiple ^{31}P NMR signals (experimental section) and complicated ^{1}H C***H***=C***H*** peak patterns, as depicted in Figure 5-1.

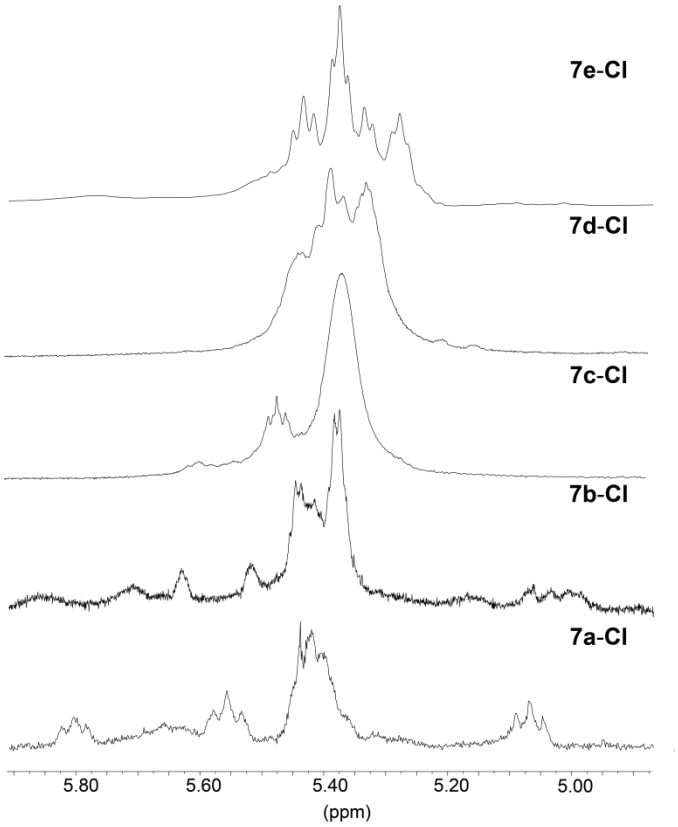

Figure 5-1. The C*H*=C*H* region of the ^{1}H NMR spectra of **7a-e-Cl**.

As illustrated in Scheme 5-4, the final step of route II would be a threefold C=C hydrogenation which proved challenging. Despite various modifications of the reaction conditions, $ClRh(PPh_3)_3$, the hydrogenation catalyst employed for route I,[85] only

reduced a fraction of the double bonds. Adams's catalyst, PtO_2, has been successfully employed with other families of gyroscope like complexes.[20,22-25] Thus, a THF solution of **7c**-**Br** was treated with H_2 (1 atm) in the presence of PtO_2 (15 mol%) at room temperature. A chromatographic workup gave the hydrogenation product *trans*-Fe(CO)(NO)(Br)(P((CH$_2$)$_{14}$)$_3$P) (**9c**-**Br**)[119] as a red brown solid in 31% yield. However, a $^{31}P\{^1H\}$ NMR spectrum exhibited two peaks at 45.1 and 48.2 ppm in a 75:25 area ratio. The former was assigned as the product peak, as it agreed with the $^{31}P\{^1H\}$ NMR spectrum of **9c**-**Br** from route I (45.2 ppm). The mass spectrum of the crude product showed the molecular ion and no ions of higher masses.

As depicted in Scheme 5-2, route III to the gyroscope like complexes **9** involves ring closing metathesis after the first but before the second ligand substitution at iron – i.e., at the stage of the cationic dicarbonyl nitrosyl complexes $\mathbf{5}^+$ BF_4^-. As shown in Scheme 5-5, a 0.0020 M CH_2Cl_2 solution of *trans*-[Fe(CO)$_2$(NO)(P((CH$_2$)$_6$CH=CH$_2$)$_3$)$_2$]$^+$ BF_4^- ($\mathbf{5c}^+$ BF_4^-)[119] was refluxed with Grubbs' catalyst. Workup afforded *trans*-[Fe(CO)$_3$(P((CH$_2$)$_6$CH=CH(CH$_2$)$_6$)$_3$P)]$^+$ BF_4^- ($\mathbf{8c}^+$ BF_4^-)[119] in 57% yield as a red brown waxy solid. The $^{31}P\{^1H\}$ spectrum exhibited two peaks 60.9 ppm (82%) and 60.1 ppm (18%), consistent with the presence of multiple *Z*/*E* C=C isomers. A similar reaction of $\mathbf{5e}^+$ BF_4^- afforded crude *trans*-[Fe(CO)$_3$(P((CH$_2$)$_8$CH=CH(CH$_2$)$_8$)$_3$P)]$^+$ BF_4^- ($\mathbf{8e}^+$ BF_4^-), which was not further analyzed.

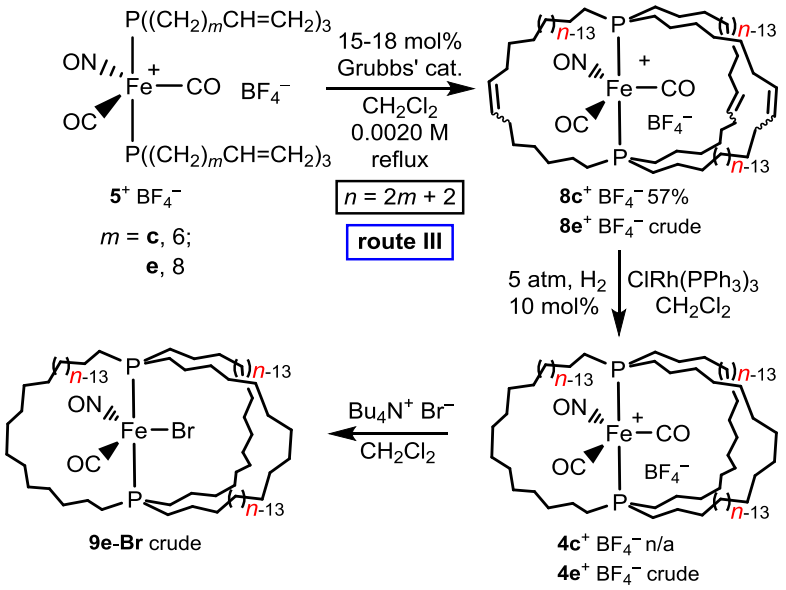

Scheme 5-5. Route III to the title complexes; alkene metathesis during the substitution sequence.

Attempted hydrogenations of **8c**,**e**$^+$ BF_4^- gave mixed results. With **8c**$^+$ BF_4^-, substantial amounts of the starting material were always recovered under varied reaction conditions. In contrast, when **8e**$^+$ BF_4^- was treated with H_2 (5 atm) in the presence of $ClRh(PPh_3)_3$, a ^1H spectrum of an aliquot showed no residual C***H***=C***H*** signals. However, the ^{31}P NMR spectrum of this crude *trans*-$[Fe(CO)_2(NO)(P((CH_2)_{18})_3P)]^+$ BF_4^- (**4e**$^+$ BF_4^-)[119] indicated a purity of only 80%. Nevertheless, it was further reacted with Bu_4N^+ Br^-. A chromatographic workup gave crude *trans*-$Fe(CO)(NO)(Br)(P((CH_2)_{18})_3P)$ (**9e-Br**),[119] which exhibited $^{31}P\{^1H\}$ NMR signals at 45.4 (5%), 45.0 (80%), and 44.8 (15%) ppm. The $^{31}P\{^1H\}$ NMR spectrum of **9c-Br** synthesized by route I exhibited a signal at 45.2 ppm. In accord with dependence of the

$^{31}P\{^{1}H\}$ NMR chemical shift on macrocycle size in other gyroscope like complexes,[85] the signal of **9e-Br** should be slightly upfield from that of **9c-Br**. The product peaks do not vary enough to make a definite assignment, but the peak at 45.0 is most consistent with the expected product. The mass spectrum showed a molecular ion and fragmentation pattern consistent with the presence of **9e-Br**.

5.2.2 Molecular and lattice structures

Structural data were sought for as many of the gyroscope like complexes as possible. Single crystals of **9c-Cl**, **9c-Br**, and **9c-CN** could be grown. Thus, X-ray data were collected, and the structures were solved as summarized in the experimental section and Table 5-2. Key metrical parameters are given in Table 5-3.

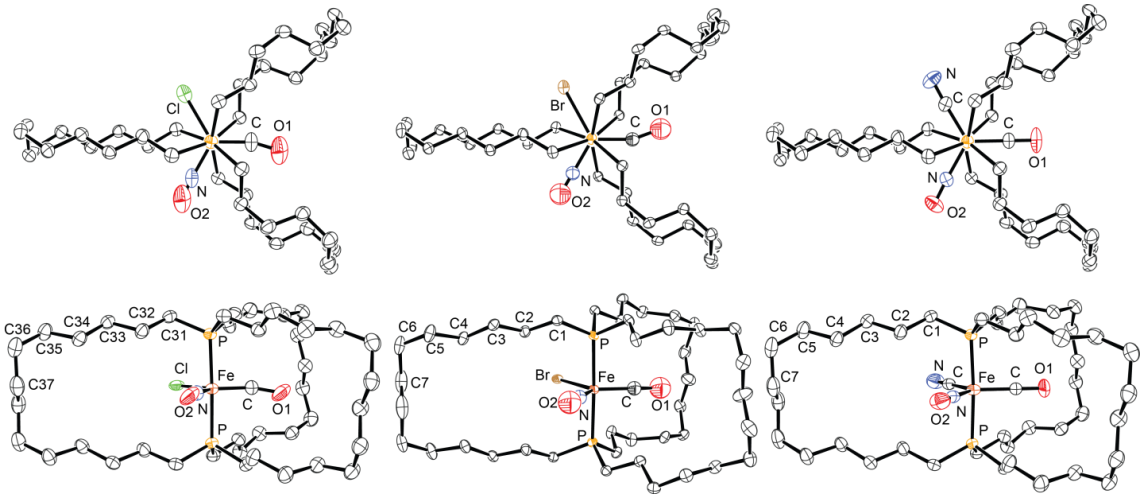

Figure 5-2. Thermal ellipsoid plots (50% probability) of the dominant conformations of **9c-Cl**, **Br**, **CN** (left to right). *Crystal structures were obtained by Dr. Dirk Skaper, but all figures and analyses were done by the author.

Thermal ellipsoid representations of **9c-Cl**, **9c-Br**, and **9c-CN** are provided in Figure 5-2. In all three structures, the CO/NO/X ligands were disordered over three positions. In the case of **9c-Cl**, the ligands could nonetheless be distinguished (33% occupancy, each position); for refinement, the CO and NO positions were arbitrarily assigned in accord with the overall symmetry. In the structure of **9c-Br**, the bromide ligand exhibited 33% occupancy at each position, but the CO and NO ligands could not be distinguished. For refinement, they were assigned equal occupancies in each position. In the case of **9c-CN**, none of the ligands could be distinguished and were presumed to be equally disordered over three positions. Refinement was carried out with fixed occupancy factors as described in the experimental section.

As a result, the positions of the ligands shown in Figure 5-2 are arbitrary, and the bond lengths and angles must be interpreted with caution. In each structure, the dibridgehead diphosphine moiety exhibits a crystallographic C_2 axis coincident with the carbonyl ligand Fe-C linkage (the oxygen atom can deviate from this axis). In all complexes, the substituents along the P-Fe-P axes adopted staggered conformations (Figure 5-2, top). An analogous symmetry axis and conformation is found in the crystal structure of the tricarbonyl complex **3c** (Scheme 5-2), which has been analyzed in previous papers.[85]

Table 5-2. Summary of crystallographic data.[a]

Complex	**9c-Cl**	**9c-Br**	**9c-CN**
empirical formula	$C_{43}H_{84}ClFeNO_2P_2$	$C_{43}H_{84}BrFeNO_2P_2$	$C_{44}H_{84}FeN_2O_2P_2$
formula weight	800.35	844.81	790.92
crystal system	monoclinic	monoclinic	monoclinic
space group	*C*2/c	*C*2/c	*C*2/c
unit cell dimensions			
a [Å]	21.4367(4)	21.2190(8)	21.4114(6)
b [Å]	13.8586(4)	13.9660(8)	13.9998(2)
c [Å]	18.3518(5)	18.1727(2)	18.2960(5)
α [°]	90	90	90
β [°]	122.459(1)	121.002(4)	122.681(9)
γ [°]	90	90	90
volume [$Å^3$]	4600.3(2)	4616.1(3)	4616.1(3)
Z	4	4	4
ρ_{calcd} [Mg/m^3]	1.156	1.216	1.138
μ [mm^{-1}]	0.489	1.295	0.431
F(000)	1752	1824	1736
crystal size [mm^3]	0.35 × 0.30 × 0.20	0.30 × 0.30 × 0.30	0.35 × 0.20 × 0.20
range for data collection	2.37 to 27.44	2.92 to 27.57	2.26 to 27.50
index ranges	$-27 \le h \le 27$	$-27 \le h \le 27$	$-27 \le h \le 27$
	$-17 \le k \le 17$	$-18 \le k \le 18$	$-18 \le k \le 17$
	$-23 \le l \le 23$	$-23 \le l \le 23$	$-23 \le l \le 23$
reflections collected	9763	39777	9935
independent reflections	5244	5278	5286
data/restraints/parameters	5244/3/234	5278/0/230	5286/0/232
goodness-of-fit on F^2	1.062	1.026	0.984
final R indices [I>2σ(I)]	R_1 = 0.0503, wR_2 = 0.1496	R_1 = 0.0613, wR_2 = 0.1595	R_1 = 0.0346, wR_2 = 0.0900
R indices (all data)	R_1 = 0.0648, wR_2 = 0.1612	R_1 = 0.0857, wR_2 = 0.1774	R_1 = 0.0464, wR_2 = 0.0960
largest diff. peak & hole [e $Å^{-3}$]	0.975/–1.014	2.200/–2.197	0.219/–0.772

[a]Data common to all structures: T = 173(2) K; λ = 0.71073 Å.

Table 5-3. Intramolecular and intermolecular distances involving rotator and stator atoms in gyroscope like complexes (Å), and selected bond and torsion angles (°).

Complex	**9c-Cl**	**9c-Br**	**9c-CN**
Fe-P	2.2527(6)	2.2705(8)	2.2310(3)
FeCO	2.86	2.70	2.98[a]
FeNO	2.75	2.95	2.88[a]
FeX	2.363(4)	2.5280(19)	2.98[a]
radius of rotator[b]	4.38	4.22	4.50
Fe-C_a[c]	7.89	7.91	7.93
Fe-C'_a[c]	7.89	7.91	7.93
Fe-C_b[c]	6.65	6.73	6.62
Fe-C'_b[c]	7.46	7.37	7.43
Fe-C_c[c]	7.46	7.37	7.43
Fe-C'_c[c]	6.65	6.73	6.62
Fe-C_{distal}–vdW[d]	4.95	5.03	4.92
Fe-C_{distal}–vdW[e]	6.19	6.21	6.23
Fe-$C_{neighbor}$[f]	5.99	6.06	6.04
Fe-$C_{neighbor}$–vdW[g]	4.29	4.36	4.34
∠ P-Fe-P	177.9	178.2	176.1
$P(\underline{\mathbf{C}}H_2)_3$/$P(\underline{\mathbf{C}}H_2)_3$[h]	6.02	6.08	5.98
$\underline{\mathbf{C}}_a$P-Fe-P$\underline{\mathbf{C}}_a$[i]	6.04	6.12	5.98
$\underline{\mathbf{C}}_b$P-Fe-P$\underline{\mathbf{C}}_b$	6.16	6.20	6.12
$\underline{\mathbf{C}}_c$P-Fe-P$\underline{\mathbf{C}}_c$	6.16	6.20	6.12
C_a-P-P-C_a[j]	38.4	38.2	38.5
C_b-P-P-C_b	37.9	37.5	38.2
C_c-P-P-C_c	37.9	37.5	38.2

[a]These values represent the two distinct distances in the structure. Due to refinement constraints, two of the distances are identical. [b]The FeCO distance (the FeCO distance is the longest of the previous values) plus the van der Waals radius of the oxygen atom (1.52 Å). [c]The distance from iron to the two remote carbon atoms of the three macrocycles (macrocycle A contains the idealized C_2 axis) that are closest to the plane of the rotator (Fe-C_{distal}). [d]The shortest of the previous six distances, minus the van der Waals radius of the carbon atom (1.70 Å). [e]The longest of the previous six distances, minus the van der Waals radius of the carbon atom. [f]The distance from iron to the nearest carbon atom of a neighboring gyroscope like molecule.[g]The previous entry minus the van der Waals radius of the carbon atom. [h]The distance between planes defined by the three carbon atoms attached to each phosphorus atom, taken at the centroid of the three carbon atoms. [i]The distance between the P$\underline{\mathbf{C}}H_2$ carbon atoms of each macrocycle. [j]The C-P-P-C torsion angle within the three macrocycles (a, b, c).

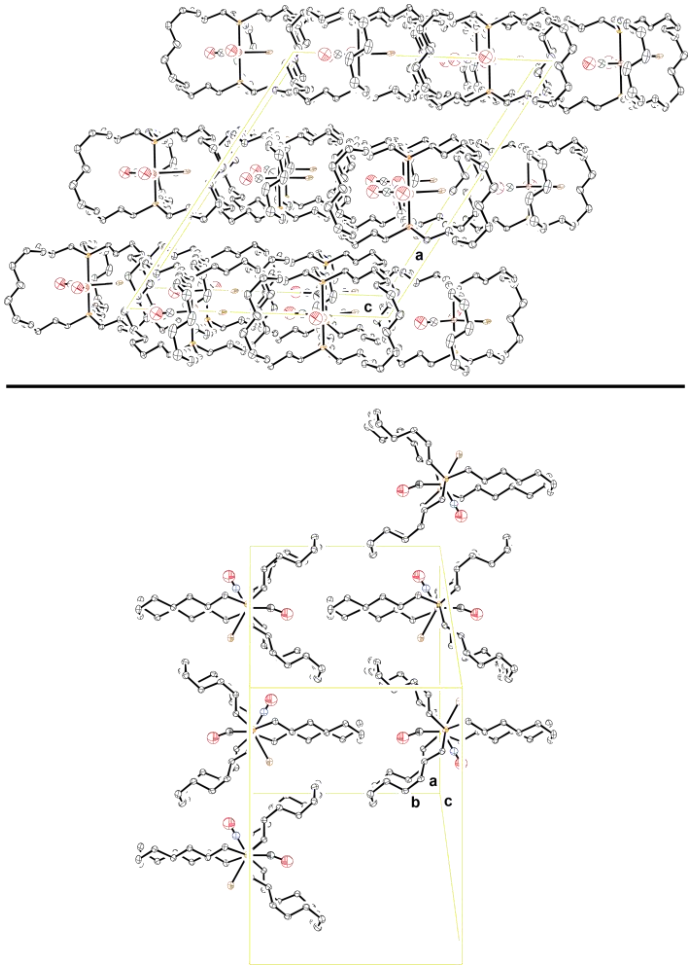

Figure 5-3. The crystal lattice of 9c-Br as viewed along (top) and perpendicular (bottom) to the b axis.

The packing in the crystal lattice of all three structures is analogous to that in **3c**.[85] A representative lattice, that of **9c-Br**, is shown in Figure 5-3. The molecules pack in well-defined layers as shown in Figure 5-3 (top). All of the P-Fe-P axes are parallel. Within each layer the individual molecules alternate between two different orientations (Figure 5-3, bottom).

A model for approximating the void space available for rotation of the rotators within the gyroscopic cages has been developed in several previous papers.[20b,22a,72,85] Figure 5-4 applies this paradigm to **9c-Cl**. At the outset, the rotator radius is determined by taking the distance from iron to the most remote atom on the rotator and adding the corresponding van der Waals radius. In the complexes presented above, the Fe-CO distance is the longest (2.70-2.98 Å) with 2.86 Å for **9c-Cl**. The van der Waals radius of oxygen (1.52 Å)[37] is then added to the Fe-CO distance, giving a radius of 4.38 Å for **9c-Cl**. The corresponding values for **9c-Br** and **9c-CN** are given in Table 5-3 and span a relatively narrow range (4.22-4.50 Å). The analogous distances and radii calculated for the other ligands in **9c-Cl**, **9c-Br**, and **9c-CN** are as follows: Fe-Cl, 2.36/4.11 Å; Fe-Br, 2.53/4.38 Å; Fe-NO, 2.75-2.95/4.27-4.47 Å; Fe-CN 2.98/4.53 Å. Thus, despite the diminished reliabilities of the individual bond lengths as a result of the disorder noted above, the reliance upon the Fe-CO linkages as radius determining seems secure.

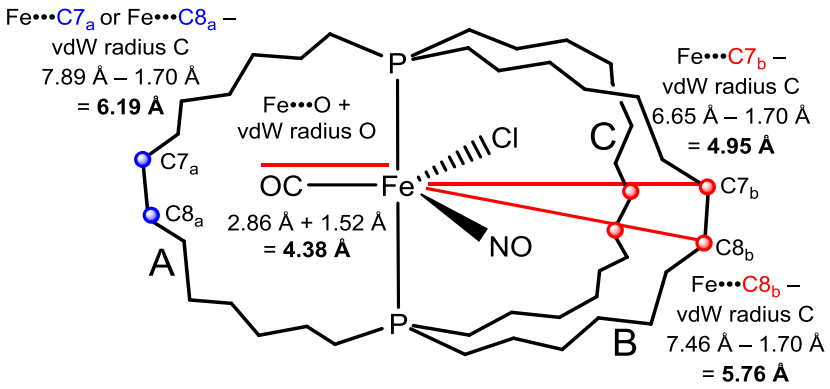

Figure 5-4. Spatial relationships involving the iron atom, rotator, and $(CH_2)_{14}$ bridges in **9c-Cl**; see text and Table 5-3 (vdW = van der Waals; A/B/C refer to the macrocycle labels in Table 5-3).

The "horizontal clearance" for the rotator is then estimated. First, the distances from iron to the most distant carbon atoms on all three of the methylene chains are determined. Since all of the structures possess $P(CH_2)_{14}P$ linkages, the remote carbon atoms should be C7 and C8. The van der Waals radius of a carbon atom is subtracted from these distances.[41] In order to determine the minimum clearance available we employ the shortest of the six values (see Fe-C_{distal}-vdW, Table 5-3).[43] For **9c-Cl**, **9c-Br**, and **9c-CN** the "horizontal clearance" is larger than that of the radius rotator. This indicates that there is indeed enough clearance within the cage for the rotator to rotate. The smallest difference between the clearance and the rotator radius is found in **9c-CN** (4.92 vs. 4.50 Å).

Another issue concerns the feasibility of rotator rotation in the crystal lattice. Here, there is the additional consideration of interference from neighboring molecules. Of most interest are the cases where the distances between the iron atom of one molecule to the nearest non-hydrogen atoms of a neighboring complex are *greater* than the radius of the rotator, once adjusted for the van der Waals radius of the neighboring non-hydrogen atom. This guarantees sufficient steric spacing.

Data obtained from the crystal structures illustrated above are presented in Table 5-3 ("Fe-$C_{neighbor}$–vdW"). These distances are quite similar for all three complexes (5.99, 6.06, and 6.04 Å for **9c-Cl**, **9c-Br**, and **9c-CN**), giving 4.29, 4.36, and 4.34 Å after the van der Waals correction. The values are comparable to those of the rotator radii (4.35, 4.44, and 4.50 Å). Furthermore, the carbon atom on the neighboring molecule that exhibits the shortest distance is markedly removed from the plane of the rotator, bringing

the degree of interaction into question. The next nearest atom, which is barely removed from the rotator plane, allows for more clearance (4.44 Å, 4.48 Å, and 4.55 Å after van der Waals correction). These relationships are exemplified in Figure 5-5. In any case, there appears to be no significant barrier to rotator rotation imposed by the crystal lattices.

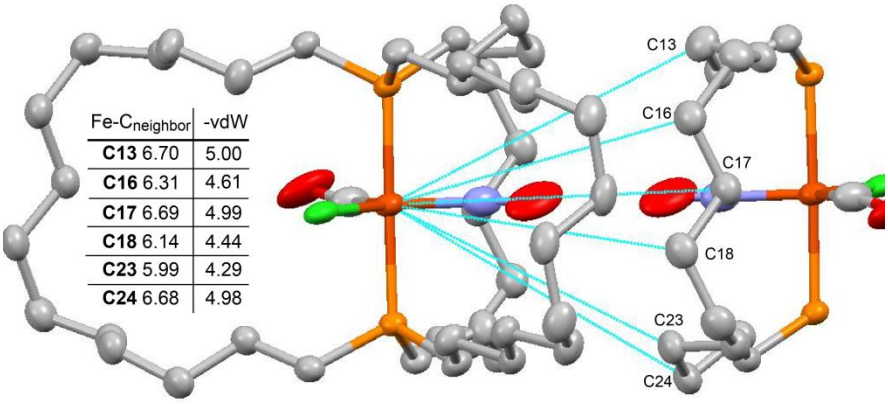

Figure 5-5. Distances from the iron atom of crystalline 9c-Cl to the six nearest atoms of a neighboring molecule

5.3 Discussion

5.3.1 Syntheses

In the context of Scheme 5-2, Schemes 5-3 to 5-5 have established several routes by which gyroscope like iron complexes with dipolar rotators can be accessed. Through route I it has been demonstrated that the title complexes *trans*-Fe(CO)(NO)(X)(P((CH$_2$)$_{14}$)$_3$P) (**9c**) can be accessed in good yield by direct substitution of dicarbonyl nitrosyl complexes *trans*-[Fe(CO)$_2$(NO)(P((CH$_2$)$_{14}$)$_3$P)]$^+$ BF$_4^-$ (**4c**$^+$ BF$_4^-$;

Scheme 5-3). Route II involves the ring closing metathesis reactions of previously reported complexes **6a-e-X** (Scheme 5-4). Some of these were successful, and others not. But importantly, the yields were considerably lower than for the metathesis reactions depicted in Scheme 5-2 for route 1.[85] Furthermore, the standard hydrogenation conditions could not be applied. For example, PtO_2 is a better hydrogenation catalyst than $ClRh(PPh_3)_3$ in the synthesis of **9e-Br**. Route III requires metatheses reactions of cationic complexes. The initial results with **5b,e**$^+$ BF_4^-, and the subsequent hydrogenations and reactions with Bu_4N^+ Br^- (Scheme 5-5), are not particularly promising, at least from the standpoint of giving easily purified products. In any case, the clear conclusion is that complexes **9** are most readily accessible through substitution of cage complexes **4**$^+$ BF_4^- as opposed to "late stage: metathesis reactions of **5**$^+$ BF_4^- or **6**.

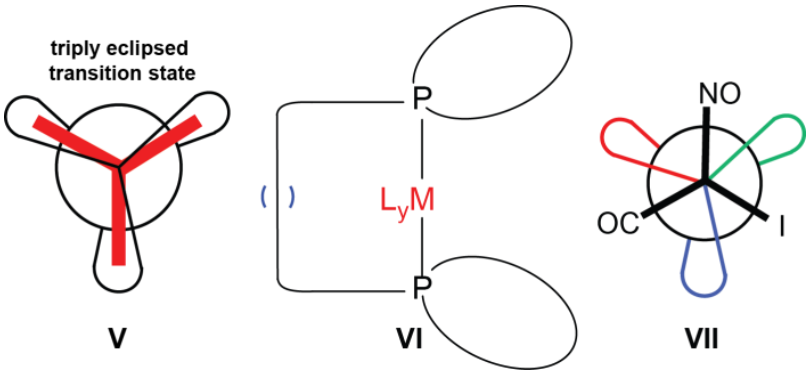

Figure 5-6. Compounds relevant to discussion section.

A possible complication that was not raised in the discussion section involves alternative modes of ring closing metatheses. In a previous paper dealing with octahedral osmium gyroscope like complexes,[22a] a second ring closing metathesis product was determined to have the general structure **VI** shown in Figure 5-6 . These less symmetrical species, derived in part from *intra*ligand metatheses, give more complicated ^{1}H NMR spectra that resemble some of the products of the ring closing metathesis reactions of **7a**-**X**. Perhaps some of the iron substituents or counter anions unique to routes 2 and 3 have an influence on the selectivity.

5.3.2 Rotational behavior

The three sets of $P(CH_2)_{n/2}$ signals in the $^{13}C\{^{1}H\}$ NMR spectrum from **9c-I** indicates that rotation of the Fe(CO)(NO)(I) moiety is slow on the NMR timescale at room temperature. These signals could be ascribed to the three unique macrocycles illustrated in **VII** in Figure 5-6. With respect to the concept of horizontal clearance introduced above, one would add the van der Waals radius of iodide (1.98 Å)[41] to a typical iron-iodine bond length in an iron carbonyl diphosphine complex. Some representative complexes exhibit iron-iodine distances of 2.610(1)-2.695(1) Å.[120] These correspond to radii of 4.59-4.68 Å, all of which are lower than the range of horizontal clearances in Table 5-3 (4.92-5.03 Å).

Thus, it was considered whether the vertical clearance could represent a limiting factor to rotation. Figure 5-7 explores the spatial relationships between the rotator ligands and the C-P-Fe-P-C linkages of **9c-X** and relevant data are reported in Table 5-3.

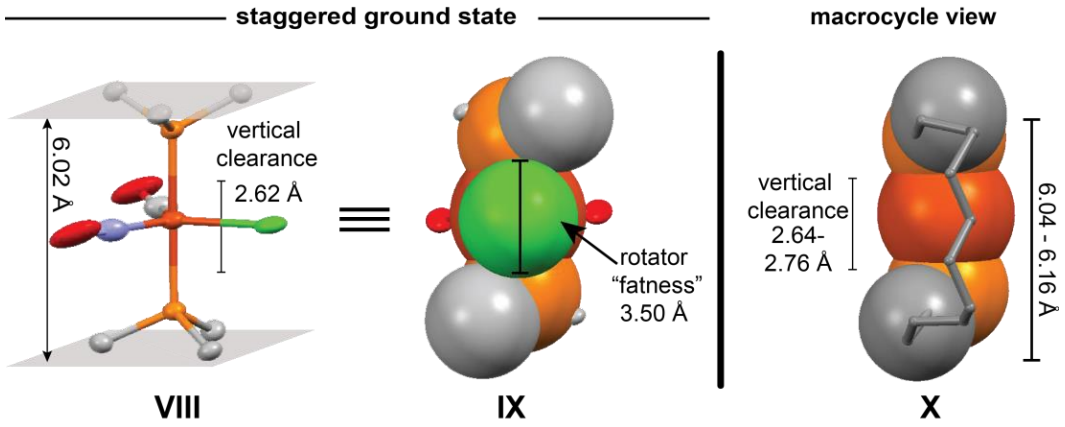

Figure 5-7. Steric relationships between atoms in **9c-Cl** relevant to "vertical clearance" of the rotator. **VIII**: separation of planes defined by the P***C***H_2 carbon atoms. **IX**: rotated 90° from **VIII** so that the Cl atom points out of the page and with selected atoms at van der Waals radii (e.g., the P***C***H_2 carbon atoms that most closely flank a rotator ligand, which are from different macrocycles). **X**: relationship of the two P***C***H_2 carbon atoms within a macrocycle.

First, in **9c-Cl** the distance between the two planes defined by the three methylene carbon atoms on phosphorus, is 6.02 Å (6.08 Å and 5.98 Å for **9c-Br** and **9c-CN** respectively; **VIII**). Subtracting the van der Waals radius of two P***C***H_2 carbon atoms (3.40 Å) yields a vertical clearance of 2.62 Å (2.68 Å and 2.58 Å for **9c-Br** and **9c-CN**). The second relevant clearance is provided by the distance between the P***C***H_2 carbon atoms on each macrocycle (**X**). For **9c-Cl** this distance ranges from 6.04 to 6.16 Å (6.08-6.20 Å and 5.98-6.12 Å for **9c-Br** and **9c-CN**). Subtracting the van der Waals radii of

the P***C***H_2 carbon atoms gives a vertical clearance of 2.64-2.76 Å (2.68-2.80 Å and 2.58-2.72 Å for **9c-Br** and **9c-CN**).

With the dimensions of the stator detailed, the final relevant measurement is that of rotator 'fatness,' approximated by the van der Waals diameter of the largest ligand on the rotator (**IX**). This value increases as the X ligand progresses from CN (3.40 Å), Cl (3.50 Å), Br (3.70 Å), to I (3.96 Å).[41] In order to rotate, the X ligands must pass through the three macrocycles. Figure 5-6 (**V**) illustrates the three eclipsing interactions in the rotational energy maximum. From the metrical data discussed, the vertical clearances are smaller than the rotator fatness. The tightness of this squeeze can be mitigated by conformational changes within the macrocycle itself as previously discussed.[85] Since the $^{13}C\{^1H\}$ NMR spectra of **9c-Cl**, **9c-Br** and **9c-CN** indicate that rotation of the Fe(CO)(NO)(X) moiety is fast on the NMR timescale at room temperature, there should be a value where the rotator becomes too "fat" for the conformational changes in the macrocyles to allow the rotator to pass through. This value would logically be between 3.70 and 3.96 Å.

In previous work[72] we described the synthesis of gyroscope like complexes that are based on dibridgehead diarsine cages. These possessed iron-arsenic distances that were 4% greater than the iron-phosphorus distances, with an 11% increase in vertical clearance. This extension proved advantageous, resulting in decreased rotational barriers. Replacement of the two phosphorus donor atoms in **9c-I** by arsenic atoms could provide the additional vertical clearance to allow the Fe(CO)(NO)(I) rotator to rotate at room temperature.

5.3.3 Cage effects

One impetus of this project was to identify any "cage effects" between acyclic complexes **6** and gyroscope like complexes **9**. Comparing the spectral data in Table 5-1 to similar data reported previously for the relevant acyclic complexes,[32] few significant differences can be identified. The $^{31}P\{^{1}H\}$ NMR signals of the gyroscope like complexes are generally 2-3 ppm downfield of those of the acyclic analogs. The ***C***O signals in the $^{13}C\{^{1}H\}$ spectra of **9** are always ~2 ppm upfield from those of the corresponding complexes **6**. Finally, the IR ν_{CO} and ν_{NO} values are greater in the caged complexes; this trend is most pronounced for **9c-I** vs. **6c-I** (1911 and 1691 cm^{-1} vs. 1905 and 1681 cm^{-1}).

5.3.4 Towards molecular gyroscopes

As discussed in the introduction. a characteristic of molecular gyroscopes that our previous complexes lacked was unidirectional rotation of the rotator. Rather, Brownian motion – i.e., both clockwise and counterclockwise directions – would be expected. However, the gyroscope like complexes *trans*-Fe(CO)(NO)(X)(P($(CH_2)_n$)$_3$P) consisting of Fe(CO)(NO)(X) rotators could support unidirectional rotation driven by an external electric field.[9] Four promising characteristics of these gyroscope like complexes have been identified: (1) Their dipole moment is localized on the rotator. (2) Because these complexes are neutral, there are no counter ions which could increase the barrier to rotation. (3) All axes are parallel in the crystal lattices. This should facilitate the

activation of *all* rotators with respect to unidirectional rotation. (4) The rotators are protected from interactions with neighboring molecules by the steric shielding of the methylene chains.

The synthesis of these complexes is just the beginning. The next steps should involve a more in depth study into the rotational properties of the rotators. A study of the dielectric properties of the dipole moment itself would provide information for future projects that could improve upon the design of molecular compasses.

5.4 Experimental section

General data**:** all reactions were conducted under N_2 or H_2 atmospheres. Chemicals were treated as follows: CH_2Cl_2, ether, and hexanes, dried and degassed using a Glass Contour solvent purification system; $CDCl_3$, C_6D_6, (2 × Cambridge Isotope Laboratories), $Bu_4N^+ X^-$ (X = Cl or CN, Aldrich, 95-97%; Br, TCI, 99%; I, Alfa Aesar, 98%), Grubbs' catalyst ($Ru(=CHPh)(PCy_3)_2(Cl)_2$; Strem), SiO_2 (Silicycle, 40-63 μm, 230-400 mesh), neutral Al_2O_3 (Macherey-Nagel), Celite (EMD), used as received.

NMR spectra (^1H, $^{13}C\{^1H\}$, $^{31}P\{^1H\}$) were recorded on standard 400 or 500 MHz spectrometers at ambient probe temperatures and referenced as follows (δ, ppm): ^1H, residual internal C_6D_5H (7.15), $CHCl_3$ (7.26); ^{13}C, internal C_6D_6 (128.0), $CDCl_3$ (77.0); ^{31}P, external H_3PO_4 (0.00). IR spectra were recorded using a Shimadzu IRAffinity-1 spectrometer with a Pike MIRacle ATR system (diamond/ZnSe crystal). Mass spectra data were recorded on a Micromass Zabspec instrument. Melting points

were determined on an Electrothermal IA 9100 apparatus or a Stanford Research Systems (SRS) MPA100 (Opti-Melt) automated device. Microanalyses were conducted on a Carlo Erba EA1110 instrument or by Atlantic Microlab.

***trans*-Fe(CO)(NO)(Cl)(P((CH$_2$)$_{14}$)$_3$P) (9c-Cl)**. A Schlenk flask was charged with *trans*-[Fe(CO)$_2$(NO)(P((CH$_2$)$_{14}$)$_3$P)]$^+$ BF$_4^-$ (**4c**$^+$ BF$_4^-$;[85] 0.060 g, 0.068 mmol) and CH_2Cl_2 (15 mL). Then Bu_4N^+ Cl^- (0.028 g, 0.102 mmol) was added with stirring. After 18 h, the solvent was removed by oil pump vacuum. Then CH_2Cl_2 (10 mL) was added and the mixture was filtered through silica (2.5 × 5.0 cm) with CH_2Cl_2. The solvent was removed from the filtrate by oil pump vacuum to give **9c-Cl** as a pale orange solid (0.044 g, 0.055 mmol, 81%), mp 139-141 °C (capillary). Anal. Calcd. for $C_{43}H_{84}ClFeNO_2P_2$ (799.50): C 64.53, H 10.58; found: C 64.18, H 10.63.

NMR ($CDCl_3$, δ in ppm): ^{1}H NMR (500 MHz): 1.98-1.86 (m, 12H, C***H***$_2$), 1.66-1.48 (m, 12H, C***H***$_2$), 1.44-1.37 (m, 12H, C***H***$_2$), 1.36-1.27 (m, 48H, C***H***$_2$); ^{13}C{^{1}H} NMR (126 MHz) 218.9 (t, $^2J_{CP}$ = 37.4 Hz, ***C***O), 30.6 (virtual t, $^3J_{CP}$, $^5J_{CP'}$ = 6.5 Hz,[37] PCH$_2$CH$_2$***C***H$_2$), 27.9 (s, ***C***H$_2$), 27.6 (s, ***C***H$_2$), 26.9 (s, ***C***H$_2$), 26.80 (s, ***C***H$_2$), 26.75 (virtual t, $^1J_{CP}$, $^3J_{CP'}$ = 12.9 Hz,[37] P***C***H$_2$), 23.5 (s, ***C***H$_2$); ^{31}P{^{1}H} NMR (202 MHz): 48.7 (s).

IR (powder film, cm^{-1}): 2926 (w), 2856 (w), 1905 (s, ν_{CO}), 1678 (s, ν_{NO}), 1458 (w), 1409 (w), 1087 (w), 803 (w), 760 (w), 719 (w). MS:[76] *m/z* 801 (**9c-Cl**$^+$, 5%), 771 ([**9c-Cl**–CO]$^+$, 30%), 741 ([**9c-Cl**–CO–NO]$^+$, 100%), 738 ([**9c-Cl**–NO–Cl]$^+$, 65%), 684

([**9c-Cl**–CO–NO–Cl–Fe+2O]$^+$, 65%), 668 ([**9c-Cl**–CO–NO–Cl–Fe+O]$^+$, 40%), 652 ([**9c-Cl**–CO–NO–Cl–Fe]$^+$, 20%).

***trans*-Fe(CO)(NO)(Br)(P((CH$_2$)$_{14}$)$_3$P) (9c-Br)**. **Route I**. A Schlenk flask was charged with *trans*-[Fe(CO)$_2$(NO)(P((CH$_2$)$_{14}$)$_3$P)]$^+$ BF_4^- (**4c**$^+$ BF_4^-;[85] 0.107 g, 0.122 mmol) and CH_2Cl_2 (20 mL). Then Bu_4N^+ Br^- (0.079 g, 0.244 mmol) was added with stirring. After 18 h, the solvent was removed by oil pump vacuum. Then CH_2Cl_2 (10 mL) was added and the mixture was filtered through silica (2.5 × 5.0 cm) with CH_2Cl_2. The solvent was removed from the filtrate by oil pump vacuum to give **9c-Br** as a pale orange solid (0.082 g, 0.097 mmol, 79%), mp 150-152 °C (capillary). Anal. Calcd. for $C_{43}H_{84}BrFeNO_2P_2$ (843.45): C 61.13, H 10.02; found: C 61.42, H 10.07. **Route II**. A Fischer-Porter bottle was charged with **7c-Br** (0.158 g, 0.198 mmol), PtO_2 (0.007 g, 0.030 mmol, 15 mol%), THF (20 mL), and H_2 (1 atm). The solution was stirred at 23 °C. After 48 h, the solvent was removed by oil pump vacuum. The residue was filtered through neutral alumina (2.5 × 5.0 cm) with THF. The solvent was removed from the filtrate by oil pump vacuum to give **9c-Br** as a red-brown solid. (0.049 g, 0.061 mmol, 31%).

NMR ($CDCl_3$, δ in ppm): ^{1}H NMR (500 MHz): 2.17-1.80 (m, 12H, C***H***$_2$), 1.68-1.47 (m, 12H, C***H***$_2$), 1.44-1.36 (m, 12H, C***H***$_2$), 1.36-1.18 (m, 48H, C***H***$_2$); ^{13}C{^{1}H} NMR (100 MHz): 218.6 (t, $^2J_{CP}$ = 36.5 Hz, ***C***O), 30.3 (virtual t, $^3J_{CP}$, $^5J_{CP'}$ = 7.8 Hz,[37] PCH$_2$CH$_2$***C***H$_2$), 27.7 (s, ***C***H$_2$), 27.3 (s, ***C***H$_2$), 26.8 (s, ***C***H$_2$), 26.6 (s, ***C***H$_2$), 26.5 (virtual

t, $^{1}J_{CP}$, $^{3}J_{CP'}$ = 12.9 Hz,[37] P***C***H_2), 23.2 (s, ***C***H_2); $^{31}P\{^{1}H\}$ NMR (202 MHz): 45.2 (s); **Route II** $^{31}P\{^{1}H\}$ (162 MHz) 48.2 (s, 25% impurity), 45.1 (s, 75%).

IR (powder film, cm^{-1}): 2926 (w), 2853 (w), 1907 (s, ν_{CO}), 1683 (s, ν_{NO}), 1456 (w), 1409 (w), 1234 (w), 1087 (w), 791 (w), 758 (w), 718 (w). MS:[76] *m/z* 815 ([**9c**-**Br**–CO]$^+$, 20%), 785 ([**9c**-**Br**–CO–NO]$^+$, 100%), 736 ([**9c**-**Br**–CO–Br]$^+$, 35%), 734 ([**9c**-**Br**–NO–Br]$^+$, 40%), 704 ([**9c**-**Br**–CO–NO–Br]$^+$, 5%), 664 ([**9c**-**Br**–CO–NO–Br–Fe+O]$^+$, 10%), 648 ([**9c**-**Br**–CO–NO–Br–Fe]$^+$, 25%); **Route II** MS:[76] *m/z* 801 (**9c**-**Br**$^+$).

***trans*-Fe(CO)(NO)(I)(P((CH$_2$)$_{14}$)$_3$P) (9c-I)**. A Schlenk flask was charged with *trans*-[Fe(CO)$_2$(NO)(P((CH$_2$)$_{14}$)$_3$P)]$^+$ BF_4^- (**4c**$^+$ BF_4^-;[85] 0.090 g, 0.102 mmol) and CH_2Cl_2 (20 mL). Then Bu_4N^+ I^- (0.030 g, 0.114 mmol) was added with stirring. After 18 h, the solvent was removed by oil pump vacuum. Then CH_2Cl_2 (10 mL) was added and the mixture was filtered through silica (2.5 × 5.0 cm) with CH_2Cl_2. The solvent was removed from the filtrate by oil pump vacuum to give **9c-I** as a pale orange solid (0.069 g, 0.077 mmol, 75%), mp 162-164 °C (capillary; dec.). Anal. Calcd. for $C_{43}H_{84}FeINO_2P_2$ (891.44): C 57.91, H 9.49; found: C 57.77, H 9.60.

NMR ($CDCl_3$, δ in ppm): ^{1}H NMR (500 MHz): 2.34-1.89 (m, 24H, C***H***$_2$), 1.78-1.58 (m, 24H, C***H***$_2$), 1.52-1.46 (m, 12H, C***H***$_2$), 1.46-1.39 (m, 12H, C***H***$_2$), 1.39-1.30 (m, 12H, C***H***$_2$); $^{13}C\{^{1}H\}$ NMR (125 MHz): 218.7 (t, $^{2}J_{CP}$ = 35.5 Hz, ***C***O), 30.5, 30.2, 29.9

(overlapping multiplets, $3PCH_2CH_2\boldsymbol{C}H_2$), 28.0-26.8 (overlapping signals, $\boldsymbol{C}H_2$), 24.1, 23.7, 23.5 (overlapping multiplets, $3PCH_2\boldsymbol{C}H_2$; $^{31}P\{^1H\}$ NMR (202 MHz): 41.6 (s).

IR (powder film, cm^{-1}): 3076 (w), 2926 (w), 2853 (w), 1911 (s, ν_{CO}), 1691 (s, ν_{NO}), 1459 (w), 1409 (w), 1262 (w), 1089 (w), 1019 (w), 799 (w), 756 (w), 718 (w). MS:[76] *m/z* 892 (**9c-I**$^+$, 5%), 864 ([**9c-I**–CO]$^+$, 25%), 834 ([**9c-I**–CO–NO]$^+$, 100%), 767 ([**9c-I**–I]$^+$, 5%), 737 ([**9c-I**–NO–I]$^+$, 25%), 684 ([**9c-I**–CO–NO–I–Fe+2O]$^+$, 100%), 668 ([**9c-I**–CO–NO–I–Fe+O]$^+$, 15%), 652 ([**9c-I**–CO–NO–I–Fe]$^+$, 10%).

***trans*-Fe(CO)(NO)(CN)(P((CH$_2$)$_{14}$)$_3$P) (9c-CN)**. A Schlenk flask was charged with *trans*-$[Fe(CO)_2(NO)(P((CH_2)_{14})_3P)]^+$ BF_4^- (**4c**$^+$ BF_4^-;[85] 0.050 g, 0.056 mmol) and CH_2Cl_2 (15 mL). Then Bu_4N^+ CN^- (0.030 g, 0.114 mmol) was added with stirring. After 16 h, the solvent was removed by oil pump vacuum Then CH_2Cl_2 (10 mL) was added and the mixture was filtered through silica (2.5 × 5.0 cm) with CH_2Cl_2. The solvent was removed from the filtrate by oil pump vacuum to give **9c-CN** as a pale orange solid (0.036 g, 0.046 mmol, 83%), mp 141-143 °C (capillary; dec.). Anal. Calcd. for $C_{44}H_{84}FeN_2O_2P_2$ (790.54): C 63.95, H 10.25; found: C 64.01, H 10.22.

NMR ($CDCl_3$, δ in ppm): ^1H NMR (500 MHz): 2.11-1.97 (m, 12H, C$\boldsymbol{H}_2$), 1.86-1.74 (m, 12H, C$\boldsymbol{H}_2$), 1.61-1.48 (m, 60H, C$\boldsymbol{H}_2$); $^{13}C\{^1H\}$ NMR (126 MHz): 218.3 (t, $^2J_{CP}$ = 30.1 Hz, ***C***O), 140.7 (t, $^2J_{CP}$ = 40.6 Hz, ***C***N), 30.7 (virtual t, $^3J_{CP}$, $^5J_{CP'}$ = 6.9 Hz,[37] $PCH_2CH_2\boldsymbol{C}H_2$), 29.3 (virtual t, $^1J_{CP}$, $^3J_{CP'}$ = 13.5 Hz,[37] P***C***H_2), 27.9 (s, ***C***H_2),

27.8 (s, *C*CH_2), 27.0 (s, ***C***H_2), 26.7 (s, ***C***H_2), 23.8 (s, ***C***H_2); $^{31}P\{^1H\}$ NMR (202 MHz): 58.2 (s).

IR (powder film, cm^{-1}): 2924 (w), 2852 (w), 2098 (w, ν_{CN}), 1917 (s, ν_{CO}), 1703 (s, ν_{NO}), 1458 (w), 1307 (w), 1238 (w), 1089 (w), 985 (w), 759 (w), 736 (w), 721 (w), 619 (s). MS:[76] *m/z* 791 (**9c-CN**$^+$, 15%), 762 ([**9c-CN**–CO]$^+$, 55%), 737 ([**9c-CN**–CO–CN]$^+$, 35%), 732 ([**9c-CN**–NO–CO]$^+$, 100%), 704 ([**9c-CN**–CO–NO–CN]$^+$, 5%).

***trans*-Fe(CO)(NO)(Cl)(P((CH$_2$)$_6$CH=CH(CH$_2$)$_6$)$_3$P) (7c-Cl)**. A Schlenk flask was charged with *trans*-Fe(CO)(NO)(Cl)(P((CH$_2$)$_6$CH=CH$_2$)$_3$)$_2$, (**6c-Cl**;[32] 0.127 g, 0.145 mmol), CH_2Cl_2 (75 mL; the resulting solution is 0.0020 M in **6c-Cl**), and Grubbs' catalyst (0.022 g, 0.026 mmol, 18 mol%), and fitted with a condenser. The solution was refluxed. After 48 h, the solvent was removed by oil pump vacuum. The residue was filtered through neutral alumina (2.5 × 2.5 cm) using 2:1 v/v hexane/CH_2Cl_2. The solvent was removed from the filtrate by oil pump vacuum to give **7c-Cl** as red-brown waxy solid (0.046 g, 0.054 mmol, 37%, mixture of *E/Z* isomers).

NMR ($CDCl_3$, δ in ppm): ^1H (500 MHz) 5.48-5.20 (m, 6H, C***H***=), 2.04-1.93 (m, 12H, C***H***$_2$), 1.88-1.64 (m, 12H, C***H***$_2$), 1.62-1.47 (m, 12H, C***H***$_2$), 1.41-1.28 (m, 36H, C***H***$_2$); $^{31}P\{^1H\}$ (202 MHz) 50.4 (s, 77%), 49.8 (s, 23%).

***trans*-Fe(CO)(NO)(Br)(P((CH$_2$)$_6$CH=CH(CH$_2$)$_6$)$_3$P) (7c-Br)**. A Schlenk flask was charged with *trans*-Fe(CO)(NO)(Br)(P((CH$_2$)$_6$CH=CH$_2$)$_3$)$_2$, (**6c-Br**;[32] 0.157 g,

0.170 mmol), CH_2Cl_2 (85 mL; the resulting solution is 0.0020 M in **6c-Br**), and Grubbs' catalyst (0.025 g, 0.031 mmol, 18 mol%), and fitted with a condenser. The solution was refluxed. After 48 h, the solvent was removed by oil pump vacuum. The residue was filtered through neutral alumina (2.5 × 2.5 cm) using 1:1 v/v hexane/CH_2Cl_2. The solvent was removed from the filtrate by oil pump vacuum to give **7c-Br** as red-brown waxy solid (0.047 g, 0.053 mmol, 31%, mixture of *E/Z* isomers).

NMR ($CDCl_3$, δ in ppm): ^{1}H (500 MHz) 5.43-5.15 (m, 6H, C***H***=), 2.10-1.90 (m, 12H, C***H***$_2$), 1.91-1.66 (m, 12H, C***H***$_2$), 1.64-1.45 (m, 12H, C***H***$_2$), 1.42-1.27 (m, 36H, C***H***$_2$); ^{31}P{^{1}H} (202 MHz) 50.4 (s, 63%), 49.8 (s, 15%), 47.8 (s, 22%).

***trans*-Fe(CO)(NO)(I)(P((CH$_2$)$_6$CH=CH(CH$_2$)$_6$)$_3$P) (7c-I)**. A Schlenk flask was charged with *trans*-Fe(CO)(NO)(I)(P((CH$_2$)$_6$CH=CH$_2$)$_3$)$_2$, (**6c-I**;[32] 0.232 g, 0.239 mmol), CH_2Cl_2 (120 mL; the resulting solution is 0.0020 M in **6c-I**), and Grubbs' catalyst (0.035 g, 0.043 mmol, 18 mol%), and fitted with a condenser. The solution was refluxed. After 19 h, additional catalyst was added (0.012 g, 0.014 mmol, 6 mol%). After another 24 h, the solvent was removed by oil pump vacuum. The residue was filtered through neutral alumina (2.5 × 2.5 cm) using CH_2Cl_2. The solvent was removed from the filtrate by oil pump vacuum to give **7c-I** as red-brown waxy solid (0.091 g, 0.096 mmol, 40%, mixture of *E/Z* isomers).

NMR ($CDCl_3$, δ in ppm): ^{1}H (500 MHz) 5.47-5.20 (m, 6H, C***H***=), 2.12-1.47 (m, 36H, C***H***$_2$), 1.46-1.28 (m, 36H, C***H***$_2$); ^{31}P{^{1}H} (202 MHz) 44.9 (s, 63%), 42.0 (s, 15%).

***trans*-Fe(CO)(NO)(CN)(P((CH$_2$)$_6$CH=CH(CH$_2$)$_6$)$_3$P) (7c-CN)**. A Schlenk flask was charged with *trans*-Fe(CO)(NO)(CN)(P((CH$_2$)$_6$CH=CH$_2$)$_3$)$_2$, (**6c-CN**;[32] 0.162 g, 0.187 mmol), CH_2Cl_2 (95 mL; the resulting solution is 0.0020 M in **6c-CN**), and Grubbs' catalyst (0.028 g, 0.034 mmol, 18 mol%), and fitted with a condenser. The solution was refluxed. After 48 h, the solvent was removed by oil pump vacuum. The residue was filtered through neutral alumina (2.5 × 2.5 cm) with CH_2Cl_2. The solvent was removed from the filtrate by oil pump vacuum to give **7c-CN** as red-brown waxy solid (0.038 g, 0.045 mmol, 24%, mixture of *E/Z* isomers).

NMR ($CDCl_3$, δ in ppm): ^{1}H (500 MHz) 5.41-5.17 (m, 6H, C***H***=), 2.08-1.90 (m, 12H, C***H***$_2$), 1.89-1.60 (m, 12H, C***H***$_2$), 1.61-1.46 (m, 12H, C***H***$_2$) 1.46-1.26 (m, 36H, C***H***$_2$); ^{31}P{^{1}H} (202 MHz) 60.2 (s, 75%), 59.6 (s, 15%), 59.4 (s, 22%).

***trans*-Fe(CO)(NO)(Cl)(P((CH$_2$)$_7$CH=CH(CH$_2$)$_7$)$_3$P) (7d-Cl)**. A Schlenk flask was charged with *trans*-Fe(CO)(NO)(Cl)(P((CH$_2$)$_7$CH=CH$_2$)$_3$)$_2$, (**6d-Cl**;[32] 0.101 g, 0.104 mmol), CH_2Cl_2 (55 mL; the resulting solution is 0.0020 M in **6d-Cl**), and Grubbs' catalyst (0.015 g, 0.018 mmol, 18 mol%), and fitted with a condenser. The solution was refluxed. After 48 h, the solvent was removed by oil pump vacuum. The residue was filtered through neutral alumina (2.5 × 2.5 cm) using 2:1 v/v hexane/CH_2Cl_2. The solvent was removed from the filtrate by oil pump vacuum to give **7d-Cl** as red-brown waxy solid (0.032 g, 0.037 mmol, 35%, mixture of *E/Z* isomers).

NMR ($CDCl_3$, δ in ppm): ^{1}H (500 MHz) 5.44-5.24 (m, 6H, C***H***=), 2.31-2.11 (m, 12H, C***H***$_2$), 2.09-1.94 (m, 12H, C***H***$_2$), 1.89-1.64 (m, 12H, C***H***$_2$), 1.64-1.49 (m, 12H,

C***H***$_2$), 1.50-1.18 (m, 48H, C***H***$_2$); $^{31}P\{^1H\}$ (202 MHz) 42.1 (s, 25%), 42.0 (s, 25%), 41.9 (s, 20%), 39.7 (s, 30%).

***trans*-Fe(CO)(NO)(Br)(P((CH$_2$)$_7$CH=CH(CH$_2$)$_7$)$_3$P) (7d-Br)**. A Schlenk flask was charged with *trans*-Fe(CO)(NO)(Br)(P((CH$_2$)$_7$CH=CH$_2$)$_3$)$_2$, (**6d-Br**;[32] 0.110 g, 0.109 mmol), CH_2Cl_2 (55 mL; the resulting solution is 0.0020 M in **6d-Br**), and Grubbs' catalyst (0.016 g, 0.020 mmol, 18 mol%), and fitted with a condenser. The solution was refluxed. After 16 h, additional catalyst was added (0.005 g, 0.007 mmol, 6 mol%). After another 20h, the solvent was removed by oil pump vacuum. The residue was filtered through neutral alumina (2.5 × 2.5 cm) using 1:1 v/v hexane/CH_2Cl_2. The solvent was removed from the filtrate by oil pump vacuum to give. **7d-Br** as a red-brown waxy solid (0.030 g, 0.033 mmol, 30%, mixture of *E/Z* isomers).

NMR ($CDCl_3$, δ in ppm): ^1H (500 MHz) 5.46-5.21 (m, 6H, C***H***=), 2.15-1.88 (m, 12H, C***H***$_2$), 1.84-1.52 (m, 24H, C***H***$_2$), 1.50-1.00 (m, 54H, C***H***$_2$); $^{31}P\{^1H\}$ (202 MHz) 42.2 (s, 23%), 42.0 (s, 30%), 41.9 (s, 12%), 39.7 (s, 12%), 39.7 (s, 23%).

***trans*-Fe(CO)(NO)(Cl)(P((CH$_2$)$_8$CH=CH(CH$_2$)$_8$)$_3$P) (7e-Cl)**. A Schlenk flask was charged with *trans*-Fe(CO)(NO)(Cl)(P((CH$_2$)$_8$CH=CH$_2$)$_3$)$_2$, (**6e-Cl**;[32] 0.131 g, 0.125 mmol), CH_2Cl_2 (65 mL; the resulting solution is 0.0020 M in **6e-Cl**), and Grubbs' catalyst (0.019 g, 0.023 mmol, 18 mol%), and fitted with a condenser. The solution was refluxed. After 12 h, additional catalyst was added (0.006 g, 0.008 mmol, 6 mol%). After 24 h, the solvent was removed by oil pump vacuum. The residue was filtered through neutral alumina (2.5 × 2.5 cm) using 2:1 v/v hexane/CH_2Cl_2. The solvent was removed

from the filtrate by oil pump vacuum to give **7e-Cl** as red-brown waxy solid (0.049 g, 0.051 mmol, 41%, mixture of *E/Z* isomers).

NMR ($CDCl_3$, δ in ppm): ^{1}H (500 MHz) 5.45-5.25 (m, 6H, C***H***=), 2.07-1.82 (m, 24H, C***H***$_2$), 1.80-1.64 (m, 12H, C***H***$_2$), 1.64-1.44 (m, 24H, C***H***$_2$), 1.42-1.14 (m, 42H, C***H***$_2$); ^{31}P{^{1}H} (202 MHz) 49.3 (s, 57%), 49.1 (s, 41%), 48.9 (s, 2%).

***trans*-Fe(CO)(NO)(Br)(P((CH$_2$)$_8$CH=CH(CH$_2$)$_8$)$_3$P) (7e-Br)**. A Schlenk flask was charged with *trans*-Fe(CO)(NO)(Br)(P((CH$_2$)$_8$CH=CH$_2$)$_3$)$_2$, (**6e-Br**;[32] 0.125 g, 0.115 mmol), CH_2Cl_2 (60 mL; the resulting solution is 0.0020 M in **6e-Br**), and Grubbs' catalyst (0.017 g, 0.021 mmol, 18 mol%), and fitted with a condenser. The solution was refluxed. After 48 h, the solvent was removed by oil pump vacuum. The residue was filtered through neutral alumina (2.5 × 2.5 cm) using 1:1 v/v hexane/CH_2Cl_2. The solvent was removed from the filtrate by oil pump vacuum to give **7e-Cl** as red-brown waxy solid (0.042 g, 0.041 mmol, 36%, mixture of *E/Z* isomers).

NMR ($CDCl_3$, δ in ppm): ^{1}H (500 MHz) 5.56-5.28 (m, 6H, C***H***=), 2.17-2.01 (m, 12H, C***H***$_2$), 1.92-1.61 (m, 24H, C***H***$_2$), 1.61-1.46 (m, 24H, C***H***$_2$), 1.44-1.10 (m, 42H, C***H***$_2$); ^{31}P{^{1}H} (202 MHz) 41.8 (s, 59%), 41.7 (s, 34%), 41.6 (s, 7%).

***trans*-[Fe(CO)$_2$(NO)(P((CH$_2$)$_6$CH=CH(CH$_2$)$_6$)$_3$P]$^+$ BF$_4^-$ (8c$^+$ BF$_4^-$)**. A Schlenk flask was charged with *trans*-[Fe(CO)$_2$(NO)(P((CH$_2$)$_6$CH=CH$_2$)$_3$)$_2$]$^+$ BF_4^- (**5c**$^+$ BF_4^-;[32] 0.151 g, 0.159 mmol), CH_2Cl_2 (80 mL; the resulting solution is 0.0020 M in **5c**$^+$ BF_4^-), and Grubbs' catalyst (0.024 g, 0.029 mmol, 18 mol%), and fitted with a

condenser. The solution was refluxed. After 48h, the solvent was removed by oil pump vacuum. The residue was filtered through celite (2.5 × 2.5 cm) with CH_2Cl_2. The solvent was removed from the filtrate by oil pump vacuum and the residue was triturated under ether. The ether was decanted and the residue dried by oil pump vacuum to give **8c**$^+$ BF_4^- as a red-brown waxy solid (0.083 g, 0.091 mmol, 57%, mixture of *E/Z* isomers).

NMR ($CDCl_3$, δ in ppm): ^{1}H (500 MHz) 5.48-5.11 (m, 6H, C***H***=), 2.36-2.13 (m, 12H, C***H***$_2$), 2.09-1.80 (m, 12H, C***H***$_2$), 1.70-1.25 (m, 48H, C***H***$_2$); ^{31}P{^{1}H} (202 MHz) 60.9 (s, 82%), 60.1 (s, 18%).

***trans*-[Fe(CO)$_2$(NO)(P((CH$_2$)$_8$CH=CH(CH$_2$)$_8$)$_3$P)]$^+$ BF$_4^-$ (8e$^+$ BF$_4^-$).** A Schlenk flask was charged with *trans*-[Fe(CO)$_2$(NO)(P((CH$_2$)$_8$CH=CH$_2$)$_3$)$_2$]$^+$ BF_4^- (**5e**$^+$ BF_4^-;[21] 0.300 g, 0.266 mmol), CH_2Cl_2 (175 mL, the resulting solution is 0.0015 M in **5e**$^+$ BF_4^-), Grubbs' catalyst (ca. half of 0.023 g, 0.027 mmol, 10 mol%), and fitted with a condenser. The solution was refluxed. After 24 h, the remaining catalyst was added. After another 24 h, the solvent was removed by oil pump vacuum to give crude **8e**$^+$ BF_4^- as a red-brown oil (0.308 g, 0.296 mmol).

NMR (C_6D_6, δ in ppm): ^{1}H (400 MHz): 5.80-5.47 (m, 6H, C***H***=), 2.50 (m, 12H, C***H***$_2$), 2.07 (m, 24H, C***H***$_2$), 1.47-1.33 (m, 60H, C***H***$_2$); ^{31}P{^{1}H} (162 MHz): 58.7 (s, 68%), 58.3 (s, 27%), 57.6 (s, 3%), 57.1 (s, 2%).

***trans*-[Fe(CO)$_2$(NO)(P((CH$_2$)$_{18}$)$_3$P)]$^+$ BF$_4^-$ (4e$^+$ BF$_4^-$).** A Fischer-Porter bottle was charged with crude **8e**$^+$ BF_4^- (0.308 g, 0.295 mmol), $ClRh(PPh_3)_3$ (0.028 g, 0.030

mmol, 10 mol%), CH_2Cl_2 (30 mL), and H_2 (5 atm). The solution was stirred at 23 °C. After 24 h, the solvent was removed by oil pump vacuum to give crude **4e**$^+$ BF_4^- as a red-brown crude product (0.320 g, 0.305mmol).

NMR (C_6D_6, δ in ppm): ^{1}H (400 MHz): 1.53 (m, 24H, C***H***$_2$), 1.34 (m, 84H, C***H***$_2$); ^{31}P{^{1}H} (162 MHz): 56.8 (overlapping peaks, 5% impurity), 55.9 (s, 80%), 55.4 (overlapping peaks, 10% impurity), 55.1 (overlapping peaks, 5% impurity).

***trans*-Fe(CO)(NO)(Br)(P((CH$_2$)$_{18}$)$_3$P) (9e-Br)**. A Schlenk flask was charged with crude **4e**$^+$ BF_4^- (0.320 g, 0.305 mmol) and CH_2Cl_2 (40 mL). Then Bu_4N^+ Br^- (excess) was added with stirring. After 16 h, the solvent was removed by oil pump vacuum. The residue was filtered through a plug of silica (2.5 × 2.0 cm) using CH_2Cl_2. The solvent was removed from the filtrate by oil pump vacuum to give crude **9e-Br** as a pale orange solid.

^{31}P{^{1}H} NMR (162 MHz, C_6D_6, δ in ppm): 45.4 (s, 5% impurity), 45.0 (s, 80%, **9e-Br**), 44.8 (overlapping peaks, 15% impurity).

MS**:**[76] *m/z* 1011 (**9e-Br**$^+$, 5%), 984 ([**9e-Br**–CO]$^+$, 20%), 954 ([**9e-Br**–CO–NO]$^+$, 100%), 903 ([**9e-Br**–CO–Br]$^+$, 60%), 818 ([**9e-Br**–CO–NO–Br–Fe]$^+$, 30%), 836 ([**9e-Br**–CO–NO–Br–Fe+O]$^+$, 20%), 852 ([**9e-Br**–CO–NO–Br–Fe+2O]$^+$, 5%).

*All mass spectra and successful hydrogenation reactions for this section were done by Dr. Dirk Skaper.

5.5 Crystallography

A concentrated CH_2Cl_2 solution of **9c-Cl** was layered with MeOH and kept at room temperature. After 4 d, data were collected on one of the orange prisms as outlined in Table 5-2. A concentrated CH_2Cl_2 solution of **9c-Br** was layered with MeOH and kept at room temperature. After 4 d, data were collected on one of the deep red prisms as outlined in Table 5-2. A concentrated CH_2Cl_2 solution of **9c-CN** was layered with MeOH and kept at room temperature. After 4 d, data were collected on one of the pale orange prisms as outlined in Table 5-2.

Cell parameters were obtained from 10 frames using a 10° scan and refined with the following numbers of reflections: **9c-Cl**, 5268; **9c-Br**, 280; **9c-CN**, 5177. Lorentz, polarization, and absorption corrections were applied.[78] The space groups were determined from systematic absences and subsequent least-squares refinement. The structures were solved by direct methods. The parameters were refined with all data by full-matrix-least-squares on F^2 using SHELXL-97.[79] Non-hydrogen atoms were refined with anisotropic thermal parameters. The hydrogen atoms were fixed in idealized positions using a riding model. Scattering factors were taken from the literature.[80] In the structure of **9c-Cl**, the Cl, NO, and CO ligands were disordered over three positions (33% occupancy). For refinement, the CO and NO positions were arbitrarily assigned in accord with the overall symmetry. In the structure of **9c-Br**, the bromine atom was disordered over three positions (33% occupancy). The NO and CO ligands were also disordered over three positions, and furthermore could not be distinguished. For refinement, they were assigned 50% occupancy within each of the three conformations.

In the structure of **9c-CN**, the CN, NO, and CO ligands were equally disordered over three positions. Refinements were carried out with fixed occupancy factors for each position (2/3 C + 1/3 N for the ligating atom and 2/3 O + 1/3 N for the non-ligating atom).

6. SUMMARY AND CONCLUSION

Since their first mention in the chemical literature in 1985, synthetic approaches to molecular gyroscopes have made rapid progress. Section 1 described the synthetic evolution of these complexes to include the Gladysz type gyroscope with *trans*-disposed donors that are tethered by three methylene spokes encasing ML_y rotators. The work in this dissertation focused on the synthesis, substitution, and dynamic behavior of these types of complexes.

Section 2 described the synthesis of gyroscope like complexes *trans*-$Fe(CO)_3(P((CH_2)_n)_3P)$ via ring closing metatheses and subsequent hydrogenation reactions. The $Fe(CO)_3$ rotators were then desymmetrized by substituting one carbonyl ligand for a nitrosyl by reaction with NO^+ BF_4^-. A second route of desymmetrization was by reaction with $[H(OEt_2)_2]^+$ BAr_f^-. The dynamic behavior of these complexes was then studied by variable temperature $^{13}C\{^1H\}$ NMR. Rotational barriers were determined from these data.

Section 3 extended the chemistry of section 2 to include arsenic as the *trans* donor ligands. This modification increased the metal to ligand bond distances by 4%. Detailed structural analyses revealed that this increase induced larger changes throughout the gyroscope molecular structure ultimately lowering rotational barriers in analogous complexes to those in section 2.

The goal of section 4 was to investigate substitution reactions of metathesis precursors from section 2, *trans*-$Fe(CO)_3(P((CH_2)_mCH{=}CH_2)_3)_2$. These complexes were first reacted with NO^+ BF_4^- and further reacted with halides or pseudohalides to yield complexes of the formula *trans*-$Fe(CO)(NO)(X)(P((CH_2)_mCH{=}CH_2)_3)_2$. Twenty acyclic compounds with Fe(CO)(NO)(X) rotators were synthesized by employing different chain lengths (m = 4-8) and different halides and pseudohalides (Cl, Br, I, and CN). These complexes were synthesized with two objectives: (1) cataloging spectral characteristics for comparison to future complexes in search of a cage effect and (2) investigating the efficiency of ring closing metathesis around dipolar rotators.

Section 5 established that gyroscope like complexes *trans*-$[Fe(CO)_2(NO)(P((CH_2)_n)_3P)]^+$ BF_4^-could be reacted with ammonium salts of different halides and pseudohalides (Cl, Br, I, and CN) to give a complex with a dipolar rotator. This section detailed the metathesis and hydrogenation reactions of complexes from section 4 establishing that substitution is best done after the complex has undergone metathesis and hydrogenation. Such 'late stage' metathesis reactions led to impure products with much lower yields and further hydrogenation was problematic.

The studies in this dissertation have greatly expanded the scope of the iron based gyroscopes and provided detailed structural and dynamic properties providing relevant insight for related complexes. Future studies could focus on the solid state behavior and modification of the stator to allow for a more rigid frame. Some cage effects were noted in Section 5. Another route to determining a cage effect would be to react *trans*-

$[Fe(CO)_2(NO)(P((CH_2)_mCH{=}CH_2)_3)_2]^+$ BF_4^- and *trans*-$[Fe(CO)_2(NO)(P((CH_2)_n)_3P)]^+$ BF_4^- with different halide salts and determine if there are differing substitution rates. The caged complex could have slower reactions than the open complex. Finally, a more in depth study into the rotational properties of the dipolar rotators could be the next step for chemistry discussed in Section 5. Also, determination of the dielectric properties of the dipole would provide information to future projects which could improve the design of gyroscope like complexes that could be used as molecular compasses.

REFERENCES

(1) Schalley, C. A. *Angew. Chem. Int. Ed.* **2002**, *41*, 1513-1515. *Angew. Chem*. **2002**, *114*, 1583-1586.

(2) Day, A. I.; Blanch, R. J.; Arnold, A. P.; Lorenzo, S.; Lewis, G. R.; Dance, I. *Angew. Chem. Int. Ed.* **2002**, *41*, 275-277. *Angew. Chem*. **2002**, *114*, 285-287.

(3) von Bohnenberger, J. G. F. *Gilbert's Annalen der Physik* **1818**, *60*, 60-71.

(4) Cousins, F.W. *The Anatomy of the Gyroscope-Part III (AGARDograph No. 313)*, J. L. Hollington (ED.); AGARD: Neuilly sur Seine, 1990. AGARD: Advisory group for Aerospace Research and Development of the North Atlantic Treaty Organization (NATO).

(5) Skopek, K.; Hershberger, M. C.; Gladysz, J. A. *Coord. Chem. Rev.* **2007**, 1723-1733.

(6) http://www.gyroscopes.org/uses.asp.

(7) Kottas, G. S.; Clarke, L. I.; Horinek, D.; Michl, J. *Chem. Rev.* **2005**, *105*, 1281-1376.

(8) (a) Khuong, T.-A. V.; Nuñez, J. E.; Godinez, C. E.; Garcia-Garibay, M. A. *Acc. Chem. Res.* **2006**, *39*, 413-422. (b) Vogelsberg, C. S.; Garcia-Garibay, M. A. *Chem. Soc. Rev.* **2012**, *41*, 1892-1910. (c) Pérez-Estrada, S.; Rodríguez-Molina, B.; Xiao, L.; Santillan, R.; Jiménez-Osés, G.; Houk, K. N.; Garcia-Garibay, M. A. *J. Am. Chem. Soc*. **2015**, *137*, 2175-2178. (d) Arcos-Ramos, R. Rodríguez-Molina, B.; Gonalez-Rodriguez, E.; Ramirez-Montes, P. I.; Ochoa, M. E.; Santillan, R.; Farfán, N.; Garcia-Garibay, M. A. *RSC Adv.* **2015**, *5*, 55201-55208. (e) Jiang, X.; O'Brien, Z. J.; Yang, S.; Lai, L. H.;

Buenaflor, J.; Tan, C.; Khan, S.; Houk, K. N.; Garcia-Garibay, M. A. *J. Am. Chem. Soc.* **2016**, *138*, 4650-4656.

(9) (a) Bermudez, V.; Capron, N.; Gase, T.; Gatti, F. G.; Kajzar, F.; Leigh, D. A.; Zerbetto, F.; Zhang, S. *Nature* **2000**, *406*, 608-611. (b) Horansky, R. D.; Clarke, L. I.; Price, J. C.; Khuong, T.-A. V.; Jarowski, P. D.; Garcia-Garibay, M. A. *Phys. Rev. B* **2005**, *72*, 014302-1 to 014302-5. (c) Horansky, R. D.; Clarke, L. I.; Winston, E. B.; Price, J. C.; Karlen, S. D.; Jarowski, P. D.; Santillan, R.; Garcia-Garibay, M. A. *Phys. Rev. B* **2006**, *74*, 054306-1 to 054306-12. (d) Dhar, P.; Swayne, C. D.; Fischer, T. M.; Kline, T.; Sen, A. *Nano Lett.* **2007**, *7*, 1010-1012. (e) Arcenegui, J. J.; García-Sánchez, P.; Morgan, H.; Ramos, A. *Phys. Rev. E* **2013**, *88*, 033025-1 to 033025-8.

(10) Boitrel, B.; Lecas, A.; Renko, Z.; Rose, E. *New J. Chem.* **1989**, *13*, 73-99.

(11) Gray, G. M.; Duffey, C. H. *Organometallics* **1994**, *13*, 1542-1544.

(12) Ng, P. L.; Lambert, J. N. *Synlett* **1999**, 1749-1750.

(13) (a) Setaka, W.; Yamaguchi, K. *J. Am. Chem. Soc.* **2013**, *135*, 14560-14563. (b) Setaka, W.; Inoue, K.; Higa, S.; Yoshigai, S.; Kono, H.; Yamaguchi, K. *J. Org. Chem.* **2014**, *79*, 8288-8295. (c) Shionari, H.; Inagaki, Y.; Yamaguchi, K.; Setaka, W. *Org. Biomol. Chem*. **2015**, *13*, 10511-10516. (d) Nishiyama, Y.; Inagaki, Y.; Yamaguchi, K. *J. Org. Chem.* **2015**, *80*, 9959-9966.

(14) Bauer, E. B.; Ruwwe, J.; Martín-Alvarez, J. M.; Peters, T. B.; Bohling, J. C.; Hampel, F. A.; Szafert, S.; Lis, T.; Gladysz, J. A. *Chem. Commun*. **2000**, 2261-2262.

(15) Bauer, E. B.; Hampel, F. A.; Gladysz, J. A. *Organometallics* **2003**, *22*, 5567-5580.

(16) Frampton, M. J.; Anderson, H. L. *Angew. Chem. Int. Ed.* **2007**, *46*, 1028-1064. *Angew. Chem.* **2007**, *119*, 1046-1083.

(17) Horn, C. R.; Martín-Alvarez, J. M.; Gladysz, J. A. *Organometallics* **2002**, *21*, 5386-5393.

(18) (a) Butikov, E. *Eur. J. Phys.* **2006**, *27*, 1071-1081. (b) Kleppner, D.; Kolenkow, R. J. *An Introduction to Mechanics*; Cambridge University Press: Cambridge, 2010; Chapters 7.3-7.5.

(19) Stahl, J.; Bohling, J. C.; Bauer, E. B.; Peters, T. B.; Mohr, W.; Martín-Alvarez, J. M.; Hampel, F.; Gladysz, J. A. *Angew. Chem. Int. Ed.* **2002**, *41*, 1872-1876. *Angew. Chem*. **2002**, *114*, 1951-1957.

(20) (a) Nawara, A. J.; Shima, T.; Hampel, F.; Gladysz, J. A. *J. Am. Chem. Soc.* **2006**, *128*, 4962-4963. (b) Nawara-Hultzsch, A. J.; Stollenz, M.; Barbasiewicz, M.; Szafert, S.; Lis, T.; Hampel, F.; Bhuvanesh, N.; Gladysz, J. A. *Chem. Eur. J.* **2014**, *20*, 4617-4637. (c) Taher, D.; Nawara-Hultzsch, A. J.; Bhuvanesh, N.; Hampel, F.; Gladysz, J. A. *J. Organomet. Chem.* **2016**, in press (available on the web). DOI: 10.1016/j.jorganchem.2016.03.022.

(21) Shima, T.; Hampel, F.; Gladysz, J. A. *Angew. Chem. Int. Ed.* **2004**, *43*, 5537-5540. *Angew. Chem.* **2004**, *116*, 5653-5656.

(22) (a) Fiedler, T.; Bhuvanesh, N.; Hampel, F.; Reibenspies, J. H.; Gladysz, J. A. *Dalton Trans.* **2016**, *45*, 7131-7147. (b) Fiedler, T.; Chen, L.; Wagner, N. D.; Russell, D. R.; Gladysz, J. A. *Organometallics* **2016**, *35*, in press (available on the web). DOI: 10.1021/acs.organomet.6b00249.

(23) Wang, L.; Hampel, F.; Gladysz, J. A. *Angew. Chem., Int. Ed. Engl.* **2006**, *45*, 4372-4375; *Angew. Chem.* **2006**, *118*, 4479-4482.

(24) (a) Wang, L.; Shima, T.; Hampel, F.; Gladysz, J. A. *Chem. Commun.* **2006**, 4075-4077. (b) Estrada, A. L.; Jia, T.; Bhuvanesh, N.; Blümel, J.; Gladysz, J. A. *Eur. J. Inorg. Chem.* **2015**, *2015*, 5318-5321.

(25) Hess, G. D.; Hampel, F.; Gladysz, J. A. *Organometallics* **2007**, *26*, 5129-5131.

(26) (a) Guix, M.; Mayorga-Martinez, C. C.; Merkoçi, A. *Chem. Rev*. **2014**, *114*, 6285-6322. (b) Abendroth, J. M.; Bushuyev, O. S.; Weiss, P. S.; Barrett, C. J. *ACS Nano* **2015**, *9*, 7746-7768.

(27) (a) Vives, G.; Tour, J. M. *Acc. Chem. Res.* **2009**, *42*, 473-487. (b) García-López, V.; Chu, P.-L. E.; Chiang, P.-T.; Sun, J.; Martí, A. A.; Tour, J. M. *Asian J. Org. Chem*. **2015**, *4*, 1308-1314.

(28) Various representative examples: (a) Lemouchi, C.; Iliopoulos, K.; Zorina, L.; Simonov, S.; Wzietek, P.; Cauchy, T.; Rodríguez-Fortea, A.; Canadell, E.; Kaleta, J.; Michl, J.; Gindre, D; Chrysos, M.; Batail, P. *J. Am. Chem. Soc.* **2013**, *135*, 9366-9376. (b) Zhou, Z.; Zhang, X.; Liu, Q.; Yan, Z.; Lv, C.; Long, G. *Inorg. Chem.* **2013**, *52*, 10258-10263. (c) Liu, Z.-q.; Kubo, K.; Noro, S.-i.; Akutagawa, T.; Nakamura, T. *Cryst. Growth Des.* **2014**, *14*, 537-543. (d) Chen, J.; Kistemaker, J. C. M.; Robertus, J.; Feringa, B. L. *J. Am. Chem. Soc.* **2014**, *136*, 14924-14932. (e) Zigon, N.; Hosseini, M. W. *Chem. Commun.* **2015**, *51*, 12486-12489. (f) Prack, E.; O'Keefe, C. A.; Moore, J. K.;

Lai, A.; Lough, A. J.; Macdonald, P. M.; Conradi, M. S.; Schurko, R. W.; Fekl, U. *J. Am. Chem. Soc.* **2015**, *137*, 13464-13467.

(29) Skopek, K.; Gladysz, J. A. *J. Organomet. Chem.* **2008**, *693*, 857-866.

(30) Zeits, P. D.; Rachiero, G. P.; Hampel, F.; Reibenspies, J. H.; Gladysz, J. A. *Organometallics* **2012**, *31*, 2854-2877.

(31) Zheng, X.; Mulcahy, M. E.; Horinek, D.; Galeotti, F.; Magnera, T. F.; Michl, J. *J. Am. Chem. Soc.* **2004**, *126*, 4540-4542 and references therein.

(32) Lang, G. M.; Skaper, D.; Shima, T.; Otto, M.; Wang, L.; Gladysz, J. A. *Aust. J. Chem.* **2015**, *68*, 1342-1351.

(33) Since complexes of the phosphine $P((CH_2)_7CH{=}CH_2)_3$ have been synthesized,[88] it seems helpful to assign a sequential letter to each methylene chain length (missing index **d** for $m = 7$ ($n = 16$)).

(34) (a) $Ru(=CHPh)(PCy_3)_2(Cl)_2$; (b) $Ru(=CHPh)(H_2IMes)(PCy_3)(Cl)_2$, H_2IMes = 1,3-dimesityl-4,5-dihydroimidazol-2-ylidene.

(35) Shima, T.; Bauer, E. B.; Hampel, F.; Gladysz, J. A. *Dalton Trans.* **2004**, 1012-1018.

(36) (a) Garrou, P. E. *Chem. Rev.* **1981**, *81*, 229-266. (b) Gorenstein, D. G. *Phosphorus-31 NMR-Principles and Applications*; Academic Press, Inc.: Orlando, FL, 1984; Chapter 1. (c) The variation with ring size has been analyzed in terms of shift tensor components. Lindner, E.; Fawzi, R.; Mayer, H. A.; Eichele, K.; Hiller, W. *Organometallics* **1992**, *11*, 1033-1043.

(37) The *J* values given for virtual triplets or multiplets approximating doublets

of doublets represent the *apparent* couplings, and not the mathematically rigorous coupling constants. Hersh, W. H. *J. Chem. Educ.* **1997**, *74*, 1485-1488.

(38) Resonances were assigned as follows. First, the PC***H***$_2$C***H***$_2$C***H***$_2$ ^{1}H NMR signals of *E,E,E*-**3a** and **5c**$^+$ BF_4^- were identified via ^{1}H,^{1}H COSY experiments. The P***C***H$_2$***C***H$_2$***C***H$_2$ ^{13}C signals were then identified by ^{1}H,^{13}C HSQC experiments. The coupling constant and chemical shift trends thus established were used to assign the P***CH***$_2$***CH***$_2$***CH***$_2$ signals of the other complexes.

(39) Boddien, A.; Gärtner, F.; Jackstell, R.; Junge, H.; Spannenberg, A.; Baumann, W.; Ludwig, R.; Beller, M. *Angew. Chem., Int. Ed.* **2010**, *49*, 8993-8996; *Angew. Chem.* **2010**, *122*, 9177-9181.

(40) Since the three FeCO distances are usually within experimental error or "three esd values", the average, as opposed to the longest, is employed.

(41) (a) Cordero, B.; Gómez, V.; Platero-Prats, A. E.; Revés, M.; Echeverría, J.; Cremades, E.; Barragán, F.; Alvarez, S. *Dalton Trans*. **2008**, 2832-2838. (b) Bondi, A. *J. Phys. Chem*. **1964**, *68*, 441-451. (c) Mantina, M.; Chamberlin, A. C.; Valero, R.; Cramer, C. J.; Truhlar, D. G. *J. Phys. Chem. A* **2009**, *113*, 5806-5812.

(42) The van der Waals radii of sp^3 and sp^2 carbon atoms are identical (1.70 Å); for simplicity the same value is applied to CO carbon atoms.

(43) For example, since the carbon chains are conformationally mobile in solution, it may be more appropriate to take an average distance for Fe-C_{distal}.

(44) (a) Johnson, B. F. G.; Segal, J. A. *J. Chem. Soc. Dalton Trans.* **1972**, 1268-1271. See also: (b) Touchard, D.; Le Bozec, H.; Dixneuf, P. *Inorg. Chim. Acta.* **1979**, *33*, L141-L142. (c) Ahmed, F. R.; Roustan, J. L. A.; Al-Janabi, M. Y. *Inorg. Chem.* **1985**, *24*, 2526-2532. (d) Crooks, G. R.; Johnson, B. F. G. *J. Chem. Soc. A* **1968**, 1238-1240.

(45) (a) Ashford, P. K.; Baker, P. K.; Connelly, N. G.; Kelly, R. L.; Woodley, V. A. *J. Chem. Soc., Dalton Trans.* **1982**, 477-479 and earlier work referenced therein. (b) Richter-Addo, G. B.; Legzdins, P. *Metal Nitrosyls*; Oxford University Press, Inc.: NY, 1992; Chapter 2, pp 37-38. (c) Connelly, N.; Geiger, W. E. *Chem. Rev.* **1996**, *96*, 877-910.

(46) Kochi, J. K. *J. Organomet. Chem*. **1986**, *300*, 139-166.

(47) Sowa, J. R. Jr.; Zanotti, V.; Facchin, G.; Angelici, R. J. *J. Am. Chem. Soc.* **1991**, *113*, 9185-9192.

(48) Brookhart, M.; Grant, B.; Volpe, A. F. *Organometallics* **1992**, *11*, 3920-3922.

(49) The IR ν_{MH} bands are, by analogy to those of the osmium hydride complexes *mer, trans*-$[Os(H)(CO)_3(PR_3)_2]^+ Z^-$, expected to be much weaker than the ν_{CO} bands (and at lower frequencies): Laing, K. R.; Roper, W. R. *J. Chem. Soc. A* **1969**, 1889-1891. See also Franke, O.; Wiesler, B. E.; Lehnert, N.; Tuczek, F. *Z. Anorg. Allg. Chem.* **2002**, *628*, 2395-2402.

(50) Siegel, J. S.; Anet, F. A. L. *J. Org. Chem*. **1988**, *53*, 2629-2630.

(51) Budzelaar, P. H. M., *gNMR: NMR Simulation Program,* Version 5.0.6.0, Adept Scientific: Luton, U.K. 2006.

(52) Karlen, S. D.; Garcia-Garibay, M. A. *Top. Curr. Chem.* **2005**, *262*, 179-227.

(53) Fyfe, C. A. *Solid-State NMR for Chemists*; CFC Press: Guelph, Ontario, Canada, 1983; pp 199-209.

(54) Duncan, T. M. *A Compilation of Chemical Shift Anisotropies*; Farragut Press: Chicago, IL, 1990; p C-35.

(55) Cluff, K. J.; Bhuvanesh, N.; Blümel, J. *Chem. Eur. J.* **2015**, *21*, 10138-10148.

(56) The program "dmfit" was applied: Massiot, D.; Fayon, F.; Capron, M.; King, I.; Le Calvé, S.; Alonso, B.; Durand, J.-O.; Bujoli, B.; Gan, Z.; Hoatson, G. *Magn. Reson. Chem.* **2002**, *40*, 70-76.

(57) Hilliard, C. R. doctoral dissertation, Texas A&M University, College Station, TX, 2013.

(58) Kirkland, T. A.; Grubbs, R. H. *J. Org. Chem.* **1997**, *62*, 7310-7318.

(59) (a) Conrad, J. C.; Eelman, M. D.; Silva, J. A. D.; Monfette, S.; Parnas, H. H.; Snelgrove, J. L.; Fogg, D. E. *J. Am. Chem. Soc.* **2007**, *129*, 1024-1025. (b) Monfette, S.; Fogg, D. E. *Chem. Rev.* **2009**, *109*, 3783-3816.

(60) Almenningen, A.; Anfinsen I. M.; Haaland, A.; Jerslev, B.; Schäffer, C. E.; Sunde, E.; Sorenson, N. A. *Acta Chem. Scand.* **1970**, *24*, 43-49.

(61) Lee, C. W.; Grubbs, R. H. *Org. Lett.* **2000**, *2*, 2145-2147.

(62) (a) Albers, M. O.; Coville, N. J. *Coord. Chem. Rev.* **1984**, *53*, 227-259. (b) Luh, T.-Y. *Coord. Chem. Rev.* **1984**, *60*, 255-276.

(63) Pankowski, M.; Bigorgne, M. *J. Organomet. Chem.* **1971**, *30*, 227-234.

(64) (a) Fischer, E. O.; Kiener, V. *J. Organomet. Chem*. **1970**, *23*, 215-233. (b) For derivatization protocols, see Semmelhack, M. F.; Tamura, R. *J. Am. Chem. Soc*. **1983**, *105*, 4099-4100.

(65) Scherer, A. doctoral dissertation, Universität Erlangen-Nürnberg, 2009, Chapter 4.

(66) (a) Tam, W.; Lin, G.-Y.; Wong, W.-K.; Kiel, W. A.; Wong, V. K.; Gladysz, J. A. *J. Am. Chem. Soc.* **1982**, *104*, 141-152. (b) Tam, W.; Lin, G.-Y.; Gladysz, J. A. *Organometallics* **1982**, *1*, 525-529.

(67) Liu, L.; Guo, Q.-X. *Chem. Rev.* **2001**, *101*, 673-696.

(68) Marahatta, A. B.; Kanno, M.; Hoki, K.; Setaka, W.; Irle, S.; Kono, H. *J. Phys. Chem. C* **2012**, *116*, 24845-24854.

(69) Commins, P.; Nuñez, J. E.; Garcia-Garibay, M. A. *J. Org. Chem*. **2011**, *76*, 8355-8363.

(70) (a) Karlen, S. D.; Ortiz, R.; Chapman, O. L.; Garcia-Garibay, M. A. *J. Am. Chem. Soc.* **2005**, *127*, 6554-6555. (b) Czajkowska-Szczykowska, D.; Rodríguez-Molina, B.; Magaña-Vergara, N. E.; Santillan, R.; Morzycki, J. W.; Garcia-Garibay, M. A. *J. Org. Chem.* **2012**, *77*, 9970-9978.

(71) Iron tetracarbonyl phosphine and arsine complexes of the formula $Fe(CO)_4(E(o\text{-tol})_3)$ have been crystallographically characterized. The Fe-As bond is 3.6% longer than the Fe-P bond: (a) Howell, J. A. S.; Palin, M. G.; McArdle, P.; Cunningham, D.; Goldschmidt, Gottlieb, H. E.; Hezroni-Langerman, D. Z. *Inorg. Chem*. **1991**, *30*, 4683-4685. (b) Howell, J. A. S.; Palin, M. G.; McArdle, P.; Cunningham, D.;

Goldschmidt, Z.; Gottlieb, H. E.; Hezroni-Langerman, D. *Inorg. Chem*. **1993**, *32*, 3493-3500. (c) The Fe-As bonds in closely related iron tricarbonyl complexes with *cis* As-Fe-As and P-Fe-P linkages are 6.6-3.8% longer: Brown, D. S.; Bushnell, G. W. *Acta Cryst*. **1967**, *22*, 296-299; Hogarth, G. *J. Organomet. Chem.* **1991**, *406*, 391-398.

(72) Lang, G. M.; Bhuvanesh, N.; Reibenspies, J. H.; Gladysz, J. A. manuscript submitted to *Organometallics*.

(73) Lang, G. M.; Skaper, D.; Hampel, F.; Gladysz, J. A. manuscript in preparation.

(74) Data were treated as recommended by Cammenga, H. K.; Epple, M. *Angew. Chem., Int. Ed. Engl.* **1995**, *34*, 1171-1187; *Angew. Chem.* **1995**, *107*, 1284. The T_e values best represent the temperature of the phase transition.

(75) This melting point was determined under argon using a sample that had been washed with hexane prior to drying. Two independently prepared samples that were not so treated showed darkening and shrinkage at ca. 50 °C.

(76) FAB, 3-NBA, m/z (relative intensity, %); the most intense peak of the isotope envelope is given.

(77) These data do not indicate an analytically pure sample, but are provided nonetheless to illustrate the best fit obtained to date.

(78) (a) Nonius, B. V. *Collect*, data collection software; 1998. (b) Otwinowski, Z.; Minor, W. *Scalepack*, data processing software: in *Methods in Enzymology* **1997**, *276* (*Macromolecular Crystallography, Part A*), 307.

(79) Sheldrick, G. *Acta Crystallogr. A* **2008**, *64*, 112-122.

(80) Cromer, D. T.; Waber, J. T. In *International Tables for X-ray Crystallography*; Ibers, J. A., Hamilton, W. C., Eds.; Kynoch: Birmingham, U.K., 1974.

(81) Dolomanov, O. V.; Bourhis, L. J.; Gildea, R. J.; Howard, J. A. K.; Puschmann, H. *J. Appl. Crystallogr*. **2009**, *42*, 339-341.

(82) "iPhone 4's New Gyroscope", Jobs, S. (YouTube) https://youtu.be/ORcu-c-qnjg (accessed 12 May 2016).

(83) See also (a) Bedard, T. C.; Moore, J. S. *J. Am. Chem. Soc.* **1995**, *117*, 10662-10671. (c) Wang, G.; Xiao, H.; He, J.; Xiang, J.; Wang, Y.; Chen, X.; Che, Y.; Jiang, H. *J. Org. Chem.* **2016**, *81*, 3364-3371.

(84) Fiedler, T.; Gladysz, J. A. Multifold Ring Closing Olefin Metatheses in Syntheses of Organometallic Molecules with Unusual Connectivities. In *Olefin Metathesis*: *Theory and Practice,* Grela, K., Ed.; Wiley/VCH: Weinheim, 2013, 311-328.

(85) Lang, G. M; Shima, T.; Wang, L.; Cluff, K. J.; Hampel, F.; Blümel, J.; Gladysz, J. A. *J. Am. Chem. Soc.* **2016**, *138*, in press (available on the web). DOI: 10.1021/jacs.6b03178.

(86) Zingaro, R. A.; Merijanian, A. *Inorg. Chem*. **1964**, *3*, 580-584.

(87) Roux, M.-C.; Paugam, R.; Rousseau, G. *J. Org. Chem.* **2001**, *66*, 4304-4310.

(88) Nawara-Hultzsch, A. J.; Skopek, K.; Shima, T.; Barbasiewicz, M.; Hess, G. D.; Skaper, D.; Gladysz, J. A. *Z. Naturforsch. B: Anorg. Chem., Org. Chem*. **2010**, *65b*, 414-424.

(89) Krasovskiy, A.; Knochel, P. *Synthesis* **2006**, 890-891.

(90) Howell, J. A. S.; Johnson, B. F. G.; Josty, P. L.; Lewis, J. *J. Organomet. Chem.* **1972**, *39*, 329-333.

(91) (a) Keiter, R. L.; Benson, J. W.; Keiter, E. A.; Harris, T. A. *et al. Organometallics* **1997**, *16*, 2246-2253.

(92) Lin, J. T.; Lin, Y. F.; Wang, S. Y.; Sun, J. S.; Yeh, S. K. *Bull. Inst. Chem., Academia Sinica* **1989**, *36*, 63-71.

(93) (a) Touchard, D.; Fillaut, J.-L.; Dixneuf, P. H.; Toupet, L. *J. Organomet. Chem*. **1986**, *317*, 291-299. (b) Touchard, D.; Lelay, C.; Fillaut, J.-L.; Dixneuf, P. H. *J. Chem. Soc., Chem. Commun.* **1986**, 37-38. (c) Petz, W. *J. Organomet. Chem*. **1988**, *346*, 397-402.

(94) Glaser, R.; Yoo, Y.-H.; Chen, G. S.; Barnes, C. L. *Organometallics* **1994**, *13*, 2578-2586.

(95) (a) Blanch, S. W.; Bond, A. M.; Colton, R. *Inorg. Chem*. **1981**, *20*, 755-761. (b) See also Baker, P. K.; Connelly, N. G.; Jones, B. M. R.; Maher, J. P.; Somers, K. R. *J. Chem. Soc., Dalton Trans.* **1980**, 579-585.

(96) (a) Ansyln, E. V.; Dougherty, D. A. *Modern Physical Organic Chemistry*, University Science Books, Sausalito, California; **2006**, pp 97-98. (b) Eliel, E. N.; Wilen, S. H. *Stereochemistry of Organic Compounds*, Wiley, New York; **1994**, pp 624-629 and 1142-1155.

(97) Baker, J.; Blümel, J. unpublished results, Texas A&M University.

(98) *trans*-$Fe(CO)_3(PPh_3)(SbMe_3)$: Fe-P 2.199(1) Å; Fe-Sb 2.4627(7) Å. Lorenz, I.-P.; Rudolph, S.; Piotrowski, H.; Polborn, K. *Eur. J. Inorg. Chem.* **2005**, 82-85.

(99) $Fe(CO)_4(SbPh_3)$: Fe-Sb 2.472(1) Å. Bryan, R. F.; Schmidt, W. C., Jr. *J. Chem. Soc., Dalton Trans.* **1974**, 2337-2340.

(100) (a) $Fe(CO)_4(Sbt\text{-}Bu_3)$: Fe-Sb 2.547(1) Å. Rheingold, A. L.; Fountain, M. E. *Acta Cryst.* **1985**, *C41*, 1162-1164. (b) $Fe(CO)_4(Pt\text{-}Bu_3)$: Fe-P 2.364(1) Å. Pickardt, J.; Rösch, L.; Schumann, H. *J. Organomet. Chem*. **1976**, *107*, 241-248.

(101) $Fe(CO)_4(Bit\text{-}Bu_3)$: Fe-Bi 2.6269(9) Å. Breunig, H. J.; Borrmann, T.; Lork, E.; Moldovan, O.; Rat, C. I.; Wagner, R. P. *J. Organomet. Chem.* **2009**, *694*, 427-432.

(102) For the $^{13}C\{^1H\}$ NMR spectra of **6a-c**$^+$ BAr_f^-, GARP ^1H decoupling sequences were employed as opposed to WALTZ-16 (Varian NMRS 500 MHz). Otherwise, residual couplings were apparent.

(103) APEX2. *Program for Data Collection on* Area *Detectors*. BRUKER AXS Inc., Madison, WI, USA.

(104) SADABS, Sheldrick, G.M. Program for Absorption Correction of Area Detector Frames. BRUKER AXS Inc., Madison, WI, USA.

(105) Spek, A. L.; PLATON. A Multipurpose Crystallographic Tool. *J. Appl. Cryst*. **2003**, *36*, 7-13.

(106) (a) Setaka, W.; Ohmizu, S.; Kabuto, C.; Kira, M. *Chem. Lett.* **2007**, *36*, 1076-1077. (b) Setaka, W.; Ohmizu, S.; Kira, M. *Chem. Lett.* **2010**, *39*, 468-469. (d) Setaka, W.; Yamaguchi, K. *Proc. Nat. Acad. Sci. U.S.A.* **2012**, *109*, 9271-9275. (e) Setaka, W.; Koyama, A.; Yamaguchi, K. *Org. Lett.* **2013**, *15*, 5092-5095.

(107) (a) Dinh, L. V.; Hampel, F.; Gladysz, J. A. *J. Organomet. Chem*. **2005**, *690*, 493-503. (b) de Quadras, L.; Stahl, J.; Zhuravlev, F.; Gladysz, J. A. *J. Organomet.*

Chem. **2007**, *692*, 1859-1870.

(108) Brookhart, M. Nelson, G. O. *J. Organomet. Chem.* **1979**, *164*, 193-202.

(109) The $^{1}H,^{1}H$ COSY experiment allowed assignment of the $PC\underline{H}_2$, $PCH_2C\underline{H}_2$, and $PCH_2CH_2C\underline{H}_2$ signals, and the $^{1}H,^{13}C$ HSQC experiment in turn correlated these to the $P\underline{C}H_2\underline{C}H_2\underline{C}H_2$ signals.

(110) X = CN: Dolcetti, G.; Busetto, L.; Palazzi, A. *Inorg. Chem*. **1974**, *13*, 222-225.

(111) X = Cl, Br, I: Carroll, W. E.; Deeney, A. F.; Lalor, F. J. J. Chem. Soc., Dalton Trans. **1974**, 1430-1433.

(112) (a) Jänicke, M.; Hund, H. –U.; Berke, H. *Chem. Ber.* **1991**, *124*, 719-723. (b) For Tables 3 and 4 in this paper, the labels **a** and **c** (denoting the phosphorus donor ligand) for compounds **5** and **7** are reversed.

(113) See also Roustan, J. L. A.; Merour, J. Y.; Forgues, A. *J. Organomet. Chem.* **1980**, *186*, C23-C26.

(114) Bitterwolf, T. E.; Steele, B. *Inorg. Chem. Commun*. **2006**, *9*, 512-513.

(115) http://www.unisys.com/about-us/company-history

(116) http://findingaids.hagley.org/xtf/view?docId=ead/1915.xml

(117) Since fictional characters can often be useful in outreach lectures, we note that the presence of gyro stabilizers in Iron Man's suit was first reported in *Iron Man*, April 1976, Vol. 1, #85. Were Tony Stark a real person, he would have very likely wanted his molecular gyroscopes to be based upon iron.

(118) (a) Dominguez, Z.; Khuong, T.-A.; Dang, H.; Sanrame, C. N.; Nuñez, J. E.; Garcia-Garibay, M. A. *J. Am. Chem. Soc*. **2003**, *125*, 8827-8837. (b) Khuong, T.-A.; Zepeda, G.; Ruiz, R.; Khan, S. I.; Garcia-Garibay, M. A. *Cryst. Growth Des*. **2004**, *4*, 15-18. (c) Rodriguez-Molina, B.; Ochoa, M. E.; Farfán, N.; Santillan, R.; Garcia-Garibay, M. A. *J. Org. Chem*. **2009**, *74*, 8554-8565.

(119) Throughout this section, *trans* refers to the disposition of the two phosphine ligands, usually in a trigonal bipyramidal coordination geometry.

(120) (a) $Fe(CO)_2(I)(PEt_3)_2$: Fe-I 2.610(1) Å. Kandler, H.; Gauss, C.; Bidell, W.; Rosenberger, S.; Bürgi, T.; Eremenko, I. L.; Veghini, D.; Orama, O.; Burger, P.; Berke, H. *Chem. Eur. J*. **1995**, *1*, 541-548. (b) $Fe(CO)_2(I)(Me)(P(Me)_3)_2$: Fe-I 2.695(1) Å. Bellachioma, G.; Cardaci, G.; Macchioni, A.; Reichenbach, G.; Foresti, E.; Sabatino, P. *J. Organomet. Chem*. **1997**, *531*, 227-235. (c) $Fe(CO)_2(I)(Ph)(P(Me)_3)_2$: Fe-I 2.61(3) Å. Venturi, C.; Bellachioma, G.; Cardaci, G.; Macchioni, A. *Inorg. Chim. Acta*. **2004**, *357*, 3712-3720.

APPENDIX A

Variable temperature information from Section 3: additional NMR data (alternative solvents and temperatures).

5a^{+} BF_4^- (C_6D_5Cl, δ in ppm): $^{13}C\{^1H\}$ (125 MHz, 23 °C) 208.7 (s, ***C***O), 28.6 and 28.3 (2s, $2AsCH_2CH_2\boldsymbol{C}H_2$ and $1AsCH_2CH_2\boldsymbol{C}H_2$), 26.91 and 26.86 (2s, $1\boldsymbol{C}H_2$ and $2\boldsymbol{C}H_2$), 26.0 and 25.9 (2s, $2As\boldsymbol{C}H_2$ and $1AsCH_2$), 25.85 and 25.0 (2s, $2\boldsymbol{C}H_2$ and $1\boldsymbol{C}H_2$), 23.1 and 22.7 (2s, $1AsCH_2\boldsymbol{C}H_2$ and $2AsCH_2\boldsymbol{C}H_2$); $^{13}C\{^1H\}$ (125 MHz, 110 °C) 208.6 (s, ***C***O), 28.9 and 28.8 (2s, $2AsCH_2CH_2\boldsymbol{C}H_2$ and $1AsCH_2CH_2\boldsymbol{C}H_2$), 27.1 and 26.98 (2s, $1\boldsymbol{C}H_2$ and $2\boldsymbol{C}H_2$), 26.95 and 26.8 (2s, $2As\boldsymbol{C}H_2$ and $1AsCH_2$), 26.4 and 26.0 (2s, $2\boldsymbol{C}H_2$ and $1\boldsymbol{C}H_2$), 23.5 and 23.2 (2s, $1AsCH_2\boldsymbol{C}H_2$ and $2AsCH_2\boldsymbol{C}H_2$).

5b^{+} BF_4^- (CD_2Cl_2, δ in ppm): ^1H (500 MHz, 23 °C) 2.38-2.21 (m, 12H, $AsC\boldsymbol{H}_2$), 1.70-1.49 (m, 24H, $AsCH_2C\boldsymbol{H}_2$ and $AsCH_2CH_2C\boldsymbol{H}_2$), 1.48-1.36 (m, 12H, $C\boldsymbol{H}_2$), 1.36-1.19 (m, 24H, remaining $C\boldsymbol{H}_2$); $^{13}C\{^1H\}$ (125 MHz, 23 °C) 207.5 (s, ***C***O), 29.6 (s, $AsCH_2CH_2\boldsymbol{C}H_2$), 27.8 (s, $\boldsymbol{C}H_2$), 27.4 (s, $As\boldsymbol{C}H_2$), 27.3 (s, $\boldsymbol{C}H_2$), 26.2 (s, $\boldsymbol{C}H_2$), 24.2 (s, $AsCH_2\boldsymbol{C}H_2$); ^1H (500 MHz, –60 °C) 2.29-2.14 (m, 12H, $AsC\boldsymbol{H}_2$), 1.60-1.40 (m, 24H, $AsCH_2C\boldsymbol{H}_2$ and $AsCH_2CH_2C\boldsymbol{H}_2$), 1.39-1.16 (m, 36H, remaining $C\boldsymbol{H}_2$); $^{13}C\{^1H\}$ (125 MHz, –60 °C) 206.5 (s, ***C***O), 28.9 and 28.8 (2s, $1AsCH_2CH_2\boldsymbol{C}H_2$ and $2AsCH_2CH_2\boldsymbol{C}H_2$), 26.4 and 26.3 (2s, $2\boldsymbol{C}H_2$ and $1\boldsymbol{C}H_2$), 26.3 and 26.2 (2s, $2As\boldsymbol{C}H_2$ and

1AsCH_2), 26.0 and 25.9 (2s, 2***C***H_2 and 1***C***H_2), 24.5 and 24.4 (2s, 2***C***H_2 and 1***C***H_2), 23.21 and 23.17 (2s, 1AsCH_2***C***H_2 and 2AsCH_2***C***H_2).

5c$^+$ BF_4^- (CD_2Cl_2, δ in ppm): ^{1}H (500 MHz, 23 °C) 2.33-2.25 (m, 12H, As***C****H*$_2$), 1.61-1.47 (m, 24H, AsCH_2***C****H*$_2$ and AsCH_2CH_2***C****H*$_2$), 1.40-1.28 (m, 48H, remaining ***C****H*$_2$); ^{13}C{^{1}H} (125 MHz, 23 °C) 207.3 (s, ***C***O), 30.6 (s, AsCH_2CH_2***C***H_2), 27.9 (s, As***C***H_2), 27.8 (s, ***C***H_2), 27.4 (s, ***C***H_2), 27.0 (s, ***C***H_2), 26.5 (s, ***C***H_2), 25.1 (s, AsCH_2***C***H_2); ^{13}C{^{1}H} (125 MHz, –90 °C) 206.0 (s, ***C***O), 29.9 (s, AsCH_2CH_2***C***H_2), 26.9 (s, As***C***H_2), 26.7 (s, ***C***H_2), 25.13 (s, ***C***H_2), 25.09 (s, ***C***H_2), 24.5 (s, ***C***H_2), 23.5 (s, AsCH_2***C***H_2).

6a$^+$ BAr_f^- (C_6D_5Cl, δ in ppm): ^{1}H (500 MHz, 23 °C) 8.43-8.37 (m, 8H, C_6***H***$_3$ *o* to B), 7.79-7.75 (m, 4H, C_6***H***$_3$ *p* to B), 1.83-1.74 (m, 8H, C***H***$_2$), 1.72-1.66 (m, 4H, C***H***$_2$), 1.50-1.27 (m, 48H, C***H***$_2$), –9.52 (s, 1H, Fe***H***); ^{13}C{^{1}H} (125 MHz, 23 °C; ***C***H_2 peaks only) 28.8 and 28.2 (2s, 2AsCH_2CH_2***C***H_2 and 1AsCH_2CH_2***C***H_2), 26.6 and 26.5 (2s, 2***C***H_2 and 1***C***H_2), 26.48 and 26.3 (2s, 2As***C***H_2 and 1As***C***H_2), 25.9 (s, ***C***H_2), 22.9 and 22.0 (2s, 2AsCH_2***C***H_2 and 1AsCH_2***C***H_2); ^{1}H (500 MHz, 110 °C) 8.15-8.10 (m, 8H, C_6***H***$_3$ *o* to B), 7.66-7.60 (m, 4H, C_6***H***$_3$ *p* to B), 1.83-1.69 (m, 8H, C***H***$_2$), 1.69-1.63 (m, 4H, C***H***$_2$), 1.50-1.38 (m, 12H, C***H***$_2$), 1.37-1.21 (m, 36H, C***H***$_2$), –9.47 (s, 1H, Fe***H***); ^{13}C{^{1}H} (125 MHz, 110 °C; ***C***H_2 peaks only) 29.2 and 28.6 (2s, 2AsCH_2CH_2***C***H_2 and 1AsCH_2CH_2***C***H_2), 27.4 and 27.3 (2s, 2***C***H_2 and 1***C***H_2), 26.84 and 26.76 (2s, 2As***C***H_2

and 1As***C***H_2), 26.59 and 25.56 (2s, 1***C***H_2 and 2***C***H_2), 23.4 and 22.6 (2s, 2AsCH_2***C***H_2 and 1AsCH_2***C***H_2).

6b$^+$ BAr_f^- (CD_2Cl_2, δ in ppm): ^{1}H (500 MHz, 23 °C) 7.75-7.69 (m, 8H, C_6***H***$_3$ *o* to B), 7.59-7.54 (m, 4H, C_6***H***$_3$ *p* to B), 2.07-1.98 (m, 12H, As***C***H_2), 1.64-1.55 (m, 12H, AsCH_2***C***H_2), 1.55-1.47 (m, 12H, AsCH_2CH_2***C***H_2), 1.47-1.39 (m, 12H, ***C***H_2), 1.38-1.26 (m, 24H, remaining ***C***H_2), –9.46 (s, 1H, Fe***H***); ^{13}C{^{1}H} (125 MHz, 23 °C; ***C***H_2 peaks only) 29.6 (s, AsCH_2CH_2***C***H_2), 28.6 (s, As***C***H_2), 27.7 (s, ***C***H_2), 27.3 (s, ***C***H_2), 26.7 (s, ***C***H_2), 24.1 (s, AsCH_2***C***H_2); ^{1}H (500 MHz, –90 °C) 7.79-7.66 (m, 8H, C_6***H***$_3$ *o* to B), 7.59-7.47 (m, 4H, C_6***H***$_3$ *p* to B), 2.07-1.84 (m, 12H, As***C***H_2), 1.54-1.04 (m, 72H, AsCH_2***C***H_2, AsCH_2CH_2***C***H_2, and remaining ***C***H_2), –9.65 (s, 1H, Fe***H***); ^{13}C{^{1}H} (125 MHz, –90 °C; ***C***H_2 peaks only) 27.9 and 27.6 (2s, 2AsCH_2CH_2***C***H_2 and 1AsCH_2CH_2***C***H_2), 26.8 (s, As***C***H_2), 26.4 and 26.1 (2s, 2***C***H_2 and 1***C***H_2), 25.8 and 25.7 (2s, 1***C***H_2 and 2***C***H_2), 25.4 and 25.1 (2s, 1***C***H_2 and 2***C***H_2), 24.3 (s, ***C***H_2), 22.4 (s, ***C***H_2).

6c$^+$ BAr_f^- (CD_2Cl_2, δ in ppm): ^{1}H (500 MHz, 23 °C) 7.76-7.69 (m, 8H, C_6***H***$_3$ *o* to B), 7.59-7.54 (m, 4H, C_6***H***$_3$ *p* to B), 2.09-1.99 (m, 12H, As***C***H_2), 1.63-1.53 (m, 12H, AsCH_2***C***H_2), 1.53-1.44 (m, 12H, AsCH_2CH_2***C***H_2), 1.43-1.35 (m, 12H, ***C***H_2), 1.36-1.25 (m, 36H, remaining ***C***H_2), –9.56 (s, 1H, Fe***H***); ^{13}C{^{1}H} (125 MHz, 23 °C; ***C***H_2 peaks only) 30.4 (s, AsCH_2CH_2***C***H_2), 28.2 (s, As***C***H_2), 28.0 (s, ***C***H_2), 27.8 (s, ***C***H_2), 27.39 (s, ***C***H_2), 27.37 (s, ***C***H_2), 24.7 (s, AsCH_2***C***H_2); ^{1}H (500 MHz, –90 °C) 7.78-7.67 (m, 8H, C_6***H***$_3$ *o* to B), 7.58-7.50 (m, 4H, C_6***H***$_3$ *p* to B), 2.03-1.87 (m, 12H, As***C***H_2), 1.53-1.39

(m, 12H, $AsCH_2C\boldsymbol{H}_2$), 1.29-1.05 (m, 48H, $AsCH_2CH_2C\boldsymbol{H}_2$ and remaining $C\boldsymbol{H}_2$), –9.68 (s, 1H, Fe***H***); $^{13}C\{^1H\}$ (125 MHz, –90 °C; $\boldsymbol{C}H_2$ peaks only) 29.3 (s, $AsCH_2CH_2\boldsymbol{C}H_2$), 26.7 (s, $As\boldsymbol{C}H_2$), 26.5 (s, $\boldsymbol{C}H_2$), 25.9 (s, $\boldsymbol{C}H_2$), 25.6 (s, $\boldsymbol{C}H_2$), 25.1 (s, $\boldsymbol{C}H_2$), 23.7 (s, $AsCH_2\boldsymbol{C}H_2$).

Additional Calculations Regarding Rotational Barriers. The above NMR data for **5a**$^+$ BF_4^- and **6a**$^+$ BAr_f^- were used to bound $\Delta G^{\ddagger}$ values for $Fe(CO)_2(NO)^+$ and $Fe(CO)_3(H)^+$ rotation. This involved application of the equation $\Delta G^{\ddagger} = RT_c[\ln(k_B/h) - \ln(k/T_c)]$, where R is the gas constant (1.987×10^{-3} kcal/mol·K), k_B is the Boltzmann constant (3.300×10^{-27} kcal/K), h is the Planck constant (1.584×10^{-37} kcal·s), and $k = \pi\delta\upsilon/\sqrt{2}$, with $\delta\upsilon$ taken as the peak separation (Hz) at the low temperature limit (298 K). When a coalescence temperature (T_c) of 383 K is entered (separate signals are still observed at 383 K), $\Delta G^{\ddagger}_{383K}$ values of 19.4 kcal/mol and 18.9 kcal/mol are calculated (average from five and three signals, respectively). The true values must (since the actual coalescence temperatures are greater) be higher.

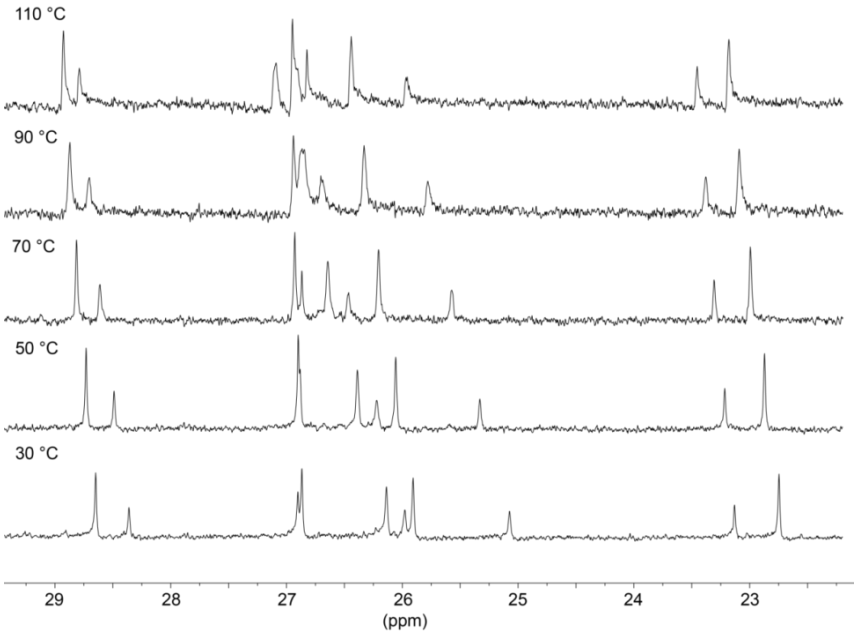

Figure A-1. The CH_2 region of the $^{13}C\{^1H\}$ NMR spectrum of **5a**$^+$ BF_4^- at different temperatures (C_6D_5Cl).

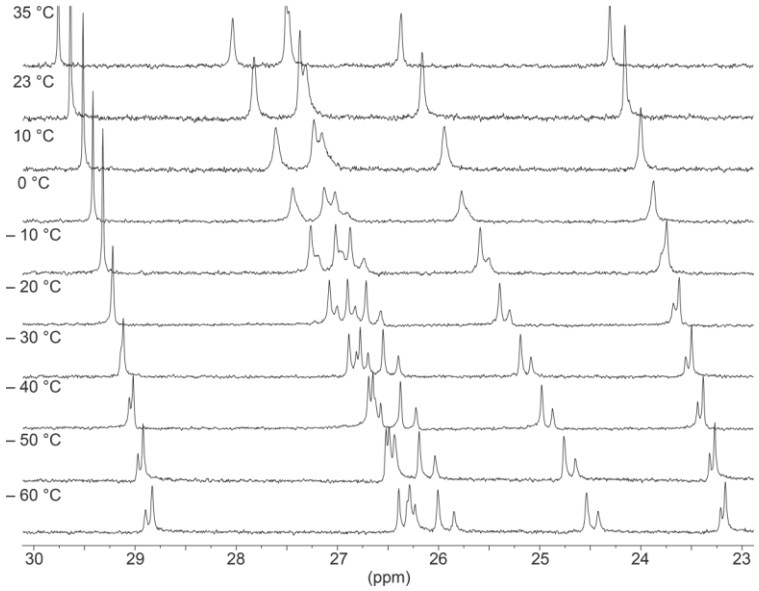

Figure A-2. The CH_2 region of the $^{13}C\{^1H\}$ NMR spectrum of **5b**$^+$ BF_4^- at different temperatures (CD_2Cl_2).

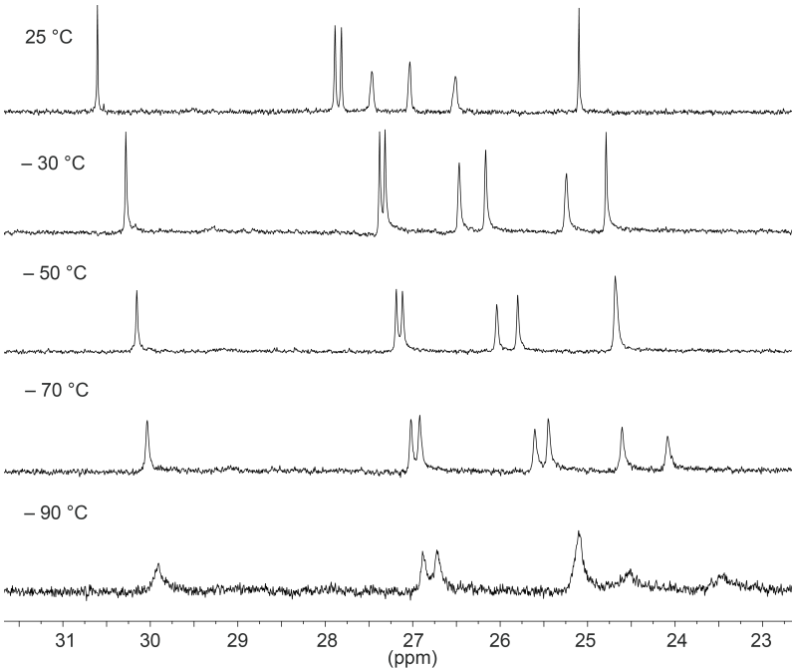

Figure A-3 The CH_2 region of the $^{13}C\{^1H\}$ NMR spectrum of **5c**$^+$ BF_4^- at different temperatures (CD_2Cl_2)**.**

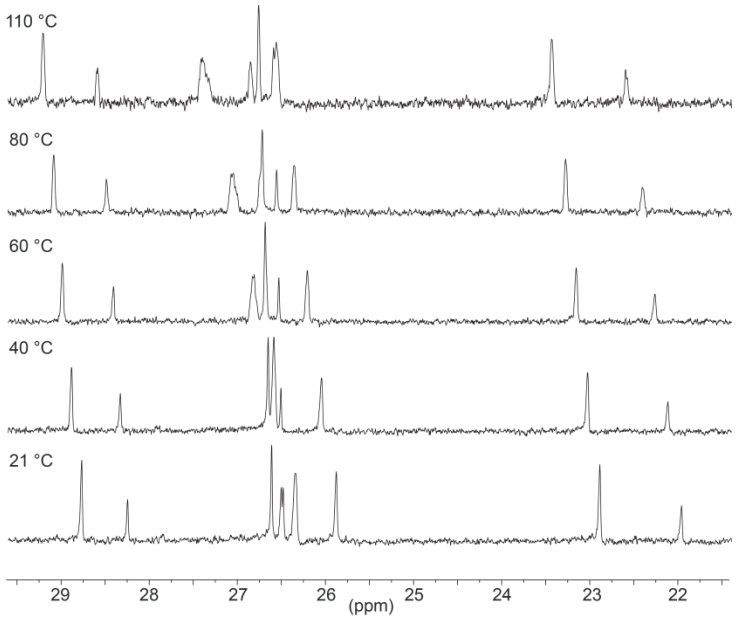

Figure A-4. The CH_2 region of the $^{13}C\{^1H\}$ NMR spectrum of **6a**$^+$ BAr_f^- at different temperatures (C_6D_5Cl).

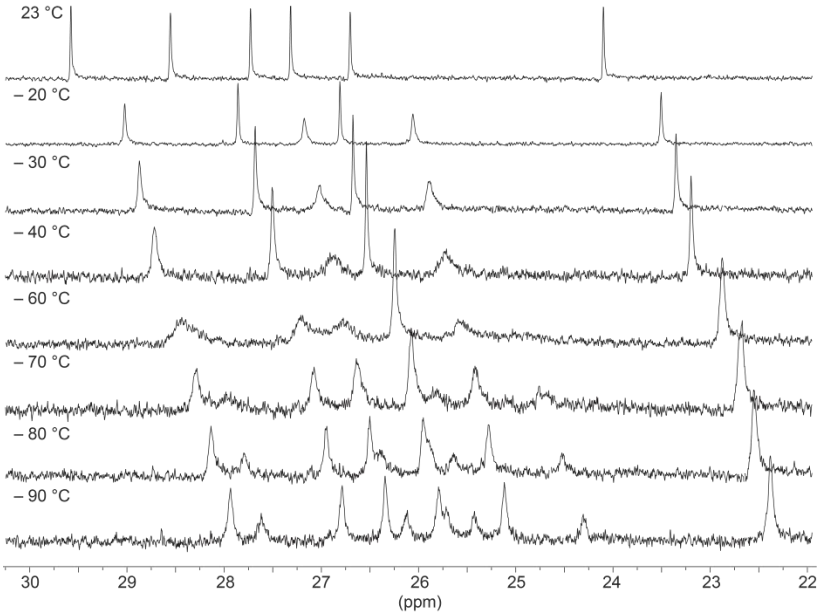

Figure A-5. The CH_2 region of the $^{13}C\{^1H\}$ NMR spectrum of **6b**$^+$ BAr_f^- at different temperatures (CD_2Cl_2).

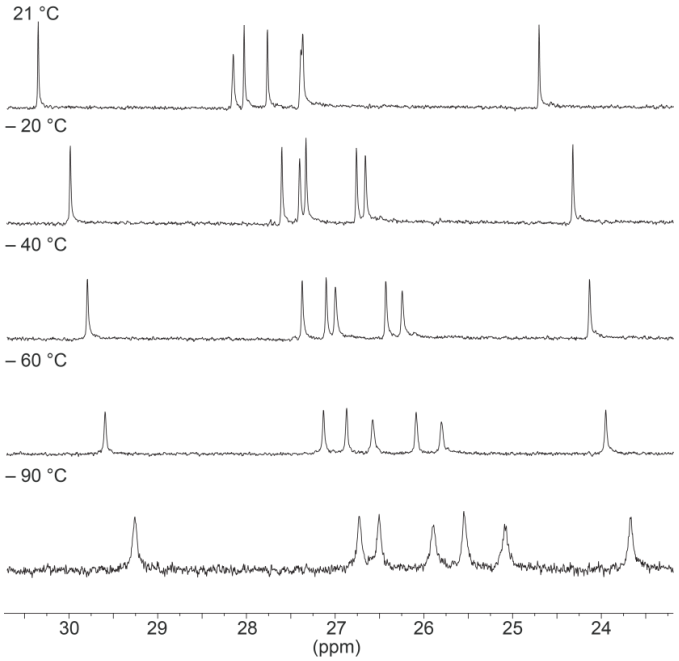

Figure A-6. The CH_2 region of the $^{13}C\{^1H\}$ NMR spectrum of **6c**$^+$ BAr_f^- at different temperatures (CD_2Cl_2).

APPENDIX B

DSC data from Sections 2 and 3.

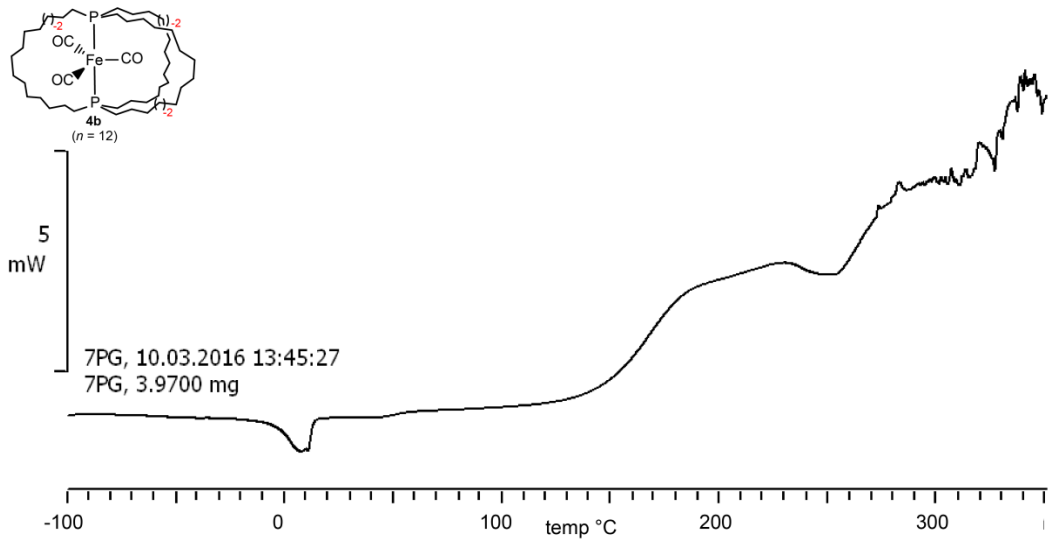

Figure B-1. DSC trace of **4b** (Section 2).

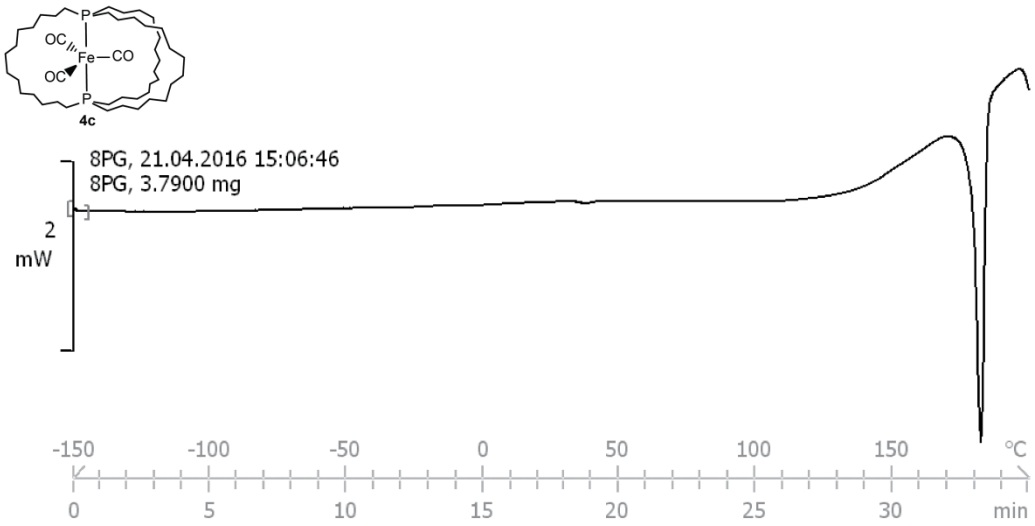

Figure B-2. DSC trace of **4c** (Section 2).

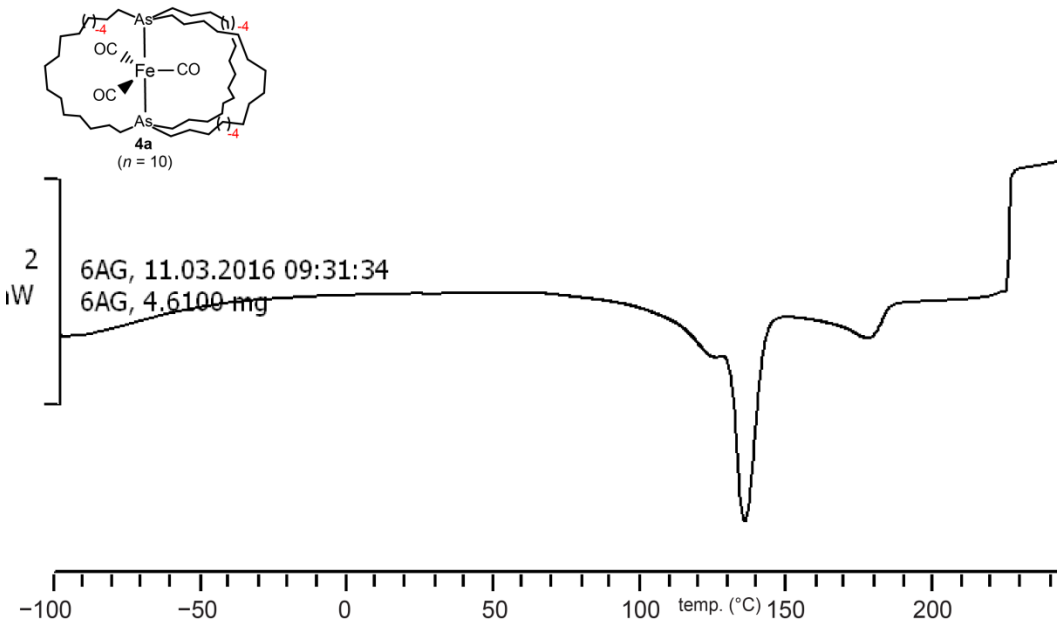

Figure B-3. DSC trace of **4a** (Section 3).

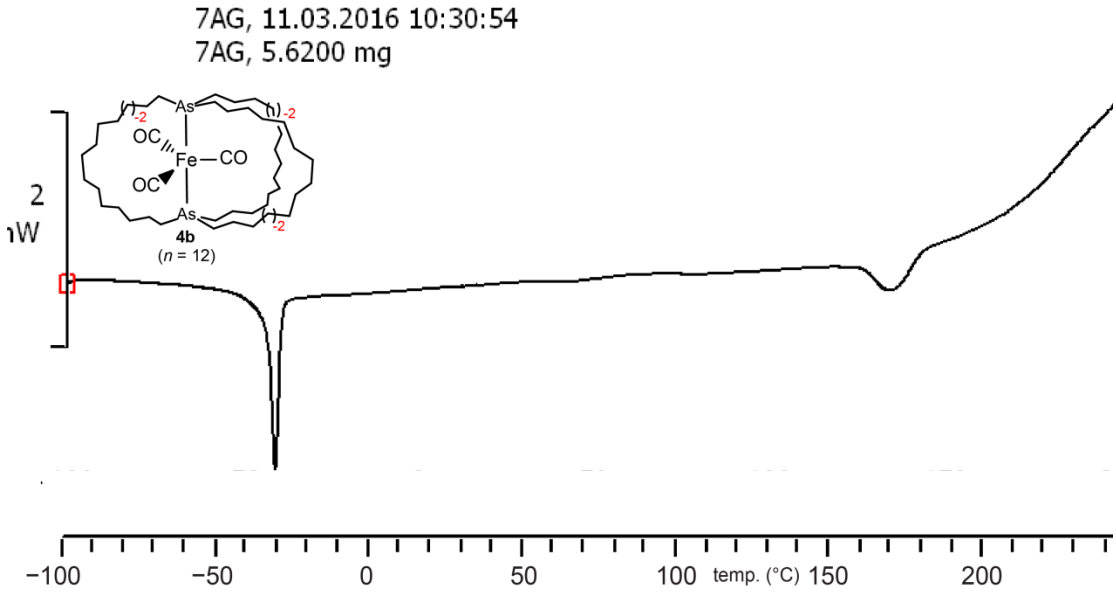

Figure B-4. DSC trace of **4b** (Section 3).

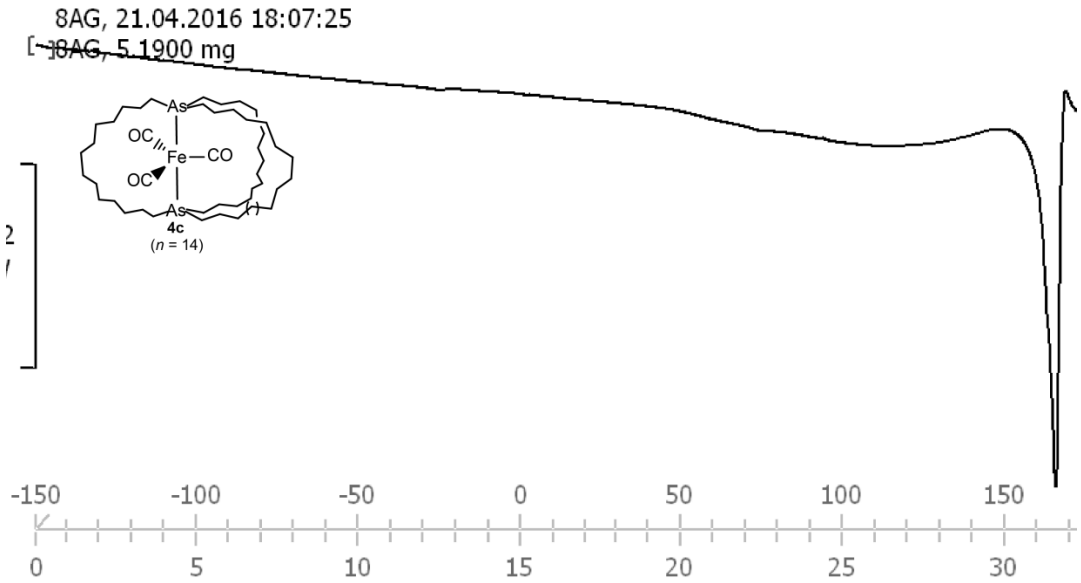

Figure B-5. DSC trace of **4c** (Section 3).